Curtin Medical School
Faculty of Health Sciences

The Role of Amyloidogenic Peptides in Disruption of Insulin Secretion and Action

Joanne Elizabeth Rowles

0000-0002-6066-3581

This thesis is presented for the Degree of
Doctor of Philosophy
Of
Curtin University

October 2023

DECLARATION

To the best of my knowledge and belief, this thesis contains no material previously published by any other person except where due acknowledgement has been made.

This thesis contains no material that has been accepted for the award of any other degree or diploma from any university.

Name of Student: Joanne E. Rowles

Signature:……

Date: 13 October 2023

ABSTRACT

Type 2 Diabetes (T2D) and Alzheimer's disease (AD) are chronic diseases with many similarities, including shared risk factors and patient demographics. Both diseases also demonstrate accumulations of amyloidogenic plaque in vital organs that disrupt cellular function and metabolism, eventually leading to cell death. Mounting evidence shows that two amyloidogenic peptides in particular, AD-associated beta-amyloid (Aβ) and T2D-associated islet amyloid polypeptide (IAPP), co-aggregate and co-deposit together in the brain and pancreatic islets. The effects of the interaction between these amyloidogenic peptides on different cell types within the brain and peripheral tissues are not understood. With a focus on tissues relevant to T2D, the thesis aimed to determine and compare the effects of Aβ, IAPP, and the combination of both, on pancreatic β-cells and skeletal muscle cells.

Initially, pancreatic islets were analysed from transgenic mice expressing human Aβ-Precursor Protein (APP) or human IAPP, and a novel double transgenic (DTG) mouse expressing both APP and IAPP. Amyloid plaque deposition, insulin function, inflammation, and cell stress markers within the islets were analysed by immunofluorescent microscopy. Amyloid plaque was only detected in IAPP and DTG mice, with significantly increased amyloid detected in islets of DTG mice. Insulin staining was reduced, and levels of macrophages were increased in DTG mice compared to other models, and these changes correlated with amyloid severity. These results indicated an exacerbated pancreatic pathology associated with increased amyloid accumulation in mice expressing both IAPP and APP, suggesting that co-aggregation of Aβ and IAPP have greater impact on islet (and in particular β-cell) function, compared to either peptide alone.

To explore this further BRIN-BD11 rat pancreatic β-cells were treated with IAPP, Aβ and IAPP-Aβ combinations. IAPP-Aβ combinations significantly reduced cell viability and enhanced stress markers compared to IAPP or Aβ alone. Although all amyloid treatments reduced insulin secretion, IAPP-Aβ aggregates induced the greatest reduction in glucose-stimulated insulin

secretion (GSIS). Apart from a reduction in GSIS, Aβ did not alter β-cell viability or metabolism. Mitochondrial function was reduced similarly by both IAPP-Aβ and IAPP, despite differences in cytotoxicity. These *in vivo* and *in vitro* findings support the hypothesis that IAPP and Aβ cross-seed in pancreatic islets to exacerbate amyloid accumulation and increase cell toxicity.

Skeletal muscle is an insulin-sensitive tissue that can be impacted by insulin resistance / T2D. Few studies have explored the effects of amyloidogenic peptides in muscle and none have yet explored the impact of IAPP-Aβ. To address this, Human Skeletal Muscle Myoblasts (HSMMs) that had been differentiated into mature myotubes were treated with IAPP, Aβ, and IAPP-Aβ The IAPP-Aβ combination significantly reduced cell viability and increased cell stress in differentiated HSMM cells compared to other amyloid treatments. All amyloid treatments reduced glucose uptake regardless of toxicity. IAPP and IAPP-Aβ aggregates again reduced mitochondrial function in a similar manner, despite differences in overall toxicity. In summary, this thesis has provided novel insight into an understudied area on how Aβ and the cross-seeding of IAPP-Aβ impact peripheral tissues relevant to T2D. The findings demonstrate a greater propensity for IAPP-Aβ to be cytotoxic in these tissues and provided insight into underlying mechanisms. Surprisingly, unlike in neuronal cells, Aβ did not induce significant cytotoxicity in pancreatic β-cell or muscle cells, suggesting that Aβ requires cross-seeding to have a role in T2D pathology. These findings could have significant implications for the knowledge, treatment, and management of T2D.

DEDICATION

This thesis is dedicated to my son,

Ellis Mark Rowles

I will love and miss you always, my Angel

ACKNOWLEDGEMENTS

Firstly, I would like to acknowledge the traditional custodians of this land (Whadjuk Noongar Booja) on which I have lived and worked, and pay my respects to their elders, past, present, and emerging. My sincere appreciation to the Curtin Medical School, the Faculty of Health Sciences, Curtin University, and the Australian Government Research Training Program for funding my PhD project. Thank you also to the CHIRI and Building 305 administration, support staff, and technicians who have worked tirelessly to make this possible. I would like to acknowledge the hard work and dedication of my supervisors A / Prof. Giuseppe Verdile and Dr. Imran Khan, my incredible mentor Dr. Kevin Keane, and my thesis chair Dr. Kylie Munyard. Thank you for all the times you have supported, guided, and encouraged me. Thank you for this opportunity, for the things I have learnt from you all, and the many fun times we have had. I would not have been able to finish this journey without you all.

A heartfelt thank you to all past and present members of my two lab groups, who are too numerous to name, but they know who they are! Thank you all for your help and friendship over the years, especially Prashant Bharadwaj (for the collaboration, material donations, knowledge, and laughter), and Jordan Rowlands (for the all-nighters, pep talks, and shenanigans). This extends to all those I have worked with in TC3, Lab 3, and Office 145 / HDR Hub 1 over the years, including Andrea Goncalves (for being your incredibly compassionate and fun self), and Alex Richards (for being my lab wife). I would also like to send apologies to those I have shared these rooms with for the almost constant giggles and occasional terrible singing. To Nikita Walz, who is included in all the above categories, you have often been the first person I have gone to for advice, celebration, encouragement, and comfort during my PhD. Without our laughter and adventures, this experience would have been incomplete. Thank you for everything.

To all my wonderful friends outside of the lab, especially my SBC girls, St Francis boys, and their families: thanks for many years of friendship, always cheering me on (or up), and of course, all the cute pet and baby pictures that

have never failed to brighten my day. To my amazing Pradella, Rowles, Allerton, Hagger, Mallet, and Vickery family members: thank you for believing in me, making me laugh every day, comforting me when I needed it, and for being my most ardent supporters. An extra special thank you to Patricia and Stephen Rowles for treating me like one of your own since I was 16, because I cannot tell you what it means to me. To my parents, Barbara and Steven Pradella, there are no words to fully express my gratitude. Thank you for your unwavering love, all the sacrifices you have made to help me get here, and for always having a hug and a cup of tea waiting for me. I could not have asked for better or more loving parents. In all of you, I have been blessed with the world's best support network which has been with me through my best and worst times. All of you have always been willing to run alongside me to help tackle any obstacles that might be in my way (probably literally).

Finally, I have saved the biggest and most important acknowledgement for last. To my husband, my best friend, the father of my children, and my soulmate, Mark Rowles: having you beside me has made every day brighter, every breath easier, and every step lighter. From bringing dinner to the lab when I am working late because you wanted me to have a home-cooked meal, to helping me rearrange sentences that were not reading right, to comforting me when I needed it the most. There has not been a single moment that you have not done your best to support me. I could write a whole new thesis on all the ways you have been so wonderful and still never manage to mention it all. Your patience, kindness, reassurance, resilience, good humour, and love have been endless and superhuman. I love you, my darling, and thank you for everything. It has been such a gift.

- Joanne E. Rowles (née Pradella)

FINANCIAL SUPPORT

Joanne E. Rowles was supported by a scholarship from the Australian Government Research Training Program (formerly the Australian Postgraduate Award), Curtin University Office of Research and Development, Curtin Medical School, and Faculty of Health Sciences, Curtin University.

LIST OF PUBLICATIONS

- **Rowles JE**, Keane KN, Gomes Heck T, Cruzat V, Verdile G, Newsholme P. Are Heat Shock Proteins an Important Link between Type 2 Diabetes and Alzheimer Disease? International Journal of Molecular Sciences. 2020;21(21):8204. doi:10.3390/ijms21218204

- Bharadwaj P, Solomon T, Sahoo BR, Ignasiak, K, Gaskin, S, **Rowles, JE**, Verdile, G, Howard, MJ, Bond, CS, Ramamoorthy, A, Martins, RN, Newsholme, P. Amylin and beta amyloid proteins interact to form amorphous heterocomplexes with enhanced toxicity in neuronal cells. Sci Rep. 2020;10(1):10356. doi:10.1038/s41598-020-66602-9

- Rowlands J, Walz N, **Rowles JE**, Keane KN, Carlessi R, Newsholme P. Method Protocols for Metabolic and Functional Analysis of the BRIN-BD11 β-Cell Line: A Preclinical Model for Type 2 Diabetes. Methods Mol Biol. 2019;1916:329-340. doi:10.1007/978-1-4939-8994-2_32

- Verdile G, Keane KN, Cruzat VF, Medic, S, Sabale, M, **Rowles, JE**, Wijesekara, N, Martins, RN, Fraser, PE, Newsholme, P. Inflammation and Oxidative Stress: The Molecular Connectivity between Insulin Resistance, Obesity, and Alzheimer's Disease. Mediators Inflamm. 2015;2015:105828. doi:10.1155/2015/105828

HOW TO READ THIS THESIS

- This thesis is written in the style of a traditional thesis and includes no unstated publications.
- This thesis is designed to be read as a digital copy, with hyperlinks available on underlined words, page numbers, and citations to direct the reader to relevant sections, though can also be read easily in hard-copy form.
- A table of contents, an index of tables and figures, and a list of abbreviations are available for ease of reference.
- Chapter 1 is a literature review which aims to summarise the current literature in the field and the significance of the work. This includes a statement of the specific research aims.
- Chapter 2 is a materials and methods section subdivided into two main sections; a section on techniques involving murine tissue samples and a section on techniques involving *in vitro* cell lines.
- Chapter 3 , Chapter 4 , and Chapter 5 feature the results of the project, including a chapter-specific abstract, introduction, aim, materials and methods, and discussion.
    - Essentially, these chapters are designed to be read as both the results chapters of a traditional thesis and as stand-alone manuscripts.
- Chapter 6 is a final discussion, where the findings of the results chapters are compiled, examined, and considered in the context of the current literature.
- Chapter 7 and Chapter 8 are the references and appendices, respectively, cited throughout the project where necessary.
- Enjoying a hot beverage is recommended while reading, unless the time is suitable to switch to a cold beverage of your choice.

TABLE OF CONTENTS

LIST OF ABBREVIATIONS

2-DG	2-Deoxy-glucose
2-NBDG	2-(N-[7-Nitrobenz-2-oxa-1,3-diazol-4-yl] Amino)-2-Deoxyglucose
Aβ	Beta-Amyloid
Active Cas3	Activated (Cleaved) Caspase-3
AD	Alzheimer's Disease
Akt	Protein Kinase B (PKB)
ApoE	Apolipoprotein E
APP	Amyloid Precursor Protein
ATF4	Activating Transcription Factor 4
β2M	β-2 Microglobulin
BBB	Blood Brain Barrier
BCA	Bicinchoninic Acid
BiP	Binding Immunoglobulin Protein
BSA	Bovine Serum Albumin
CHO	Chinese Hamster Ovary
COXIV	Complex 4 (Cytochrome C Oxidase)
CSF	Cerebrospinal Fluid
CTRL	Control
Cys2	Cysteine Residue 2 of IAPP structure
Cys7	Cysteine Residue 7 of IAPP structure
DAMPs	Danger Associated Molecular Patterns
DTG	Double Transgenic
DMEM	Dulbecco's Modified Eagle Medium
DMSO	Dimethyl Sulfoxide
ECAR	Extracellular Acidification Rate
ECL	Enhanced Chemiluminescent
ERR-α	Estrogen-Related Receptor-α
ETC	Electron Transport Chain
FBS	Foetal Bovine Serum
FCCP	Carbonyl cyanide 4-trifluoromethoxyphenylhydrazone
FFA	Free Fatty Acid
FOXO1	Forkhead Box O1
FOXO3	Forkhead Box O3
GOx	Glucose Oxidase
GLUT2	Glucose Transporter Isoform 2
GLUT4	Glucose Transporter Isoform 4

HBSS	Hank's Balanced Salt Solution
HEPES	4-(2-hydroxyethyl)-1-piperazineethanesulfonic acid
HFIP	Hexafluoro-2-propanol
hIAPP	Human Islet Amyloid Polypeptide
HRP	Horseradish Peroxidase
HSMM	Human Skeletal Muscle Myoblasts
HSP	Heat Shock Protein
HSR	Heat Shock Response
IAPP	Islet Amyloid Polypeptide
IFN-γ	Interferon-Gamma
IgG	Immunoglobulin G
IL-1β	Interleukin-1β
iNOS	Inducible Nitric Oxide Synthase
KRBB	Kreb's Ringer Bicarbonate Buffer
LRP-1	Lipoprotein Receptor-related Protein 1
MHC2	Myosin Heavy Chain 2
MTT	Methylthiazol Tetrazolium
MYOG	Myogenin
NF-κB	Nuclear Factor κB
NT	Nontransgenic
OCR	Oxygen Consumption Rate
pAkt	Phosphorylated Akt
pAkt S473	Phosphorylated Akt at Serine 473
pAkt T308	Phosphorylated Akt at Threonine 308
PBMCs	Peripheral Blood Mononuclear Cells
PGC-1α	Peroxisome Proliferator-Activated Receptor Gamma Coactivator 1-α
PPAR-α	Peroxisome Proliferator-Activated Receptor-α
PPAR-γ	Peroxisome Proliferator-Activated Receptor-γ
PS1 / 2	Presenilin 1 / 2
pTau	Phosphorylated Tau protein
PBS	Phosphate-Buffered Saline
PCR	Polymerase Chain Reaction
PER	Proton Efflux Rate
PI	Propidium Iodide
ROS	Reactive Oxygen Species
rIAPP	Rodent Islet Amyloid Polypeptide
RIPA	Radioimmunoprecipitation Assay
RT-PCR	Real Time Polymerase Chain Reaction
SD	Standard Deviation

SDS-PAGE	Sodium Dodecyl Sulphate – Polyacrylamide Gel Electrophoresis
SEM	Standard Error of the Mean
SIRT1	Sirtuin-1
STP	Staurosporin
T2D	Type 2 Diabetes
TBS	Tris-Buffered Saline
TBS-T	TBS with 0.05% TWEEN® 20
ThioS	Thioflavin S
THP	Thapsigargin
TNNT3	Troponin Type 2
TNFα	Tumor Necrosis Factor-α
UPR	Unfolded Protein Response
UPS	Ubiquitin-Proteasome-System

LIST OF TABLES AND FIGURES

CHAPTER 1 Literature Review

1.1 Introduction

Type 2 diabetes mellitus (T2D) is a metabolic disorder characterised by chronic hyperglycaemia that (if not managed appropriately) can cause irreversible damage to vital organs and tissues [1]. In recent years, there has been extensive evidence for an association between T2D and Alzheimer's disease (AD), a neurodegenerative disorder characterised by progressive cognitive decline, behavioural changes, and reduced activities of daily living and executive function leading to eventual death [2-5]. At first glance, there appears to be little connection between these two diseases, but there are many clinical, epidemiological, and pathological links between T2D and AD.

Both T2D and AD are chronic diseases affecting older populations, and both can result in the death of the patient [1, 5]. They also share risk factors, including genetic susceptibility, obesity, age, sedentary lifestyle, and affect shared populations of people [1, 5]. Evidence suggests that a diagnosis of T2D increases the risk of developing AD by 65% [2, 3], while patients with AD have an increased risk of developing insulin resistance and T2D [4]. In addition to epidemiology, there are also common physiological links. T2D and AD both have dysfunction in insulin signalling [6-9], chronic inflammation [10-12], oxidative stress [10, 13, 14], and the focus of this thesis, plaque accumulation composed of amyloidogenic peptides in vital organs [15, 16].

'Amyloidogenic' is a term given to proteins and polypeptides that have a high propensity to misfold and aggregate into abnormal and / or unregulated conformations. Currently, a total of 37 pathological human amyloid proteins have been documented to play a role in human diseases. A further 4 amyloid proteins have been found not to be associated with disease and are functional in the human body in their aggregated states [17, 18]. Despite originating in different tissues and having dissimilar structures and functions, these proteins progressively aggregate from monomeric peptides to oligomeric intermediates, and finally into an insoluble fibrillar morphology with a β-sheet secondary structure [19, 20]. Insoluble fibrillar amyloidogenic peptides can

deposit in vital tissues as amyloidogenic plaque and the intermediate aggregates can contribute to a variety of disorders. In T2D and AD, the relevant amyloidogenic peptides are islet amyloid polypeptide (IAPP) and β-amyloid (Aβ) [21, 22].

IAPP is a small hormone-polypeptide known to aggregate and deposit in the pancreatic islets, and has been associated with islet dysfunction in T2D [23]. Similarly to the mechanism(s) of pancreatic dysfunction, the peptide Aβ accumulates in the brain in patients causing neuronal dysfunction and death [16]. Importantly, recent research indicates that IAPP and Aβ may cross-seed and co-localise in common tissues, predominantly the brain and pancreatic islets [24, 25]. Although the impact of IAPP on T2D is well-established, the role of Aβ (individually and in combination with IAPP) has not yet been explored. This chapter aims to explore the literature on IAPP and Aβ in the pathophysiology of T2D.

1.2 Type 2 Diabetes Mellitus

1.2.1 Definition and Risk Factors

In Australia, an estimated 5.6% of the adult population (approximately 1.3 million people) have a form of diabetes [26-28]. Globally, approximately 1 in 2 (46%) of those with diabetes are not diagnosed and, therefore, untreated. However, in Australia, only 1 in 4 Australians (25%) with diabetes are suspected to be undiagnosed [28]. This discrepancy has been largely attributed to differences in quality of health care and income level, since low- and middle-income countries account for 87% of global diabetes-related deaths, only spending 35% of global diabetes-related health expenditure, and are predicted to have a higher increase in the number of cases of diabetes by 2045 (up to a 143% increase in the predicted cases compared to the global average of a 51% increase) [27]. Despite this, according to the Australian Institute of Health and Welfare National Mortality Database, 16700 preventable deaths were directly attributed to diabetes or a diabetic complication in 2018 alone [29].

Diabetes is divided into individual subtypes, depending on the particular type of insulin action deficiency, including Type 1 Diabetes (T1D), T2D, Gestational Diabetes, and other rarer forms with a genetic cause. T1D is predominantly characterised by a deficiency in insulin production resulting from an autoimmune reaction that destroys insulin-secreting pancreatic β-cells. Although T1D occurs more frequently in children, it can occur at any age and often occurs suddenly [30]. In comparison, T2D (the most prevalent form of the disease, accounting for 85-90% of total diabetic cases [31]) has a more gradual onset and occurs more frequently in older adults (mainly > 60 years).

The predominant risk factor for development of T2D is obesity, typically determined by body mass index (BMI), a ratio of body weight to height, intended to give an insight into an approximate amount of body fat. Research indicates that the risk of T2D has a positive causal association with BMI [32-34]. Ageing is another important risk factor, as the risk of developing T2D increases with age, although recent studies indicate an increase in the diagnosis of T2D in young adults and adolescents [35-37]. This is predominantly believed to be the result of increased obesity in younger populations, as BMI was found to have a direct correlation with the age of onset of T2D, such that adults who were more obese at a younger age had a higher risk of developing T2D than those who were obese at a later age. [35, 38, 39]. Studies also suggest that men are more likely to develop T2D than women, probably as a result of a higher accumulation of abdominal visceral fat due to male sex hormones (known as “android” obesity) [40]. Consistent with these findings, transwomen who have undergone hormone therapy and / or orchiectomy are less likely to develop diabetes-associated pathology than cis-men [41].

In addition, genetics and inheritance play an important role in determining who will develop T2D. For example, people of Asian, Hispanic, and African descent are more at risk than those of Northern European descent in US populations [42]. Indigenous populations, such as those in the US and Australia, are also more likely to develop T2D than non-indigenous populations [36, 43]. Similarly, those with a family history of T2D are more likely to develop it themselves, evidenced by 74-100% of people recently diagnosed with T2D in the US and

the UK having first- or second-degree family members with T2D [37, 44]. However, phenotype-based risk models that use nongenetic variables such as age, sex, BMI, and diet, are still more likely to predict a future diagnosis of T2D than current genotype-based risk models, indicating that genetics alone is not enough to accurately determine the probability of developing T2D [45].

1.2.2 Pathophysiology of Type 2 Diabetes

The hallmark of T2D, chronic hyperglycaemia, results from an inability of pancreatic islets to produce enough insulin, ineffective use of the insulin by peripheral tissues, or a combination of both [29]. Under heathy physiological conditions, an increase in blood glucose triggers β-cells of the pancreatic islets to release insulin, which promotes glucose transport into peripheral tissues for use in energy production and storage [46, 47]. Elevations in blood glucose result in an increased passive entry of glucose into β-cells via Glucose Transporter 2 (GLUT2) channels, which is rapidly converted to pyruvate by glycolysis for entry into the TCA cycle in mitochondria (Figure 1A) [48]. Increased mitochondrial activity results in an enhanced ATP : ADP ratio in the β-cell, closing ATP-sensitive K^+ channels [49]. Closure of these channels causes depolarisation of the cellular membrane, opening voltage-gated calcium (Ca^{2+}) channels and resulting in an influx of Ca^{2+} that triggers insulin exocytosis into the blood [48, 49].

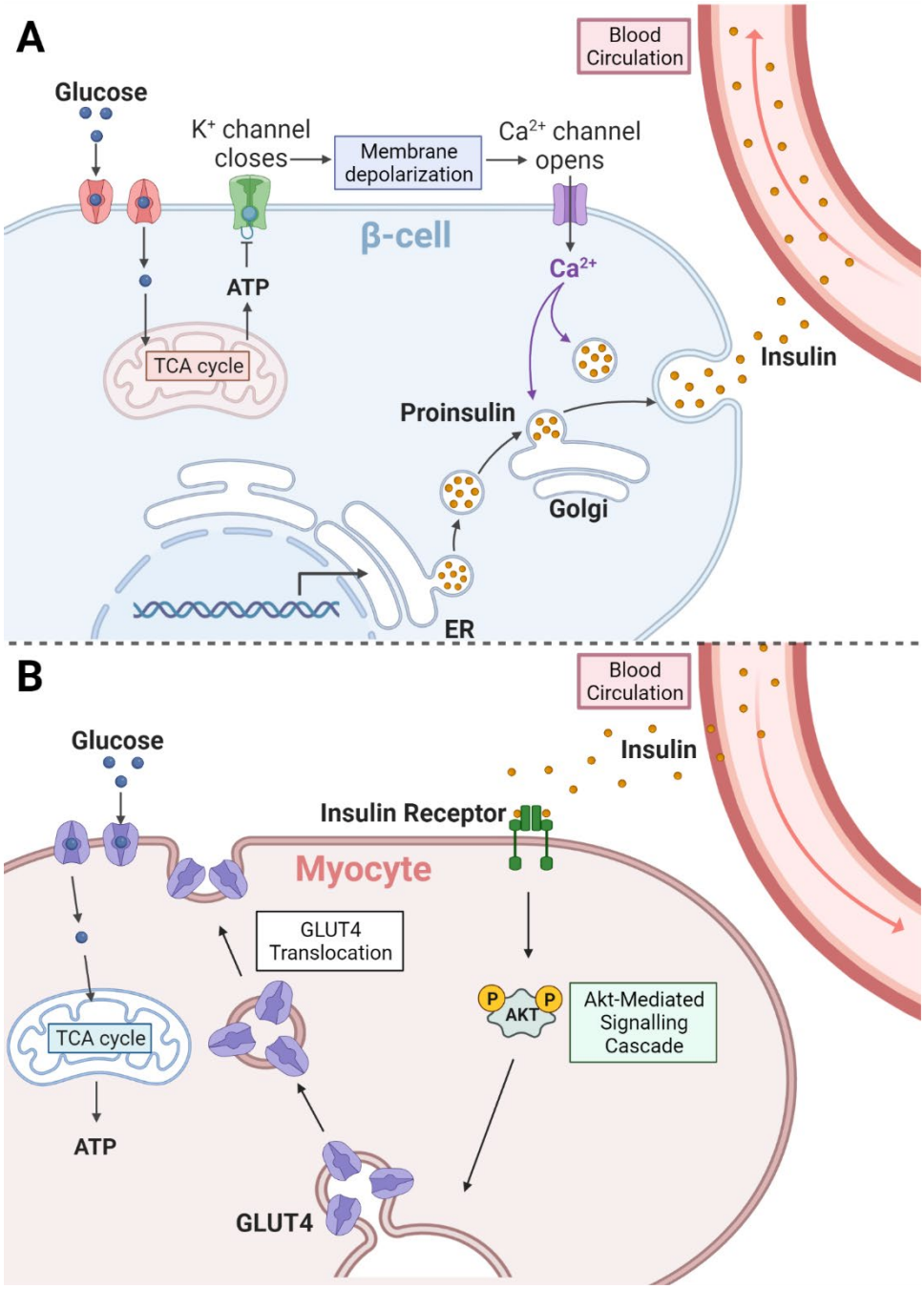

Figure 1. Insulin function in healthy individuals. Glucose enters pancreatic β-cells via specialised GLUT2 receptors and is broken down into key metabolites to enter the TCA cycle inside mitochondria. The subsequent increase in ATP output closes ATP-sensitive K^+ channels on the cell membrane, resulting in membrane depolarisation and the opening of voltage-dependent Ca^{2+} channels. The influx of intracellular Ca^{2+} triggers insulin exocytosis (A). Insulin is transported in the bloodstream to peripheral tissues (such as myocytes) where insulin receptors are located. Binding to insulin receptors activates downstream signalling cascades, mediated by activated (phosphorylated) Akt, to translocate GLUT4 receptors to the cellular membrane, allowing the passage of glucose into the cell. Retrieved and adapted from 'Insulin Production Pathway' template by author with Biorender.com (2023).

In insulin-sensitive peripheral tissues, including the liver, skeletal muscle, and adipose tissue, insulin binds to the insulin receptor on the cell membrane [50]. This activates downstream signalling cascades mediated by activation of Akt via phosphorylation at the residues of threonine 308 (T308) and serine 473 (S473) [50]. Although the effects of phosphorylated Akt (pAkt) are widespread, the resultant effect is the translocation of intracellular glucose transporter isoform 4 (GLUT4) channels to the cell membrane to allow the influx of glucose for cell respiration and energy production (Figure 1B) [51]. A deficiency in insulin production, or a decrease in insulin receptor affinity for insulin, results in hyperglycaemia, reduced mitochondrial oxidative phosphorylation, impaired fatty acid oxidation, intracellular lipid accumulation, reduced glycogen synthesis, increased cytotoxic reactive oxygen species (ROS), and activation of inflammatory signalling pathways in peripheral tissues [52-54].

Peripheral insulin resistance occurs early in disease progression, often in a prediabetic state [1]. The cause of insulin resistance is poorly understood, although there are several important risk factors associated with its development, including factors similar to T2D such as obesity, age, poor diet, genetics, sedentary lifestyle, and hormonal dysregulation [11, 55-57]. In addition, chronic systemic inflammation can contribute significantly to the development and severity of insulin resistance [10, 11]. Regardless, when peripheral tissues develop a resistance to insulin, glucose cannot be properly transported and used, resulting in hyperglycaemia. As a result, insulin demand increases and T2D eventually develops when the β-cells fail to sufficiently compensate for the insulin resistance [58, 59].

In healthy individuals, there is a hyperbolic relationship between insulin secretion and peripheral insulin sensitivity, where decreases in insulin sensitivity result in increases in insulin secretion [7, 60]. However, in insulin-resistant individuals, pancreatic islets eventually undergo functional adaptations to enhance glucose-stimulated insulin secretion (GSIS), such as increased β-cell mass, greater amplitudes of action potentials, modified exocytotic efficiency, and increased intracellular Ca^{2+} to compensate [61]. As insulin resistance increases and / or worsens, chronic compensatory hyperinsulinemia promotes islet dysfunction, including reduced intercellular

communication between individual β-cells, reduced density of ATP-sensitive K^+ channels, and impaired cell cycle progression [62-64]. Furthermore, factors external to islet function, such as hyperlipidaemia and inflammatory cytokines, contribute to β-cell distress and dysfunction [7, 60]. Eventually, the β-cell mass and function declines due to increased β-cell apoptosis under stress [7, 62].

Although islet dysfunction and peripheral insulin resistance are the defining features of T2D, an additional key pathological feature is the accumulation of intra-islet amyloid plaque. Approximately 90% of individuals with T2D show pancreatic amyloid deposition on post-mortem examination [21, 65-67]. In comparison, up to 15% of non-diabetics show amyloid plaque pathology [66-69]. Comparing islet plaque composition, 40% of these non-diabetic individuals show general amyloidosis [69], while the islet amyloid plaque identified in diabetic patients is primarily composed of the hormone peptide IAPP (also called IAPP) [65]. IAPP can begin to deposit early in T2D disease development, and has been associated with both a progressive decline of β-cell mass and increased disease severity [70, 71].

1.3 Islet Amyloid Polypeptide

1.3.1 Synthesis, Secretion, and Clearance

IAPP is a 37 amino acid hormone polypeptide co-secreted with insulin from pancreatic islet β-cells (Figure 2) [72]. IAPP is primarily defined in the literature by its propensity to misfold and aggregate into cytotoxic oligomeric and fibrillar structures that deposit in critical tissues in the body, such as the pancreas [73]. However, under healthy non-amyloidogenic conditions, IAPP assists insulin in the regulation and management of postprandial glucose levels, where it stimulates the satiety response, regulates gastric emptying, and suppresses glucagon secretion from the α-cells in the pancreatic islet [59]. Although IAPP mRNA is found in many tissues in the body, including the central nervous system and gastrointestinal (GI) tract, the vast majority of IAPP synthesis and secretion occurs in pancreatic islets [74-76].

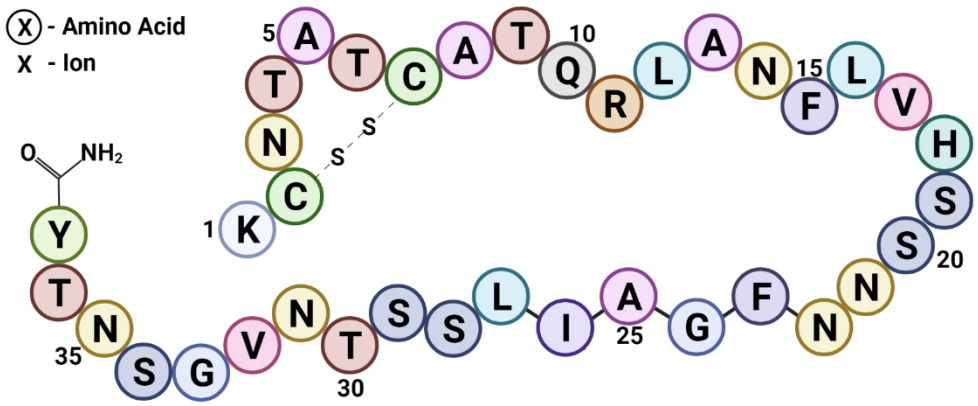

Figure 2. Monomeric Structure of human IAPP. IAPP, also called Amylin, is a pancreatic peptide hormone comprised of 37 amino acids, with a disulphide bond between resides 2 and 7 and an amidated C-terminus. Figure adapted from Hayden et al. [77].

The IAPP gene is located on chromosome 12 [78]. Human IAPP synthesis begins with PreproIAPP, an 89 amino acid coding sequence that is rapidly cleaved at the N-terminus to produce the 69 amino acid ProIAPP, the precursor protein to IAPP. Subsequently, ProIAPP is processed in the endoplasmic reticulum (ER) to form the disulphide bond between cysteine residues 2 (Cys2) and 7 (Cys7) before progressing down the secretory pathway for further post-translational modifications and cleavage in both terminal domains to form mature IAPP [72]. The amidated C-terminus and disulphide bond are important structural features necessary for the full biological function of IAPP [78].

Once fully mature, IAPP is stored in the dense core of β-cell secretory granules, surrounded by insulin [79]. Due to the nature of the close relationship between IAPP and insulin, they share many transcription and secretory regulators, including glucose, amino acids, and free fatty acids (FFA) [80-84]. Although IAPP is secreted in a ratio of approximately 1-5 parts of IAPP to 100 parts of insulin [59, 85, 86], under certain conditions the molar ratio can be altered. Studies on concurrent insulin and IAPP secretion have shown that increased expression of inflammatory cytokines, such as tumour necrosis factor-α (TNFα) and monocyte chemoattractant protein-1, can increase IAPP secretion while insulin secretion is unaffected or reduced in isolated islets and murine cell lines [87, 88]. In addition, pathological conditions such as elevated

glucocorticoid levels, obesity, and T2D can not only induce aberrant IAPP secretion relative to insulin secretion but can even upregulate the amount of pancreatic IAPP mRNA [89-96]. This selective increase in IAPP is believed to be due to Golgi-dependent mechanisms [97].

Unsurprisingly, insulin and IAPP also share similar mechanisms of clearance from the circulation. Insulin degrading enzyme (IDE) is a metalloprotease that is ubiquitously distributed in tissues of the human body, although abundantly expressed in the liver, skeletal muscle, and brain, where insulin and IAPP bind [98]. As its name suggests, IDE is predominantly responsible for insulin degradation, although studies examining IAPP clearance have found that IAPP is also a substrate of IDE, where insulin degradation by IDE was altered in the presence of IAPP (suggesting competitive binding) [99, 100]. Despite the similarities, there are still some differences in their mechanism of clearance between insulin and IAPP. Under healthy conditions, 50% of insulin is cleared from the circulation via hepatic IDE during its initial passage through the liver [101, 102]. After this, a further 25% of the circulating insulin is cleared by the kidney via renal proteases and filtration, with excess then degraded by IDE (and other nonspecific proteases) in insulin target tissues, including the brain, skeletal muscle, liver, and adipose tissue [101, 103, 104]. IDE appears to have a 4-fold higher affinity for insulin over IAPP [99], possibly explaining limited IAPP clearance via hepatic IDE, particularly under the hyperinsulinaemic conditions of pre-T2D insulin resistance [105, 106]. Hence, circulating IAPP is cleared primarily via renal peptidases in the kidney [105, 107, 108].

At an intracellular level, the mechanisms of IAPP degradation are still debated. In tissues that secrete or bind IAPP, cytosolic IDE still appears to play an important role in its clearance and degradation [109], although other mechanisms are also involved. One such mechanism includes the ubiquitin-proteasome system, which recognises and degrades superfluous and dysfunctional proteins from the cytoplasm and nucleus [110]. To briefly summarise this complex process, proteins are flagged for degradation by the covalent attachment of ubiquitin molecules to target proteins, and subsequently proteolysed by large enzymes known as the proteasome [111]. In addition to the ubiquitin-proteasome system, the autophagy-lysosomal

pathway is another important potential degradation mechanism for IAPP [109, 112]. During this process, proteins and other cytoplasmic components are engulfed by double-membrane bound vesicles called autophagosomes, which then fuse with lysosomes containing degradative enzymes [113].

The ubiquitin-proteosome system and autophagy-lysosomal pathway have typically been considered independent mechanisms, although evidence is emerging for a significant amount of cooperation between the two. For example, ubiquitin is a common regulatory molecule in both pathways, as autophagy can be mediated by ubiquitin. In addition, both pathways are also known to share substrates, including IAPP [114]. However, because IAPP is an amyloidogenic peptide, the effectiveness of IAPP clearance may be influenced by its aggregation state. Pancreatic islets (where amyloidogenic IAPP aggregates and accumulates) contain resident macrophages that assist in maintaining islet health and the removal of disease-causing agents [115]. However, when the amyloid burden becomes too great, circulating macrophages can be recruited to the islet to help remove the aggregated IAPP [116].

1.3.2 Amyloidogenicity of IAPP

As an amyloidogenic peptide, IAPP is prone to 'misfold' [117]. This is believed to be due to interactions between aromatic residues in their structure, particularly within the region of residues 20-29 (Figure 2) [117, 118]. In amyloidogenic peptides, aromatic residues are notable for their propensity to interact with each other primarily through highly hydrophobic reactions (in addition to the other hydrophobic residues), resulting in misfolding of IAPP [119, 120]. Further evidence for the importance of the 20-29 residue region in amyloidogenic misfolding and aggregation of IAPP lies in the comparison between human IAPP (hIAPP) and non-amyloidogenic rodent IAPP (rIAPP). A total of five of the six substitutions differentiating the structure of hIAPP and rIAPP reside within this region, with a notable absence of aromatic and hydrophobic residues in rIAPP, suspected of inhibiting its ability to aggregate [121]. Moreover, some mammalian species, including some felines, birds, and nonhuman primates, retain aromatic residues in this region (despite other

sequence differences of up to six substitutions) and similarly form amyloidogenic IAPP aggregates [73, 121-123].

Misfolded amyloidogenic monomers, such as IAPP, aggregate in 3 distinct phases, known as the nucleation phase, the elongation phase, and the saturation phase [124, 125]. During the nucleation phase, monomeric amyloidogenic peptides undergo a conformational change ('misfold') and begin to aggregate into oligomeric complexes, where they function as 'seeds' for the conformational change of surrounding amyloidogenic monomers [125, 126]. As more peptides are added, oligomers grow in size and complexity [124-126] (although all oligomers share a common backbone structure [127]). The nucleation phase is also called the 'lag phase', as it is a process that is comparatively slower than the next step, the elongation phase. During the elongation phase, the oligomeric complexes reach a critical mass (approximately 6 nm in size for IAPP specifically [128]), which triggers a rapid elongation process of the oligomeric complexes into protofibrils until they reach the saturation phase of mature insoluble fibrils with β-sheet structures [126]. The entire IAPP aggregation process from monomers to fibrils can occur in as little as 4 h [129, 130].

1.4 IAPP aggregates in Type 2 Diabetes

1.4.1 IAPP-mediated Cytotoxicity

An association between T2D and IAPP-derived amyloid plaque has been identified since the early 1990s, where increased plaque deposition was found in pancreatic islets of patients with severe T2D [121]. Aggregated IAPP is cytotoxic to β-cells in a dose-dependent manner with distinct apoptotic features observed, including membrane blebbing, DNA fragmentation, and increased active caspase-3 activity [133, 134, 138]. This cytotoxic effect has been observed in various models *in vitro*, including cultured human islets [134, 139, 140], cultured rodent islets [141, 142], and β-cell lines [20, 142-144]. Overexpression models of human IAPP have similarly shown that IAPP causes apoptosis of pancreatic β-cells in vitro [145, 146] and may induce spontaneous diabetes-like pathology in rodent models [147-149]. Interestingly, despite sharing the pancreatic islets with β-cells, α-cells (responsible for

glucagon secretion and important for glucose homeostasis), are less susceptible to cytotoxicity under the same culture conditions, although the reason for this is currently unknown [150]

Early research following the discovery of IAPP focused primarily on the amyloid plaque composed of insoluble IAPP fibrils, where it was believed to accumulate in the extracellular space of β-cells within the pancreatic islet, forming a mechanical barrier and altering cellular function significant enough to cause apoptosis [131]. However, the theory that plaque / fibrils were directly responsible for β-cell dysfunction and death appears to be a misconception. Early work mainly relied on transgenic animal models where the aggregate species of IAPP were unspecified [131], or synthetic IAPP preparations that were not given enough time for complete fibrillisation to occur [132-134]. In essence, the early research on IAPP were likely not exclusively using fibrils, but an unknown mixture of monomers, oligomeric complexes, and fibrils. More recent research, however, has demonstrated that the transient soluble oligomers formed in the nucleation / lag phase have a stronger correlation with β-cell cytotoxicity, with protofibrils and fibrils becoming progressively less toxic and more inert [20, 125, 128, 135-137]. Although more inert than the oligomers, fibrils are not completely harmless, as they can deplete proteostatic mechanisms, function as reservoirs for oligomer storage / release, and act as catalysts for misfolding and aggregation [18].

1.4.2 Ionic Dysregulation and Oxidative Stress

There are several proposed mechanisms by which amyloidogenic IAPP oligomers exert their toxicity. Primary among them is the theory of ionic dysregulation, where IAPP permeabilises cell membranes by forming inappropriate pores and channels [132, 138, 139]. This is believed to occur due to the microstructures formed by the aggregating oligomers. Essentially, monomeric IAPP forms an α-helical conformation at the N-terminus supported by the disulphide bond between Cys2 and Cys7, but as misfolding and aggregation occurs, this converts to β-sheet structures, creating oligomers with varying conformations during the transition [138-142]. Although both α-helical and β-sheet rich structures are capable of forming pores in membranes, β-sheet rich structures appear to form larger and more disruptive pores [138,

139, 143]. Other studies have also suggested a possible detergent-like effect of membrane disruption by developing fibrils on the cell surface [144].

The disruption of the semipermeable membrane creates unregulated ionic movement into and out of the cell, leading to dysregulated intracellular ion concentrations and disruption of important cellular processes, including mitochondrial function [132, 145]. When mitochondrial dysfunction occurs, this can result in an accumulation of cytoplasmic ROS [146]. When intracellular ROS levels increase, the nuclear factor erythroid 2-related factor 2 (NRF2) transcription factor is activated, resulting in increased expression of cytoprotective antioxidant enzymes such as superoxide dismutase (SOD) and catalase (CAT) [147]. SOD catalyses the conversion of superoxide radicals (O_2^-) into oxygen (O_2) and (still cytotoxic) hydrogen peroxide (H_2O_2), whereupon CAT will further neutralise H_2O_2 into H_2O and O_2 [148]. Furthermore, NRF2 also upregulates the expression of glutathione and its associated enzymes, glutathione peroxidase (GPx) and glutathione reductase (GR), which form the glutathione redox system [147-149]. GPx oxidises glutathione and, in the process, reduces H_2O_2 to H_2O. GR then catalyses the reduction of oxidised glutathione back to its original form, allowing the process to begin again [148]. Although efficient, if overwhelmed, ROS accumulation of ROS can lead to additional mitochondrial dysfunction and oxidative stress, as well as activation of inflammatory signalling and intrinsic apoptotic pathways [13, 150-152].

Evidence confirms that IAPP is indeed capable of inducing ionic dysregulation, mitochondrial dysfunction, and oxidative stress in β-cells, where it alters oxygen consumption, ATP production, and mitochondrial membrane potential [150, 153-155]. This effect could be amplified by two significant factors that make β-cells prone to an increased risk of oxidative stress; a high endogenous ROS production rate and lower expressions of antioxidant enzymes (including SOD, CAT, and GPx) compared to other cell types, such as liver cells [149, 156]. Additionally, IAPP could potentially begin to aggregate intracellularly into oligomers prior to secretion, where it may damage mitochondrial membranes in a similar manner to the external membrane, exacerbating oxidative stress and mitochondrial-mediated stress signals [157].

1.4.3 Perturbation of Insulin Secretion

The IAPP-induced dysregulation of intracellular ion concentrations can also affect important β-cell functions, such as insulin secretion. In particular, Ca^{2+} homeostasis is vital for healthy functioning of β-cells, where it is both an important trigger for insulin exocytosis, as previously described (1.2; Figure 1A, page 11), and a crucial component of mitochondrial machinery [158-160]. In addition, disruptions to β-cell Ca^{2+} metabolism could negatively affect delicate intracellular signalling mechanisms, such as those involving calmodulin or Protein Kinase C (PKC), both signalling molecules which have a multiplicity of functions, including regulation of secretory mechanisms [161-168]. Therefore, ionic dysregulation of Ca^{2+} can affect insulin secretion specifically in several ways: directly by impairing Ca^{2+} influx and mitochondrial depolarisation, and indirectly by reducing the ATP : ADP ratio to trigger the influx of Ca^{2+} [169-171]. In essence, ionic dysregulation and the resulting oxidative stress should theoretically cause significant impairment of GSIS. However, when this theory has been tested, the impact of IAPP on GSIS has been disputed.

Although some studies have shown dose-dependent decreases in GSIS after exposure to IAPP in rodent islets *ex vivo* [172-174] and *in vitro* [150], others have not observed significant changes [175, 176]. This discrepancy is attributed to the concentration of IAPP since dosages < 5 μM appear to have no significant effect on GSIS. Although concentrations of ≥ 5 μM are supraphysiological for circulating plasma levels of IAPP (typically 2-20 pM depending on prandial state and diabetic condition [177, 178]), estimates of IAPP concentration in secretory granules have been up to 4 mM [179] and up to 400 μM in the local islet environment immediately after secretion [180]. Furthermore, knowing that insulin secretion is typically increased during the initial development of T2D to overcome peripheral resistance, it is possible that local islet IAPP concentrations are higher in the islets of prediabetic and diabetic patients. Thus, intracellular aggregation of IAPP or accumulation of IAPP on the external cellular membrane can reach sufficient concentrations to impact GSIS *in vivo*.

1.4.4 Inflammation and Alteration of Proteostasis

Although ionic dysregulation and oxidative stress contribute significantly (if not predominantly) to islet dysfunction in the presence of IAPP, additional mechanisms of toxicity have also been identified. In particular, inflammation can play a significant role in T2D, contributing to the burden of the disease [10, 181]. Dysfunctions in ionic dysregulation, particularly intracellular Ca^{2+}, could inhibit β-cell signalling machinery and further contribute to cellular inflammation. For example, Calmodulin and PKC, multifunctional signalling molecules mentioned above (1.4.3, page 20), also have roles in the regulation of energy metabolism, inflammation, and apoptosis, which could be negatively impacted by IAPP-induced ionic dysregulation [161-163, 167, 182, 183]. In addition, PKC signalling has been noted to be involved in the upregulation of IAPP expression in murine pancreatic islets through pro-inflammatory and fatty acid-induced mechanisms [81, 87], further compounding the toxic effect.

In addition to these mechanisms, oxidative stress and ROS generation are known causes of inflammation in pancreatic β-cells [184-186]. As β-cells are damaged or distressed, they release endogenous danger signals known as danger-associated molecule patterns (DAMPs). DAMPs are recognised by macrophages, which secrete pro-inflammatory cytokines in response [187-189]. These cytokines then bind to receptors on the cell surface to signal pro-inflammatory pathways, including binding to death receptors to initiate the extrinsic pathway of apoptosis, if necessary [190]. Macrophage infiltration of pancreatic islets is a feature of T2D, where macrophages are recruited from the circulation to assist the resident islet macrophages [116, 191-193]. Although acute inflammation is a well-established defence mechanism against pathogens or injury, chronic inflammation can be detrimental [194].

β-cell exposure to inflammatory cytokines can simultaneously inhibit GSIS and increase IAPP expression [87, 95, 96, 195]. Studies have also shown that macrophage exposure to IAPP results in increased secretion of pro-inflammatory cytokines, particularly Interleukin-1β (IL-1β) and TNFα [196-200], creating a feedback loop of sustained of inflammation. Different aggregate species of IAPP also appear to elicit different responses from macrophages via distinct pathways, where early IAPP aggregates lead to increased

expression of IL-1β's precursor, proIL-1β, compared to later more complex aggregates, which lead to increased secretion of mature IL-1β [199]. Interestingly, IAPP can act as a pro-inflammatory agent itself, as evidence has suggested that it can activate Fas-associated membrane death receptors in isolated human and murine islets, as well as β-cell lines [201, 202].

In addition to inflammation, β-cells are equipped with other stress management mechanisms. Two of these internal mechanisms, the ubiquitin-proteasome and autophagy-lysosomal-systems, have previously been discussed for their role in the clearance of monomeric IAPP (1.3.1, page 13). However, their function may be impaired by toxic IAPP aggregates, as evidence shows a reduced effectiveness of these systems in the presence of IAPP aggregation [109, 110, 203-205], leading to detrimental ER stress [206]. Other mechanisms of proteotoxic stress management in β-cells includes recruitment of molecular chaperones known as heat shock proteins (HSPs).

HSPs are ubiquitous in almost all known organisms and are essential in healthy cellular function, where they assist in protein formation, stabilisation, monitoring, and transport [207]. Additionally, HSPs can assist the autophagy-lysosomal pathway through chaperone-mediated autophagy and cooperate with the ubiquitin-proteasome system in the treatment of proteotoxic stress [208, 209]. In the event of a cellular stressor, the expression of HSPs can be greatly enhanced to restore / refold damaged proteins and flag those damaged beyond repair for degradation, called the 'heat shock response' [210]. Although named for its discovery during thermal shock experiments, other stressors (including injury, oxidative stress, proteotoxicity, inflammation, and heavy metal poisoning) can elicit the same response [211-215]. Studies have shown that HSPs can help prevent and remove IAPP aggregation [216, 217]. However, the role of HSPs in the development of T2D is complex and multilayered.

In older obese individuals (a population highly susceptible to T2D), HSP expression and function is reduced [218, 219]. Dysfunctional insulin signalling and inflammation, both significant features of T2D, are also correlated with reductions in HSP expression [220, 221]. This combination of factors means

that cells from patients with T2D likely have limited ability to respond to stressors. Furthermore, studies show that HSPs can prevent aggregation and progression to fibril formation, but in doing so, can maintain peptides in toxic chaperone-oligomer complexes, also creating a more stressful environment [222].

Often, the same HSP can function differently under different conditions. For example, binding immunoglobulin protein (BiP), a constitutively expressed HSP in the ER known as the “master regulator” of many ER functions, can also have a stress-induced increase in expression in response to an abundance of unfolded / misfolded proteins [223, 224]. *In vitro* studies have identified BiP as an HSP capable of binding IAPP and preventing its aggregation [225], with elevated expression of BiP found in β-cells of transgenic mice expressing human IAPP [226]. However, under pronounced ER stress, BiP translocates to the cell surface and acts as a pro-apoptotic receptor for inflammatory cytokines [227-229], and can even be secreted from β-cells to function as a DAMP [227]. In this role, it can promote hyperglycaemia and peripheral insulin resistance [230] Furthermore, BiP, which is also known as Glucose-Regulated Protein 78 (GRP78) due to its upregulation during times of glucose starvation, could theoretically have increased expression in peripheral tissues of T2D patients as insulin resistance could lead to a hypoglycaemic intracellular environment [231]. Other key HSPs noted to play complex roles in the β-cell response of cells to amyloid toxicity, include HSP72 [216, 217, 232], HSP90 [233, 234], and HSP60 [235, 236]. For more detailed information on the role of these HSPs (and others) in the context of T2D, refer to my published review in Appendix A (8.1, page 234) [214].

In summary, the accumulation of aggregated IAPP in pancreatic islets results in ionic dysregulation, oxidative stress, insulin dysfunction, and inflammation of β-cells, as well as activation of clearance mechanisms including the β-cell’s heat shock response, ubiquitin-proteasome system, and autophagy-lysosomal pathway. As IAPP can also induce dysfunction of clearance mechanisms, the β-cell can quickly become overwhelmed by ER stress, ROS, and mitochondrial dysfunction [13, 151]. Contributing to this dysfunction, the inflammatory environment of T2D can reduce the capacity of the β-cell to respond to

stressors and exacerbate insulin dysfunction and cell stress [151, 202, 237]. As a result, the β-cell is unable to recover, and apoptotic signalling pathways are activated (Figure 3).

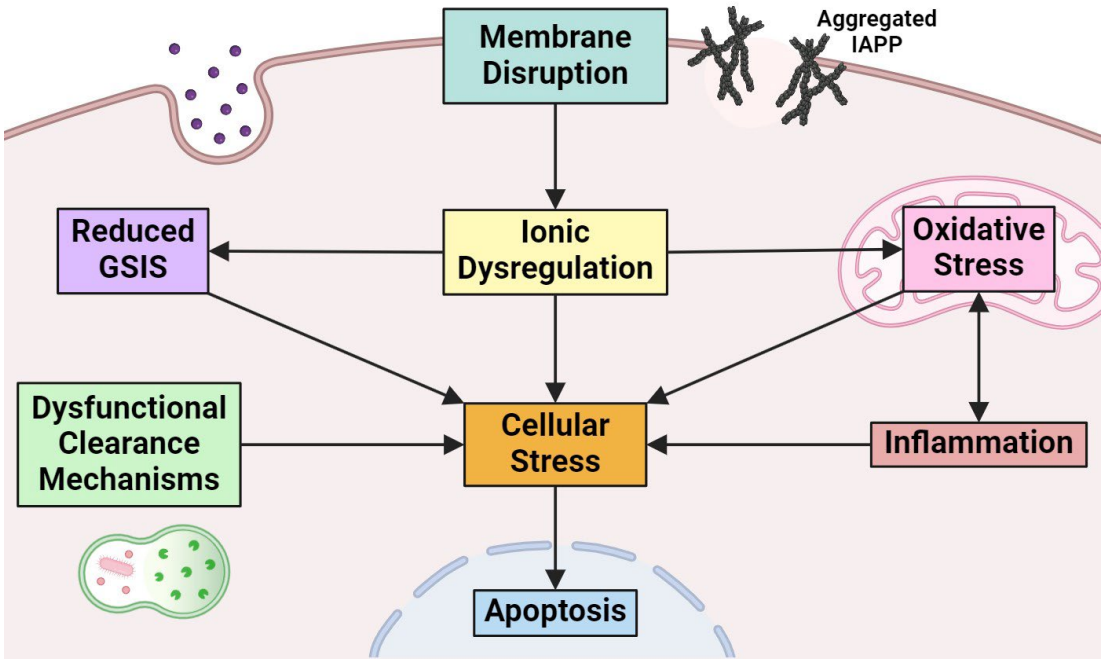

Figure 3. Aggregated IAPP interacts with β-cell membranes to reduce β-cell function and viability. Islet Amyloid Polypeptide (IAPP) forms pores in pancreatic β-cell membranes, affecting ionic homeostasis. Ionic dysregulation results in oxidative stress, reduced glucose-stimulated insulin secretion (GSIS), and up-regulation of pro-inflammatory signalling. In addition, IAPP aggregates cause downregulation in clearance mechanisms. Once the stress management mechanisms of the β-cell have been overwhelmed, the cell will initiate apoptotic signalling.

1.4.5 IAPP in Peripheral Insulin Sensitivity

As reviewed above (1.2.2, page 10), T2D is not singly characterised by pancreatic islet dysfunction. In fact, peripheral insulin resistance, in tissues such as skeletal muscle, adipose, and the liver, generally occurs early in disease progression and is a strong contributor to the development of pancreatic β-cell stress. Aside from the pancreas, IAPP can aggregate in many different vital tissues including the brain, liver, skeletal muscle, and heart [238-240]. Considering its co-secretion with insulin, early works on IAPP focused heavily on its role in insulin signalling. In these studies, IAPP was found to downregulate glucose uptake, glycogen synthesis, and insulin signalling in animal models *in vivo* and *ex vivo* [23, 241, 242]. In addition, insulin resistant

individuals were noted to have an exaggerated IAPP to insulin ratio in the presence of hyperglycaemia [243].

Unfortunately, the majority of these early studies are not necessarily reliable indications of the true effect of IAPP on peripheral insulin signalling. Firstly, many used supraphysiological levels of IAPP, and when animal models have been infused with physiological levels expected in the blood, there have been no known effects on insulin signalling [94, 244]. Secondly, follow-up studies have noted that IAPP has a reduced clearance rate compared to insulin, making the measurement of IAPP to insulin ratios in hyperglycaemic environments possibly misleading [94]. Finally, and very importantly, much early research on IAPP did not yet fully understand IAPP binding / aggregation kinetics, and therefore it cannot be guaranteed which species was used (monomers, oligomers, or fibrils).

Very few studies have been conducted since the original exploration into IAPP in peripheral tissues. Later studies have shown that monomeric IAPP is capable of beneficial effects in human adipose tissue and primary adipocytes via activation of multiple signalling pathways, including phosphorylation of STAT3, Akt and ERK, pathways shared in insulin signalling [245]. Furthermore, monomeric IAPP and IAPP analogues like Pramlintide can improve leptin signalling and weight loss in obese animal models [246]. In a recent study involving a transgenic animal model expressing amyloidogenic human IAPP, no significant difference in hepatic insulin resistance was noted between transgenic animals and nontransgenic littermates [247]. Due to the lack of clarity on the subject, it is abundantly clear that investigation into the role of IAPP in peripheral insulin resistance should be revisited.

1.4.6 Cross-seeding and Co-aggregation with other Proteins

IAPP is not unique in its ability to misfold and aggregate into insoluble fibrils. Approximately 40 different proteins have been identified as amyloidogenic *in vivo*, and amyloidogenic peptides have been associated with up to 50 different diseases in humans [17, 248]. Despite dissimilar sequences and structures, all amyloidogenic peptides form comparable microstructures of rigid, non-branching, straight fibrils with a β-sheet secondary structure once fully

aggregated [19]. As described above (1.3.2, page 16), amyloid proteins aggregate with an initial nucleation phase [249]. The nucleation phase occurs slowly, as proteins gradually misfold and begin to aggregate until a sufficient size is reached for the elongation phase to begin. However, the nucleation stage can be accelerated by preformed amyloid aggregate seeds[249, 250].

Amyloid seeds can trigger confirmational changes in stable monomeric and properly folded proteins through prion-like activity. Therefore, a misfolded IAPP monomer can initiate misfolding and aggregation in surrounding IAPP monomers, which themselves can become seeds for further aggregation. When this occurs in monomers of the same protein, it is called 'homologous seeding' [250]. However, many amyloidogenic peptides are also capable of 'heterologous seeding' or 'cross-seeding', where a misfolded amyloid protein catalyses the aggregation of a different protein.

Cross-seeding among amyloid proteins appears to be more complex than homologous seeding, as not all pairs of amyloid proteins can promote aggregation amongst each other [249]. IAPP has been noted for its ability to mutually cross-seed many amyloid proteins, including the Prion protein (PrP) [251, 252], Parkinson's disease-associated α-synuclein [253-255], and AD-associated proteins, Tau [256] and Aβ [257, 258]. Studies show cross-seeding by IAPP can potentially increase the rate of aggregation of other peptides [259]. Furthermore, research is also beginning to suggest that IAPP may also co-aggregate with many of these proteins, as experiments investigating IAPP's cross-seeding action have discovered fibrils composed of both peptides [259].

Although related, the terms "cross-seeding" and "co-aggregation" have distinct meanings. Co-aggregation refers to the ability for one species of protein to aggregate with a different protein into shared heterocomplexes [18, 249]. This can occur between an amyloidogenic protein and a non-amyloidogenic protein, such as human IAPP with insulin [260], Tau protein [256], and rat IAPP [261, 262]. However, co-aggregation of two amyloidogenic peptides can potentially exacerbate disease burdens. IAPP can co-aggregate with many of the same proteins it cross-seeds with, including α-synuclein [253-255], PrP [251, 252], and Aβ [24, 25], contributing to the pathology of their associated diseases.

The co-aggregation potential of IAPP with both Tau and Aβ, two amyloidogenic proteins that are heavily implicated in the pathology of AD, is particularly notable. Current research indicates that IAPP not only cross-seeds and co-aggregates with Aβ and Tau in neuronal cells [24, 256], but potentially in other areas of the body, such as within pancreatic islets [25, 251, 263]. Furthermore, recent studies also strongly indicate that co-aggregated heterocomplexes of IAPP-Aβ have exacerbated cytotoxicity compared to either peptides alone [129, 155, 247], which could hasten the disease process in both AD and T2D.

1.5 β-Amyloid

1.5.1 Synthesis, Secretion, and Clearance

In the brain, the Aβ peptide is mainly synthesised and secreted by neuronal and neuroglial cells (Figure 4) [264]. Although the function of Aβ is highly complex and not well understood, studies have shown that monomeric Aβ is neuroprotective, with noted antioxidant and antimicrobial properties [265-267]. Aβ can also aid in intracellular cholesterol transport [268], and can function as a transcription factor [269]. Like IAPP, Aβ can also aggregate into cytotoxic oligomers and insoluble fibrils in vital tissues. Accumulated Aβ aggregates are the primary component of amyloid plaque in the brains of AD patients [270, 271].

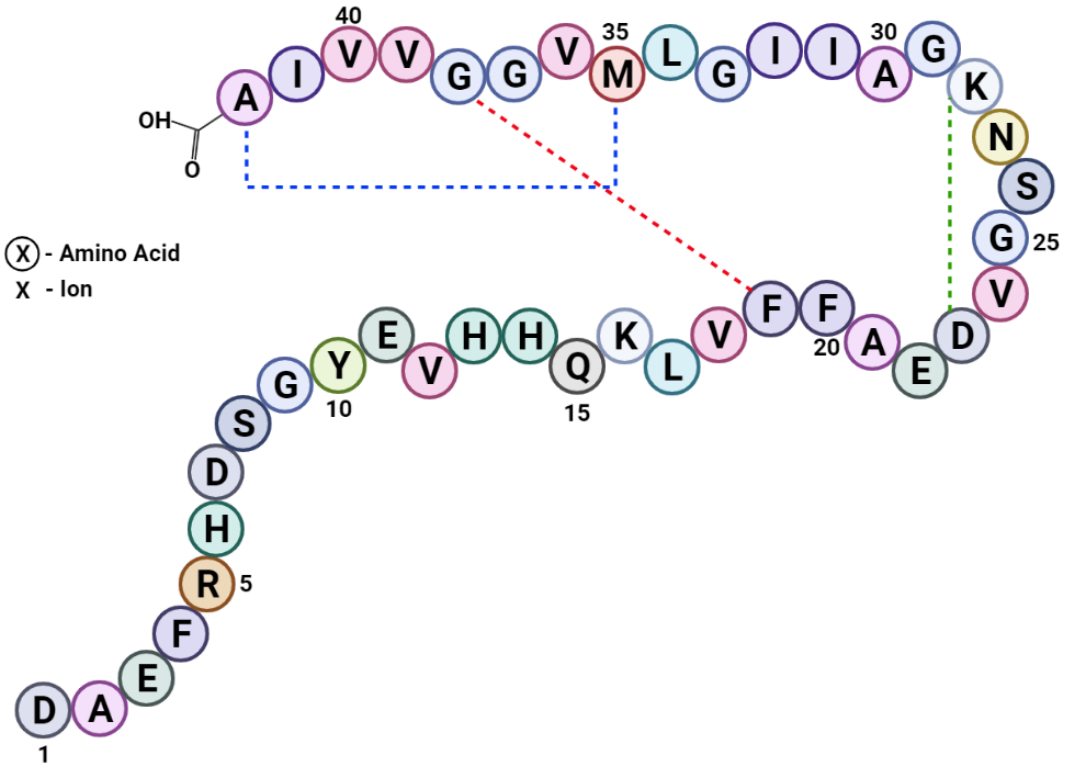

Figure 4. Monomeric structure of human Aβ42. Aβ is a neuropeptide composed of 38-43 amino acids, with Aβ40 and Aβ42 being the most common. Aβ42, shown here, is thought to be the more toxic and amyloidogenic species of Aβ. Molecular interactions occur between resides 19 and 38 (blue dashed line), and 35 and 42 (red dashed line). The turn conformation is stabilised by a salt bridge between 23 and 28 (green dashed line), as well as hydrophobic interactions of surrounding residues. Figure adapted from Scheidt et al. [272].

Aβ is derived from a larger integral membrane protein of up to 770 amino acids, aptly named Aβ Precursor Protein (APP), with APP695 being the most common isoform expressed in the human brain [273]. APP is initially synthesised in the ER before transportation via the Golgi apparatus and trans-Golgi network to the cell membrane [274]. APP has several biological functions of its own, with known roles in neurite outgrowth, synaptogenesis, transcription regulation, axonal transport, and receptor-mediated cell signalling [275]. In tissues, the highest expression of APP is found in nervous tissue, particularly the brain, although APP expression is also observed in endocrine tissues and the digestive system, including accessory digestive organs such as the liver and pancreas [264, 276]. APP is also highly expressed in platelet cells, which

are believed to be a major source of circulating APP in the periphery [277, 278].

To form mature Aβ, APP undergoes significant post-translational modifications, including proteolytic processing, glycosylation, and phosphorylation [279]. During proteolytic processing, APP can be competitively cleaved within the N-Terminus by either α-secretase or β-secretase before successive processing by γ-secretase within its C-Terminus [280, 281]. If APP is initially cleaved by α-secretase, Aβ is not generated and as such, this process is referred to as the 'non-amyloidogenic' processing pathway. For amyloidogenic Aβ to be formed, APP must undergo the initial cleavage of N-Terminus by β-secretase prior to γ-secretase processing [280, 281]. The regulation of these pathways and factors that determine initial enzyme cleavage remained to be fully understood. Factors such as substrate binding and lipid membrane composition, as well as protein, inflammatory, and / or hormonal modulators all have potential roles in determining the initial cleavage enzyme [282-287].

The γ-secretase cleavage of APP can generate Aβ peptides of varying lengths, those identified include between 38 and 43 amino acids long. The most abundant Aβ peptides in the CNS and periphery are the Aβ40 and Aβ42 amino acid forms. The Aβ42 is a highly amyloidogenic isoform and the primary form found in cerebral plaque deposits [288]. Aβ40 is the most abundantly expressed isoform in the brain under normal physiological conditions and, compared to Aβ42, aggregates more slowly and is less neurotoxic [289]. In the development of AD, the ratio of Aβ42 to Aβ40 appears to be crucial, as Aβ40 has been reported to slow the rapid aggregation of Aβ42 [290, 291]. As such, any increase in the ratio of Aβ42 to Aβ40 is likely to result in a more rapid formation of cytotoxic oligomers and insoluble fibrillar plaques which hamper impacting on the intracellular clearance mechanisms [288, 289].

The clearance of Aβ is remarkably similar to IAPP. The clearance mechanisms include enzymatic (e.g. IDE, neprilysin), and cellular degradation pathways including the ubiquitin-proteasome system, and the autophagy-lysosomal pathway [292]. Furthermore, in the central nervous system, microglia (the

resident brain macrophages) clear Aβ aggregates by phagocytosis, similar to IAPP by macrophages in the pancreatic islet [292, 293]. In the periphery, the liver and kidneys clear the bulk of Aβ from the circulation in as little as 15 min [294, 295]. However, there are still some minor differences. The majority of Aβ production occurs in the brain, so systemic clearance of Aβ first requires transport across the blood-brain barrier (BBB) from the cerebrospinal fluid (CSF) to the blood plasma. This process is mediated by low-density lipoprotein receptor-related protein 1 (LRP-1), a multiligand receptor commonly involved in endocytosis [296, 297]. Any decrease in the expression or effectiveness of LRP-1 in the BBB can result in Aβ accumulation within the brain [296]. In a vicious cycle, the function of LRP-1 itself is impeded by excessive accumulation of amyloidogenic Aβ, particularly Aβ42, but also by ageing and certain genetic AD variants [296].

Another important mediator of Aβ efflux from the brain is apolipoprotein E (ApoE), a cholesterol transporter and distributer [297]. Currently, the multifaceted role of ApoE in AD is well documented but not yet fully understood. Although early research suggested direct ApoE-Aβ binding interactions, more recent studies have shown that ApoE lipoproteins may compete with Aβ for the same clearance pathways through LRP-1 in an isoform-dependent manner [297, 298]. Specifically, the ApoE4 isoform inhibits Aβ clearance from the brain and periphery and promotes the accumulation of neuronal Aβ [296, 297, 299-301]. In addition, a related protein, ApoJ (the most expressed apolipoprotein in the brain), has important roles in cellular debris removal and apoptosis as a molecular chaperone related to HSPs [302, 303]. Studies have shown that ApoJ is present in amyloid plaque deposits in the brain and that its expression level is increased in patients with AD, likely as part of a protective response [296]. ApoJ binds to Aβ, preventing neurotoxicity and fibril formation, and promotes transport of Aβ across the BBB via LRP-2 receptors (a ‘relative’ of LRP-1 in the same superfamily of receptors, also known to decrease with age) [304].

1.5.2 Amyloidogenicity of Aβ

Despite very little structural similarity between Aβ and IAPP, Aβ is similarly amyloidogenic and capable of misfolding and aggregating into insoluble fibrils with a β-sheet secondary structure [305]. Aβ also undergoes similar stages of nucleation, elongation, and saturation to IAPP. However, this process takes considerably longer for Aβ than for IAPP, often taking more than 72 h to reach the saturation stage *in vitro* [129, 130]. Interestingly, some studies have shown Aβ aggregates can form different oligomeric species, some species eventually forming fibrils, while others remain as large nonfibrillar oligomers [306].

In contrast to IAPP, Aβ lacks aromatic residues in its structure. However, Aβ does have hydrophobic residues that make up a C-terminal hydrophobic region. Interactions between these residues are believed to be significant enough to initiate the aggregation of monomeric Aβ, particularly in the Aβ42 [307-309]. The specific residues that are responsible for misfolding / aggregation are still highly debated and poorly understood, although early work indicated residues 17-20 and 30-35 were critical for aggregation [310]. However, much of this work examined fragments of Aβ, which may have missed interactions between residues at opposite ends of the structure. For example, the increased aggregation of Aβ42 compared to Aβ40 is suspected to be related to interactions between Ala42 and Arg5 [311]. More recently, 3 histidine residues have been repeatedly implicated in Aβ aggregation: His6, His13, and His14 [312, 313], with His14 critical for neurotoxicity [314]. To support this evidence, one of three substitutions distinguishing human β-amyloid from non-amyloidogenic rat amyloid is a replacement of His13 with arginine [315].

1.6 Aβ aggregates in Alzheimer's Disease

1.6.1 The Alzheimer's Brain

Alzheimer's disease (AD) is the most common form of dementia, a spectrum of progressive neurodegenerative disorder characterised by a gradual decline in cognition, memory loss, and executive functioning; reduced activities of daily living and eventual death [5, 316]. In 2022, the Australian Burden of Disease

study conducted by the Australian Institute of Health and Welfare determined that AD and other dementias are the second leading cause of disease burden in Australia. This disease burden has increased between 2011 and 2022, rising from the fourth leading cause [317]. Due to the growth and ageing of the Australian population, the incidence of AD is expected to more than double by 2058. Although age is the main risk factor for dementias, obesity, physical inactivity, chronic stress, hypertension, and hyperglycaemia are also important risk factors often shared with T2D [5, 316, 317].

Accounting for approximately 60-70% of total dementia cases, AD is a neurodegenerative disease characterised by brain atrophy, particularly in the hippocampus and cerebral cortex. [318]. Upon postmortem investigation, brain samples from AD patients have neurofibrillary tangles composed of hyperphosphorylated Tau protein [319-321] and accumulation of extracellular amyloid plaque, similar to that seen in the pancreatic islets of patients with T2D. In the 1980s, brain plaque deposits were purified by liquid chromatography and were found to be composed primarily Aβ peptides [271]. Since then, further research indicates AD brains exhibit higher levels of the more aggregation prone Aβ42 compared to controls [322].

1.6.2 Aβ-mediated Cytotoxicity

Numerous studies have demonstrated the cytotoxic effects of Aβ on neuronal cells, both *in vivo* and *in vitro* [14, 22, 129, 323, 324]. In parallel to the findings of IAPP, the extracellular plaque composed of insoluble fibrils appears to be less toxic in comparison to the soluble oligomeric species of Aβ. Although neuritic plaques can contribute to an inflammatory environment within the brain, no clear association has been identified between plaque deposits and cognitive decline [318]. Healthy individuals have been found to have amyloid deposits, while some AD patients have minimal plaque deposition [324, 325]. Amyloid plaques are regarded as an important hallmark of progression to Alzheimer's disease, as it accumulates up to 2-3 decades prior to the onset of dementia symptoms [326]. The early loss of synapses is thought to be as a result of accumulation of soluble Aβ aggregates rather than insoluble fibrils [135, 136, 325]. Subsequent microglia and astrocyte activation and

accumulation of hyperphosphorylated Tau, drive the process of neurodegeneration and neuronal loss.

Soluble Aβ aggregates induce apoptosis and expression of cellular stress markers in a variety of *ex vivo* and *in vitro* models, including neuronal cell lines, and primary rodent neurons and neuroglia [14, 129, 327-329]. Similarly, rodent models that express human Aβ exhibit advanced plaque deposition, neurodegeneration, and cognitive decline in an age-related manner [247, 330, 331]. Many pathways of toxicity have been identified, most of which are shared with IAPP, including ionic dysregulation, inflammation, mitochondrial dysfunction, and induction of oxidative stress.

1.6.3 Ionic Dysregulation and Oxidative Stress

Aβ can act directly on neuronal cell membranes, promoting ionic dysregulation and oxidative stress [306, 332, 333]. Similar to IAPP, Aβ aggregates are capable of direct insertion into the cell membrane to form aberrant channels, increasing cell membrane permeability [333]. Additionally, Aβ aggregates can interact with and disrupt regular functions of intramembranous lipids to exert further cytotoxicity [332, 334]. For example, Aβ can bind strongly to gangliosides on the surface of neurons and inhibit their function, affecting long-term potentiation, a process involving persistent strengthening of neuronal synapses to promote synaptic plasticity and improve memory and learning [335]. Moreover, Aβ aggregates accelerate membrane lipid peroxidation through ROS production, resulting in decreased membrane fluidity and integrity. This effect is amplified by aggregates of higher molecular weight compared to lower molecular weight [336].

Aβ aggregates can also affect ionic movement by interacting with cell surface receptors. Neuronal glutamate receptors for n-methyl-d-aspartate (NMDA) and α-amino-3-hydroxy-5-methyl-4-isoxazolepropionic acid (AMPA) play critical roles in synaptic plasticity [14]. Aβ can bind to these glutamate receptors and alter ion channel activity, causing ionic dysregulation [337-339]. In addition, Aβ aggregates also act as a ligand for the Receptor for Advanced Glycation End products (RAGE). RAGEs are involved in clearance of AGEs and mediate Aβ influx into the brain. RAGE expression is increased in AD brains, which could

mean increased Aβ influx [338]. Increased influx of Aβ by RAGE combined with reduced efflux from the brain through LRP-1, increases Aβ concentration in brain to promote aggregation. Additionally, Aβ-RAGE interactions can induce and enhance oxidative stress and apoptosis [338]. Furthermore, Aβ binds with high affinity to α7-Nicotinic Acetylcholine Receptor (α7nAChR), where it raises intracellular Ca^{2+} levels [340].

Ionic dysregulation, particularly increased intracellular Ca^{2+}, is a known cause of mitochondrial dysfunction in neurons [341]. As described above (1.4.2; page 18) disruption of mitochondrial Ca^{2+} homeostasis can be detrimental, resulting in increased ROS production, reduced ATP generation, and apoptosis through intrinsic mechanisms [155, 306]. In addition, Aβ aggregates have a high affinity for haem iron molecules, likely due to histidine residues in their structure [342]. The formation of Aβ-haem complexes reduces the pool of haem in the cell, which is vital to maintain complex IV of the electron transport chain [342-344]. Aβ-haem complex formation decreases expression and activity of complex IV in human neuroblastoma cells *in vitro*, upregulating oxidant production. Additionally, the Aβ-haem complex can function as a peroxidase, further contributing to oxidative stress [342]. Neuronal cells are highly susceptible to oxidative stress due to a high lipid content, a high energetic requirement, and lower antioxidant defence mechanisms [10].

1.6.4 Inflammation and Alteration of Proteostasis

Aβ-induced oxidative stress can be both a cause and consequence of neuroinflammation. Important contributors are microglial cells, the resident macrophage cells of the central nervous system, which play a critical albeit complex role in AD pathogenesis. On the one hand, microglia have important functions in the innate immune response and clearance of Aβ aggregates from the brain. Pattern recognition receptors known as scavenger receptors (SRs) on the surface of microglia can detect and bind with Aβ, activating the microglia to clear Aβ aggregates [345]. On the other hand, once activated, microglia can contribute to AD pathology by up-regulation of pro-inflammatory signalling [194, 346, 347]. The inflammatory mediators IL-2, IL-6, IL-1β, and TNF-α are increased in AD post-mortem brain samples, CSF, and blood plasma subjects similarly to T2D [347, 348]. Aβ can even function as a DAMP to directly

stimulate pro-inflammatory signalling of microglia in a manner similar to IAPP-in macrophages [349].

Disruption of microglial function is associated with AD pathogenesis. In a transgenic AD mouse model, the microglia of older mice had reduced Aβ uptake, a two to five times decrease in the SRs expression and a two to three times increase in pro-inflammatory cytokines. Paradoxically, this appears to be due to the pro-inflammatory microenvironment, as IL-1β and TNF-α also decreased Aβ uptake through a reduction in SR expression of SRs in cultured N9 murine microglia in the same study [350]. Furthermore, in addition to reducing Aβ clearance, pro-inflammatory mediators can enhance amyloidogenic Aβ production and promote its aggregation and deposition [283, 346, 351, 352]. In essence, a vicious cycle of inflammation forms as Aβ accumulation, activated microglia, and pro-inflammatory cytokines simultaneously augment neuroinflammation and Aβ aggregation.

As in pancreatic β-cells, neuronal cells initially respond to Aβ accumulation by upregulating intracellular clearance mechanisms such as the ubiquitin-proteosome and autophagy-lysosomal systems. While these mechanisms can compensate for each other to some extent if problems arise in either [114, 353], the efficiency of both mechanisms is simultaneously reduced in response to aging and oxidative stress, both common features of AD brains [114, 354, 355]. Further exacerbating the pathology, impairment in autophagy can increase γ-secretase activity and expression of Presenilin 1 (PS1), a core protein component of the γ-secretase known to regulate APP processing [356]. This alteration can significantly accelerate Aβ production, as observed in HEK293 cells *in vitro* [357]. When autophagy and ubiquitin-mediated mechanisms are diminished, HSPs are upregulated to maintain cellular homeostasis [358, 359]. These proteins are thought to have a protective role against Aβ in neuronal cells. In particular, HSP90 and HSP70 (with their co-chaperone HSP40) have important cytoprotective roles, including inhibition of Aβ aggregation, remodelling of Aβ oligomers, and up-regulation of Aβ clearance [214, 360, 361]. Other HSPs have less clear roles, such as HSP60, a mitochondrial chaperone [362]. Although HSP60 overexpression is protective of Aβ-induced mitochondrial dysfunction [363], HSP60 has also

been implicated in the localisation of APP and Aβ directly in mitochondria in C17.2 murine neuronal stem cells [236].

While the heat shock response is characterised as a universal cell stress response, studies of cultured primary rodent neurons and Y79 human neuroblastoma cells reveal a potential tissue-specific response. In neurons, particularly in the hippocampus, a dampened heat shock response has been detected compared to neuroglia and other cells, even within the same animals [364-366]. Furthermore, human and other animal neurons also have a higher threshold for activation of the heat shock response than neuroglia [366]. This effect appears to be caused by disruptions in the signalling of the transcription factor Heat Shock Factor 1 (HSF1) in neurons, such as its reduced expression, function, or activity [366-369]. While there is some ability of supporting glial cells to transfer their HSPs to neurons to supplement their protection [370-372], the lack of a robust heat shock response may confer an innate vulnerability to neurons during times of cellular stress. An extensive discussion of the role of HSPs in AD and T2D is available in our published review [214] (Appendix A; 8.1, page 234).

Overall and when put in the larger context of oxidative stress, pro-inflammatory signalling, and impaired clearance mechanisms, Aβ accumulation is detrimental to neuronal cells and remarkably analogous to the effect of IAPP on pancreatic β-cells (Figure 3).

1.6.5 Tau Pathophysiology

Another major AD hallmark, the accumulation of hyperphosphorylated Tau protein to form neurofibrillary tangles, together with Aβ, plays an important role in driving the loss of neurons [373, 374]. The Tau protein is a microtubule-associated protein important for maintaining the structure and stability of microtubules in neuronal axons [375, 376]. Tau is also involved in microtubule-mediated axonal transport and intracellular signal transduction [376-378]. Phosphorylation of Tau proteins at specific sites modulates its activity, but dysregulation of this mechanism can result in hyperphosphorylation of Tau [270, 379]. This abnormal hyperphosphorylation can cause Tau to bind to other Tau proteins rather than microtubules, forming aggregates of paired helical

filaments and neurofibrillary tangles [380]. Eventually, tangles and aggregates lead to the destabilisation of microtubules and a loss of neuronal integrity (Figure 5).

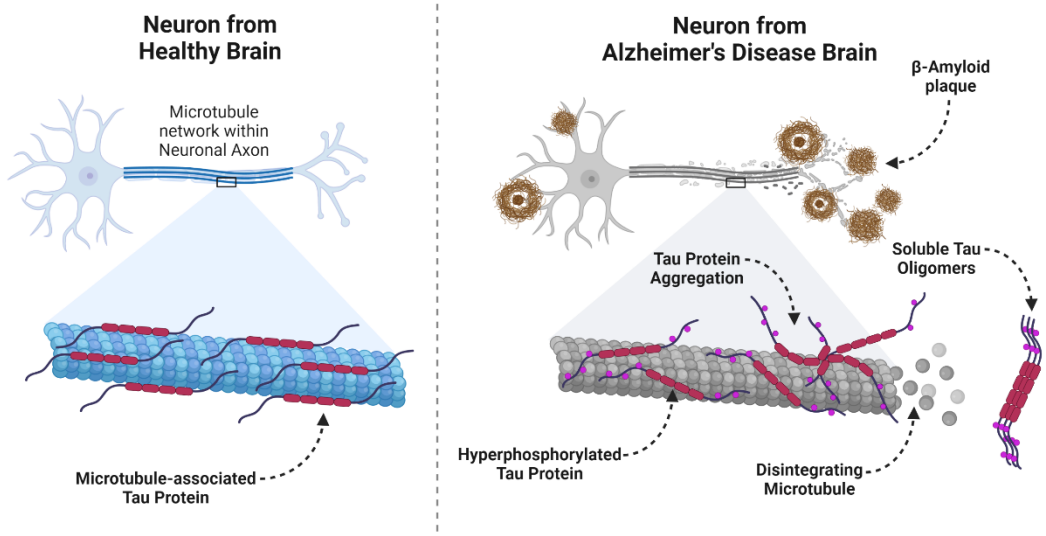

Figure 5. Tau aggregation in AD brains leads to disruption of microtubules and neurofibrillary tangles. Hyperphosphorylation of the microtubule-associated Tau protein results in aggregation of Tau, disrupting the microtubule network within neuronal axons. This aggregation eventually becomes neurofibrillary tangles, altering neuronal structure and function, leading to cell death. In addition, hyperphosphorylated Tau can dissociate from microtubules and accumulate into soluble Tau oligomers, capable of exacerbating cellular stress, amyloid aggregation, and neurofibrillary tangle formation. Retrieved and adapted from 'Pathology of Alzheimer's Disease 2" by author from the Biorender.com (2023).

Tau and Aβ share some characteristics. Before the formation of insoluble tangles, Tau aggregates can form soluble oligomers, which are thought to be more cytotoxic than insoluble Tau deposits, similarly to amyloids [379, 380]. Oligomers of Tau and Aβ are increased in the brain and CSF of AD patients compared to healthy controls (although, unlike amyloids, Tau aggregation is entirely hyperphosphorylation-dependent) [379, 380]. Interestingly, Aβ and Tau are capable of cross-seeding and co-aggregation in a similar manner to Aβ and IAPP [381, 382]. Furthermore, IAPP is also capable of cross-seeding Tau to form heterocomplexes [256]. Tau is also widely present in pancreatic islets, where ablation can severely impact β-cell function, GSIS, glucose tolerance, suggesting an important role for Tauopathy in T2D [383].

1.7 Aβ aggregates in Type 2 Diabetes

1.7.1 Aβ in the Diabetic Pancreas

As early as 1996, aggregated Aβ has been found in pancreatic islets of transgenic AD mouse models [384]. A study by Miklossy et al. [25] examined postmortem pancreatic tissue from diabetic patients. The authors reported the presence of aggregated Aβ together with IAPP aggregates in pancreatic islet plaque. Furthermore, the same study also found increased Tau expression and hyperphosphorylation associated with plaque deposit, which also stained positively for ubiquitin and ApoE [25]. It remains to be determined how Aβ is deposited in pancreatic islets, although it has been suggested that Aβ undergoes efflux from the brain and then uptake from the periphery. This notion is based on studies that indicate transgenic mouse models that express APP in the brain exclusively do not accumulate pancreatic plaque unless human IAPP is also present [296, 385, 386]. Another scenario includes the generation and secretion of Aβ from islet cells. Pancreatic β-cells express the genes for APP and the necessary processing enzymes to produce mature Aβ within the islet itself (the only islet cells that do so) [25, 387, 388]. Furthermore, a recent study noted that transient increases in plasma Aβ are synchronous with increase in plasma insulin and decreased Aβ immunostaining within β-cells, suggesting potential co-secretion of Aβ with insulin (and therefore IAPP) [389].

The role of APP and Aβ in the islet are still unknown, although evidence indicate a role in GSIS and glucose homeostasis. A study of transgenic APP / PS1 mice found that APP in pancreatic islets exhibited autocrine / paracrine function and increases insulin secretion from β-cells [385]. This function of APP is further supported by an obese mouse model that identified the APP gene as an important regulator of insulin secretion through a network-based modelling analysis of genes associated with T2D [390]. Potentially, aggregates of Aβ have a negative impact on insulin secretion through corruption of this pathway. Recent research indicates that in islets of older mice, Aβ decreases insulin secretion, implying not only that Aβ may exert a different effect than APP, but that it may be an age-dependent effect relevant to T2D [389, 390].

However, Aβ does not exist in pancreatic islets in isolation. Several studies have identified an accelerated aggregation of Aβ in the presence of IAPP (and vice versa) due to cross-seeding [259, 391-393]. Although the information on the topic is extremely limited, a few animal studies have begun to explore how IAPP-Aβ combinations impact disease progression and severity of both AD and T2D. In transgenic fruit flies (*Drosophila Melanogaster*) expressing both human IAPP and Aβ, lifespan was reduced compared to transgenic flies that expressed only IAPP or Aβ [392]. Moreover, a paper by Wijesekara et al. [247] has provided one of the most in-depth analyses to date of Aβ and IAPP in a shared disease model. A cross-bred double transgenic mouse model expressing human APP and IAPP showed significant exacerbations in AD and T2D disease burdens, including amyloid plaque loading in the brain and pancreas, peripheral and central insulin insensitivity, and neurodegeneration. Data relevant to this thesis from this publication are available as Appendix B (8.2, page 235) for reference.

Insight into how IAPP-Aβ together exacerbate AD and T2D disease processes at a cellular level is lacking. In a study by collaborators Bharadwaj et al. [129], IAPP-Aβ co-oligomerisation resulted in large amorphous aggregates distinct from those of Aβ and IAPP. Key findings from this study have been included in Appendix C (8.3, page 236). Bharadwaj et al. further state that these IAPP-Aβ co-aggregates have enhanced cytotoxicity, where they reduced cell viability 3-4 times compared to Aβ or IAPP alone. However, this toxicity profile was only examined in neuronal cell lines with reference to AD, and not in pancreatic tissue where Aβ and IAPP also co-localise *in vivo*. More research is needed to investigate the impact of Aβ and Aβ-IAPP aggregates on vital insulin-secreting pancreatic β-cells to fully elucidate the pathology of T2D.

1.7.2 Aβ in Central and Peripheral Insulin Resistance

Insulin resistance plays an important role in the pathology of AD. Compared to peripheral insulin signalling which primarily mediates glucose uptake, insulin receptor activation in the CNS promotes synaptic plasticity, neuronal growth and repair, and memory formation [394]. Dysregulation of this pathway through the induction and exacerbation of CNS insulin resistance provides another potential link between AD and T2D. A study involving cultured primary cortical

neurons of rats demonstrated that Aβ can bind to insulin receptors and downregulate both their function and expression [395]. Aβ oligomers are also suspected to bind to synaptic membranes, altering their conformation and further disrupting insulin binding / signalling [396]. AD-related hyperphosphorylation of Tau and loss of Tau function can also negatively impact insulin signalling in the CNS, exacerbating this effect [397, 398]. Furthermore, the neuroinflammatory environment within the AD brain can further downregulate insulin signalling, potentially leading to severe central insulin resistance [399].

However, as noted above, Aβ does not exist only in the CNS. Similar to IAPP, Aβ is able to aggregate in many of the insulin-sensitive peripheral tissues, including the liver, skeletal muscle, and heart [400]. Aβ is known to aggregate in skeletal muscle cells in a disease known as inclusion body myositis (IBM) [401, 402]. As a result of an inflammatory immune reaction that causes damage to proteostatic mechanisms and the ER, protein aggregates, such as Aβ, can accumulate in skeletal muscle cells, triggering further oxidative and ER stress [403, 404]. This process leads to reduced cell viability and function [403, 404]. However, outside of this specific disease, there is little evidence to suggest plaque accumulation occurs comparable to the degree found in the pancreas or brain in insulin-sensitive tissues of patients with T2D and / or AD.

Although these tissues lack significant amyloid aggregation, amyloidogenic peptides can still impact the viability and function of cells. Several distinct transgenic mouse models of Aβ overexpression have shown an increased glucose intolerance, metabolic dysfunction, and peripheral insulin resistance compared to controls in the presence of a high-fat diet [247, 405-409]. Although this can be the result of disruption to the hypothalamic regulation of insulin signalling (or even inflammation), there is evidence that Aβ could disrupt insulin signalling directly in peripheral tissues. As Aβ can bind to insulin receptors in the CNS, it can also potentially do this in peripheral tissues, down regulating insulin signalling [410, 411]. In hepatocytes from an APP / PS1 transgenic mouse model, Aβ can also disrupt insulin signalling both *in vivo* and *in vitro* by up-regulation of suppressor of cytokine signalling 1 (SOCS1)

through activation of the Janus kinase 2 (JAK2) / signal transducer and activator of transcription 3 (STAT3) pathway [412, 413].

Few studies have examined a dual T2D / AD phenotype in relation to metabolic dysfunction and peripheral insulin resistance. A study of APP / PS1 mice crossed with the *db /* + transgenic model of obesity and T2D with a mutation in the leptin receptor gene, reported exacerbated insulin resistance and glucose intolerance compared to *db /* + mice only [6]. These results are consistent with other studies such as transgenic APP / PS1 mice of AD crossbred with a diabetic mice model overexpressing IGF-2 [414], a transgenic APP model combined with both a mouse model of obesity, and with a mouse strain bred for its glucose intolerance [415, 416]. These studies observed worse metabolic deficits in diabetic mice models in the presence of human APP and Aβ. However, investigation of human IAPP is notably absent from these studies.

With little agreement on the role of aggregated IAPP in insulin sensitivity alone, the effect of IAPP-Aβ heterocomplexes in peripheral tissues is even less well known. Wijesekara et al. [247] demonstrated that although transgenic human APP mice exhibited reduced insulin sensitivity, a double transgenic model expressing both human APP and human IAPP displayed both insulin resistance and hyperglycaemia, indicating an exacerbated diabetic disease burden (Appendix C; 8.3, page 236). In this model, disruption of glucose homeostasis and high levels of plasma Aβ were observed before Aβ plaque deposits were identified in the brain, suggesting that metabolic disruption occurred early in the pathology. Whether this is the result of extrinsic mechanisms, such as hypothalamic regulatory disruption, chronic inflammation, or more intrinsic mechanisms such as IAPP-Aβ aggregates disruption of cells in peripheral tissues remains to be determined. As both diseases heavily feature insulin resistance, understanding the role of systemic IAPP-Aβ aggregates in insulin signalling is important to understanding the pathogenic mechanisms of both AD and T2D

1.8 Conclusion

In summary, studies have shown co-localisation of IAPP and Aβ in common tissues, including the brain, pancreas, and insulin-sensitive peripheral tissues. Emerging research further suggests that co-aggregation of these amyloidogenic peptides could enhance their cytotoxicity. As such, evidence supports the hypothesis proposed in this thesis that either IAPP and / or Aβ can potentially promote β-cell dysfunction and peripheral insulin resistance. To date, the cellular mechanisms remain to be fully determined. In addition, the combined effect of these proteins have not been widely explored. This will be investigated through the following research aims.

1.9 Research Aims

1.9.1 To assess pancreatic islet amyloid load, insulin, inflammation, and cellular stress in a novel transgenic mouse model expressing both human IAPP and Aβ

1.9.2 To investigate the impact of Aβ, alone and in combination with IAPP, on insulin secretion, viability, and metabolism of pancreatic β-cells *in vitro*

1.9.3 To investigate the impact of Aβ, alone and in combination IAPP, on insulin sensitivity, cellular viability, and metabolism on insulin-sensitive peripheral tissues *in vitro*

CHAPTER 2 Materials and Methods

2.1 *Ex Vivo* Murine Studies

2.1.1 Murine Models

A double transgenic (DTG) murine model exhibiting both pancreatic and cerebral amyloid was developed by the laboratory of Prof. Paul Fraser, Medical Biophysics, University of Toronto by cross-breeding a transgenic mouse model overexpressing human APP with another transgenic mouse model overexpressing human IAPP [247]. The transgenic APP mice featured both the Swedish and Indiana human APP695 mutations resulting in increased levels of amyloidogenic human Aβ in the central nervous system, while the transgenic IAPP mice featured increased levels of human IAPP in pancreatic tissue. As a result, the crossbred DTG mice retained both of these features. Nontransgenic littermates (NT) were used as controls to be compared with DTG, APP and IAPP mice (Table 1). As female mice presented a less severe phenotype, male mice were selected and placed on a 45% high-fat diet from 3 weeks of age to exacerbate symptoms further, then sacrificed at 16 or 24 weeks for analysis. Paraffin-embedded 5 µm sections of murine pancreatic tissue were prepared by the Fraser laboratory and three consecutive tissue sections were mounted per microscopic slide prior to being sent to Curtin University for examination [247].

Table 1. Comparison of transgenic, double transgenic, and nontransgenic murine models used in *ex vivo* examination of pancreatic tissue sections

Murine Model	Genetic / Transgenic Background	Gene Promoter / Expression Pattern	Model Features	Number of Animals per group	
				16W	24W
NT	50% FVB 25% C57BL / 6 25% CH3	N/A	N/A	7	7
APP	TgCRND8: APP KM670 / 671NL [Swedish]	Hamster Prion Protein (PrP) gene promoter	Model features increased levels of Aβ production, AD-like	5	5

	APP V717F [Indiana]	Protein expression localised to central nervous system neurons and (to a much lesser extent) astrocytes [417]	amyloid plaque deposition, Tau hyperphosphorylation, and cognitive impairment [417]		
IAPP	FVB / N-Tg [Ins2-IAPP] RHFSoel / J	Rat Insulin II gene promoter Protein expression localised to pancreatic tissue [418]	The model features T2D-like islet amyloid deposition and impaired insulin secretion [418]	6	8
DTG	APP x IAPP As above	As above	Exhibits features of both APP and IAPP transgenic models, including overexpression of human APP and IAPP [247]	9	7

2.1.2 De-Paraffinisation and Rehydration

The paraffin-embedded pancreatic tissue sections were deparaffinised by heating at 65 °C in a fan-forced oven for 20 min, then washed three times in 100% Xylene for 5 min. The sections were then washed twice in 100%, 70%, 50%, then 30% ethanol for 5 min each, respectively, before gentle washing in running RO water for 5 min to rehydrate the tissues. From this point on, the tissue sections were not allowed to dry.

2.1.3 Antigen Retrieval

Antigen retrieval, when required according to the experimental design, was carried out by immersing slides in sodium citrate buffer (10 mM sodium citrate, 0.05% TWEEN® 20, pH 6.0) in a microwave-safe slide rack and container. Using a 1100-watt microwave at 50% power, the slides were heated for 30 min (3 min rotations) at 95 °C, being careful to avoid tissue dissociation from the

slide caused by the solution boiling. The slides were cooled at room temperature for 10 min and then washed in RO water for 5 min.

2.1.4 Thioflavin S Staining

Thioflavin S (ThioS) staining, when required according to the experimental design, was performed after antigen retrieval and prior to immunofluorescent staining. The slides were immersed in 1% w / v filtered ThioS (Sigma Aldrich) for 10 min at room temperature, protected from light. After incubation, slides were required to be kept continually protected from light and were washed twice in 80% ethanol for 3 min, once in 90% ethanol for 3 min, and three times in RO water for 1 min.

2.1.5 Immunofluorescent Staining

The slides were washed in Tris-buffered saline (TBS) for 5 min with gentle agitation on a plate rocker. A hydrophobic barrier pen was used to surround the tissues and confine the reagents to each specific tissue section on each slide. Once applied, a blocking solution of 10% normal goat serum (NGS) in TBS with 0.05% TWEEN® 20 (TBS-T; Sigma Aldrich) was added to each section and incubated in a humid chamber for 60 min at room temperature. The slides were drained of blocking solution and primary antibodies diluted in 1% NGS in TBS-T were added (Table 2). The slides were then incubated at 4 °C overnight in a humid chamber. Optimal antibody dilutions were obtained by optimisation of antibody dilution factors on spare sections prior to use on test samples.

Table 2. Primary antibodies used in immunofluorescent staining of murine pancreatic tissue sections

Antigen	Epitope	Isotype (IgG)	Dilution	Supplier	Cat No.
Insulin	Information Unavailable	Guinea Pig	1:500	Abcam	Ab7842
Iba1	Information Unavailable	Rabbit	1:250	Abcam	Ab178846
Tau	~Asp430	Rabbit	1:250	Cell Signaling	46687
Phospho-Tau	Ser202 & Thr205	Mouse	1:200	Thermofisher	MN1020

Cleaved Caspase-3	~Asp175	Rabbit	1:250	Cell Signaling	9664

Following primary antibody incubation, slides were washed three times in TBS-T for 5 min with gentle agitation on a plate rocker. Fluorophore-conjugated secondary antibodies in 1% NGS in TBS-T were incubated at room temperature for 60 min in a humid chamber, protected from light (Table 3). After incubation, if ThioS staining had not been done earlier, slides were now required to remain continuously protected from light and were washed three times in TBS-T for 5 min with gentle agitation on a plate rocker.

Table 3. Fluorophore-conjugated secondary antibodies used in immunofluorescent staining of murine pancreatic tissue sections

Antigen	Fluorophore	Isotype	Dilution	Supplier	Cat No.
Guinea Pig IgG	AF647	Goat IgG	1:500	Abcam	Ab6908
Rabbit IgG	AF594	Goat IgG	1:250	Cell Signaling	8889
Mouse IgG	AF647	Goat IgG	1:250	Cell Signaling	4410

2.1.6 Hoescht Stain

0.02 µg / µL of Hoescht solution in TBS was added to each slide and left to incubate at room temperature in a humid container. After incubation, the slides were washed for 15 min in TBS with gentle agitation on a plate rocker.

2.1.7 Mounting slides

A single drop (approximately 10 µL) of ProLong™ Diamond Antifade Mountant (Invitrogen) was added to each section of a slide and a 22 x 40 mm coverslip was placed per slide. The slides were then allowed to dry overnight, protected from light.

2.1.8 Microscopic Imaging

Microscopic imaging was performed on a Nikon A1 confocal microscope and viewed on NIS Elements Viewer Software Version 4.11.0. A minimum of five islets were chosen at random per tissue section and imaged. All images were taken at 20x magnification. Care was then taken to ensure that the same islets and regions of interest were captured over the serial sections on the same

microscopy slide. Laser power and detection settings were optimised for each antibody according to manufacturer recommendations.

2.1.9 Image Quantification and Data Analysis

Images were analysed using ImageJ software. The islets were identified and the isolated by threshold gating, and appropriate background corrections were applied to each antibody. Each individual islet was then quantified into intensity and / or the percentage of islet area of antibody staining. The intensity of antibody staining was measured using the mean grey value, where each pixel within the gated islet area is given as a continuous value on a grey scale between 0 (black; absence of staining) and 255 (white; complete saturation of staining). The grey value of all pixels (with a given value of between 1-255) was then averaged to give a mean grey value per islet. The percentage of islet area stained positively by antibodies was measured by each pixel within the gated islet area being given a binary categorical value depending on the presence or absence of staining. The area of all pixels positive for antibody staining was then given a percentage value of the total gated islet area occupied.

Statistical analysis was performed using GraphPad Prism version 8 software. Data underwent normality testing and, if found to be normally distributed, one-way ANOVA with Tukey multiple comparisons Post-Hoc testing were performed to compare means between groups, while two-way ANOVA tests with Sidak's multiple comparisons Post-Hoc testing were used to determine changes between groups at 16 and 24 w. If data was not normally distributed, nonparametric Kruskal-Wallis test with Dunn's Post-Hoc tests were instead used to compare the mean rankings of each group. All graphed data is expressed as Mean ± Standard Deviation (SD). The statistical significance limit was set at 0.05 or less ($p < 0.05$).

2.2 *In Vitro* Cell Line Studies

2.2.1 Preparation of Amyloid Peptides

The preparation of amyloidogenic peptides into oligomeric species followed well-established protocols [129, 419, 420]. Synthetic powdered preparations of human IAPP (Abbiotec) and the 42-residue isoform of Aβ (Keck Institute) were solubilised in Hexafluoro-2-propanol (HFIP) at a final concentration of 1 mM. After 30 min of incubation at room temperature, the solution was vortexed for 1 min and then separated into 100 µL aliquots in individual 1.5 mL microtubes. The HFIP in each tube was evaporated under a gentle and steady stream of oxygen-free nitrogen (N_2) gas, leaving a dried film of IAPP or Aβ peptides. The films were stored at -20 °C until required, but no longer than 3 months.

To resuspend the dried protein film, 20 µL of dimethyl sulfoxide (DMSO) was added, carefully scraping the sides of the microtube. The microtubes were vortexed for 1 min, pulse centrifuged, then sonicated for 10 min at room temperature, with successive 10 sec cycles and 5 sec breaks between cycles in Biorupter® Plus Sonication Device (Diagenode). After sonication, 980 µL of Ham's F-12 medium without FBS and without Phenol Red (Gibco) was added to give a final concentration of 100 µM per microtube. Following resuspension in in F-12, amyloidogenic peptides were incubated at 4 °C for 24 h to allow oligomerisation. The oligomeric amyloidogenic stock solution was stored at 4 °C and used within 7 days.

2.2.2 Cell Culture

2.2.2.1 BRIN-BD11 cells

BRIN-BD11 (CellBank Australia) is a hybrid β-cell line created by electrofusion of primary rat islets with RINm5F, a rat insulinoma cell line [421]. Cells were cultured primarily in T75 flasks in RPMI 1640 medium (Sigma Aldrich) supplemented with 11.1 mmol / L glucose, 2 mmol / L L-glutamine, 10% v / v foetal bovine serum (FBS), and 1% v / v penicillin streptomycin. The cells were maintained at 37 °C with 5% CO_2 and subcultured at approximately 70-80% confluence. Before treatment, BRIN-BD11 cells were seeded at optimised cell

densities in subculture plates (96-, 24- or 6-well plates) as required by experimental conditions and left to adhere overnight.

2.2.2.2 HSMM cells

Human Skeletal Muscle Myoblasts (HSMM; Lonza) are primary human undifferentiated mononucleated myoblasts isolated from the quadriceps or psoas muscles of healthy adult donors [422, 423]. According to the manufacturer's recommendations, HSMM cells were cultured at 37 °C and 5% CO_2 in SkBMTM-2 basal medium (Lonza) supplemented with 10% v / v FBS, 50 µg / mL of bovine fetuin, 10 ng / ml human recombinant epidermal growth factor, 1 ng / ml human recombinant fibroblast growth factor, and 0.4 µg / mL of dexamethasone (SkGMTM-2 Skeletal Muscle Myoblasts SingleQuotsTM supplements, Lonza). Cells were subcultured at approximately 50-60% confluence to prevent spontaneous differentiation, and growth medium was changed every 2-3 days.

2.2.2.3 Differentiation of HSMM cells

HSMM cells were seeded in Growth Medium in subculture plates required by experimental conditions (96-, 24- or 6-well plates) and left to adhere overnight. The supernatant was discarded and replaced with a fusion medium of 1:1 Dulbecco modified Eagles Medium (DMEM) and Ham's F12 nutrient mixture (Sigma Aldrich) supplemented with 2% horse serum. Cells were cultured in this medium for 5 days, ensuring that the differentiation medium was changed at least every 2-3 days. After 5 days, the cells were prepared for treatment.

2.2.2.4 Cell Counting and Subculturing

Once the necessary confluency of cells (variable depending on cell type) had been reached, the cells were ready to be counted and / or subcultured into cell culture flasks or plates as needed. The following reagent measurements were optimised for the T75 subculture flask but can be scaled for other flask sizes. First, the conditioned media was discarded from the cell culture flask and the cells were briefly washed with 10 mL of phosphate-buffered saline (PBS; depending on the size of the flask). The PBS was then discarded, and cells were incubated with 5 mL of 0.25% trypsin for 5 min at 37 °C with 5% CO_2 to detach cells from the flask. After incubation, trypsin was neutralised with an

equal volume (5 ml) of appropriate fresh growth medium containing 10% FBS. The flask contents were collected in a 15 mL test tube, and cells were pelleted by centrifugation for 5 min (500 x *g* for BRIN-BD11 cells, 200 x *g* for HSMM cells). The supernatant was again discarded, and the cell pellet was resuspended in ~3 mL of appropriate fresh growth medium. A 50 µL sample of cell suspension was added to 50 µL of 0.4% Trypan Blue (Thermofisher) solution to stain cells and a Neubauer haemocytometer was used to calculate the cell density per millilitre. cells were seeded into a fresh flask at an appropriate seeding density in fresh growth media.

2.2.3 Methylthiazol Tetrazolium (MTT) Assay

The MTT assay is a colourimetric assay used as a measurement of cell viability, as only live cells reduce the soluble MTT to insoluble formazan crystals. After treatment, 5 mg / ml of MTT solution was added to the supernatant within the wells in a 1 : 10 ratio (e.g., 10 µL of MTT to 100 µL supernatant). The plate was left to incubate for 4 h at 37 °C and 5% CO_2, protected from light. The MTT / supernatant solution was eluted from the wells, and 100 µL of DMSO was added per well to solubilise formazan crystals. The plate was then gently shaken on an orbital plate shaker for 1 min and absorbance was read at 570 nm on a PerkinElmer Ensight™ multimode plate reader. Results were expressed as relative fold change from control.

2.2.4 Cell Cycle Analysis (Flow Cytometry)

After treatment, cells were harvested using 0.25% trypsin and collected into 15 mL test tubes. Cells were pelleted by centrifugation at 500 x *g* and room temperature, resuspended in PBS to wash and then were pelleted again. The PBS was decanted, and the cells were gently resuspended in 1 mL of -20 °C 70% ethanol to permeabilise the cell membrane and fix the cells. Cells were then stored at -20 °C overnight. After overnight incubation, cells were pelleted via centrifugation by 500 x *g* and room temperature, then cells were washed a total of three times in PBS. Cells were resuspended in 200 µL of PBS containing 10 µg / mL RNAse and 40 µg / mL Propidium Iodide (PI) a red-fluorescent DNA stain that cannot penetrate the semipermeable cell membrane, then incubated for 30 min at room temperature, protected from

light. A BD LSRFortessa flow cytometer (BD Biosciences) was used to determine and analyse the stained cells. PI staining was detected in the FL2 channel of the flow cytometer.

Cell debris and aggregate cell populations were excluded via gating and single cell populations were shown on a histogram displaying event count versus PI fluorescence (using a minimum of 10000 events). Using this histogram, the phases of cell cycle can be determined as PI staining creates a fluorescence signal proportionate to the amount of DNA present. Cells entering into the process of mitosis (G_2 / M) contain twice the amount of DNA than resting cells or cells preparing for DNA duplication (G_0 / G_1). Cells in the transitional process of DNA duplication (S Phase) and necrotic or apoptotic cellular fragments (Sub-G_1) can also be detected. The phases of the cell cycle were detected and analysed using FloJo v10 software.

2.2.5 Bicinchoninic Acid (BCA) Protein Assay

The BCA Assay was performed using the Pierce™ BCA Assay Kit (Thermofisher) according to manufacturer's protocol. Briefly, BCA reagents were mixed according to the manufacturer's instructions (50 parts A to 1 part B), and 200 µL of the mixture was added to 25 µL of cell lysate sample per well in a 96-well plate. The plate was then incubated at 37 °C for 30 min before absorbance was recorded at 560 nm on a PerkinElmer Ensight™ multimode plate reader. The results were compared to a standard curve of known concentrations of bovine serum albumin (BSA; 0-2000 µg) prepared on the same plate to determine the protein concentration in µg / mL.

2.2.6 Glucose Stimulated Insulin Secretion (GSIS)

As directed by previously established laboratory protocols [424] post-treatment supernatant was removed, and the wells were washed with PBS. Warm (37 °C) Kreb's Ringer bicarbonate buffer (KRBB: 115 mM of NaCl 4.7 mM of KCl, 1.28 mM of $CaCl_2.2H_2O$, 1.2 mM of KH_2PO_4, 1.2 mM of $MgSO_4.7H_2O$, 10 mM of $NaHCO_3$, 10 mM of HEPES, 0.5% BSA; pH 7.4) supplemented with 1.1 mM glucose was added to each well and the cells were left to acclimate for 40 min at 37 °C with 5% CO_2. After acclimation, the supernatant was removed and fresh warm KRBB was added to each well supplemented with 1.1 mM glucose,

for basal stimulation, or 16.7 mM glucose and 10 mM Alanine, for maximum stimulation. The plates were incubated for 20 min at 37 °C with 5% CO_2 before collecting the supernatant and stored at -80 °C for future testing. RIPA cell lysis buffer was added to each well before incubation at 4 °C for 30 min. Cell lysates were stored at -20 °C and a BCA Assay (2.2.5, page 51) was used to determine protein quantification for normalisation.

2.2.7 Insulin ELISA

Insulin quantification was determined via Ultrasensitive Rat Insulin ELISA kit (Mercodia) according to the manufacturer's protocols. Briefly, 25 µL of Insulin Calibrators were added to 96-well coated ELISA plates with samples generated from Glucose Stimulated Insulin Secretion (2.2.6, page 51). 100 µL of enzyme conjugate solutions per well were added, and the plate was incubated on an orbital plate shaker at room temperature for 2 h. After incubation, the plate was washed 6 times with 350 µL of wash buffer, then 200 µL of Substrate TMB was added to each well and the plate was incubated for 15 min at room temperature protected from light. 50 µL of Stop Solution per well was added and the plate was briefly placed on an orbital plate shaker to ensure adequate mixing. The absorbance was read at 450 nm on a PerkinElmer Ensight™ multimode plate reader. Insulin quantification was performed using known concentrations of insulin calibrators and normalised via protein quantification BCA Assay (2.2.5, page 51). Results were expressed as insulin concentration in µg / L / µg of protein, or as a relative fold change from control.

2.2.8 Western Blot Analysis

2.2.8.1 Sample Preparation

After treatment, cells were washed with cold Hank's balanced salt solution (HBSS; Gibco). 100 µL of RIPA buffer with cOmplete™ ULTRA protease inhibitor cocktail (Roche) was added to wells, and wells were scraped to enhance lysing of cells and protein output. Lysate solution was collected into 0.5 mL microtubes, vortexed for 1 min, then incubated at 4 °C for 1 h. Post-incubation, the samples were vortexed again for 1 min then sonicated for 3 min at 4 °C, with successive 15 sec cycles and 5 sec breaks between cycles in

Biorupter® Plus Sonication Device (Diagenode). Samples were vortexed for 1 min and centrifuged at 10000 x *g*, then the supernatant was aspirated and transferred to a fresh 0.5 mL microtube. Concentration of proteins in samples was determined by BCA Assay (2.2.5, page 51). Samples were stored at -20 °C.

2.2.8.2 *Sodium Dodecyl Sulphate – Polyacrylamide Gel Electrophoresis (SDS-PAGE)*

Samples were prepared for SDS-PAGE by adding NuPAGE™ LDS Sample Buffer and NuPAGE™ Sample Reducing Agent (Invitrogen) to at least 15 µg of protein per sample as per manufacturer instructions. Sample mixture was vortexed for 1 min, then heated to 70 °C for 10 min. Samples were separated by electrophoresis in either a pre-cast Bolt™ 4 – 12% Bis-Tris Plus Gel or using 10% hand-cast gels made via the SureCast Gel Handcast System (Invitrogen). Electrophoresis was performed using a Mini Gel Tank in NuPage™ MOPS SDS Running Buffer (Invitrogen) at a constant voltage of 80 V for 90 min.

2.2.8.3 *Protein Transfer*

After electrophoresis, the acrylamide gels were transferred to a nitrocellulose membrane via a wet transfer method. Briefly, the nitrocellulose membrane and acrylamide gel were enclosed in filter paper and fibre/sponge padding, then loaded into cartridges and into a Tetra Blotting Module (Bio-Rad). Cartridges were submerged in Transfer Buffer (25 mM Tris, 192 mM Glycine, 10% Methanol) alongside a frozen cooling block. Transfer was performed at 4 °C for 105 min at a constant amperage of 250 mA or overnight at a constant voltage of 20 V. After transfer completion, Ponceau S Solution (Sigma-Aldrich) was applied to membranes to verify successful protein transfer, then rinsed from the membrane using warm TBS.

2.2.8.4 *Immunoblotting*

Following Ponceau S staining and removal, membranes were incubated in blocking solution of 3% BSA or 5% skim milk in TBS-T for 1 h at room temperature. Following blocking, membranes were incubated with primary antibodies in 1% BSA or 1% skim milk in TBS-T overnight at 4 °C (Table 4).

Table 4. Primary antibodies used in immunoblotting of *in vitro* cell lines

Target	Epitope	Isotype (IgG)	Dilution	Supplier	Cat No.
α/β-Tubulin	~Tyr36	Rabbit	1:1000	Cell Signaling	2128
Cleaved Caspase-3	~Asp175	Rabbit	1:1000	Cell Signaling	9664
Akt – Total	~C-Terminus	Rabbit	1:1000	Cell Signaling	9272
Akt – Phospho (S473)	~Ser473	Rabbit	1:1000	Cell Signaling	9271
Akt – Phospho (T308)	~Thr308	Rabbit	1:1000	Cell Signaling	4056
ATF4	~C-Terminus	Rabbit	1:1000	Cell Signaling	11815
β-Actin	~N-Terminus	Rabbit	1:1000	Cell Signaling	4970
BCL-XL	Information Unavailable	Rabbit	1:1000	Abcam	Ab32370
BiP	~Arg26	Rabbit	1:1000	Cell Signaling	3183
CHOP	Information Unavailable	Mouse	1:1000	Cell Signaling	2895
COXIV	~Lys29	Rabbit	1:300	Cell Signaling	4850
GAPDH	~Lys260	Rabbit	1:1000	Cell Signaling	5174
HSP60	~Trp68	Rabbit	1:1000	Cell Signaling	12165
iNOS	Ser1118 - Gly1129	Rabbit	1:1000	Abcam	Ab136918
Sirt1	Information Unavailable	Mouse	1:1000	Cell Signaling	8469
SUR1	Information Unavailable	Rabbit	1:1000	Abcam	Ab32844

Membranes were then washed three times in TBS-T for 5 min each, then incubated with HRP-linked secondary antibodies in 1% BSA or 1% skim milk in TBS-T for 1 h at room temperature (Table 5). After incubation, membranes were washed three times in TBS-T for 5 min each then incubated for 5 min in Clarity™ Western Enhanced Chemiluminescent (ECL) Substrate (Bio-Rad) at room temperature, protected from light.

Table 5. HRP-linked secondary antibodies used in immunoblotting of *in vitro* cell lines

Target	Isotype	Dilution	Supplier	Cat No.
Rabbit IgG	Goat	1:2000	Dako	P0448
Mouse IgG	Goat	1:2000	Dako	P0447

2.2.8.5 Imaging and Quantification of Protein Banding

Membranes were transferred to a ChemiDoc™ MP Imaging System (Bio-Rad) and imaged using the Chemi Hi Resolution application protocol in ImageLab® Software (Bio-Rad). Using the same software, lanes and bands were identified and densitometry analysis of protein banding was used to quantify changes in protein expression. Target protein expression was normalised by housekeeping protein expression and expressed as relative expression for comparison between groups.

2.2.9 PI Staining (Flow Cytometry)

PI staining of cells (without prior membrane permeabilisation as was performed in Cell Cycle Analysis (2.2.4, page 50) is a more direct measure of cell death as only membrane-compromised (typically late-stage apoptotic cells) are detected. After treatment, both the supernatant and cells were collected in 14 mL test tubes to include all living and dead cells. The cells were pelleted via centrifugation at 500 x *g* and room temperature, then resuspended in Phosphate-Buffered Saline (PBS) to wash and were pelleted again. The PBS was decanted, and the cells were resuspended and incubated in fresh PBS with 40 µg / mL PI (Thermofisher) for 5 min, protected from light. Cells were vortexed for 1 min, transferred to 5 mL flow cytometer tubes then briefly kept on ice. A BD LSRFortessa Flow Cytometer (BD Biosciences) was used to determine and analyse the stained cells. Using a minimum of 10000 events, cell debris and aggregate cell populations were excluded via gating and single cell populations were shown on a histogram displaying event count versus PI fluorescence. Using FloJo v10 Software, PI positive cells were identified and expressed as percentage of total events.

2.2.10 CM-H2DCFDA Intracellular Oxidative Stress Indicator (Flow Cytometry)

On the day of the assay, the CM-H2DCFDA probe was prepared to a stock concentration of 250 µM in DMSO. After treatment, cells were washed with PBS, then incubated for 30 min with 1 µM of the ROS Probe CM-H2DCFDA in Phenol Red-free serum-free DMEM at 37 °C with 5% CO_2, protected from light. Continually protected from light, the cells were washed again with PBS, then harvested using 0.25% trypsin. The cells were pelleted via centrifugation, then resuspended in 1 mL of fresh PBS. All samples were vortexed for 1 min, transferred to 5 mL flow cytometer tubes then briefly kept on ice. A BD LSRFortessa Flow Cytometer (BD Biosciences) was used to analyse the stained cells. Using a minimum of 10000 events, cell debris, aggregate cell populations and PI positive cells (PI Staining; 2.2.9, page 55) were excluded via gating and single cell populations were shown on a histogram displaying event count versus CM-HF2DCFDA fluorescence. Using FloJo v10 Software, the intensity of CM-HF2DCFDA staining was identified as the geometric mean.

2.2.11 Seahorse XF^{e}96 Mitochondrial Stress Test

2.2.11.1 Reagents and Preparation

The Agilent Seahorse XF^{e}96 flux analyser was operated according to the manufacturer's mitochondrial stress testing protocols. Testing reagent final concentrations were successfully optimised for each cell line in order to meet the required manufacturer's criteria [232, 425]. Oligomycin, Carbonyl cyanide 4-trifluoromethoxyphenylhydrazone (FCCP), Antimycin A and Rotenone were purchased from Sigma Aldrich and solubilised in DMSO in 5 mM stock concentrations (Figure 6). Cells were seeded in specialised Seahorse XF^{e}96 cell culture plates and left to adhere overnight before undergoing treatment. During this time, the XF^{e}96 sensor plate was hydrated using calibrant solution supplied by Agilent and left to incubate for 24 h at 37 °C in a non-CO_2 incubator.

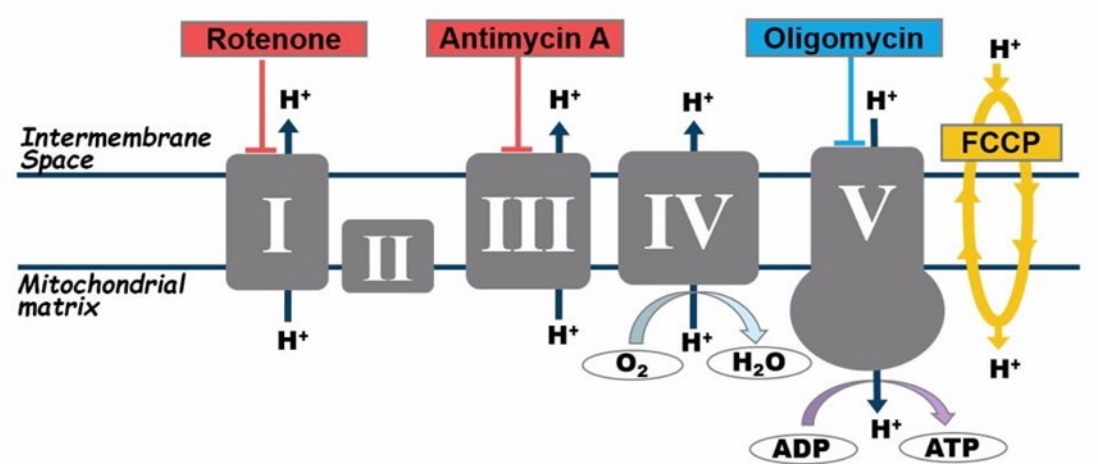

Figure 6. Electron transport chain targets of key mitochondrial modulators (sourced from Rogers, Burroughs [425]). Seahorse XFe96 mitochondrial stress testing employs the use of acute injections of mitochondrial modulators to alter mitochondrial coupling mechanisms, as well as function of ATP-Synthase and respiratory complexes I and III, to determine changes in mitochondrial function and cellular respiration after exposure to test compounds such as amyloidogenic peptides.

2.2.11.2 *Day of the Assay*

After treatment, the supernatant was discarded from the cell plate and replaced with buffer-free serum-free DMEM (Sigma Aldrich) supplemented with 1 mmol / L of sodium pyruvate and 2.5 mmol / L of glucose (pH 7.4). The plate was incubated for 1 h at 37 °C in a non-CO_2 incubator to allow the cells to acclimate to the new environment. As this occurred, the reagent injections were loaded into the sensor plate (Table 6), which was then inserted into the flux analyser to calibrate. Post-calibration, the cells had acclimated to the media change and the cell plate was inserted into the flux analyser. After basal measurements were conducted, the wells were injected with 25 µL of the buffer-free serum-free DMEM containing optimised concentrations of Oligomycin, FCCP, then a combined injection of Antimycin A and Rotenone. The injections were delivered at 21 min intervals with alternating mix / measure cycles every 3.5 min to detect Oxygen Consumption Rate (OCR). After assay completion, the BCA Assay (2.2.5, page 51) was used to quantify protein for normalisation.

Table 6. Final concentrations of mitochondrial stress testing reagents per cell line

Cell line	Injection 1: Oligomycin (µM)	Injection 2: FCCP (µM)	Injection 3: Antimycin A (µM)	Injection 3: Rotenone (µM)
BRIN-BD11	2	0.3	1	1
HSMM	2	1	1	1

2.2.11.3 Calculations and Outcomes

Oligomycin, as an inhibitor of ATP synthase [426], was used to estimate OCR coupled to ATP synthesis. FCCP, as a mitochondrial uncoupler [427], was used to measure maximal OCR. A combination of Antimycin A and Rotenone inhibits the flow of the electron transport chain (ETC) at complexes III and I respectively [428, 429], allowing measurement of non-mitochondrial respiration (Figure 6). Using current modelling, extracellular acidification and oxygen consumption can be detected and used to calculate the ATP generation, where each mol of oxygen can yield up to a 2.79 mol of ATP [430]. The basal measurements and calculations are then used to calculate further parameters such as proton leak, spare respiratory capacity and coupling efficiency percentage (Table 7, Figure 7). Results were expressed as OCR in pmol / min / µg of protein and fold change from control.

Table 7. Calculation of mitochondrial parameters from mitochondrial stress testing measurements after injections of mitochondrial modulators

Parameter	Calculation
Non-Mitochondrial Respiration	Minimum OCR after Antimycin A / Rotenone
Basal Respiration	(Final OCR before Oligomycin) – (Non-Mitochondrial Respiration)
Proton Leak	(Minimum OCR after Oligomycin) – (Non-Mitochondrial Respiration)
Maximal Respiration	(Maximum OCR after FCCP) – (Non-Mitochondrial Respiration)
ATP Production	(Basal Respiration) – (Proton Leak)
Spare Respiratory Capacity	(Maximal Respiration) – [(ATP Production) + (Non-Mitochondrial Respiration)]

Coupling Efficiency	(ATP Production) / (Basal Respiration) * 100

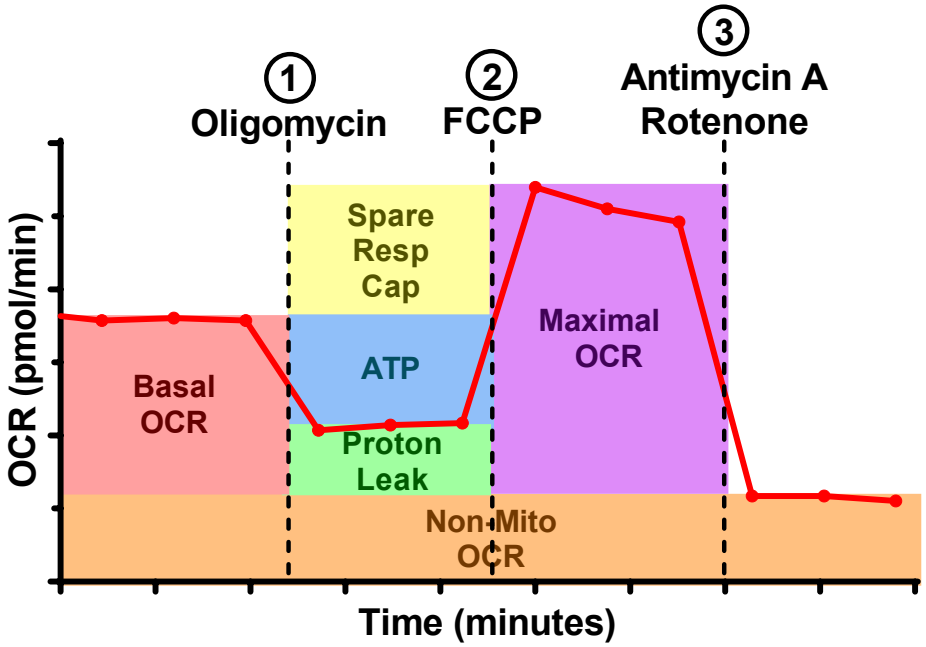

Figure 7. Example of Seahorse XFe96 Flux Analyser Mitochondrial Stress Output. Changes in oxygen consumption rate over time after exposure to mito-active drugs can be used to calculate important mitochondrial parameters, such as the basal oxygen consumption rate (Basal OCR), spare respiratory capacity (Spare Resp Cap), ATP production rate (ATP), proton leak, maximum oxygen consumption rate (Maximal OCR), and non-mitochondrial oxygen consumption rate (Non-mito OCR).

2.2.12 Seahorse XF^{e}96 Glycolytic Rate Assay

2.2.12.1 Reagents and Preparation

The Agilent Seahorse XFe96 flux analyser was operated according to the manufacturer's glycolytic rate testing protocols. Testing reagent final concentrations were successfully optimised for each cell line in order to meet the required manufacturer's criteria [431, 432]. 2-Deoxy-glucose (2-DG; Sigma) was prepared in DMEM to a stock concentration of 1 M (Figure 8). Antimycin A and Rotenone reagents where preparation was conducted identically to the Mitochondrial Stress Test (2.2.11, page 56), as was cell and sensor plate preparation.

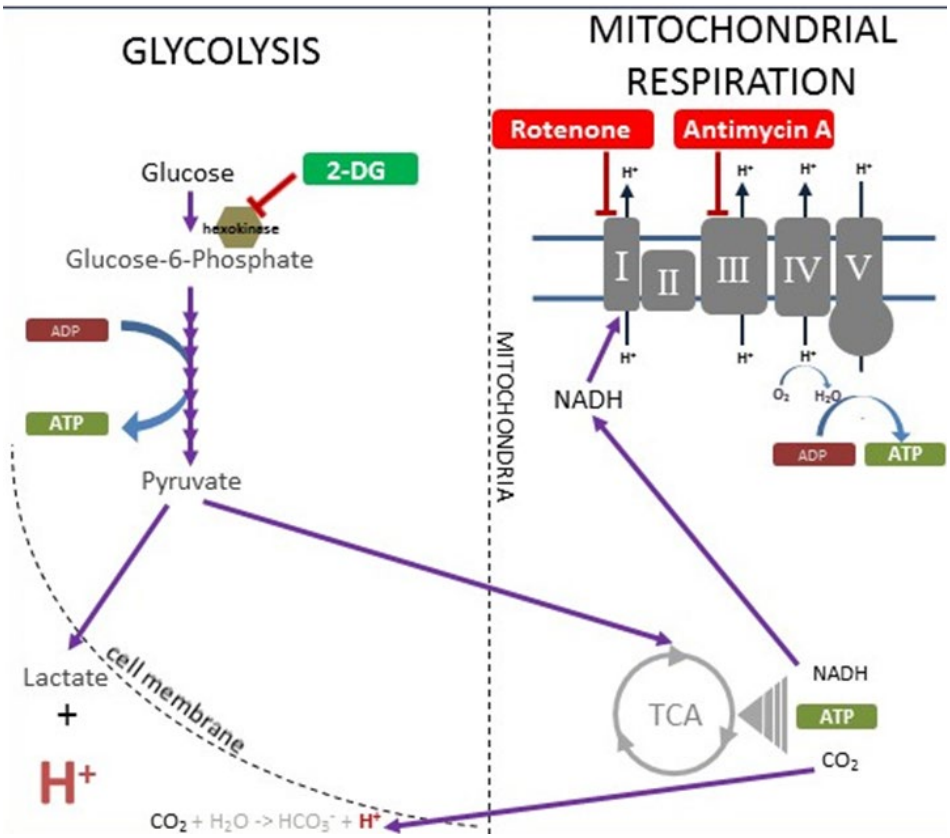

Figure 8. Targets of glycolytic rate modulators (sourced from Agilent Technologies, Inc [433]). Seahorse XFe96 glycolytic rate assay employs the use of mitochondrial modulators Antimycin A and Rotenone to inhibit oxidative phosphorylation and promote compensatory glycolytic activity. The addition of the glycolytic inhibitor 2-DG confirms the specificity of the pathway to stop glycolytic acidification.

2.2.12.2 Day of the Assay

After treatment, the supernatant was discarded and replaced with Phenol Red-free serum-free DMEM (Sigma Aldrich) supplemented with 1 mmol / L of sodium pyruvate, 2.5 mmol / L glucose, and 5 mmol / L of 4-(2-hydroxyethyl)-1-piperazineethanesulfonic acid (HEPES; Gibco) (pH 7.4). The plate was incubated for 1 h at 37 °C in a non-CO_2 incubator to allow the cells to acclimate to the new environment. The reagent injections were loaded into the sensor plate (Table 8), including injections of 5 mmol / L HCl in key blank wells to determine the Buffering Capacity of the medium, and the cartridge was inserted into the flux analyser to calibrate.

Post-calibration, the cell plate was also inserted into the flux analyser. After basal measurements were conducted, the wells were injected with 25 µL the Phenol Red-free serum-free DMEM containing either optimised concentrations

of 2-DG then a combined injection of Antimycin A and Rotenone, or HCl only (in specific cell-free wells). The injections were delivered at 21 min intervals with alternating mix / measure cycles every 3.5 min to detect Proton Efflux Rate (PER). After assay completion, the BCA Assay (2.2.5, page 51) was used to quantify protein for normalisation.

Table 8. Final concentrations of glycolytic rate testing reagents per cell line

Cell line	Injection 1: Antimycin A (µM)	Injection 1: Rotenone (µM)	Injection 2: 2-DG (mM)
BRIN-BD11	1	1	100
HSMM	1	1	100

2.2.12.3 Calculations and Outcomes

The change in pH detected after the HCl injections allowed the Buffering capacity of the media to be accurately detected. Antimycin A and Rotenone disable the ETC, resulting in a rise in compensatory glycolysis [428, 429]. The following injection of 2-DG competitively binds glucose hexokinase, inhibiting glycolysis [434] (Figure 8). Mitochondrial acidification is determined via the buffering capacity of the assay media and the CO_2 contribution factor (pre-calculated by Seahorse XF^e96 Flux Analyser) to isolate the PER attributed solely to glycolysis. From these calculations, including buffering capacity and basal measurements, key parameters of glycolytic rate were determined and expressed as both PER in pmol / min / µg of protein, and as fold change from control (Table 9; Figure 9).

Table 9. Calculation of glycolytic parameters from glycolytic rate assay measurements after injections of mitochondrial modulators

Parameter	Calculation
Mitochondrial Acidification	Pre-calculated from buffering capacity of assay media and CO_2 contribution factor of mitochondrial oxygen consumption rate
Post 2-DG Acidification	Minimum PER after 2-DG
Basal Glycolytic Rate	(Final OCR before Antimycin A / Rotenone) – [(Mitochondrial Acidification) + (Post 2-DG Acidification)]

Compensatory Glycolysis	(Maximum PER after Antimycin A / Rotenone) – (Post 2-DG Acidification)

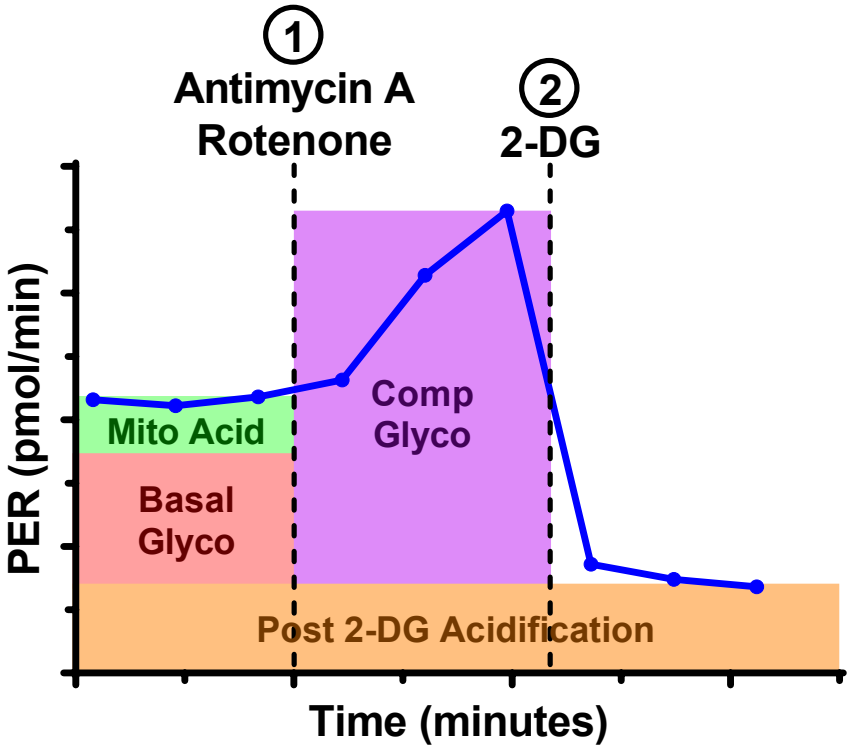

Figure 9. Example of Seahorse Xfe96 Flux Analyser Glycolytic Rate Output. Changes in pH, measured as proton efflux rate, over time after exposure to mito-active drugs can be used to calculate important mitochondrial parameters relevant to glycolytic activity, such as the basal glycolytic rate (Basal Glyco) and compensatory glycolysis (Comp Glyco) [432].

2.2.13 Real Time Polymerase Chain Reaction (RT-PCR)

2.2.13.1 RNA Extraction

Real time polymerase chain reaction (RT-PCR) was performed to determine changes in gene expression. First, RNA was extracted using TRIzol® Reagent (Life Technologies) according to the manufacturer's protocol. RNA samples were suspended in UltraPure™ DNase / RNase-free water (Life technologies) and RNA concentration (ng / µL) and purity was determined using NanoDrop Microvolume Spectrophotometer (Thermofisher). RNA samples with absorbance ratios of >1.8 A_{260} / A_{280} and 2.0 - 2.2 A_{260} / A_{230} were considered without significant contamination.

2.2.13.2 cDNA Synthesis

Synthesis of cDNA from RNA was performed using QuantiTect Reverse Transcription Kit (Qiagen). Genomic DNA was removed by adding gDNA Wipeout Buffer to RNA samples and incubating at 42 °C for 3 min, then placing immediately on ice. Reverse-Transcription Master Mix (consisting of Quantiscript Reverse Transcriptase, Reverse-Transcription Buffer, and Primer Mix) was added, and samples were incubated at 42 °C for 15 min, then 95 °C for 3 min to inactivate Reverse Transcriptase.

2.2.13.3 RT-PCR

Using a customised SYBR® Green-optimised RT^2 Profiler PCR Array (Qiagen) with RT^2 qPCR primer assays (Qiagen; Table 10), a RT-PCR was performed in a 384-well plate format using the ViiA™ 7 Real-Time PCR System (Applied Biosystems). Using a fast qPCR program, the incubation cycling parameters included an initial activation step of 95 °C for 2 min, followed by 40 cycles of 95 °C for 3 sec and final primer-specific steps of 60 °C for 1 min. Data analysis was based on comparative Ct (ΔΔCt) method normalised by housekeeping genes.

Table 10. Primers used in RT-PCR

Name	Symbol	NCBI Gene ID	Supplier	Cat No.
Myogenin	MYOG	4656	Qiagen	PPH07162C
Myosin Heavy Chain 2	MHC2	4620	Qiagen	PPH23817B
Troponin Type 3	TNNT3	7140	Qiagen	PPH09881A
β-2 Microglobulin	β2M	567	Qiagen	PPH01094E

2.2.14 Glucose Uptake (Flow Cytometry)

2–(N–[7–Nitrobenz–2–oxa–1,3–diazol–4–yl] Amino)–2–Deoxyglucose (2–NBDG), a fluorescent analogue of glucose, was used to indicate glucose uptake into HSMM cells. As per previously established laboratory protocols

[435], post-treatment cells were washed with PBS then challenged for 20 min with or without 100 nM of Insulin and 100 µM of 2-NBDG at 37 °C with 5% CO_2, protected from light. The cells were washed again with PBS, then harvested using 0.25% trypsin. The cells were pelleted via centrifugation, then resuspended in 1 mL of fresh PBS. All samples were vortexed for 1 min, transferred to 5 mL flow cytometer tubes then briefly kept on ice. A BD LSRFortessa Flow Cytometer (BD Biosciences) was used to analyse the stained cells. Using a minimum of 10000 events, cell debris, aggregate cell populations and PI positive cells (PI Staining; 2.2.9, page 55) were excluded via gating and single cell populations were shown on a histogram displaying event count versus 2-NBDG fluorescence. Using FloJo v10 Software, the intensity of 2-NBDG staining was identified as the geometric mean.

2.2.15 Data Analysis

All experiments were performed a minimum of three times in duplicate. Statistical analysis was performed using GraphPad Prism Version 8 software. Data underwent normality testing and if found to be normally distributed, one-way ANOVA with Tukey multiple comparisons Post-Hoc testing were performed to compare means between groups. If found to not be normally distributed, the equivalent nonparametric Kruskal-Wallis test with Dunn's Post-Hoc testing was used to compare the mean rankings of each group instead. Two-way ANOVA was with Sidak's multiple comparisons Post-Hoc testing was used to determine changes between groups over time. All graphed data is expressed as mean ± standard error of the mean (SEM). Statistical significance limit was set at 0.05 or less ($p \leq 0.05$).

CHAPTER 3 Exacerbation of Pancreatic Islet Pathology in a Mouse Model Expressing Both Human APP and IAPP

3.1 Abstract

Type 2 diabetes (T2D) and Alzheimer's disease (AD) are related chronic metabolic diseases that feature aggregated amyloid peptides in vital tissues, such as the brain in AD and the pancreas in T2D. Aggregation of amyloidogenic peptides is associated with cellular dysfunction and death. Recent studies suggest that AD-associated beta-amyloid (Aβ) and the T2D-associated islet amyloid polypeptide IAPP may co-localise not only in the brain, but also in insulin-producing pancreatic islets. The consequences of the combination of IAPP and Aβ in pancreatic islets are yet to be fully determined. The purpose of the study described in this chapter was to investigate the effect of human IAPP and Aβ on pancreatic islets in a novel double transgenic (DTG) mouse model expressing human APP and human IAPP. Pancreatic tissue from high-fat-fed 16- or 24-week-old mice was analysed using immunostaining and fluorescent microscopy to detect changes in amyloid aggregation, islet morphology, islet function, and inflammation. Amyloid aggregation only occurred in IAPP and DTG mice, with exacerbated amyloid accumulation in DTG mice. The severity of amyloid aggregation was strongly correlated with reductions in islet insulin and increases in islet inflammation. Furthermore, DTG mice had small but significant increases in islet size and apoptotic markers. Tau loading decreased in all groups over time with exposure to the high-fat diet. These findings provide support *in vivo* that the combination of human IAPP and Aβ exacerbates amyloid accumulation and cellular dysfunction in islets.

3.2 Introduction

T2D and AD share many common pathological features, including oxidative stress, chronic inflammation, insulin signalling dysfunction, and amyloid plaque deposition [9, 155, 173]. Furthermore, patients with T2D have an increased risk of developing AD, while patients with AD have an increased risk of developing insulin resistance in peripheral tissues, a hallmark of T2D [2-4]. With an increasingly ageing population and global cases of T2D and AD expected to increase in the coming years, it is important to investigate the pathological relationship between these two seemingly unrelated diseases [1, 5].

A potential link involves the aggregation and accumulation of toxic amyloidogenic peptides (IAPP and Aβ) into plaque in vital organs. IAPP is known to co-secrete with insulin from pancreatic β-cells and cross the BBB to co-deposit with local deposits of Aβ [24, 436]. Likewise, Aβ has been found to co-deposit with IAPP in pancreatic islets [25]. Although there is evidence of co-deposition / interaction of IAPP with Aβ, few studies have investigated the consequences of such events. An *in vitro* study has reported that IAPP-Aβ heterocomplexes enhance neurotoxicity [129]. *In vivo* studies have been hampered by the lack of appropriate animal models, as unlike human IAPP and Aβ, rodent IAPP and Aβ are non-amyloidogenic and do not aggregate [437]. To overcome these challenges, Wijesekara et al. [247] developed a double transgenic mouse model (DTG) to express both human Aβ and IAPP.

To generate this model, a transgenic human APP mouse model featuring increased Aβ expression in the brain [417] was crossbred with another transgenic mouse model featuring overexpression of human IAPP from pancreatic tissue [418], producing DTG offspring with both characteristics, as detailed in Chapter 2 (2.1.1, page 43), Table 1, and Wijesekara et al [247]. Initial characterisation revealed exacerbated pathological features of human T2D and AD [247]. The DTG mice (fed a high-fat diet from 3 weeks of age) were diabetic, with marked hyperglycaemia, peripheral insulin resistance, and exacerbated pancreatic amyloid. The DTG mice also showed reduced brain insulin signalling, neurodegeneration, and elevated cerebral amyloid and Tau

pathology. In addition, Wijesekara et al. presented some evidence of accumulation of pTau, in the islets of DTG mice. However, while highly expressed in pancreatic islets, the role of Tau in islet function is unclear [438, 439].

This thesis aims to provide mechanistic insight into the consequences of Aβ-IAPP interactions with a particular focus on β-cell function. The current chapter begins to address this overall aim *ex vivo* by using pancreatic tissue from the same DTG mice developed by our collaborator Professor Paul Fraser and described in Wijesekara et al. [247] and Appendix B (8.2, page 235), as well as tissue from the single transgenic human APP and IAPP mice, and nontransgenic littermates. This thesis expands upon the analysis of islet size, amyloid severity, islet insulin, and tau pathology performed by Wijesekara and team by examining these factors among all groups, and at both 16 and 24 weeks of age. In addition, new analyses were added to investigate markers of cell stress and inflammation to provide further insight into potential mechanisms underlying the exacerbated islet pathology associated with IAPP and Aβ accumulation.

3.3 Aim

To assess morphology, insulin content, amyloid accumulation, and cellular stress in pancreatic islets from transgenic mice expressing both human IAPP and APP (DTG) and compare with those observed in mice expressing only APP, IAPP, or nontransgenic littermates.

3.4 Materials and Methods

3.4.1 Pancreatic Tissue Samples

Paraffin-embedded pancreatic tissue samples of 16- or 24-week-old DTG, APP, IAPP, and nontransgenic (NT) mice were obtained from Prof. Paul Fraser and colleagues at the University of Toronto. Samples had been prepared by mounting three 5 μM thick, consecutively sliced sections of pancreatic tissue per microscopic slide, with four slides provided per animal. Mice were fed a high-fat diet from 3 weeks of age, then sacrificed at either 16 or 24 weeks

(Murine Models; 2.1.1, page 43). Findings on relevant parameters related to β-cell function and peripheral insulin sensitivity are described in Wijesekara et al. [247] and Appendix B (8.2, page 235).

3.4.2 Experimental Design

Tissue slides underwent De-Paraffinisation and Rehydration (2.1.2, page 44) and Antigen Retrieval (2.1.3, page 44) before Immunofluorescent Staining (2.1.5, page 45) for specific markers of β-cell morphology function and stress to determine changes between groups. An anti-insulin antibody was used to identify islets and insulin content. ThioS staining was used to identify amyloid aggregation. Anti-ionized calcium binding adapter molecule 1 (IBA1) antibody was used to identify the presence of macrophages. Despite IBA1's more common use as a marker of activated microglia in the brain, multiple studies have validated its use as a "pan-macrophage" marker in many peripheral tissues across multiple species, including specifically in pancreatic islets [440-447]. Anti-cleaved caspase-3 (Active Cas3) antibody was used as a marker of cell apoptosis. Anti-Tau antibody was used to detect Tau loading in pancreatic islets, while Anti-pTau (AT8) antibody detecting phosphorylation at the Ser202 and Thr205 residues was used to detect Tau pathology. This pTau antibody was selected as phosphorylation of Tau at the Ser202 and Thr205 residues is correlated with Aβ-induced pathology and the progression of AD [448, 449]. Primary and secondary (isotype) antibody controls were performed a minimum of three times each to confirm specific staining of pancreatic tissue.

As consecutive sections allowed for comparative investigation of the same islets in multiple sections, the first section of each slide was probed with anti-insulin antibody and ThioS to allow identification of islets and amyloid loading, followed by immunofluorescent antibodies in the second and third sections (Table 11). The experimental design per microscopic slide was as follows:

Table 11. Experimental Design of Immunofluorescent Markers

Slide Number	Section 1	Section 2	Section 3
1	Insulin / ThioS	Active Cas-3	IBA1
2	Insulin / ThioS	Tau	pTau

3.4.3 Imaging, Quantification and Statistical Analysis

Microscopic Imaging (2.1.8, page 46) was performed using a Nikon A1 confocal microscope, with a minimum of five islets per section randomly selected for investigation. Image J software was used for Image Quantification and Data Analysis (2.1.9, page 47). Each individual islet was isolated by gating and then quantified and the islet area (micron^2), the percentage of islet area stained, the intensity of the staining (mean grey value), and the integrated density (intensity * total area of staining) were identified. These results were graphed as individual islets per group and as the average per animal within each group. The results are displayed as mean ± standard deviation and GraphPad Prism software was used for statistical analysis. If data was normally distributed, one-way ANOVA with Tukey multiple comparisons Post-Hoc testing were performed to compare means between groups. If data was not normally distributed, equivalent nonparametric (e.g. Kruskal-Wallis test with Dunn's Post-Hoc) tests were instead. Two-way ANOVA tests with Sidak's multiple comparisons Post-Hoc testing were used to determine changes between groups at 16 and 24 weeks. Significance was determined as $P > 0.05$.

3.5 Results

3.5.1 Reduced islet insulin and increased islet size in pancreatic islets of DTG mice

Initial investigations aimed to determine changes in the morphology and functioning of islets in the mouse models. Insulin levels and islet size were assessed in pancreatic tissue of NT, APP, IAPP, and DTG mice by immunostaining with anti-insulin antibody. On observation, the islets appeared larger and exhibited less intensity of insulin staining in IAPP and DTG mice compared to NT and APP mice (Figure 10A). The islets of the IAPP mice appeared enlarged at 24 weeks, while in DTG mice, enlarged islets were observed at both 16 and 24 weeks.

For quantitative analysis, the 'islet size' (mean islet area in microns^2) was measured. Despite observed trends, a two-way ANOVA revealed no significant changes in mean islet size between groups or between time points (Figure 10B). The mean intensity of insulin staining in DTG mice was

significantly reduced compared to NT mice at both 16 ($p = 0.0009$) and 24 weeks ($p = 0.0375$), with no significant changes between time points (Figure 10C). The 'insulin coverage' (percentage of the islet area stained for insulin) was significantly reduced in DTG mice compared with APP mice at 16 weeks ($p = 0.0109$; Figure 10D) and NT at both 16 weeks ($p = 0.0001$) and 24 weeks ($p = 0.0051$). There were no further alterations in mean insulin coverage between 16 and 24 weeks.

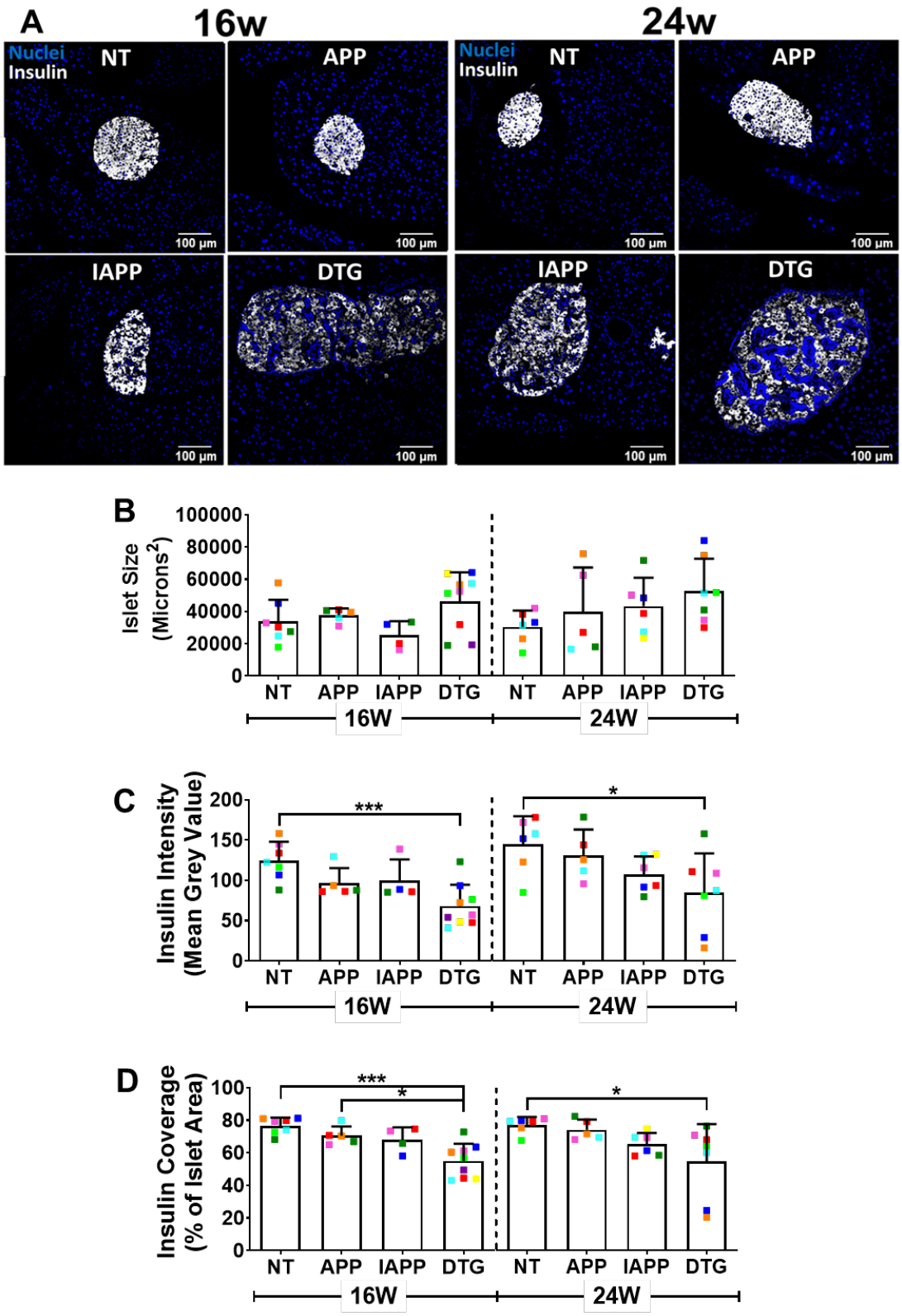

Figure 10. Crossbred double transgenic APP x IAPP mice have reduced islet insulin compared to single transgenic APP, IAPP, and nontransgenic littermates. Paraffin sections were generated from pancreatic tissue of 16- and 24-week-old mice and stained with anti-insulin antibody. (A) Representative islet images of insulin staining (anti-insulin antibody; white) and cell nuclei (Hoescht stain; blue) at 20X magnification, with scale bar set at 100 µm.

Quantitation of other parameters representative of insulin staining and islet health were performed and represented as mixed bar / scattergrams, including the mean islet size (microns^2; B), mean fluorescent intensity of insulin staining (mean grey value; C) and mean percentage (%) of islet area stained with insulin ('insulin coverage'; D) per animal. Each coloured data point represents an individual animal. All data represented as mean ± SD. N = 4-9 animals per group. NT = nontransgenic, APP = human APP transgenic, IAPP = human IAPP transgenic, DTG= human APP x IAPP double transgenic. Statistical analysis via two-way ANOVA with Tukey to determine variation between groups (*), and Sidak's multiple comparisons testing to determine variation between 16 and 24 weeks ($^{\#}$). $^{\#}$ / *p value=≤0.05, $^{\#\#}$ / **p value=≤0.01, $^{\#\#\#}$ / ***p value=≤0.001, $^{\#\#\#\#}$ / ****p value=≤0.0001.

During analysis, a large intra-animal variation of islet size and insulin loading was observed. To determine whether trends in islet size / insulin between groups were masked when calculated as mean per animal due to this variation, the results were also quantified as the total islets per group (Figure 11). Subsequently, islet size was significantly increased in DTG islets compared to NT islets at 24 weeks ($p = 0.026$; Figure 11A). The intensity of insulin staining in DTG islets was significantly reduced compared to all other groups at both 16 weeks ($p < 0.0001$ vs NT, 0.088 vs APP, and 0.0004 vs IAPP) and 24 weeks ($p < 0.0001$ vs NT, 0.0001 vs APP, and 0.0276 vs IAPP; Figure 11B). IAPP islets also had a significant reduction in insulin intensity compared to NT islets at 24 weeks ($p = 0.0010$).

Similarly, DTG islets showed a significant reduction in insulin coverage compared to all other groups at both 16 weeks ($p < 0.0001$ vs NT, p 0.0003 vs APP, 0.0104 vs IAPP) and 24 weeks ($p < 0.0001$ vs all; Figure 11B). Additionally, the IAPP islets also had a significant reduction in insulin coverage compared to the NT islets at both 16 weeks ($p = 0.0060$) and 24 weeks ($p < 0.0001$). However, there was no significant change in insulin coverage within any group between the 16- or 24-week time points. Overall, this data indicates that compared to the other mouse models, DTG mice / islets had reductions in islet insulin content and a trend toward an increase in islet size.

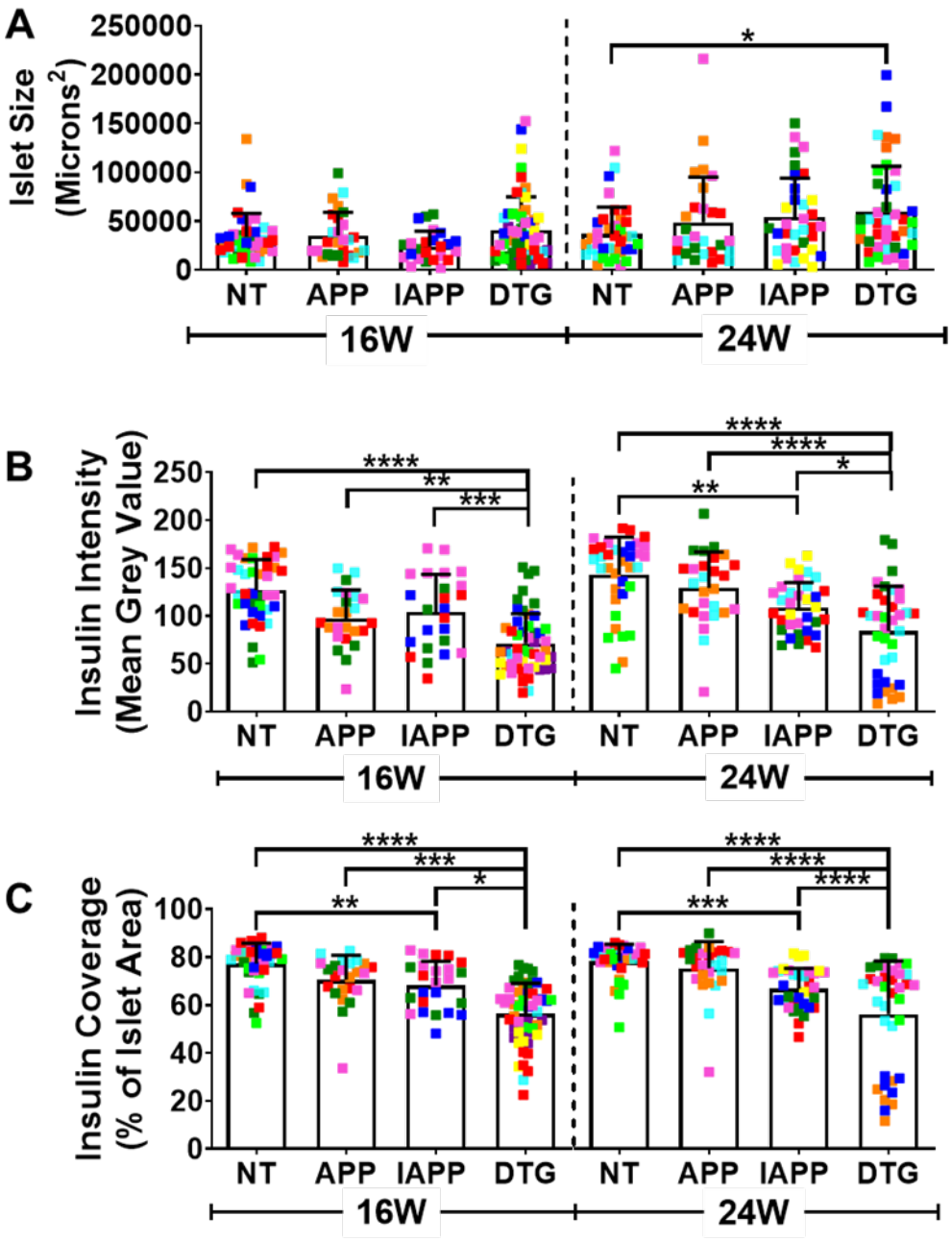

Figure 11. Individual islets of double transgenic APP x IAPP mice have exacerbated islet insulin dysfunction compared to islets of transgenic IAPP littermates. A re-examination of insulin staining parameters of 16- and 24-week-old mice, including islet size (microns; A), fluorescent intensity of insulin staining (mean grey value; B), and insulin coverage (%; C), was performed and represented as mix bar / scattergrams. Each data point represents an individual islet and each colour represents an individual animal within the group. N = 4-9 animals per group. NT = nontransgenic, APP = human APP transgenic, IAPP = human IAPP transgenic, DTG= human APP x IAPP double transgenic. Statistical analysis via two-way ANOVA with Tukey multiple comparisons testing to determine variation between groups (*), and Sidak's multiple comparisons testing to determine variation between 16 and 24 weeks ($^{\#}$), except for Islet Size (A) which was not normally distributed and nonparametric Kruskal-

Wallis test with Dunn's Post-Hoc was used instead . # / *p value = ≤0.05, ## / **p value = ≤0.01, ### / ***p value = ≤0.001, #### / ****p value = ≤0.0001.

3.5.2 Extensive amyloid aggregation in pancreatic islets of DTG mice

To determine whether reductions in insulin content were related to amyloid burden, the sections were stained with Thioflavin S (ThioS). Only IAPP and DTG mice showed any observable presence of amyloid aggregation (Figure 12A). As such, an unpaired T-Test determined that DTG mice had a significantly increased mean amyloid burden (the mean percentage of islet area stained with ThioS) compared to IAPP mice at 16 weeks ($p = 0.0252$; Figure 12B). Furthermore, a two-way ANOVA revealed a strong but not significant trend toward an increase in amyloid burden over time between 16 and 24 weeks in DTG mice ($p = 0.0521$). As with islet insulin, a large amount of intra-animal variation between islets was observed, so the total islets per group were also analysed (Figure 12C). The DTG islets had a significantly increased amyloid burden compared to the IAPP islets at 16 weeks ($p < 0.0001$) and 24 weeks ($p = 0.0043$), with a significant increase between the two time points ($p = 0.011$;), indicating increased severity over time.

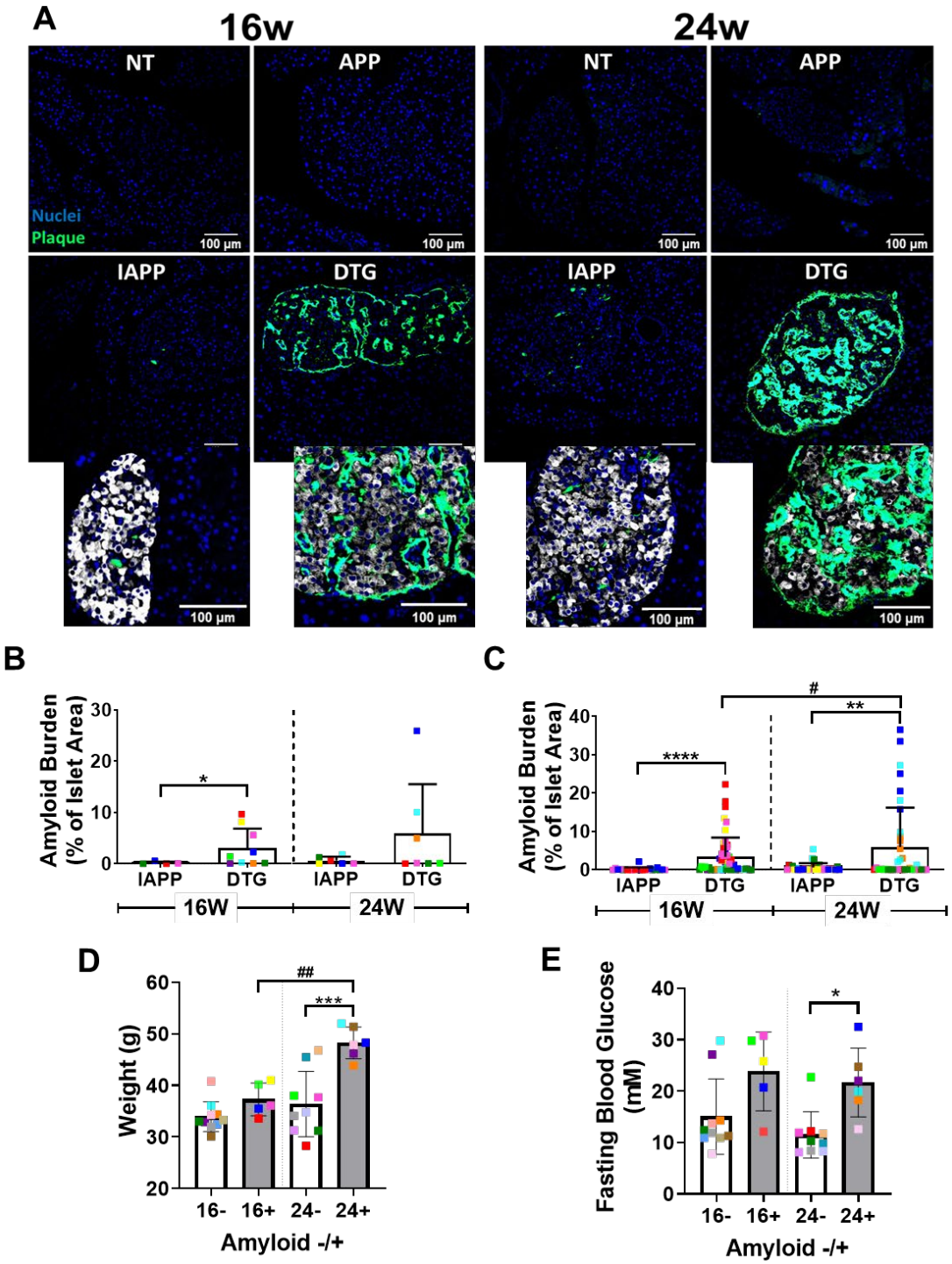

Figure 12. Amyloid burden is exacerbated in double transgenic APP x IAPP mice compared to single transgenic IAPP littermates. Paraffin sections generated from pancreatic tissue of 16- and 24-week-old mice were stained with Thioflavin S (ThioS) compound to detect the presence of amyloid proteins in pancreatic islets. (A) Representative islet images of amyloid aggregation (ThioS; green) and cell nuclei (Hoescht stain; blue) at 20X magnification, including magnified images of amyloid aggregation in the same IAPP and DTG islets including insulin staining (white). Scale bar is set at 100 µm in all images. The percentage area of islets stained positively with ThioS, called “amyloid burden”, in islets was quantified

and represented as mixed bar / scattergrams, showing the mean amyloid burden per animal (B), where each coloured data point represents an individual animal. Data was also plotted as the amyloid burden of total islets per group (C), where each data point represents an individual islet and is colour-coded to match individual animals of graph B. All data represented as mean ± SD. N = 4-9 animals per group, NT = nontransgenic, APP =human APP transgenic, IAPP = human IAPP transgenic, DTG= human APP x IAPP double transgenic. Statistical analysis via nonparametric Mann Whitney U test due to non-normal distribution (*) to determine variation between groups, and two-way ANOVA with Sidak's multiple comparisons testing to determine changes between 16 and 24 weeks ($^{\#}$). To determine what distinguishes the DTG mice that do develop amyloid (+) and those that do not (-), additional DTG phenotype data including weight (D) and fasting blood glucose (FBG; E) was stratified by amyloid status and investigated at 16 and 24 weeks. Data was quantified and represented as mixed bar / scattergrams, where each coloured data point represents an individual animals. Statistical analysis was performed via two-way ANOVA with Tukey multiple comparisons test to determine variation between groups (*), and Sidak's multiple comparisons testing to determine variation between 16 and 24 weeks ($^{\#}$). $^{\#}$ / *p value = ≤0.05, $^{\#\#}$ / **p value = ≤0.01, $^{\#\#\#}$ / ***p value = ≤0.001, $^{\#\#\#\#}$ / ****p value = ≤0.0001.

As noted in Figure 12, approximately half of the mice in the IAPP and DTG groups showed the presence of amyloid deposition. To assist in the determination of why some animals developed islet amyloid and other animals of the same transgene group did not, data pertaining to the severity of the diabetic phenotype was investigated, including differences in weight and fasting blood glucose (FBG) between amyloid positive (+) and amyloid negative (-) DTG mice at 16 and 24 weeks (Figure 12D-E). At 24 weeks, DTG mice that developed plaque had significantly increased weight (p=0.0001) and FBG (p=0.0282) compared to those that did not, indicating a relationship between a worsened T2D phenotype and amyloid deposition. Weight of DTG mice with amyloid deposition was also significantly increased over time between 16 and 24 weeks (p=0.0015). Furthermore, the specific animals / islets that developed amyloid aggregation were the same animals with greater variations in islet insulin and size (Figure 11), indicating an association between amyloid accumulation and islet dysfunction. On investigation, islet size had a moderate positive correlation with amyloid burden as determined by Pearson's correlation co-efficient (Figure 13A). Despite this trend, there were no significant differences at either time point in the size of the IAPP or DTG islets that developed amyloid aggregation (IAPP+ / DTG+) compared to

the islets of the same group that did not develop amyloid aggregation (IAPP- / DTG-; Figure 13B).

Insulin intensity was also correlated with amyloid burden, with a moderate negative relationship between the two variables (Figure 13C). Reflecting this relationship, DTG+ islets had a significant reduction in insulin intensity compared to IAPP+ and DTG- islets at both 16 weeks ($p = 0.0224$ vs DTG-, and 0.0121 vs IAPP+) and 24 weeks ($p < 0.0001$ vs DTG-, and 0.0008 vs IAPP+; Figure 13D). Insulin coverage had a similar moderate negative relationship with amyloid burden (Figure 13E), where insulin coverage of 24-week-old DTG+ islets was significantly reduced compared to DTG- islets ($p < 0.0001$; Figure 13F). In essence, amyloid aggregation in DTG islets was associated with a significant decrease in islet insulin and a trend toward an increase in islet size.

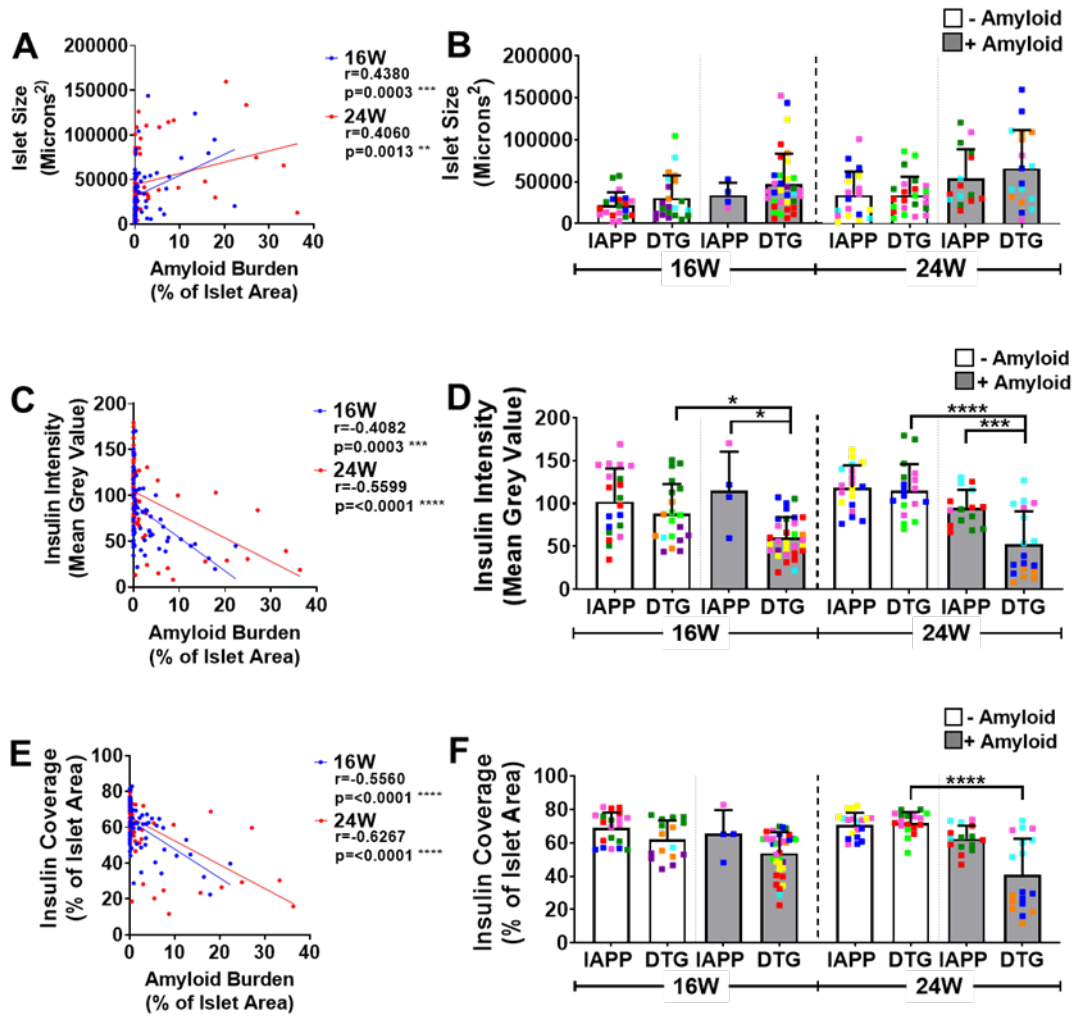

Figure 13. Changes in islet insulin correlated with amyloid burden in islets of double transgenic APP x IAPP mice. Linear regression and correlation analysis of the relationship between amyloid burden vs islet size (A), insulin intensity (C), and insulin coverage (E) in individual islets. Statistical analysis via linear regression and Pearson's correlation test. Correlation explored further via analysis of islet insulin and morphology of IAPP and DTG islets with (+) or without (-) amyloid accumulation at 16 and 24 weeks, including islet size (B), insulin intensity (D) and insulin coverage (F). All data represented as mean ± SD. N = 4-9 animals per group. NT = nontransgenic, APP = human APP transgenic, IAPP = human IAPP transgenic, DTG= human APP x IAPP double transgenic. Statistical analysis via two-way ANOVA with Tukey to determine variation between groups (*), and Sidak's multiple comparisons testing to determine variation between 16 and 24 weeks (#). # / *p value = ≤0.05, ## / **p value = ≤0.01, ### / ***p value = ≤0.001, #### / ****p value = ≤0.0001.

3.5.3 Increased presence of macrophages in islets correlated with increased amyloid burden in DTG mice

To determine whether amyloid accumulation and decreased islet insulin were associated with islet inflammation, the presence of macrophages was investigated by immunostaining with anti-IBA1 antibody (Figure 14A). The mean percentage of islet area stained for IBA1, termed ‘macrophage presence’, was quantified. According to a two-way ANOVA, there was no significant change in the mean macrophage presence in any group at 16 weeks (Figure 14B). At 24 weeks, both IAPP and DTG mice had a significant increase in mean macrophage presence compared to NT mice ($p = 0.0385$ vs IAPP, and 0.0242 vs DTG). When plotting the total islets per group, DTG islets had a significant increase in macrophage presence compared to NT and APP islets at both 16 and 24 weeks (p value=< 0.0001 for all; Figure 14C). At 24 weeks, IAPP islets also had a significant increase compared to NT and APP islets ($p = 0.0009$ and 0.0019 respectively). There was no significant change in macrophage presence between time points.

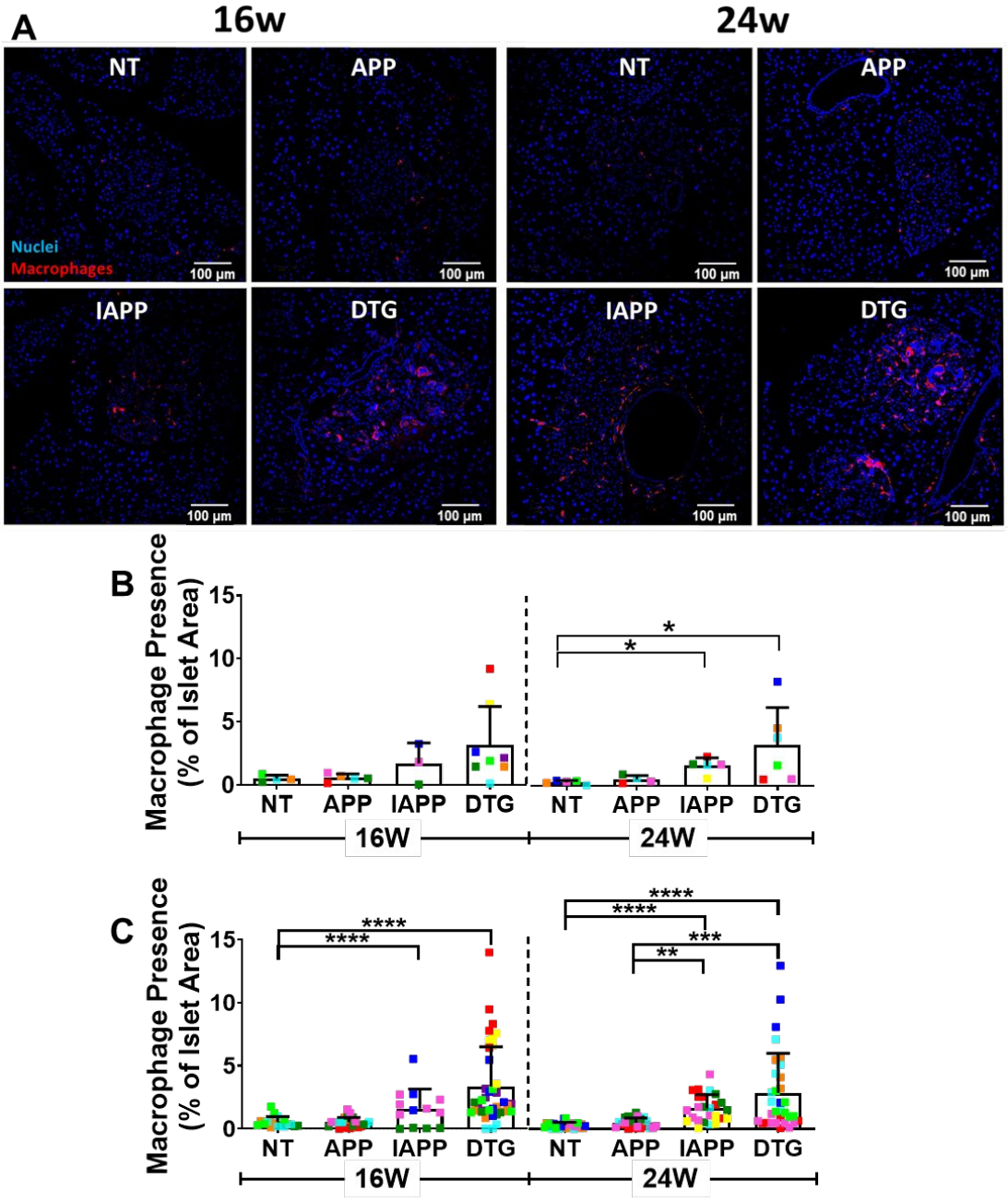

Figure 14. Increased presence of macrophages in islets of single transgenic IAPP and double transgenic APP x IAPP mice. Paraffin sections generated from pancreatic tissue of 16- and 24-week-old mice were stained with anti-IBA1 antibody to detect the presence of macrophages in pancreatic islets. (A) Representative islet images of macrophage presence (IBA1; red) and cell nuclei (Hoescht stain; blue) at 20X magnification, with scale bar set at 100 µm. The percentage area of islets stained positively with IBA1, called IBA1 coverage (%), in islets was quantified and represented as mixed bar / scattergrams, showing the mean IBA1 coverage per animal (B), where each coloured data point represents an individual animal. Data was also plotted as IBA1 coverage of total islets (%) per group (C), where each data point represents an individual islet and is colour-coded to match individual animals of graph B. All data represented as mean ± SD. N = 3-8 animals per group. NT = nontransgenic, APP =

human APP transgenic, IAPP = human IAPP transgenic, DTG= human APP x IAPP double transgenic. Statistical analysis via two-way ANOVA with Tukey to determine variation between groups (*), and Sidak's multiple comparisons testing to determine variation between 16 and 24 weeks (#). # / *p value = ≤0.05, ## / **p value = ≤0.01, ### / ***p value = ≤0.001, #### / ****p value = ≤0.0001.

Co-staining of ThioS and IBA1 showed a distinct overlap and apparent interactions between macrophages and amyloid (Figure 15A). Upon investigation, the presence of macrophages was highly correlated with amyloid burden at 16 and 24 weeks according to Pearson's correlation coefficient (Figure 15B), indicating a strong positive relationship of macrophages and amyloid aggregation in islets. Furthermore, DTG+ islets had a significantly increased macrophage presence compared to DTG- islets at both 16 weeks ($p = 0.0065$) and 24 weeks ($p < 0.0001$; Figure 15C). This data together indicated that the increased aggregation of amyloid in DTG islets was associated with in an increased level of macrophages in the same islets.

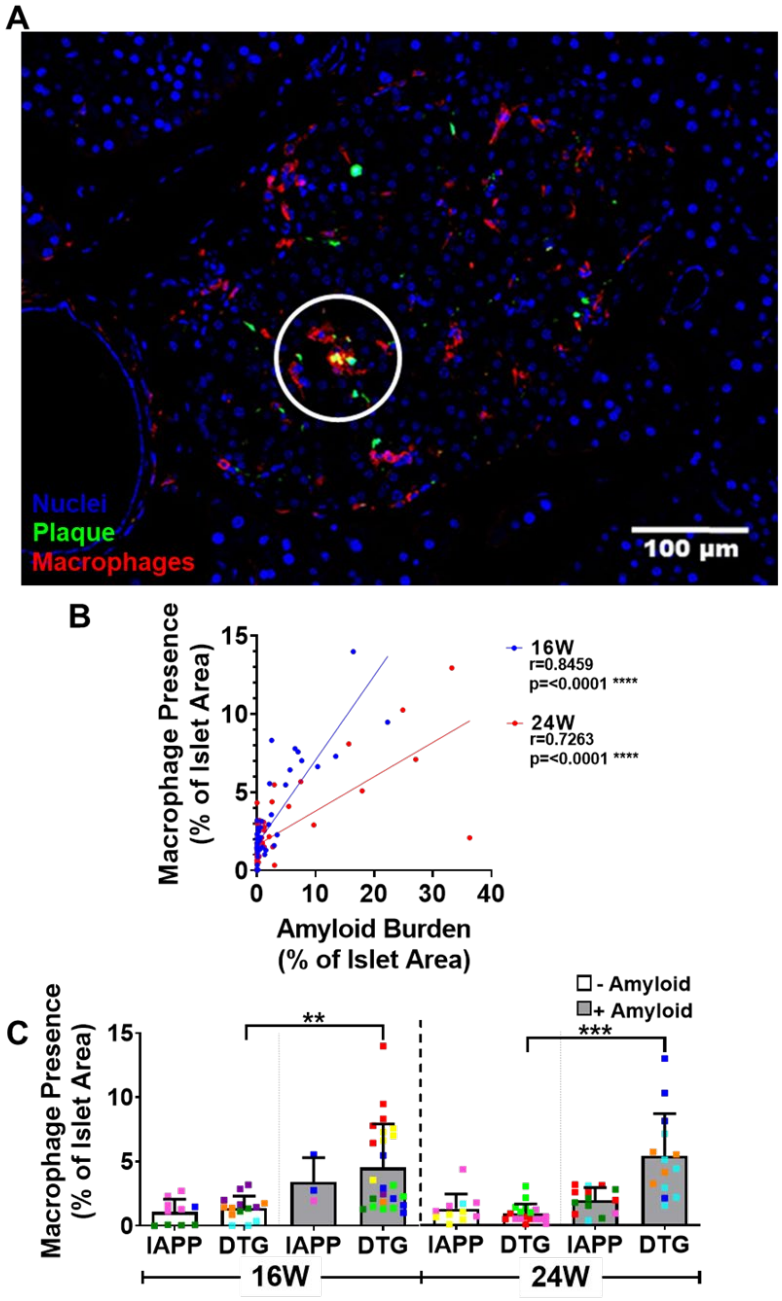

Figure 15. Increased macrophage presence in islets of transgenic IAPP and crossbred double transgenic APP x IAPP mice is highly correlated with increased pancreatic amyloid deposition. Paraffin sections generated from pancreatic tissue of 16- and 24-week-old mice were co-stained with anti-IBA1 antibody and ThioS compound to simultaneously detect the presence of macrophages in pancreatic islets and amyloid aggregation in islets, respectively. (A) A representative islet image of macrophage presence (IBA1; red), amyloid burden (ThioS; green), and cell nuclei (Hoescht stain; blue) at 20X magnification. Linear regression and correlation analysis of the relationship between amyloid burden and IBA1 coverage (B), where each data point represents an individual islet. Statistical analysis via linear regression and Pearson's correlation test. Correlation was explored further via analysis of macrophage presence in IAPP and DTG islets with (+) or without (-) amyloid accumulation

at 16 and 24 weeks (C). All data represented as mean ± SD. N = 3-8 animals per group. NT = nontransgenic, APP = human APP transgenic, IAPP = human IAPP transgenic, DTG= human APP x IAPP double transgenic. Statistical analysis via two-way ANOVA with Tukey to determine variation between groups (*), and Sidak's multiple comparisons testing to determine variation between 16 and 24 weeks (#). # / *p value = ≤0.05, ## / **p value = ≤0.01, ### / ***p value = ≤0.001, #### / ****p value = ≤0.0001.

3.5.4 Reductions in Tau in all groups at 16 and 24 weeks of age.

Tau pathology in the presence of amyloid aggregation in neurodegeneration is well documented. However, despite being expressed in islets [25, 383], its role in islet dysfunction is unclear. To assess the impact of exacerbated amyloid pathology on Tau expression in islets, pancreatic sections underwent immunofluorescent investigation for total Tau and pTau. Initial observations of Tau protein in the pancreatic samples showed extensive, uniform expression in islets of 16-week-old mice, but surprisingly, in 24-week-old mice, Tau expression was reduced and irregular expression in all groups (Figure 16A). The mean Tau coverage (mean percentage of islet area stained for Tau) was quantified, and according to a two-way ANOVA, no significant changes were identified in mean Tau coverage between groups at 16 or 24 weeks (Figure 16B). However, the mean Tau coverage of APP mice was reduced between 16 and 24 weeks ($p = 0.0453$).

The Tau coverage of individual APP islets was significantly increased compared to NT and DTG islets at 16 weeks ($p = 0.0022$ and 0.0295 respectively), but not 24 weeks (Figure 16C). In addition, Tau coverage of islets was decreased over time in all groups between 16 and 24 weeks ($p = 0.0243$ vs NT, < 0.0001 vs APP, 0.0002 vs IAPP; and 0.0004 vs DTG). Moreover, it was observed that at 16 weeks, islets exhibited higher deviation from mean and a greater range in Tau coverage than 24-week-old islets (Figure 16B and C). Tau coverage was not correlated with severity of plaque burden at either time point, with no difference between IAPP and DTG islets with or without amyloid aggregation (Figure 17A and B).

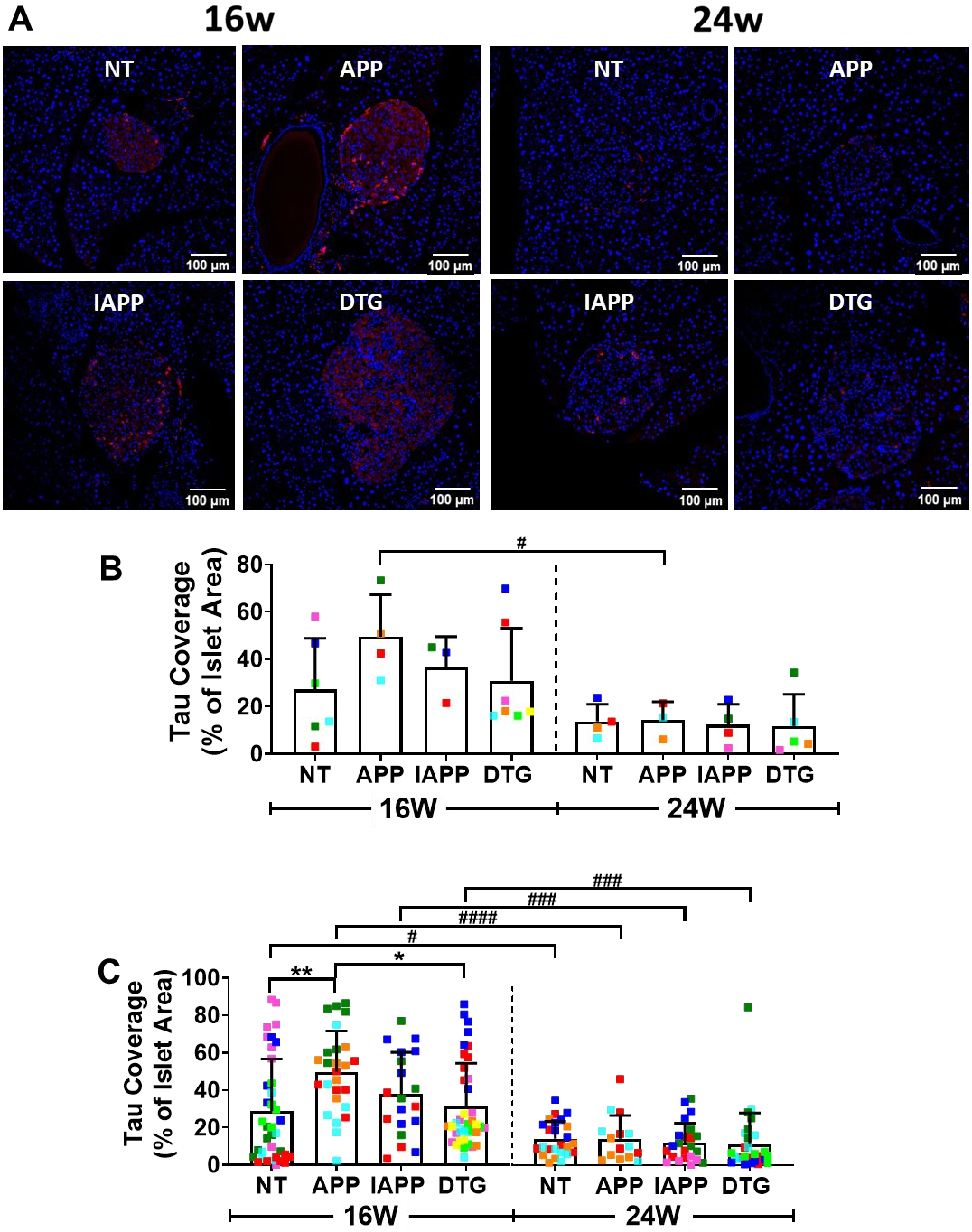

Figure 16. Tau load is reduced in islets of nontransgenic, transgenic APP, transgenic IAPP, and double transgenic APP x IAPP mice between 16 and 24 weeks. Paraffin sections were generated from pancreatic tissue of 16-and 24-week-old mice and stained with anti-Tau antibody to detect Tau protein in pancreatic islets. (A) Representative islet images of Tau staining (anti-Tau antibody; red) and cell nuclei (Hoescht stain; blue) at 20X magnification. The percentage area of islets stained positively with Tau, called Tau Coverage (%), in islets was quantified and represented as mixed bar / scattergrams, showing the mean Tau Coverage per animal (B), where each coloured data point represents an individual animal. Data was also plotted as Tau Coverage of total islets per group (C), where each data point represents an

individual islet and colour-coded to match individual animals of graph B. All data represented as mean ± SD. N = 3-7 animals per group. NT = nontransgenic, APP = human APP transgenic, IAPP = human IAPP transgenic, DTG= human APP x IAPP double transgenic. Statistical analysis via two-way ANOVA with Tukey to determine variation between groups (*), and Sidak's multiple comparisons testing to determine variation between 16 and 24 weeks (#). # / *p value = ≤0.05, ## / **p value = ≤0.01, ### / ***p value = ≤0.001, #### / ****p value = ≤0.0001.

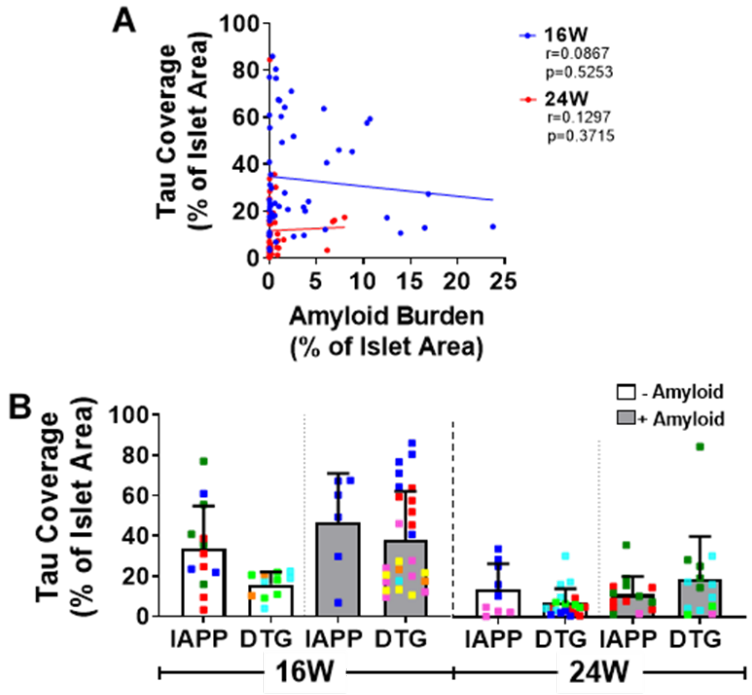

Figure 17. Tau coverage is not correlated with amyloid burden in islets of transgenic IAPP and double transgenic APP x IAPP mice. Linear regression and correlation analysis of the relationship between amyloid burden and Tau Coverage (%) (A), where each data point represents an individual islet. Statistical analysis via linear regression and Pearson's correlation test. Correlation explored further via analysis of Tau Coverage (%) in IAPP and DTG islets with (+) or without (-) amyloid accumulation at 16 and 24 weeks (B). All data represented as mean ± SD. N = 3-8 animals per group. NT = nontransgenic, APP = human APP transgenic, IAPP = human IAPP transgenic, DTG= human APP x IAPP double transgenic. Statistical analysis via two-way ANOVA with Tukey to determine variation between groups (*), and Sidak's multiple comparisons testing to determine variation between 16 and 24 weeks (#). # / *p value = ≤0.05, ## / **p value = ≤0.01, ### / ***p value = ≤0.001, #### / ****p value = ≤0.0001.

In summary, Tau loading decreased over time in all groups and was not impacted by amyloid aggregation. In addition, immunofluorescent investigation of pTau in pancreatic islets was also attempted, however (despite isotype and antibody control testing confirming specific staining) intra-islet pTau staining

was weak and present in a minimal number of islets (Appendix D; 8.4, page 237)

3.5.5 Markers of apoptosis are increased in DTG mice, but not correlated with amyloid burden

To examine if the inflammation, amyloid aggregation, and alterations in islet morphology resulted in β-cell distress, a marker of apoptosis, Active Cas3, was investigated (Figure 18A). The 'Active Cas3 coverage' (percentage of islet area stained for Active Cas3) was initially quantified as the mean per animal (Figure 18B). According to a two-way ANOVA, there was no significant difference in mean Active Cas3 coverage per animal between any of the groups or across the time points. However, a trend toward an increase in IAPP mice compared to APP mice at 16 weeks ($p = 0.0593$) was observed. When plotted as total islets per group (Figure 18C), IAPP islets had a significant increase in Active Cas3 coverage compared to APP mice at 16 weeks ($p < 0.0001$). DTG islets had an increased Active Cas3 coverage compared to APP mice at both 16 weeks and 24 weeks ($p < 0.0001$ and 0.0300 respectively).

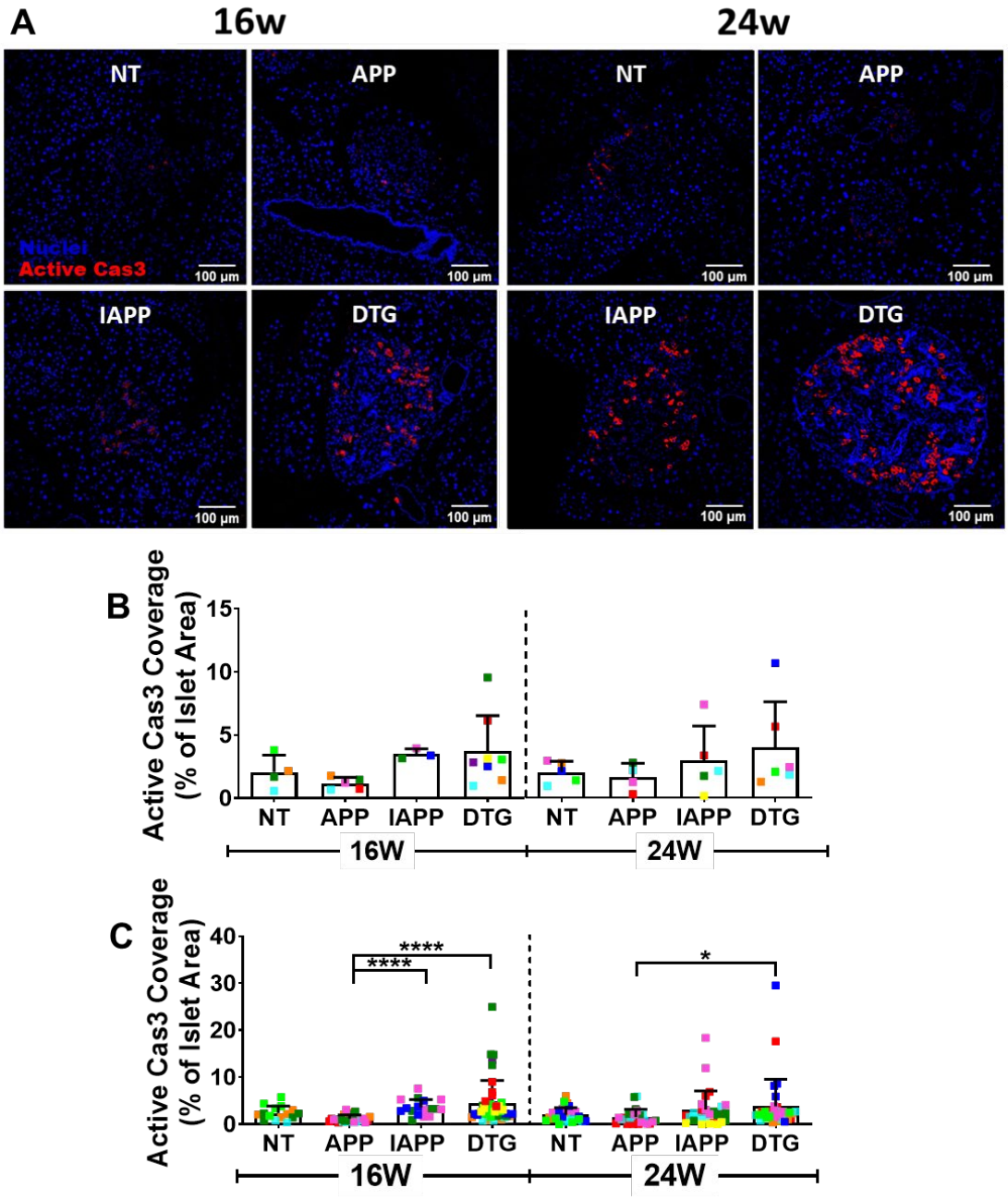

Figure 18. Increased activated caspase-3 in islets of crossbred double transgenic APP x IAPP mice. Paraffin sections were generated from pancreatic tissue of 16- and 24-week-old mice and stained with anti-Cleaved caspase-3 (Active Cas3) antibody to detect apoptosis in pancreatic islets. (A) Representative islet images of apoptosis (anti-Active Cas3 antibody; red) and cell nuclei (Hoescht stain; blue) at 20X magnification, with scale bar set at 100 µm. The percentage area of islets stained positively with Active Cas3, called Active Cas3 Coverage (%), in islets was quantified and represented as mixed bar / scattergrams, showing the mean Active Cas3 Coverage (%) per animal (B), where each coloured data point represents an individual animal. Data was also plotted as Tau Coverage (%) of total islets per group (C), where each data point represents an individual islet and colour-coded to match individual animals of graph B. All data represented as mean ± SD. N = 3-8 animals per group. NT =

nontransgenic, APP = human APP transgenic, IAPP = human IAPP transgenic, DTG= human APP x IAPP double transgenic. Statistical analysis via two-way ANOVA with Tukey to determine variation between groups (*), and Sidak's multiple comparisons testing to determine variation between 16 and 24 weeks (#). # / *p value = ≤0.05, ## / **p value = ≤0.01, ### / ***p value = ≤0.001, #### / ****p value = ≤0.0001.

Despite the significant change between some groups, Spearman's rank correlation test identified that Active Cas3 coverage in islets showed no significant relationship with amyloid burden (Figure 19A). Furthermore, there were no significant differences in Active Cas3 coverage between IAPP and DTG islets with or without the presence of amyloid aggregation (Figure 19B). In summary, the percentage of Active Cas3 are increased in DTG islets compared to APP islets, though it is not correlated with the severity of amyloid aggregation. Rather, this appears to be because APP mice had a slightly reduced Active Cas3 expression compared to other groups, though the difference was not significant.

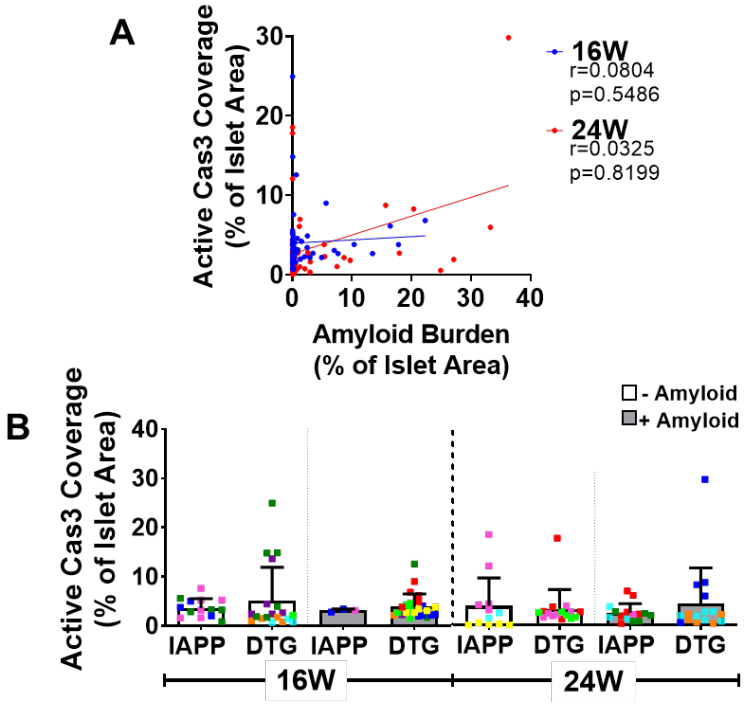

Figure 19. Active caspase-3 is not correlated with amyloid burden is islets of transgenic IAPP and crossbred double transgenic APP x IAPP mice. Linear regression and correlation analysis of the relationship between amyloid burden and Active Cas3 Coverage (A), where each data point represents an individual islet. Statistical analysis via linear regression and Pearson's correlation test. Correlation explored further via analysis of Active Cas3 Coverage (%) in IAPP and DTG islets with (+) or without (-) amyloid accumulation at 16 and 24 weeks

(B). All data represented as mean ± SD. Statistical analysis via two-way ANOVA with Tukey to determine variation between groups (*), and Sidak's multiple comparisons testing to determine variation between 16 and 24 weeks (#).

3.6 Discussion

Several animal models have been used to investigate the association between T2D and AD but have lacked relevant pathological characteristics. AD mouse models often employ the use of human APP transgenes as a solution, although common mouse models of diabetes (for example, using streptozotocin injections to destroy pancreatic β-cells) often lack amyloidogenic IAPP and peripheral insulin resistance, distinguishing characteristics of T2D [6, 416, 450]. The mouse model developed by Wijesekara et al. [247] (Appendix B; 8.2, page 235) employs the use of human APP and IAPP transgenes in a DTG model and therefore represents a more appropriate model for studying the interaction and consequences of pathologies (particularly amyloid pathology) that link T2D with AD. This chapter extends the initial characterisation of pancreatic islet pathology in the DTG model reported by Wijesekara et al., but also provides the first evidence of inflammation and cell death processes that contribute to islet dysfunction in this model.

ThioS staining demonstrated amyloid aggregation in IAPP and DTG mice, where DTG mice had increased amyloid burden compared to IAPP (Figure 12). This was in agreement with previous findings by Wijesekara et al. [247], who found an increase in amyloid severity in 16-week-old DTG mice compared to IAPP mice (Appendix B; 8.2, page 235). Extending the scope of the previous analysis, 24-week-old mice were also examined, though there was no significant increase in amyloid burden between IAPP and DTG mice at this time point, likely owing to the large standard deviation between DTG mice. Further extending the previous study by Wijesekara and team to analyse plaque burden in the individual islets of each group, this study showed that the amyloid burden was increased in both 16 and 24-week-old DTG islets, and this increase was exacerbated over time between 16 and 24 weeks.

Interestingly, not all DTG mice showed amyloid staining (hence, the stratification of the data into amyloid positive and amyloid negative mice /

islets). This was also observed for other parameters measured in this study, although all animals were confirmed to have the same genotype. Therefore, this variation may be due to variation in the expression of the transgene between mice in the same group. Alternatively, the variation may also reflect the individual response of each mouse to the high-fat diet, particularly in the development of insulin resistance. According to Wijesekara et al. [247], insulin resistance in DTG mice was highly variable, which implies that some DTG mice developed more severe insulin resistance than others in the same group despite the shared genotype, likely contributing to an exacerbated total disease burden. In support of this notion, 24-week-old DTG mice with a higher amyloid burden also demonstrated a higher bodyweight and fasting blood glucose (Figure 12C-D).

Major indicators of islet dysfunction often involve alterations in islet insulin content and increases in islet size [451]. Prior analysis by Wijesekara et al. [247] examined islet size in 16-week-old IAPP and DTG mice only, where they found an increase in islet size compared to IAPP mice. To investigate in more depth, insulin staining was performed in all transgene groups, and at both 16 and 24 weeks. In this thesis, insulin staining revealed an increase in average islet size in DTG mice compared to NT littermates, but not other transgene groups. Reasons for this discrepancy may be related to the selection of data for analysis. Wijesekara and team selected fewer mice (3 – 4) per genotype but examined a higher number of islets per mouse (15+). By comparison, we analysed a higher number of mice per genotype (5 – 9), but fewer islets per mouse (5+). As there was significant inter- and intra-animal variation, this could result in the differences between analyses.

To determine if changes in islet size were correlated with amyloid burden, sections were co-stained with the amyloid stain ThioS. However, increases in islet size were only weakly correlated with amyloid burden; and no statistically significant differences in size between islets of DTG mice with (DTG+) or without (DTG-) amyloid aggregation. Evidence suggests that islet size may increase to adapt to / overcome peripheral insulin resistance [451], a phenomenon previously documented in the DTG model, as shown in Appendix B (8.2, page 235). Overall, this suggests the small change in islet size is

potentially more closely correlated with a more advanced state of T2D as a whole than amyloid burden alone. Further research that considers peripheral insulin resistance and its relationship to islet size in this model may be warranted.

Previous analysis of insulin staining by Wijesekara et al. [247] found a reduced 'β-cell area' in islets (insulin intensity normalised by total islet area) of DTG mice. However, this was only investigated at 16 weeks, and only in IAPP vs DTG mice (Appendix B; 8.2, page 235). The analysis of insulin staining was extended in the current study to incorporate all groups at both 16- and 24-week time points. This revealed significant reductions in the intensity and coverage of islet insulin of IAPP and DTG mice at both 16 and 24 weeks (Figure 10; Figure 11). Reduced islet insulin was already present at 16 weeks and did not worsen over time, indicating that alterations in islet insulin began early in the progression of the disease. Furthermore, the relationship between islet insulin and amyloid burden was examined, revealing that amyloid accumulation was significantly correlated with decreases in islet insulin (Figure 13).

Reduced islet insulin in the presence of amyloidogenic peptides is well documented, with IAPP aggregation associated with the loss of β-cells in pancreatic islets of patients with T2D [121, 134]. Recent evidence showing the co-localisation of IAPP and Aβ in human pancreatic tissue has yet to determine the effect of this combined exposure compared to IAPP alone [25, 247]. As the combination of IAPP and APP in islets of these mice shows exacerbated insulin dysfunction compared to those from IAPP mice only. These results are consistent with Bharadwaj et al.'s [129] finding of increased cytotoxicity of combination IAPP-Aβ in neuronal cells (Appendix C; 8.3, page 236). Taken together, this data validates the hypothesis that the combination of both amyloidogenic peptides potentiates cytotoxicity compared to either alone.

Currently, limited evidence is available on the effect of Aβ alone in pancreatic islets. However, studies indicate that regardless of origin, structure, or function, aggregated amyloid peptides such as IAPP and Aβ share common mechanisms of cytotoxicity [2]. These mechanisms involve the formation of abberant pores in cellular membranes, ionic dysregulation, oxidative stress,

and mitochondrial dysfunction [13, 22, 150, 155]. Despite the evidence for aggregation and toxicity of human Aβ, the APP mice did not develop amyloid aggregation or alterations in islet insulin. This finding suggests Aβ may require the presence of IAPP to aggregate in pancreatic islets of DTG mice. Evidence suggests amyloid proteins can function as a seed for misfolding and aggregation of other amyloidogenic peptides, as discussed in Chapter 1 (1.4.6, page 25) [257]. Though ThioS uniformly stains all aggregated amyloid peptides in this study, Wijesekara et al. [247] previously identified Aβ immunoreactivity in the islets of DTG mice only (shown in Appendix B, page 235). The increase in amyloid burden between IAPP and DTG mice further supports this notion, as the higher amyloid burden may be due to both amyloidogenic peptides co-depositing in the islets of DTG mice.

As amyloid aggregation also occurs very early in disease progression in these mice (before 16 weeks), earlier time points could also be a point of future investigation. It is acknowledged as both a benefit and a limitation that this mouse model shows a very aggressive neurodegenerative and diabetic phenotype, occurring early compared to other amyloid mouse models. As a limitation, this aggressive model may limit the threshold at which changes can be detectable, obscuring the sequence of events in disease progression. Crossbreeding IAPP mice with APP knock-in mice that show slower progression of amyloid pathology (e.g. APP NL-F KI [452]) (52 weeks compared to the maximum 24 weeks for APP mice (TgCRND8) used in this study), may be a more relevant model for the goal of investigating changes over time. As this aggressive model was also sustained on a high-fat diet to exacerbate symptoms, a comparison to DTG mice on a normal diet is also advisable to address limitations with this model.

As an alternative explanation for the increase in amyloid burden in DTG mice, the more advanced disease state of DTG mice could be as a result of an increasingly inflammatory environment. Inflammatory cytokines can simultaneously inhibit insulin secretion and increase IAPP expression in β-cells [87, 95, 96, 195]. In the brain, inflammatory cytokines have also been documented to increase Aβ, both through increased production and decreased clearance [283, 351, 352]. Furthermore, the presence of Aβ and IAPP

themselves also result in increased inflammatory cytokine production through their role as DAMPs, contributing to a vicious cycle [200, 453-455]. Essentially, an exacerbated inflammatory environment in DTG mice compared to the other groups could have resulted in increased production and / or decreased clearance of IAPP and / or Aβ peptides in islets, leading to the observed increase in amyloid burden. As this study was limited to pancreatic tissue sections, future studies would benefit from an investigation into alternative tissue samples such as blood samples and pancreatic homogenates to assess pro-inflammatory cytokines in these mouse models, both systemically and localised to pancreatic islets.

Evidence of the increased inflammatory environment in DTG mice is represented by the significant increases in macrophage presence in pancreatic islets of DTG and IAPP mice (Figure 14). Macrophages have a significant role in managing chronic inflammation and removing accumulating proteins and other foreign material through phagocytosis, with increases in macrophages noted in islets of T2D patients [193]. While resident islet macrophages can assist in clearance of amyloids [456-458], when the amyloid burden becomes excessive, circulating macrophages can be recruited to infiltrate the islet [116]. While beneficial in clearing amyloids, macrophages also release pro-inflammatory cytokines that can contribute to a reduction in GSIS [198].

The current study found that an increased presence of macrophages was highly correlated with amyloid burden (Figure 15). Co-staining of amyloid aggregation and macrophages confirmed this, as macrophages were often observed co-localising and interacting with the amyloid. In addition, DTG islets with amyloid aggregation (DTG+) had a significant increase in macrophage presence compared to those without (DTG-), further highlighting the important link between amyloid accumulation and inflammation. IBA1, as a marker of macrophages and activated microglia, allowed for observation of total macrophage involvement in pancreatic islets, as it does not distinguish between resident or recruited macrophages [459]. Future studies may involve investigation into the distinct roles of resident and recruited macrophages in the clearance of amyloid aggregation in DTG mice. Additionally, another

possibility of future study could compare IBA1 staining in pancreatic tissue with brain sections of the same DTG mice.

Another potential commonality of cellular dysfunction in the context of T2D and AD involves Tau protein. Tau, a microtubule-associated protein, is well documented in the pathology of AD for its hyperphosphorylation and accumulation into neurofibrillary tangles [373, 374]. As such, reductions in total Tau in the brain is often seen as beneficial due to the reduced capacity for Tau to become phosphorylated and aggregate [460, 461]. The link between pancreatic islet Tau and T2D pathology in literature is less substantial, though limited studies have shown Tau protein may be expressed in islets [25]. The findings of the current study where Tau is present in islets in all animal models is one of the few studies that have reported the prevalence of Tau in pancreatic islets (Figure 16).

Currently, the function of Tau in pancreatic islets remains to be determined. Tau, as a microtubule stabilising protein, could act to modulate microtubule dynamics in islet β-cells [462] which is essential in insulin production, as disruption could impede the transport of pro-insulin to insulin granules, slowing down insulin biosynthesis [439, 463]. In support of this notion, a study on Tau ablation in the pancreas resulted in reduced islet insulin content, elevated pro-insulin levels, and impaired GSIS in mice, promoting a diabetic phenotype [383]. Tau pathology in islets may affect the recruitment and transport of insulin granules by disrupting the microtubule network in β-cells [464]. Additionally, as IAPP is co-secreted with insulin, this could potentially lead to reduced IAPP secretion and increased intracellular IAPP accumulation and aggregation in β cells [263].

At 16 weeks, islets of APP mice had higher Tau protein loading in islets compared to other mouse models (Figure 16). Evidence suggests that APP can regulate Tau proteostasis in cortical neurons via post-transcriptional mechanisms that were not solely mediated by Aβ production [460]. Essentially, mutant human APP, as seen in APP mice, could affect Tau loading independently of the presence of Aβ aggregation, providing a potential explanation for why the islets of APP mice had increased levels of Tau in the

absence of aggregated amyloid. The effect of an increase in total Tau expression on islet function is yet to be understood, particularly as there were no differences in islet size and islet insulin between NT and APP mice (Figure 10; Figure 11).

Despite extensive expression of Tau in all animal models at 16 weeks, Tau was comparatively reduced in all animal models at 24 weeks (Figure 16). It is known that a high-fat diet can result in metabolic dysfunction and β-cell stress [465]. This could result in the reduction in the expression of Tau (and other proteins) that are essential in healthy β-cell function across all groups over time. A comparison study with a low-fat diet, in addition to further investigation cell stress markers may address this. In addition, the current literature on whether a reduction in total Tau expression is protective or detrimental is mixed and generally limited to AD-associated neuronal studies, not islet Tau expression [466, 467]. Furthermore, it cannot be ruled out that Tau expression in islets is modulated differently under similar external stressors compared to the brain (and the effect of this modulation on cellular function). Further investigation is required to determine the role of tau in islets, and how downregulation of its expression in islets impacts islet function.

Current literature suggest amyloid pathology occurs upstream of Tau pathology in AD, where Aβ accumulation triggers phosphorylation and aggregation of Tau into neurofibrillary tangles, resulting in neuronal loss [468, 469]. Whether a similar mechanism occurs in the islets from DTG is supported by the Wijesekara et al. study [247], which showed a representative figure of evidence for pTau accumulation in the 24wk DTG mouse, but no quantitation (Appendix D, page 237). To address this and complement the total Tau data, the current study extended this to investigate and quantitate the amount of pTau present in islets across 16 and 24 week. Unfortunately, very low pTau staining was observed in islets overall (impacting on the confidence of quantitating small amounts), despite the absence of staining in primary and secondary antibody control images demonstrating the staining present was not artefact (Appendix D; 8.4, page 237). The lack of extensive intra-islet pTau staining could be a result of the lesser ability of murine Tau to pathologically phosphorylate under toxic conditions compared to human Tau. Structural

differences in the N terminal of murine and human Tau reveals that murine Tau does not form neurofibrillary tangles as human Tau does, and though murine Tau is still capable of undergoing abnormal phosphorylation in the presence of aggregated amyloid proteins, the absence of AD-like tauopathy is a limitation of this study [470, 471]. Further studies by Wijesekara et al. [263] confirmed that double transgenic human IAPP and human Tau exhibited exacerbated islet dysfunction compared to transgenic human IAPP mice with murine Tau. Future studies could investigate other transgenic human Tau models in the presence of combined human IAPP-Aβ expression.

Along with the high-fat diet, increases in inflammation and amyloid burden coupled with decreases in islet insulin could predict a significant amount of cellular stress. Active Cas3, a marker of apoptosis, was statistically increased in islets of DTG mice compared to NT littermates. However, unlike the changes in islet insulin and macrophage presence, the increase was not correlated with amyloid burden. The lack of apoptotic cells under apparent stress is possibly a result of “timing”. As amyloid aggregation, inflammation and islet insulin dysfunction are occurring at an early stage in disease progression (before 16 weeks), the majority of islet cell apoptosis could have occurred at an earlier time point, prior to investigation at 16 weeks, or could be occurring at a later time point than 24 weeks. Further studies could investigate additional inflammatory markers, such as IL-1β and TNF-α, and β-cell stress markers upstream of apoptosis, particularly those involving mitochondrial dysfunction [155], including Cytochrome C and HSP60. Moreover, additional time points in the mouse models (or similar models with a slower progression of symptoms) could also be analysed.

In conclusion, amyloid aggregation in pancreatic islets of novel DTG mice expressing both human APP and human IAPP was correlated with increases in intra-islet inflammation and reductions in islet insulin, suggesting significant islet distress and dysfunction. While apoptotic markers such as Active Cas3 were unrelated to amyloid aggregation specifically, they were still increased in DTG mice, likely as a result of the advanced disease state of DTG mice compared to its NT, APP, and IAPP littermates. Additionally, Tau loading in islets was decreased over time in the presence of a high-fat fed diet in all

groups. While reductions in Tau in neuronal cells is primarily thought of as protective, Tau's potential involvement in insulin secretion means this reduction may impact mechanisms of insulin secretion. Overall, the combination of human IAPP and Aβ in DTG mice, exacerbated T2D-like pancreatic islet pathology compared to either human IAPP or human APP alone. These findings support evidence that the combination of IAPP and Aβ may cross-seed to exacerbate amyloidogenic aggregation in pancreatic islets and promote β-cell dysfunction. Potential mechanisms will be explored *in vitro* in the next chapter.

CHAPTER 4 IAPP Cytotoxicity is Potentiated by Co-Aggregation with Aβ in BRIN-BD11 Pancreatic β-Cells

4.1 Abstract

Accumulation of the amyloidogenic peptides, Islet Amyloid Polypeptide (IAPP) and β-Amyloid (Aβ) can disrupt cellular metabolism and bioenergetics, leading to oxidative stress and apoptosis. Findings described in the previous chapter demonstrated that exacerbated amyloid deposition in mice models of IAPP and APP (Aβ) exacerbated islet dysfunction and pathology. To provide a greater understanding of underlying mechanisms, the aim of the work in this chapter was to assess the effect of human IAPP, Aβ aggregates, or a combination of both on the function of the BRIN-BD11 rat pancreatic β-cell line. BRIN-BD11 β-cells were treated with IAPP, Aβ, or a 1:1 IAPP-Aβ combination to determine changes in cell viability, insulin secretion, bioenergetics, and markers of cellular stress. Treatment of cells with the IAPP-Aβ combination significantly exacerbated apoptosis and oxidative stress, and reduced insulin secretion compared to treatment with IAPP or Aβ alone. However, despite being less cytotoxic than the IAPP-Aβ combination, IAPP had a more pronounced and significant effect on mitochondrial function. Aβ alone demonstrated limited toxicity to β-cells. These findings demonstrate the potentiation of IAPP toxicity upon co-incubation and aggregation with Aβ in pancreatic β-cells *in vitro*.

4.2 Introduction

As amyloidogenic peptides, IAPP and Aβ share a propensity for misfolding and aggregating into toxic soluble oligomers and insoluble fibrils, the latter of which accumulate in extracellular spaces as amyloid plaque [472]. IAPP and Aβ also share associations with chronic metabolic diseases, such as T2D and AD [21, 22]. Moreover, recent investigations have revealed IAPP and Aβ can co-localise in pancreatic islets where they cross-seed to form IAPP-Aβ heterocomplexes [25, 129].

Independently, IAPP has long been associated with β-cell dysfunction. Literature shows that IAPP accumulation in the extracellular space of pancreatic islets is cytotoxic to β-cells, as it increases the rate of β-cell apoptosis in a dose-dependent manner [133, 134, 473]. Though unconfirmed, there are several suspected mechanisms of toxicity, including creating a mechanical barrier in the extracellular space [131, 474], disruption of cell membrane leading to ion dysregulation [132], and activation of the extrinsic pathways of apoptosis [201]. While there is extensive literature on the role of IAPP in β-cell dysfunction, there is limited information available on the effect of Aβ aggregates on pancreatic β-cells. However, studies show that Aβ aggregates disrupt neuronal function and viability through similar mechanisms of toxicity to IAPP on β-cells [332, 334], suggesting a potentially similar effect.

Current research indicates that the pre-fibrillar soluble oligomeric aggregates of IAPP and Aβ are more cytotoxic than fibrils [20, 135, 136]. While exerting similar mechanisms of toxicity to fibrils in the extracellular space, the smaller soluble oligomers can also disrupt intracellular processes, particularly mitochondrial function and bioenergetics [13, 155, 157, 475, 476]. Disruption of mitochondrial function is highly detrimental to β-cells, as mitochondria play a vital role in the coupling of glucose-sensing to insulin secretion via glucose metabolism [49]. Additionally, the intracellular accumulation of amyloidogenic oligomers has been hypothesised to deregulate proteostasis, leading to ER stress [214, 477, 478].

Evidence is beginning to indicate that IAPP and Aβ in combination exacerbate amyloid pathology. Post-mortem examinations have revealed that AD patients have an increased frequency and extent of islet amyloid aggregation, while the duration of T2D is directly correlated with the amount of neuronal amyloid plaque [4]. Exposure to oligomeric IAPP-Aβ *in vitro* demonstrated enhanced cytotoxicity compared to IAPP or Aβ oligomers in neuronal cells in a 2020 study by Bharadwaj et al [129] (Appendix C; 8.3, page 236). Additionally, pancreatic load is markedly increased in transgenic mice expressing both human IAPP and APP, where it was associated with reduced islet function [247]. The previous chapter of this thesis further demonstrated that the same double

transgenic mouse model also featured increased inflammation, increased cell stress markers, and reduced islet insulin compared to controls.

Taken together, this data indicates that Aβ may play an important role in β-cell dysfunction and the development of T2D. This current chapter aims to provide insight into mechanisms by which IAPP and Aβ exert their toxicity on β-cells of the pancreatic islet. Pancreatic β-cells from the rat clonal BRIN-BD11 cell line were exposed to oligomeric preparations of IAPP, Aβ and IAPP-Aβ *in vitro* to assess changes in β-cell viability, insulin secretion, mitochondrial function, and overall cellular stress.

4.3 Aim

To investigate the effect of oligomeric aggregations of human Aβ, IAPP, or the combination of both on BRIN-BD11 β-cell function and cellular metabolism.

4.4 Materials and Methods

4.4.1 Amyloidogenic Peptide Preparation

Preparation of amyloidogenic peptides is described previously (2.2.1, page 48) as per established protocols [129, 419, 420]. Briefly, synthetic powdered human IAPP and Aβ was solubilised in HFIP, then dried and stored as homogenous peptide films. When required, Aβ or IAPP peptide films were resolubilised in 20 µL of DMSO, then sonicated, centrifuged, and diluted in 980 µL of Phenol Red-free Ham's F-12 media (2% v / v of DMSO) to a final concentration of 100 µM IAPP or Aβ. To create an IAPP-Aβ combination, the IAPP peptide solution was combined with Aβ peptide solution at a 1 : 1 ratio of v / v, producing an IAPP-Aβ combination solution with a final concentration of 50 µM IAPP + 50 µM Aβ. The amyloid stock solutions were then stored at 4°C overnight to allow appropriate aggregation of amyloidogenic peptides into soluble oligomeric species, as per established protocols [129, 419, 420]. Following the incubation, the 50 µM IAPP + 50 µM Aβ combination solution was referred to as "100 µM of IAPP-Aβ" and was compared to an equivalent volume of 100 µM homogenous IAPP or Aβ peptides. For example, 10 µM of homogenous IAPP or Aβ peptide treatment would be compared to "10 µM" of

IAPP-Aβ combination peptide treatment, containing 5 μM of IAPP + 5 μM of Aβ aggregated into heterogenous IAPP-Aβ oligomeric species.

4.4.2 Cell Culture

The rat clonal pancreatic β-cell line, BRIN-BD11, was cultured in RPMI-1640 growth medium supplemented with 11.1 mM glucose, 2 mM glutamine, 10% FBS and 1% penicillin streptomycin at 37 °C in a humidified atmosphere of 5% CO_2 (2.2.2.1, page 48). BRIN-BD11 cells have a doubling time of less than 20 h [421], and were maintained in a sub-confluent state (below 70-80 % confluency) until experimentation, with regular changes of growth medium every 2-3 days. As an immortal cell line, BRIN-BD11 cells are viable up to passage 50 [421] but passages above 40 were not used in this project. Prior to treatment, BRIN-BD11 cells were subcultured and counted (2.2.2.4, page 49), then seeded at optimised cell densities into cell culture plates with fresh RPMI-1640 medium and left to adhere overnight. After overnight incubation, supernatant was changed to RPMI-1640 medium supplemented with amyloidogenic peptides. The concentration of amyloidogenic peptides that β-cells were exposed to include a “low” concentration range of 0.3-1 μM, a “mid” concentration range of 1-5 μM, and a “high” concentration range of 10-50 μM. BRIN-BD11 cells were exposed to amyloidogenic peptides for up to 24 h, depending on experimental requirements. All amyloidogenic peptide treatments were accompanied by appropriate controls, including a “media control” (fresh RPMI-1640), and a vehicle control (fresh RPMI-1640 supplemented with DMSO in Phenol Red-free Ham’s F-12 media equivalent to the percentage found in amyloidogenic peptide treatment).

4.4.3 MTT Assay

A density of 1 x 10^4 BRIN-BD11 cells per well were seeded into 96-well plates and left to adhere overnight before cells were treated for 24 h with amyloidogenic peptides in quadruplicate wells. After 24 h treatment, MTT Assay (2.2.3, page 50) was performed. Results were represented as relative fold change in cell viability from the media control.

4.4.4 Cell Cycle Analysis

A density of 1 x 10^6 BRIN-BD11 cells per well were seeded into 6-well plates and left to adhere overnight before cells were treated for 24 h with amyloidogenic peptides in duplicate wells. After 24 h treatment, cells were harvested and a Cell Cycle Analysis (2.2.4, page 50) was performed using the fluorescent DNA-stain PI. Using flow cytometry, single cell populations were isolated via gating, and a minimum of 1 x 10^4 events were plotted on a histogram as event count vs mean fluorescent intensity of PI staining. An example histogram generated from control BRIN-BD11 cells below in Figure 20 demonstrates how the phases of the cell cycle were determined.

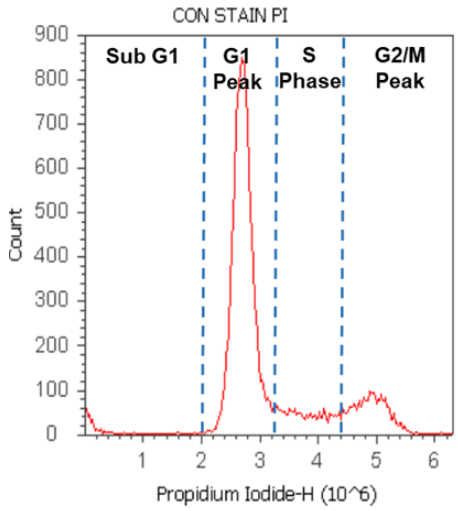

Figure 20. Representative histogram of cell cycle analysis. Event count vs fluorescent intensity of PI staining. Generated from media control sample of BRIN-BD11 cells.

4.4.5 Insulin Secretion

A density of 1.5 x 10^5 BRIN-BD11 cells per well were seeded into 24-well plates and left to adhere overnight before cells were treated for 24 h with amyloidogenic peptides in quadruplicate wells. After removal of the supernatant, the β-cells were subject to a GSIS (2.2.6, page 51) challenge, where the quadruplicate wells were exposed to KRBB supplemented with 1.1 mM glucose (for basal insulin secretion) or 16.7 mM glucose + 10 mM Alanine (for maximum insulin secretion) in duplicate wells each. Insulin level was analysed using an Insulin ELISA (2.2.7, page 52) kit. Cell lysates were collected, and protein was quantified by BCA Assay (2.2.5, page 51) for

normalisation. Results were calculated as µg insulin / L / µg protein and graphed as the fold change from the media control.

4.4.6 Western Blot Analysis

A density of 1 x 10^6 BRIN-BD11 cells per well were seeded into 6-well plates and left to adhere overnight before cells were treated for 24 h amyloidogenic peptides. Treatments of media only or a vehicle control were used as negative controls. Treatments of 1 µM of Rotenone (an inhibitor of complex I in the electron transport chain [425]), Thapsigargin (THP; induces ER stress via inhibition of ER Ca^{2+} ATPase [479]) or Staurosporin (STP; induces apoptosis via inhibition of protein kinases [480])) were used as positive controls for mitochondrial stress, ER stress and apoptosis, respectively. After 24 h treatment, cells were lysed and a BCA Assay (2.2.5, page 51) was conducted for protein quantification to prepare samples for Western Blot Analysis (2.2.8, page 52). Western blot analysis experiments were repeated a minimum of three times. Primary antibodies used in this study included Anti-BiP, Anti-Active Cas-3, anti-HSP60, anti-inducible nitric oxide synthase (iNOS), anti-B-cell lymphoma-extra-large (BCL-XL), anti-C / EBP homologous protein (CHOP), anti-pancreatic and duodenal homeobox 1 (PDX1), Sulfonylurea receptor 1 (SUR1), and anti-Cytochrome c oxidase subunit 4 (COXIV). Anti-β-actin and anti-α- / β-tubulin (both highly-conserved cytoskeletal components [481]) antibodies were used as loading controls. HRP-linked secondary antibodies used in this study include anti-Rabbit IgG and anti-Mouse IgG.

4.4.7 Intracellular ROS assay and PI Staining

A density of 1 x 10^6 BRIN-BD11 cells per well were seeded into 6-well plates and left to adhere overnight before cells were treated for 6 or 24 h with amyloidogenic peptides in duplicate wells. After treatment, cells were incubated with the CM-H2DCFDA ROS probe (2.2.10, page 56) for 30 min at 37 °C, protected from light. Cells were harvested and were incubated with 40 µg / mL of PI as per the PI Staining (2.2.9, page 55) protocol, for simultaneous co-staining of intracellular ROS and apoptotic cells. Each treatment group had additional controls with only PI or CM-H2DCFDA staining, as well as a control group absent of any staining to determine blank measurements and assist in

optimisation. Using flow cytometry, single cell populations were isolated via gating, and a minimum of 1 x 10^4 events were recorded. The percentage of PI negative (non-apoptotic) cells out of the total cell count were measured. For assessment of intracellular ROS, PI staining allowed for the exclusion of apoptotic cells prior to measurement of mean fluorescent intensity of CM-HF2DCFDA staining.

4.4.8 Mitochondrial Stress Test

A density of 1 x 10^4 BRIN-BD11 cells per well were seeded into specialised Seahorse XF^e96 cell culture plates and left to adhere overnight before cells were treated for 24 h with amyloidogenic peptides in quadruplicate wells. After 24 h treatment, a Mitochondrial Stress Test (2.2.11, page 56) was conducted according to manufacturer's protocol. Briefly, measurements of OCR (pmol / L / min) were recorded before and after three serial injections (at 21 min intervals) of the mitochondrial modulators Oligomycin, FCCP, then Antimycin A + Rotenone combination at concentrations optimised for BRIN-BD11 cells (Table 6, page 58). The OCR measurements were used to calculate multiple key parameters of mitochondrial function, including basal respiratory rate, maximum respiratory rate, ATP production, mitochondrial coupling efficiency, proton leak, and spare respiratory capacity (Figure 7, page 59). A BCA Assay (2.2.5, page 51) was used to normalise the data by protein and results were represented as the fold change from control measurements.

4.4.9 Glycolytic Rate Assay

A density of 1 x 10^4 BRIN-BD11 cells per well were seeded into specialised Seahorse cell culture plates and left to adhere overnight before cells were treated for 24 h with amyloidogenic peptides in quadruplicate wells. After 24 h treatment, a Glycolytic Rate Assay (2.2.12, page 59) was conducted according to manufacturer's protocol. Briefly, measurements of PER (pmol / L / min) were recorded before and after injection of the mitochondrial modulators Antimycin A and Rotenone combination, followed by 2-DG at concentrations optimised for BRIN-BD11 cells (Table 8, page 61). Cell-free control wells were not injected with mitochondrial modulators, but serial injections of 5 mmol / L HCl to determine buffering capacity of the media for measurement correction. PER

measurements were detected by the Agilent Seahorse XFe96 flux analyser and used to changes in glycolytic rate. A BCA Assay (2.2.5, page 51) was used to normalise the data by protein and results were represented as the fold change from control measurements.

4.4.10 Data Analysis

All experiments were repeated a minimum of three times. Statistical analysis was performed by GraphPad Prism Version 8 Software. Normality testing was performed on all data prior to analysis. If normally distributed, one-way ANOVA with Tukey multiple comparisons Post-Hoc testing was used to determine statistically significant changes between treatment groups. If not normally distributed, the equivalent nonparametric testing (Kruskal-Wallis with Dunn's multiple comparisons Post-Hoc testing) was used instead. Two-way ANOVA with Sidak's multiple comparisons Post-Hoc testing was used to determine changes between groups over time. All data is expressed as mean ± SEM. The limit of statistical significance was set at 0.05 ($p \leq 0.05$).

4.5 Results

4.5.1 Low concentrations of amyloidogenic peptides do not alter BRIN-BD11 β-cell viability or growth cycle

Initial investigations aimed to determine the effect of ≤1 μM concentrations of amyloidogenic peptides on the viability and growth of BRIN-BD11 pancreatic β-cells. Compared to other *in vitro* studies investigating human IAPP in β-cells, this concentration is relatively low [129, 150], however, human Aβ at this concentration is effective in altering neuronal cell viability and function *in vitro* [482-484]. Using a treatment time of 24 h, an MTT assay was used to measure alterations in cell viability. Only viable / living cells will reduce soluble MTT to insoluble formazan crystals within mitochondria, giving an indirect measurement of viable cells. After 24 h of exposure, there was no significant difference between treatment groups or controls (Figure 21). As the MTT assay is an indirect measurement of cell death via mitochondrial activity, the fluorescent DNA stain PI was used to validate these results.

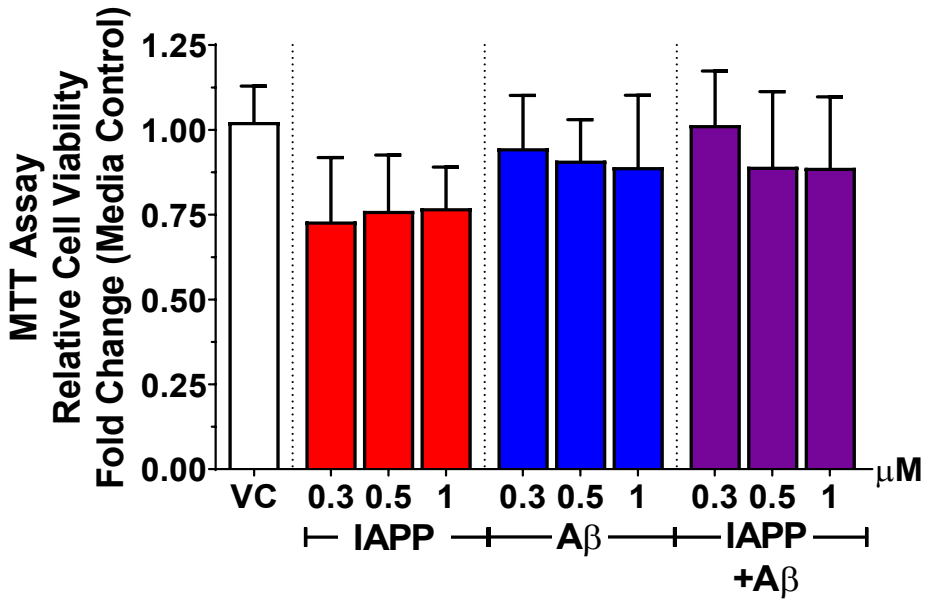

Figure 21. Low concentrations of IAPP, Aβ, or IAPP-Aβ combination over 24 h does not affect BRIN-BD11 cellular viability. BRIN-BD11 β-cells were treated with up to 1 μM of synthetic human IAPP, Aβ42 or IAPP-Aβ aggregates for 24 h before performing an MTT assay to determine changes in cell viability. Cells were also treated with media and a vehicle control containing 0.02% DMSO, equivalent to 1 μM of amyloid treatment. Results were quantified as mean ± SEM and expressed as the fold change from media control in bar graphs (N=4 in quadruplicate). IAPP-Aβ combination = 1 : 1, so 1 μM of IAPP-Aβ = 0.5 μM IAPP + 0.5 μM Aβ. Vehicle control (VC) = 0.02% DMSO (equivalent to 1 μM of treatments). Statistical analysis via one-way ANOVA with Tukey's multiple comparisons test to determine variation between treatment groups. No statistically significant changes were detected.

After permeabilisation of cells and staining with PI, the DNA content of cells was analysed to validate the MTT results, and to gain insight into whether amyloidogenic peptides interrupted regular BRIN-BD11 β-cell cycle growth, maturation, and mitosis. Phases of the growth cycle of BRIN-BD11 cells can be subdivided into the G_1 phase (non- / pre-mitotic cells with a single complement of DNA), S phase (replication of DNA content for division) or G_2 / M phase (cells with a double complement of DNA for imminent mitotic division; Figure 20). Another important parameter is the Sub-G_1 phase, which represents apoptotic bodies and cell fragments. After 24 h of exposure to 0.5 or 1 μM of IAPP, Aβ, or IAPP-Aβ combination, there was no significant difference in the percentage of total events detected in the Sub-G_1 phase between any of the treatment groups or compared to controls (Figure 22A).

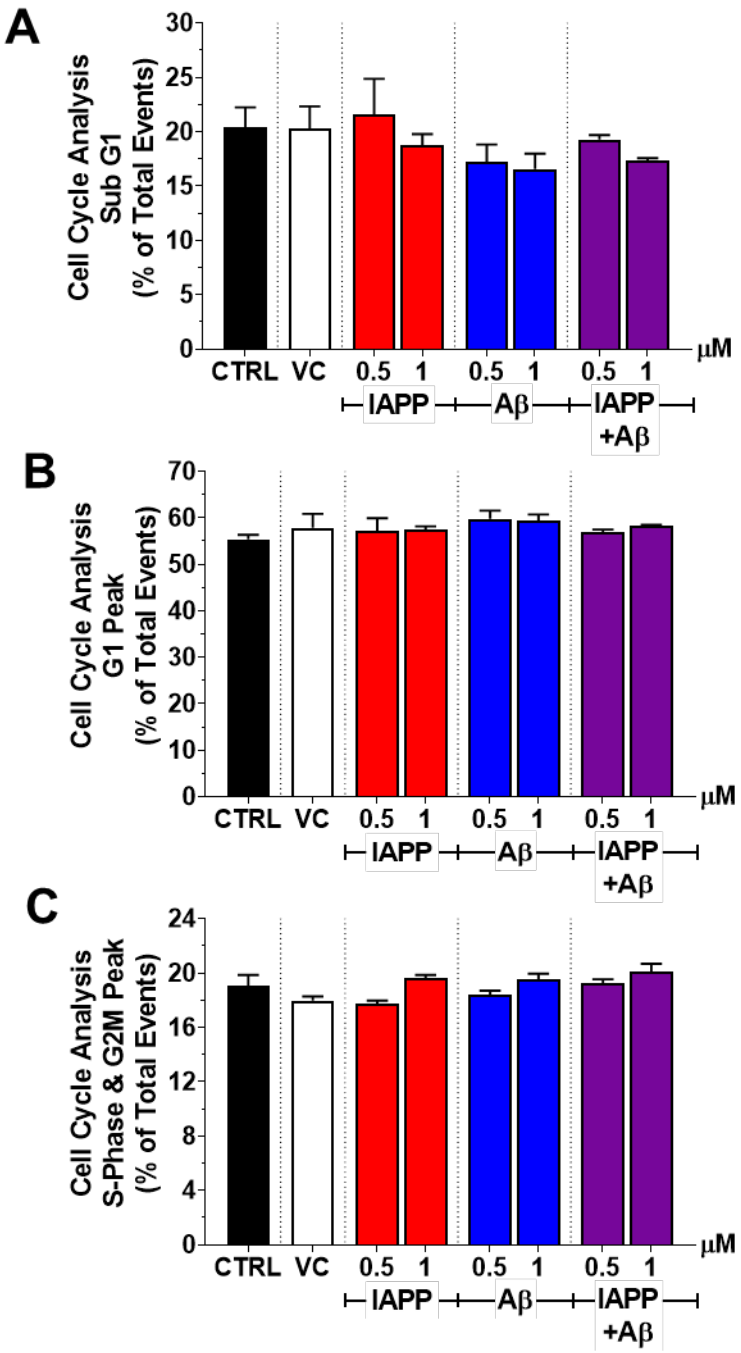

Figure 22. Low concentrations of IAPP, Aβ, or IAPP-Aβ combination over 24 h does not affect β-cell growth cycle or elicit apoptosis. BRIN-BD11 β-cells were treated with up to 1 µM of synthetic human IAPP, Aβ42 or IAPP-Aβ aggregates for 24 h before performing an cell cycle analysis to determine changes in cell viability and growth. Cells were also treated with media and a vehicle control containing 0.02% DMSO, equivalent to 1 µM of amyloid treatment. Data from separate phases of cell cycle [including (A) Sub-G_1, (B) G_1 Peak, and (C) combined S phase and G_2M Peak], were initially expressed as mean % of total events ± SEM in bar graphs (N=3 in duplicate). Statistical analysis via one-way ANOVA with Tukey's multiple comparisons test to determine variation between treatment groups. No statistically significant changes were observed.

Further investigation into the parameters of cell cycle analysis revealed no significant difference in the mean percentage of total events in the G_1 Peak between treatment groups or controls (Figure 22B). The mean percentage of total events detected in the S phase and G_2 / M peak were combined, as the rapid division of BRIN-BD11 cells meant that rarely did a G_2 / M peak appear distinct from S phase. As with the G_1 Peak, there was no significant difference identified between treatment groups or controls (Figure 22C). Taken together with the MTT results, this data shows neither cellular viability nor cellular growth cycle was affected by ≤1 μM concentrations of aggregated amyloidogenic peptides after 24 h treatment.

4.5.2 Low concentrations of amyloidogenic peptides do not alter BRIN-BD11 β-cell function and stress markers

While cell viability and growth were unaltered after treatment with amyloidogenic peptides, other essential cellular functions may have been affected. As such, the next step in the investigation was to determine if insulin secretion, the most important function of pancreatic β-cells, was altered by the same treatment. After 24 h exposure to ≤1 μM IAPP, Aβ, or IAPP-Aβ combination, BRIN-BD11 cells underwent an insulin secretion challenge, where cells were exposed to basal (1.1 mM Glucose; Figure 23A) or stimulatory (16.7 mM Glucose + 10 mM Alanine; Figure 23B) conditions. Analysis of the insulin secretion challenge revealed no significant changes in insulin secretion during either basal or stimulatory conditions between controls and treatment groups at any concentration assessed. In addition to assessing functional changes via insulin secretion, western blot analysis was also used to determine alterations in expression of key markers of β-cell function and stress (Figure 24).

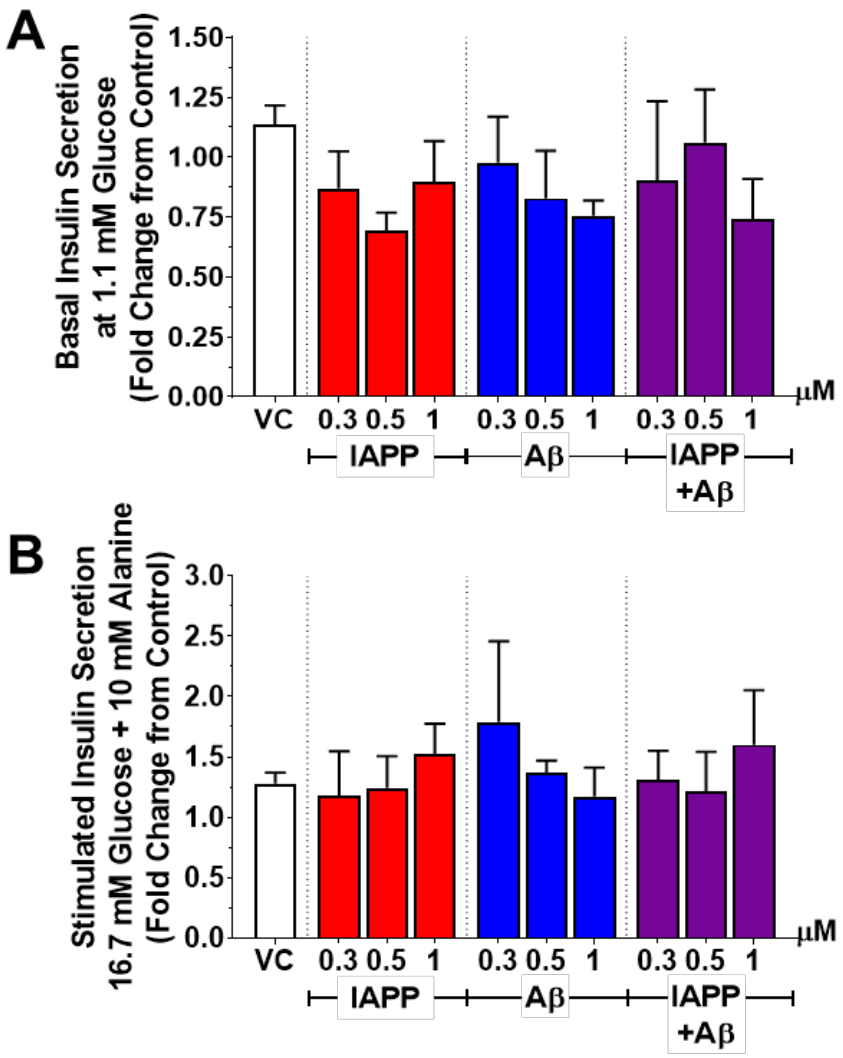

Figure 23. Low concentrations of IAPP, Aβ, or IAPP-Aβ combination over 24 h does not alter BRIN-BD11 β-cell insulin secretion. BRIN-BD11 β-cells were treated with up to 1 μM of synthetic human IAPP, Aβ42 or IAPP-Aβ aggregates for 24 h before performing an insulin secretion challenge under basal (1.1 mM glucose; A) or stimulated (16.7 mM glucose + 10 mM Alanine) conditions. Cells were also treated with media and a vehicle control containing 0.02% DMSO, equivalent to 1 μM of amyloid treatment. An insulin ELISA was used to quantify results as mean ± SEM and expressed as the fold change from media control in bar graphs (N=3 in triplicate). Statistical analysis via one-way ANOVA with Tukey's multiple comparisons test to determine variation between treatment groups. No statistically significant changes were observed.

Levels of PDX1, a marker of insulin production, was not significantly altered with any of the treatments (Figure 24C). As amyloidogenic peptides are known to exert their toxicity via inducing mitochondrial stress [150, 155], ER stress [485], and / or apoptosis [486, 487] expression of COXIV, CHOP, and Active Cas3 were also assessed. COXIV levels were similar between controls and

treatment groups (Figure 24D). Exposure of cells to 1 μM STP as a positive control led to reduction in CHOP levels (Figure 24E) and an increased ratio of active to inactive caspase-3 (Figure 24F). No changes in these measures were observed following exposure to amyloidogenic compounds compared to control (Figure 24E-F). Together, these data indicated that at concentrations of ≤1 μM, IAPP, Aβ, or IAPP-Aβ did not alter BRIN-BD11 β-cell function or viability following a 24h exposure. The effects of higher concentrations of amyloidogenic peptides were therefore assessed.

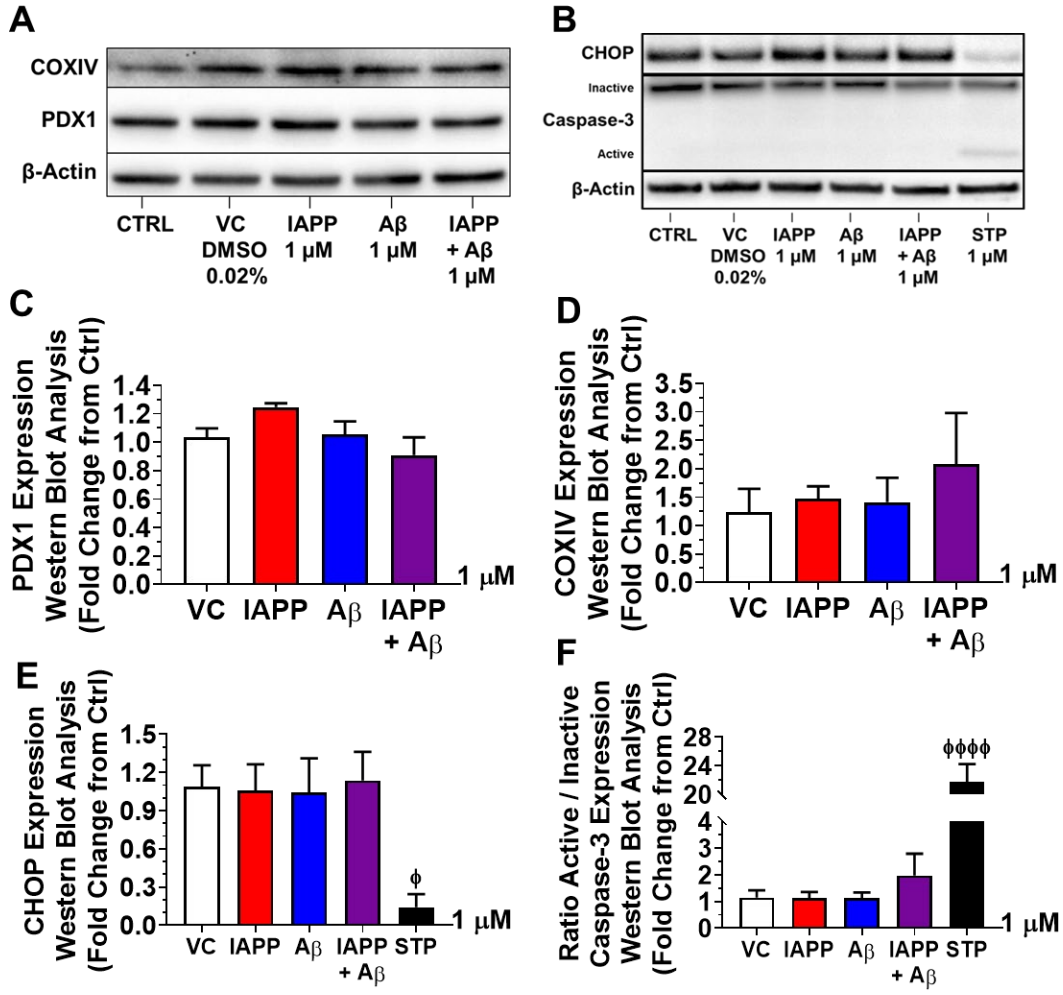

Figure 24. Low concentrations of IAPP, Aβ, or IAPP-Aβ combination over 24 h does not elicit changes in markers of BRIN-BD11 β-cell stress. BRIN-BD11 β-cells were treated with up to 1 μM of synthetic human IAPP, Aβ42 or IAPP-Aβ aggregates for 24 h before lysates were collected for western blot analysis to detect changes in protein expression (A and B). Cells were also treated with media, a vehicle control containing 0.02% DMSO, and a positive control containing 1 μM of Staurosporin (STP). Results were quantified as mean ± SEM and expressed as the fold change from media control in bar graphs (C-F; N=3). Statistical analysis

via one-way ANOVA with Tukey's multiple comparisons test to determine variation between treatment groups. Φ = statistical significance compared to respective vehicle control, * = statistical significance compared to indicated treatment group. ^{Φ} / *p < 0.05, ^{ΦΦΦΦ} / ****p value=< 0.0001.

4.5.3 Increased concentrations of IAPP-Aβ combination reduces cell viability and increases oxidative stress in BRIN-BD11 β-cells

To determine the reaction of BRIN-BD11 β-cells to higher concentrations of the amyloidogenic peptides, cells were treated with "mid-range" 1.5-5 μM or "higher-range" (10-50 μM) of amyloidogenic peptides. After 24 h of treatment, cell viability was assessed by MTT assay (Figure 25). Exposure to 1.5, 3 and 5 μM of IAPP significantly reduced cell viability compared to respective vehicle controls (p = 0.001, 0.012, and 0.004 respectively; Figure 25A). Additionally, 1.5 μM of IAPP significantly reduced cell viability compared to both Aβ and the IAPP-Aβ combination (p = 0.034 and 0.003 respectively). Comparable results were observed with higher concentrations of IAPP, where reductions were observed for 10, 25 and 50 μM treatments compared to VC controls (Figure 25B; p = 0.016, 0.017, and 0.004 respectively). In comparison to IAPP, exposure to IAPP-Aβ only reduced cell viability at 5 μM treatment (p = 0.034). Despite this, 25 and 50 μM of IAPP-Aβ resulted in a marked reduction in cell viability compared to controls (p = 0.004 and < 0.0001). Indeed, compared to IAPP and Aβ peptides, exposure to 50 μM of IAPP-Aβ significantly exacerbated cytotoxicity (p = 0.0007 and < 0.0001). Exposing the cells to Aβ peptide at any concentrations did not significantly alter viability compared to controls.

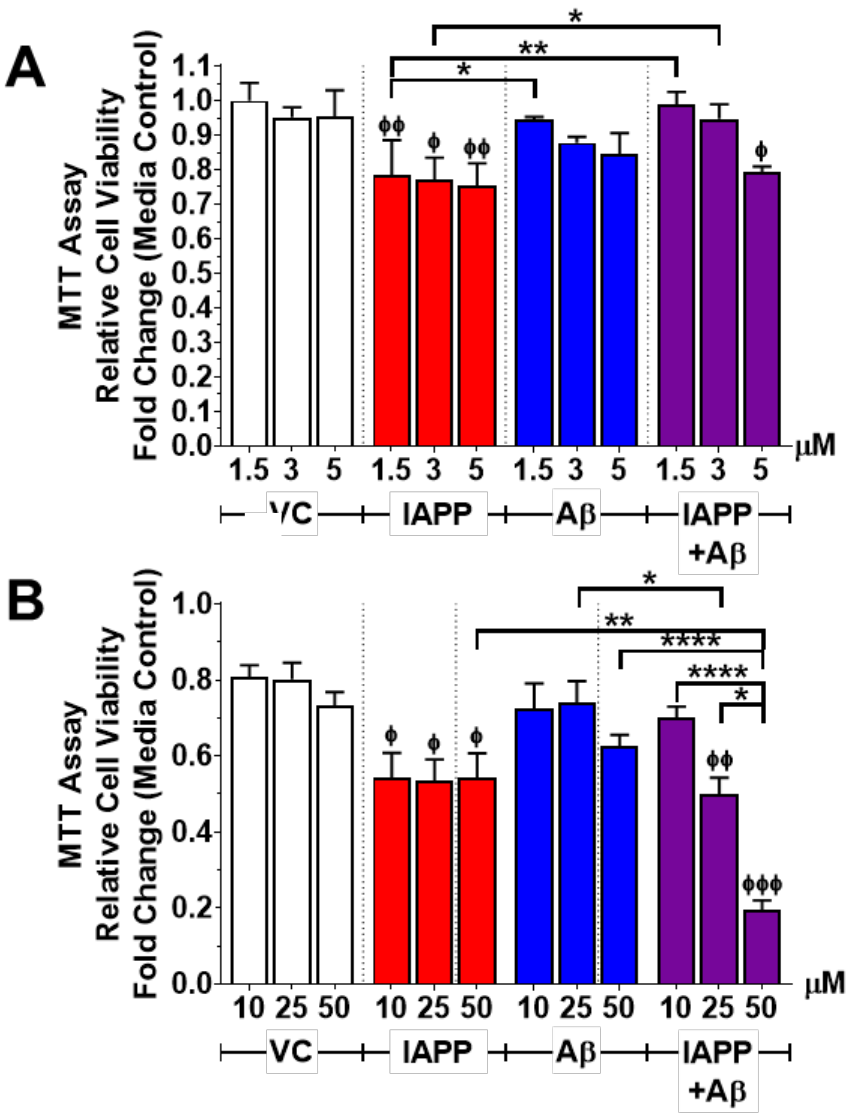

Figure 25. Higher concentrations of the IAPP-Aβ combination significantly exacerbated cytotoxicity compared to IAPP or Aβ treatments alone. BRIN-BD11 β-cells were treated with up to 1.5-5 μM (A) and 10-50 μM (B) of synthetic human IAPP, Aβ42 or IAPP-Aβ aggregates for 24 h before performing an MTT assay to determine changes in cell viability. Cells were also treated with media and vehicle controls containing 0.03-0.1% DMSO (equivalent to 1.5-5 μM of treatments; A) or 0.2-1% DMSO (equivalent to 10-50 μM of treatments; B). Results were quantified as mean ± SEM and expressed as the fold change from media control in bar graphs (N=3 in quadruplicate). Statistical analysis via one-way ANOVA with Tukey's multiple comparisons test to determine variation between treatment groups. IAPP-Aβ combination = 1 : 1, so 50 μM of IAPP-Aβ = 25 μM IAPP + 25 μM Aβ. Vehicle control (VC) = 1% DMSO (equivalent to 50 μM of treatments). Φ = statistical significance compared to respective vehicle control, * = statistical significance compared to indicated treatment group. $^{\Phi}$ / *p < 0.05, $^{\Phi\Phi}$ / **p < 0.01, $^{\Phi\Phi\Phi}$ / ***p < 0.001, $^{\Phi\Phi\Phi\Phi}$ / ****p < 0.0001.

To validate findings from the MTT assay, PI staining was performed. Here, PI staining was used on non-permeated BRIN-BD11 β-cells. As such, only cells

with a compromised cell membrane, such as those undergoing apoptosis or necrosis, were positively stained with PI. BRIN-BD11 β-cells were treated with the 50 μM of IAPP, Aβ, or IAPP-Aβ combination over two separate time points, 6 and 24 h, to determine changes over time. Following 6 h of treatment with amyloidogenic peptides, IAPP significantly reduced the percentage of PI negative (viable) cells compared to controls, Aβ, and IAPP-Aβ ($p = 0.006$, 0.001, and 0.032 respectively; Figure 26A). However, after 24 h of treatment, only IAPP-Aβ reduced the percentage of viable cells compared to controls ($p = 0.0007$). A two-way ANOVA further revealed that IAPP-Aβ was the only treatment to reduce the percentage of viable cells over time ($p = 0.001$, $F(1, 12) = 12.39$).

In addition to PI staining, the cells were simultaneously co-stained with CM-H2DCFDA, an intracellular ROS probe to detect changes in oxidative stress. CM-H2DCFDA passively diffuses into cells where it reacts with intracellular glutathione, giving a measure of the level of intracellular ROS. In accordance with the PI staining results, 6 h of IAPP treatment significantly altered BRIN-BD11 cell ROS generation, where compared to vehicle controls, IAPP was the only treatment to increase mean fluorescent intensity (Figure 26B; $p = 0.005$, 0.006, and 0.004 respectively). However, after 24 h of treatment, IAPP-Aβ had the highest levels of intracellular ROS compared to controls and other treatments ($p = 0.008$, 0.006, and 0.0029 respectively). Furthermore, a two-way ANOVA revealed that only the IAPP-Aβ combination increased intracellular ROS between 6h and 24 h (p value=0.0012; $F(1, 12) = 24.51$). The results from the MTT, PI, and intracellular ROS assays together indicate that treatment of BRIN-BD11 β-cells with IAPP led to significant cytotoxicity, which was exacerbated with the co-aggregation of IAPP and Aβ in a dose and time-dependent manner. Treating BRIN-BD11 β-cells with Aβ aggregates alone did not alter cell viability or ROS generation.

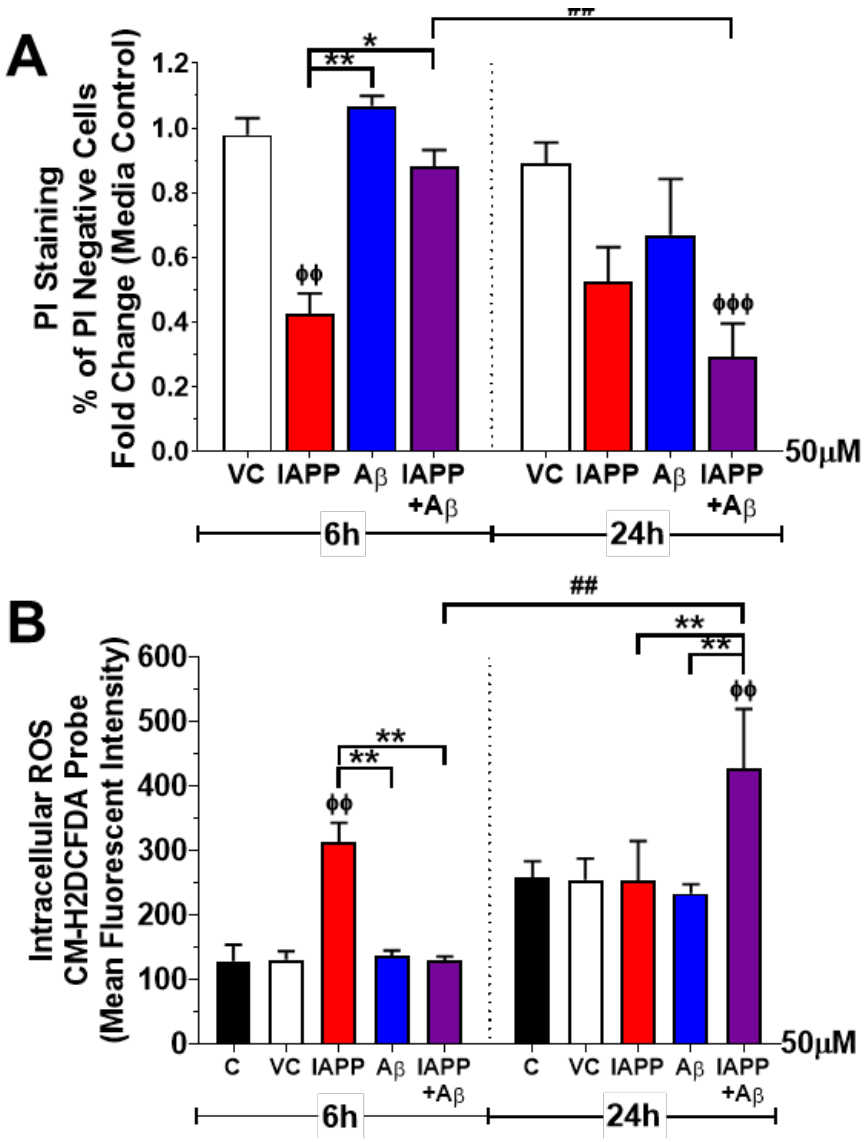

Figure 26. IAPP-Aβ combination exhibits a time-dependent decrease in BRIN-BD11 cell viability and increase in intracellular ROS generation. BRIN-BD11 β-cells were treated with 50 μM of synthetic human IAPP, Aβ42 or IAPP-Aβ aggregates for 24 h before performing Intracellular CM-H2DCFDA ROS Assay with PI staining. Cells were also treated with only media, and a vehicle control containing 1% DMSO, equivalent to 50 μM of amyloid treatment. PI staining results were quantified as mean % of PI negative cells from total events ± SEM and expressed as the fold change from media control in a bar graph (A; N=3 in duplicate). Intracellular ROS results were quantified as mean fluorescent intensity ± SEM and represented in a bar graph (B; N=3). Statistical analysis via two-way ANOVA with Sidak's multiple comparisons test to determine variation between treatment groups and over time. C = media control. Φ = statistical significance compared to respective vehicle control, # = statistical significance compared to the same treatment over time, * = statistical significance compared to indicated treatment group. ^{Φ} / $^{\#}$ / *p < 0.05, ^{ΦΦ} / $^{\#\#}$ / **p < 0.01, ^{ΦΦΦ} / $^{\#\#\#}$ / ***p < 0.01.

4.5.4 Amyloidogenic peptides reduce basal and stimulated insulin secretion from BRIN-BD11 β-cells

To determine how the effective concentrations of amyloidogenic peptides altered β-cell functioning, basal and stimulatory insulin secretion from BRIN-BD11 cells were assessed. Cells were exposed to 25 or 50 μM of IAPP, Aβ or IAPP-Aβ for 24 h, prior to an insulin secretion challenge. Compared to vehicle controls, a trend towards a reduction in basal insulin secretion was observed in 50 μM treatments, particularly IAPP-Aβ where the decrease was significant ($p = 0.027$; Figure 27A). All treatments also showed a dose-dependent decrease in basal insulin secretion between 25 and 50 μM concentrations ($p = 0.020$, 0.001, and 0.006 for IAPP, Aβ, and IAPP-Aβ respectively). Under stimulatory conditions (Figure 27B), insulin secretion was reduced following exposure to 50 μM of all amyloidogenic peptides lowest levels observed for IAPP-Aβ ($p = 0.009$, 0.0002, and < 0.0001 for IAPP, Aβ and IAPP-Aβ respectively). Additionally, both Aβ and IAPP-Aβ (but not IAPP) showed a dose-dependent reduction in stimulated insulin secretion between 25 and 50 μM ($p = 0.001$ and 0.0001). Together these data indicate that exposure of BRIN-BD11 β-cells to 50 μM of all amyloidogenic treatments led to reductions in basal and stimulated insulin secretion.

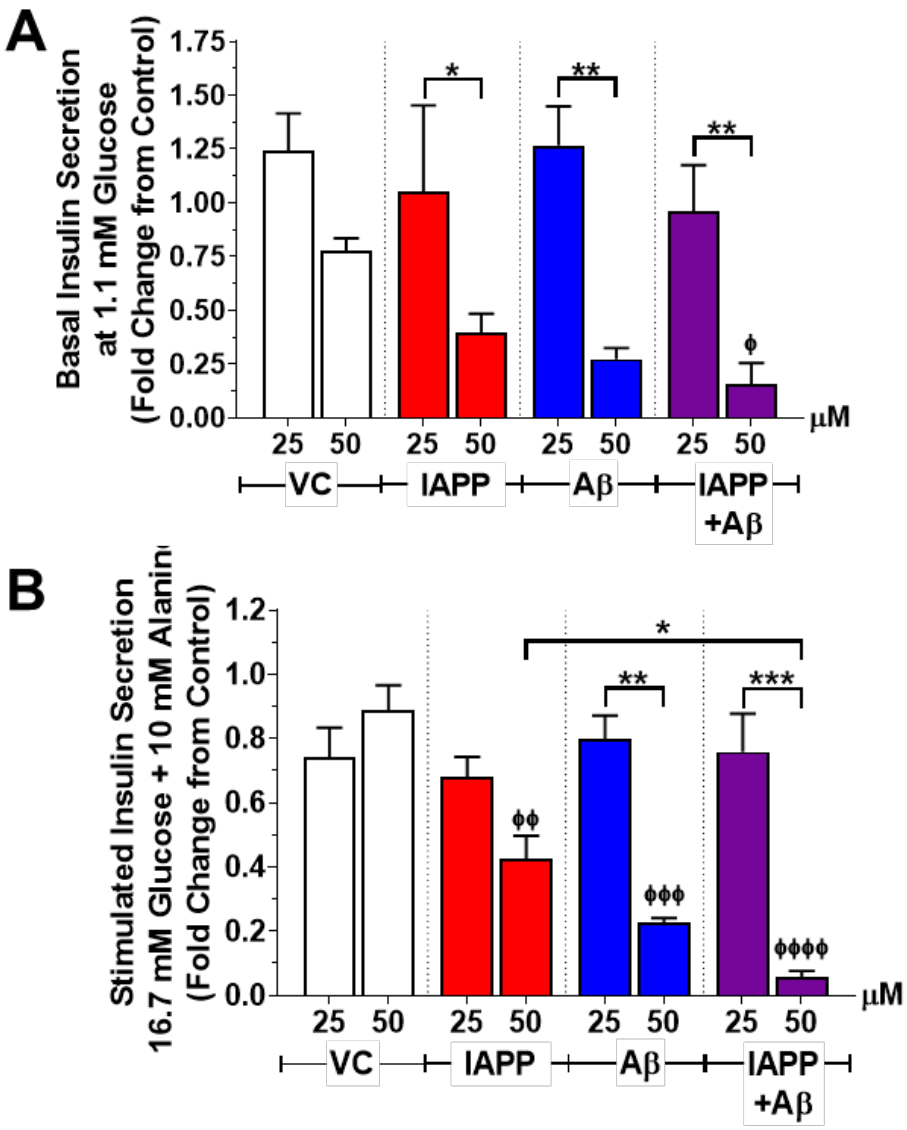

Figure 27. IAPP-Aβ combination significantly reduces both basal and glucose-stimulated insulin secretion in BRIN-BD11 β-cells. BRIN-BD11 β-cells were treated with up to 50 μM of synthetic human IAPP, Aβ42 or IAPP-Aβ aggregates for 24 h before performing an insulin secretion challenge under basal (1.1 mM glucose; A) or stimulated (16.7 mM glucose + 10 mM Alanine) conditions. Cells were also treated with media, and a vehicle control containing 0.5 or 1% DMSO, equivalent to 25 or 50 μM of amyloid treatment. An insulin ELISA was used to quantify results as mean ± SEM and expressed as the fold change from media control in bar graphs (N=3 in duplicate). Statistical analysis via one-way ANOVA with Tukey's multiple comparisons test to determine variation between treatment groups. Φ = statistical significance compared to respective vehicle control, * = statistical significance compared to indicated treatment group. $^{\Phi}$ / *p < 0.05, $^{\Phi\Phi}$ / **p < 0.01, $^{\Phi\Phi\Phi}$ / ***p < 0.001, $^{\Phi\Phi\Phi\Phi}$ / ****p < 0.0001.

4.5.5 IAPP, but not Aβ, impairs mitochondrial bioenergetics in BRIN-BD11 β-cells

The findings above indicate impaired β-cell functioning and viability associated with exposure to amyloidogenic peptides, particularly with IAPP-Aβ. Impairments in mitochondrial function is a major underlying mechanism that can lead to oxidative stress, cell death and impaired insulin secretion. Using the Seahorse XF^{e}96 Flux Analyser, key parameters of mitochondrial activity were assessed where the oxygen consumption of BRIN-BD11 β-cells was measured. The parameters included basal OCR, maximum OCR, and ATP production. Compared to vehicle control, basal OCR was reduced following 24 h of treatment with 50 μM of IAPP and IAPP-Aβ combination ($p = 0.020$ and 0.031), with only IAPP exhibiting a dose-dependent decrease between 25 and 50 μM of treatment ($p = 0.019$; Figure 28A).Treatment with Aβ did not alter basal OCR. Similar results were observed for maximal OCR (Figure 28B**;** $p = 0.049$ and 0.035 for IAPP and IAPP-Aβ, respectively). ATP production rate was reduced following treatment with 50 μM IAPP compared to controls ($p = 0.031$; Figure 28C). Neither Aβ nor IAPP-Aβ altered this parameter.

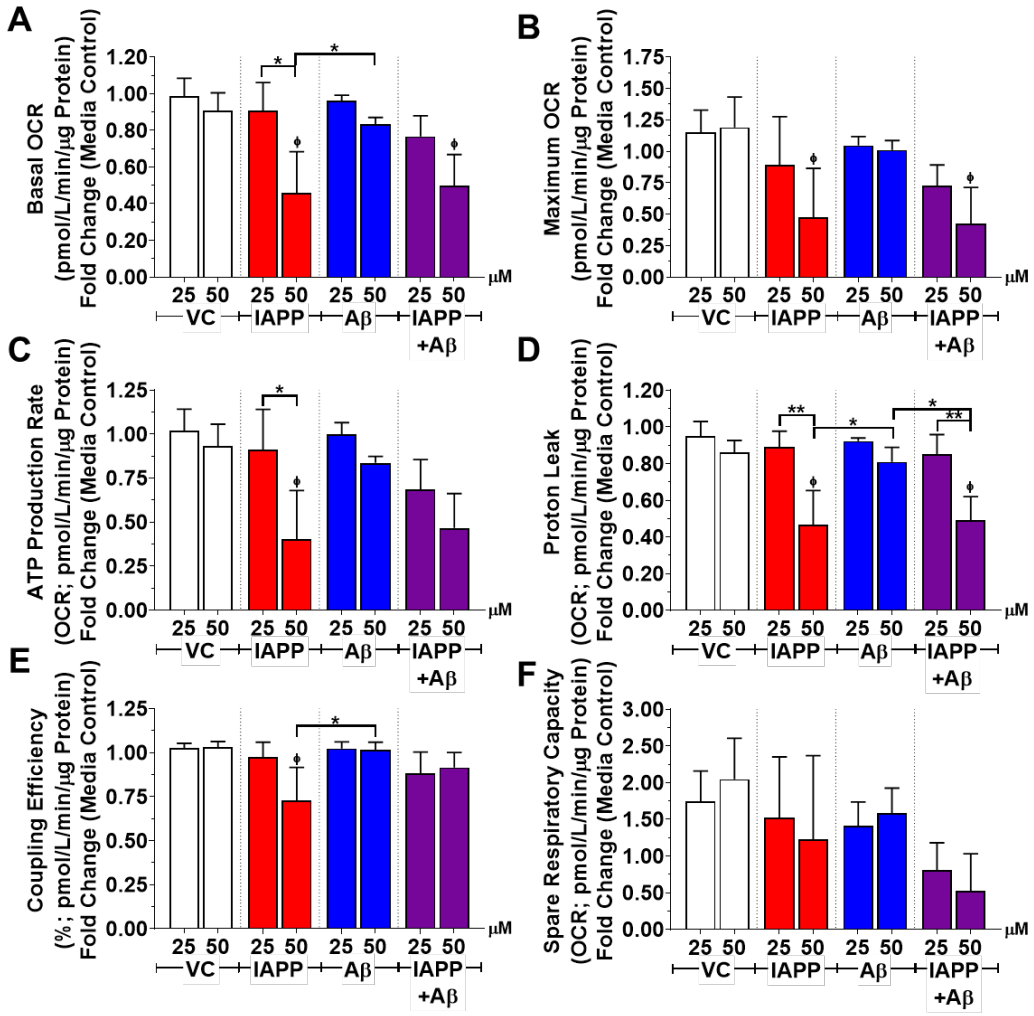

Figure 28. IAPP exacerbates mitochondrial dysfunction in BRIN-BD11 β-cells compared to Aβ or IAPP-Aβ combination. BRIN-BD11 β-cells were treated with up to 50 µM of synthetic human IAPP, Aβ42 or IAPP-Aβ aggregates for 24 h before performing mitochondrial stress testing. Cells were also treated with media, and a vehicle control containing 0.5 or 1% DMSO, equivalent to 25 or 50 µM of amyloid treatment. Using a Seahorse XF^{e}96 Flux Analyser, key parameters of mitochondrial function were identified via changes in the oxygen consumption rate (OCR) upon exposure to mitochondrial modulators. Results were quantified as mean OCR ± SEM and expressed as the fold change from media control in bar graphs (N=3 in quadruplicate), including (A) Basal OCR, (B) Maximum OCR, (C) ATP Production, (D) % Coupling Efficiency, (E) Proton Leak, and (F) Spare Respiratory Capacity. Statistical analysis via one-way ANOVA with Tukey's multiple comparisons test to determine variation between treatment groups, except for Proton Leak (D), which was not normally distributed and equivalent nonparametric Kruskal-Wallis test with Dunn's Post-Hoc was used instead. Φ = statistical significance compared to respective vehicle control, * = statistical significance compared to indicated treatment group. $^{\Phi}$ / *p < 0.05, $^{\Phi\Phi}$ / **p < 0.01.

Additional measurements of mitochondrial activity were calculated from the initial parameters, including proton leak, coupling efficiency, and the spare respiratory capacity of the cells. Proton leak is calculated as the amount of basal OCR not associated with ATP production, and is instead due to movement of protons across the inner mitochondrial membrane via leakage or uncoupling proteins [426]. Similar to the basal and maximal OCR, proton leak was reduced following treatment with 50 μM of IAPP and IAPP- Aβ combination ($p = 0.011$ and 0.016; Figure 28D). Treatment with IAPP also reduced coupling efficiency (Figure 28E; $p = 0.026$), a parameter that measures the mitochondria's ability to efficiently couple metabolism to ATP production. Treatment with Aβ or IAPP-Aβ did not alter BRIN-BD11's coupling efficiency. In addition, no changes were observed in spare respiratory capacity following treatments with any of the peptides (Figure 28F).

When mitochondrial dysfunction occurs and the mechanisms of oxidative phosphorylation have been damaged, the mitochondria can compensate through metabolic switching to increase the glycolytic rate and meet the required energy demands for the cell [488-490]. As such, investigation of alterations in glycolytic rate further elucidates changes in mitochondrial function. Exposure of cells to 25 or 50 μM of IAPP led to a trend towards an increase in basal glycolytic rate compared to controls ($p = 0.114$ and 0.080), and a significant increase compared to Aβ treated cells (Figure 29A; $p = 0.046$ and 0.041). No changes in glycolytic rate were observed after exposure to Aβ or IAPP-Aβ, and none of the peptide preparations significantly altered the glycolytic rate in response to inhibition of oxidative phosphorylation (compensatory glycolysis; Figure 29B). Overall, the data indicates that despite IAPP-Aβ exerting significantly more toxicity than IAPP or Aβ, IAPP appears to drive impairments in mitochondrial bioenergetics in the BRIN-BD11 cells.

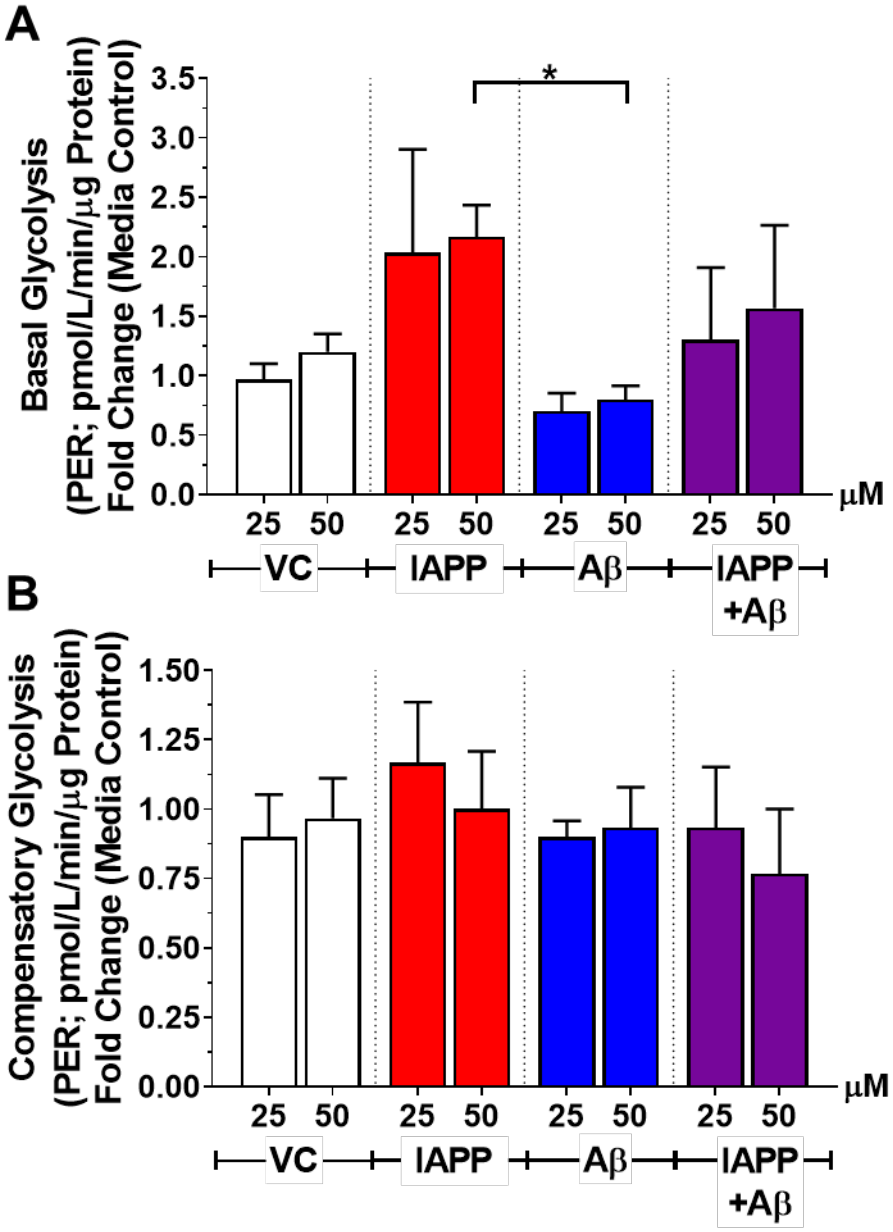

Figure 29. IAPP increases basal glycolysis in BRIN-BD11 β-cells but does not increase compensatory glycolytic rate. BRIN-BD11 β-cells were treated with up to 50 μM of synthetic human IAPP, Aβ42 or IAPP-Aβ aggregates for 24 h before performing glycolytic rate testing. Cells were also treated with media, and a vehicle control containing 0.5 or 1% DMSO, equivalent to 25 or 50 μM of amyloid treatment. Using a Seahorse XF^{e}96 Flux Analyser, key parameters of glycolysis were identified via changes in the proton efflux rate (PER) upon exposure to mitochondrial modulators. Results were quantified as mean PER ± SEM and expressed as the fold change from media control in bar graphs (N=3 in quadruplicate), including (A) Basal Glycolysis, and (B) Compensatory Glycolysis. Statistical analysis via one-way ANOVA with Tukey's multiple comparisons test to determine variation between treatment

groups. * = statistical significance compared to indicated treatment group. *p < 0.05, **p < 0.01.

4.5.6 Exposure to IAPP-Aβ combination results in mitochondrial dysfunction and apoptosis, but not ER stress in BRIN-BD11 β-cells

To validate the observed changes in mitochondrial function, western blot analysis was used to investigate the expression of proteins associated with mitochondrial stress and function, including SUR1, BCL-XL and HSP60 (Figure 30). SUR1 is a membrane protein with functions in the coupling of intracellular ATP to insulin secretion via opening / closing of voltage gated potassium channels [491]. BCL-XL is anti-apoptotic mitochondrial transmembrane protein [492, 493], and HSP60 is a mitochondrial molecular chaperone with functions in stabilising and clearing unfolded or misfolded proteins [214].

The BRIN-BD11 cells were exposed to the peptide preparations, or rotenone for 24hrs. Rotenone treatment led to an increase in SUR1 and HSP60 and a reduction in BCL-XL, consistent with its ability to impair mitochondrial function [494]. Similarly, treatment with 50 μM of IAPP and IAPP-Aβ combination led to a significant increase in SUR1 ($p = 0.043$ and 0.0142; Figure 30B), as well as a significant increase and a trend towards an increase, respectively, in HSP60 expression (Figure 30D; $p = 0.022$ and 0.077). Treatment with IAPP also led to a decrease in BCL-XL, whilst treatment with IAPP-Aβ combination did not significantly alter expression levels of this anti-apoptotic marker (Figure 30C; $p = 0.037$). Overall, this expression analysis is consistent with the mitochondrial stress test and glycolytic assay results, indicating that IAPP, alone or in combination with Aβ, can impair mitochondrial function. However, the BCL-XL expression analysis shows that only IAPP activates mitochondria-mediated apoptotic pathways. Treatment with Aβ did not significantly alter the expression of any of the mitochondrial markers assessed, consistent with its lack of effect on mitochondrial bioenergetics in BRIN-BD11 cells.

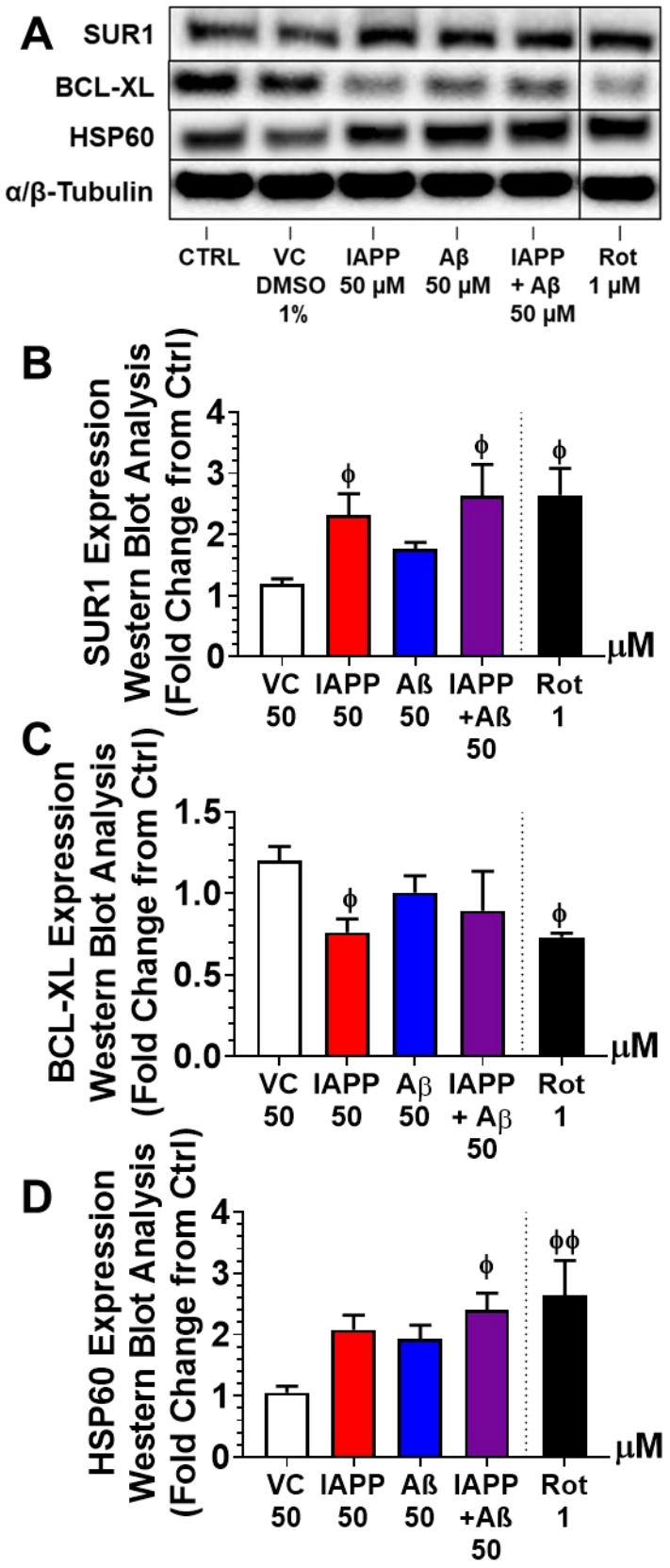

Figure 30. IAPP and IAPP-Aβ combination altered expression of mitochondrial stress markers in BRIN-BD11 β-cells. BRIN-BD11 β-cells were treated with 50 µM of synthetic

human IAPP, Aβ42 or IAPP-Aβ aggregates for 24 h before lysates were collected for western blot analysis to detect changes in protein expression associated with mitochondrial function (A). Cells were also treated with media, and a vehicle control containing 1% DMSO, equivalent to 50 μM of amyloid treatment. Results were quantified as mean ± SEM and expressed as the fold change from media control in bar graphs (B-D; N=3). 24 h treatment of 1 μM of Rotenone (Rot) used as positive control for mitochondrial dysfunction. Statistical analysis via one-way ANOVA with Tukey's multiple comparisons test to determine variation between treatment groups. Φ = statistical significance compared to respective vehicle control. $^{\Phi}p < 0.05$, $^{\Phi\Phi}p < 0.01$.

To explore effects of the amyloidogenic peptides on other stress-related markers, immunoblotting was performed to assess expression levels of Active Cas3; iNOS (a marker of cellular stress and inflammation [495, 496]) and BiP [214, 497]. Cells were also treated with STP or THP, as these agents are known to induce apoptosis and ER stress, respectively [498, 499]. Consistent with this, treatment with STP led to marked increases in Active Cas3 (Figure 31B) and iNOS (Figure 31C), and THP led to an increase in BiP levels (Figure 31E). Compared to vehicle control, exposure of cells to 50 μM IAPP and IAPP-Aβ resulted in increased expression of Active Cas3 ($p = 0.010$ and 0.001). A trend towards an increase in iNOS was also observed for IAPP-Aβ treatment ($p = 0.105$). Exposure to Aβ did not alter Active Cas3 or iNOS compared to controls. No significant changes in BiP expression were observed for any of the peptide treatments.

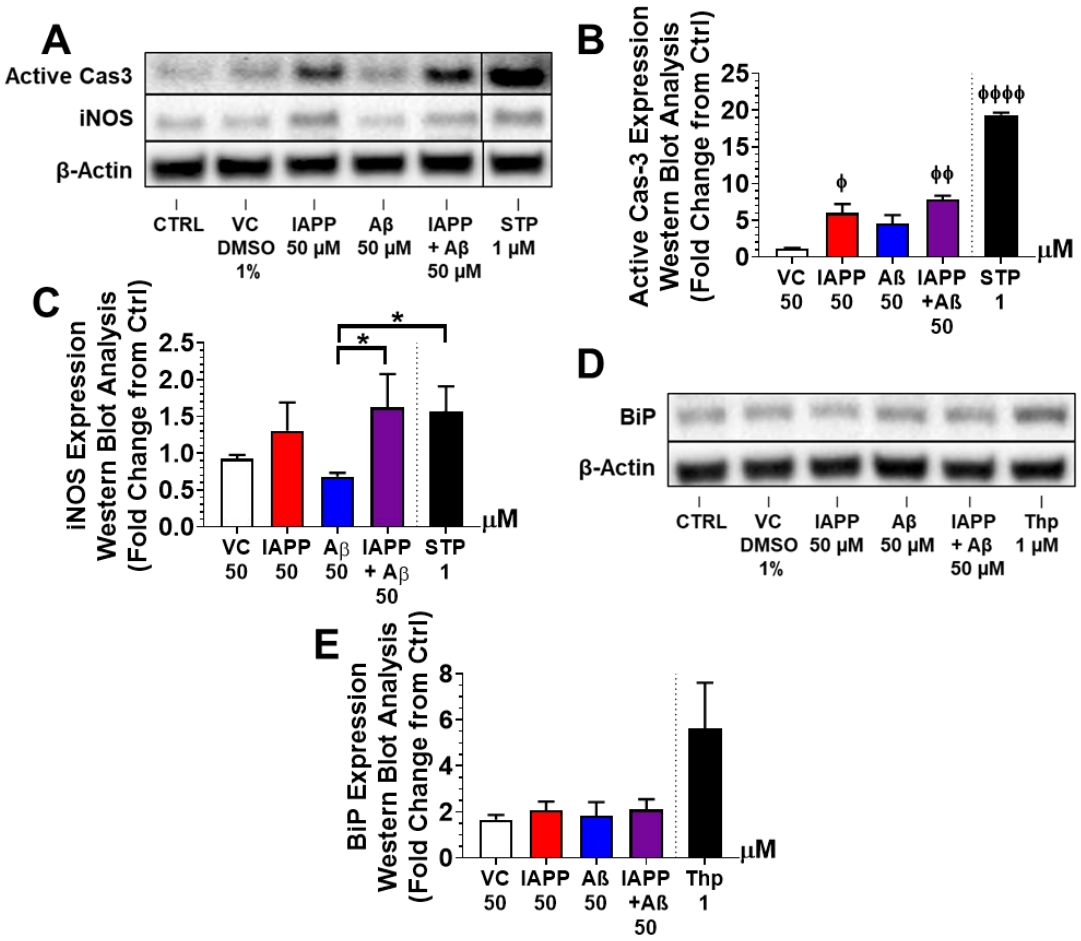

Figure 31. IAPP-Aβ combination altered expression of cellular stress markers, including apoptosis and inflammation, but not ER stress in BRIN-BD11 β-cells. BRIN-BD11 β-cells were treated with 50 µM of synthetic human IAPP, Aβ42 or IAPP-Aβ aggregates for 24 h before lysates were collected for western blot analysis to detect changes in protein expression associated with cellular stress (A and D). Cells were also treated with media, and a vehicle control containing 1% DMSO, equivalent to 50 µM of amyloid treatment. Results were quantified as mean ± SEM and expressed as the fold change from media control in bar graphs (B, C and E; N=3). 24 h treatment of 1 µM of STP used as positive control for apoptosis. 24 h treatment of 1 µM of Thapsigargin (Thp) used as positive control for ER stress. Statistical analysis via one-way ANOVA with Tukey's multiple comparisons test to determine variation between treatment groups. Φ = statistical significance compared to respective vehicle control. Φp < 0.05, ΦΦp < 0.01, ΦΦΦΦp < 0.0001.

Taken together, this data shows that significant cell stress from changes in mitochondrial function and inflammation (but not ER stress) occurred after treatment with cytotoxic concentrations of IAPP and IAPP-Aβ combination. Treatment with Aβ did not induce cellular stress as determined by a lack of

significant alterations in markers of mitochondrial, ER, and general cellular stress.

4.6 Discussion

Although extensive information is available on the role of IAPP in T2D [20, 131, 134, 157, 176], the role of Aβ in pancreatic islets (where it can co-localise and co-aggregate with IAPP [25, 129]) is still largely unexplored as discussed in Chapter 2 (1.7.1, page 38). Furthermore, the previous chapter suggested in transgenic mice that Aβ, in the absence of IAPP, did not affect pancreatic islet function, while an IAPP-Aβ combination exacerbated pancreatic islet stress compared to IAPP alone. This chapter further explored the effect of IAPP, Aβ, and IAPP-Aβ on insulin-producing pancreatic β-cells *in vitro* to gain mechanistic insights into amyloidotoxicity in T2D. Overall, the findings in this chapter indicate that the treatment of BRIN-BD11 β-cells with Aβ, IAPP, or IAPP-Aβ results in peptide-specific effects on β-cell viability, function, and bioenergetics.

The cell line selected for this study was the BRIN-BD11 rat pancreatic β-cell line. BRIN-BD11 cells are insulin-secreting and highly sensitive to glucose and other secretagogues, such as the amino acids glutamine and alanine [421, 500, 501]. As a stable, robust, immortalised cell line, it overcomes common problems in using isolated primary pancreatic cells, such as; the difficulty in isolating adequate amounts of viable islet cells [502, 503], the difficulty in maintaining islets in culture with intact insulin production [504], and hormonal and / or cellular heterogeneity between islets [505, 506]. Furthermore, while BRIN-BD11 β-cells have their limitations, including the derivation of rodent insulinoma cells, and a low tolerance for suboptimal and supraoptimal seeding densities, they also have many advantages over other commonly used β-cell lines, such as INS-1 (rat insulinoma-derived β-cells), MIN6 (mouse insulinoma-derived β-cells), and the BRIN-BD11 precursor, RINm5F (rat insulinoma-derived β-cells) [507]. These advantages include GLUT-2 expression [508], high glucose / secretagogue responsiveness [421, 507-509], appropriate cellular machinery for insulin production and secretion [421], rapid growth [421, 508], and suitability for metabolic studies [232, 508]. Furthermore, as rodent-derived cells, native IAPP and Aβ produced are non-amyloidogenic [120, 437,

510], limiting the likelihood of endogenously secreted IAPP / APP contributing to the findings presented in this chapter.

The peptide concentrations used in this study ranged from 'low' (0.5-1 μM) to 'mid' (2-10 μM), and 'high' (25-50 μM) for 24 h. Whilst these concentrations are considered supraphysiological (and the treatment times subphysiological) compared to that seen in human plasma, the treatments used within this chapter are consistent with conditions used in comparable studies. When examining the effect of amyloidogenic peptides in pancreatic cells *in vitro* (predominantly IAPP, as few studies have explored the effects of Aβ on pancreatic tissue), previous publications have used concentrations ranging from 0.5-100 μM [511, 512], with 10-40 μM commonly used in both primary islets and pancreatic cell lines [145, 513-515]. Treatment times with these concentrations generally ranged from 2-48 h [514-518]. Furthermore, the concentration of IAPP in pancreatic β-cells is estimated to be much higher than the concentration in plasma, since the concentration of IAPP in secretory granules is calculated at 0.8-4 mM in secretory granules before secretion [179] and up to 400 μM in the immediate local environment after secretion [180].

When BRIN-BD11 cells were exposed to low (≤1 μM) concentrations of IAPP, Aβ, or IAPP-Aβ combination for 24 h, no significant changes in cell viability (Figure 21; Figure 22) or insulin secretion (Figure 23) were identified, nor was there evidence of increased cell stress (Figure 24). Given the relatively low concentration compared to other studies [129, 150], this is not unexpected. Increasing the concentration to 5 μM resulted in IAPP becoming cytotoxic in BRIN-BD11 β-cells, though this was not dose dependent and appeared to plateau in toxicity by 10 μM (Figure 25). Unlike IAPP alone, the IAPP-Aβ combination became cytotoxic between 3-5 μM and exerted a time- and dose-dependent effect. Moreover, at 50 μM, IAPP exerted its cytotoxicity rapidly, with a reduced cell viability and increased intracellular ROS generation by 6 h. At the same concentration, the combination was significantly more toxic than IAPP or Aβ alone, with a marked reduction in cell viability and an increase in intracellular ROS, although this was only observed at 24 h (Figure 26).

Aβ was not cytotoxic at any concentration or at any time point. These results are in agreement with the findings of the previous chapter (3.6, page 89), where in APP (Aβ) mice only no effect on islet function was noted but combined with IAPP, resulted in increased cellular stress. However, a large body of research on Aβ establishes its cytotoxicity in neuronal cells [14, 22, 129, 323, 324]. One reason for this contrasting effect on the two cell types could be structural and electrochemical differences between neuronal and β-cell membranes. Membrane fluidity, lipid composition, and electrostatic charge are all factors known to influence the aggregation and binding kinetics of Aβ and IAPP, and which can vary between different types of cells [519-522]. In β-cells specifically, Aβ may have poor adsorption into the cell membrane compared to IAPP and IAPP-Aβ. This may be due to electrostatic repulsion of Aβ until a conformational change via aggregation reveals more positively charged amino acid residues [130]. Essentially, Aβ may be unable to bind to the negatively charged β-cell membrane until sufficient aggregation has occurred. IAPP, as a cationic peptide [522], could more readily bind to the negatively charged β-cell membrane.

Despite Aβ's lack of toxicity in β-cells, the exacerbated toxicity profile of the Aβ-IAPP combination is consistent with previous work on neuronal cells. Bharadwaj et al. [129] (Appendix C; 8.3, page 236), found that the combination of IAPP-Aβ mixtures resulted in a 3-fold increase in neurotoxicity compared to IAPP or Aβ alone. The formation of large amorphous IAPP-Aβ heterocomplexes was also demonstrated in this study, which were distinct from the IAPP or Aβ oligomers. The exacerbated toxicity found in both neuronal cells [129] and the BRIN-BD11 β-cells could result from the distinct IAPP-Aβ aggregates forming unique and potent conformations. Alternatively, the co-aggregation of Aβ and IAPP maybe be altering aggregation kinetics, promoting toxicity as a result.

A significant amount of literature demonstrates that the oligomeric species of both IAPP and Aβ are the most cytotoxic, with protofibrils and fibrils becoming progressively more inert as they enter the elongation and saturation phases of aggregation [20, 125, 128, 135-137]. IAPP rapidly undergoes fibrillisation, with aggregates found to be in the elongation or saturation phase in as little as 4 h,

while this process was still on-going after 72 h for Aβ [129, 130]. Comparatively to IAPP and Aβ aggregates, IAPP-Aβ co-aggregates took approximately 24 h to reach the elongation and saturation phases [129, 130]. In accordance with these findings, the results in this chapter have shown that IAPP has a more cytotoxic profile than the IAPP-Aβ combination after 6 h of treatment, while the IAPP-Aβ combination was significantly more toxic at 24 h (Figure 26). Essentially, the delayed but exacerbated toxic profile of the IAPP-Aβ combination could result from IAPP in the presence of Aβ aggregating more slowly but remaining in the toxic oligomeric form for a longer period of time compared to IAPP alone, as shown by Bharadwaj et al. [129] in Appendix C (8.3, page 236).

Despite Aβ's lack of cytotoxicity in BRIN-BD11 β-cells, all amyloidogenic treatments, including Aβ, reduced GSIS levels at high concentrations (Figure 27). Aβ and its precursor APP have been shown to negatively modulate GSIS, particularly in islets of older mice [389, 390]. Additionally, a network-based modelling analysis of T2D-associated genetic and clinical traits identified the APP gene as crucial in the regulation of insulin secretion in obese B6XBTBR mice [390]. In this capacity, Aβ could function as a signalling molecule to reduce GSIS in the absence of cytotoxicity. Research on the effect of IAPP on GSIS has been more abundant but still uncertain, with some studies showing dose-dependent decreases [150, 172], while other studies have not shown significant changes [175, 176]. This discrepancy has been attributed to the concentrations of IAPP used, as concentrations of less than 5 μM do not appear to significantly inhibit insulin secretion [173]. Additionally, most studies were performed in the early 1990s upon identification of the peptide, [15, 65] when IAPP's aggregation kinetics were not fully understood, which means that early IAPP treatments were likely inconsistent in their aggregation states [73, 523]. The consensus of current research appears to be that IAPP concentrations above 5 μM reduce GSIS by dysregulation of calcium channels [173]. The IAPP-Aβ combination was the only treatment in this study that reduced both basal and stimulated insulin secretion, likely due to the highly toxic nature of IAPP-Aβ treatment on BRIN-BD11 β-cells rather than any specific targeting of insulin secretion mechanisms.

With changes in insulin secretion and intracellular ROS generation observed, a detailed investigation of bioenergetics and metabolism was conducted in BRIN-BD11 (Figure 28). This revealed that both the IAPP and IAPP-Aβ aggregates had similar toxic effects on mitochondrial function, altering parameters such as basal OCR, maximal OCR, and proton leak. Additionally, the expression of HSP60 (Figure 30), involved in the clearance of unfolded or misfolded proteins from mitochondria [214], was significantly increased in the IAPP-Aβ combination, although IAPP treatment also trended towards significance. SUR1, an important link between mitochondrial metabolism and insulin secretion [491], also showed similar increases in expression after treatment with both IAPP and IAPP-Aβ, again indicating similar mechanisms of toxicity. However, some mitochondrial parameters were more strongly affected by IAPP alone, such as the ATP production rate and coupling efficiency. Furthermore, only IAPP treated cells had an increased basal glycolytic rate (Figure 29) and a decreased expression of anti-apoptotic BCL-XL indicating that mitochondrial stress was severe enough to activate compensatory aerobic glycolysis and mitochondria-mediated apoptotic pathways.

This data is in mostly in accordance with the large body of work attesting to amyloidogenic targeting of mitochondria [150, 155]. In β-cells specifically, studies have shown IAPP is capable of inducing mitochondrial dysfunction via reducing oxygen consumption, mitochondrial membrane potential, and ATP production [150, 153, 154]. While there has been little examination of the impact of Aβ on β-cell mitochondrial function, both IAPP and Aβ were found to downregulate the expression of similar mitochondrial proteins, impairing ETC function and generating ROS in a neuronal cell line (though IAPP was found to have a stronger effect than Aβ) [155]. However, in agreement with other findings in this chapter, Aβ alone demonstrated limited mitochondrial toxicity in BRIN-BD11 β-cells.

In addition to mitochondrial damage, increases in iNOS and Active Cas3 expression was noted after exposure to IAPP and IAPP-Aβ, indicating increased cell stress and inflammation leading to apoptosis (Figure 31). There are several mechanisms by which IAPP and IAPP-Aβ could increase

intracellular stress and inflammation. Amyloidogenic peptides could activate ER stress via 'overwhelming' of the unfolded protein response [206]. However, our results do not demonstrate evidence of ER stress as BiP expression was unchanged (Figure 31), though future studies could explore this in more detail. For example, BiP, as the master regulator of the unfolded protein response in the ER, has recently been discovered to translocate to the cell surface under inflammatory conditions to act as a multifunctional pro-apoptotic signalling receptor in β-cells [227-229]. Additionally, BiP can undergo stress-induced secretion from β-cells, which can then function as a pro-apoptotic signalling molecule [227]. Future studies could examine BiP translocation and secretion after amyloidogenic peptide exposure, rather than expression alone.

An alternative mechanism for the cell stress and inflammation in BRIN-BD11 β-cells upon IAPP and IAPP-Aβ exposure involves oxidative stress (Figure 32). If the amyloidogenic aggregates were to induce ionic dysregulation, as the literature indicates [132, 524], this could simultaneously disrupt β-cell function and viability via impairment of calcium ion homeostasis [525]. Calcium ion regulation is crucial to both oxidative metabolism and insulin secretion, and the disturbance of it by amyloidogenic peptides would result in impaired insulin secretion and reduced capacity for oxidative phosphorylation [169-171]. In addition, the subsequent reduction in ATP would decrease the ATP : ADP ratio, further impairing insulin secretion [169, 171]. Simultaneously, the intracellular ROS would accumulate, activating inflammatory and apoptotic signalling pathways [13, 151]. The inflammatory environment would further insult the β-cell, exacerbating cellular stress, dysfunction in insulin secretion, and apoptosis [151, 202, 237]. In essence, the literature supports that oxidative stress could be the primary agent behind the amyloid-induced changes in BRIN-BD11 β-cells [13].

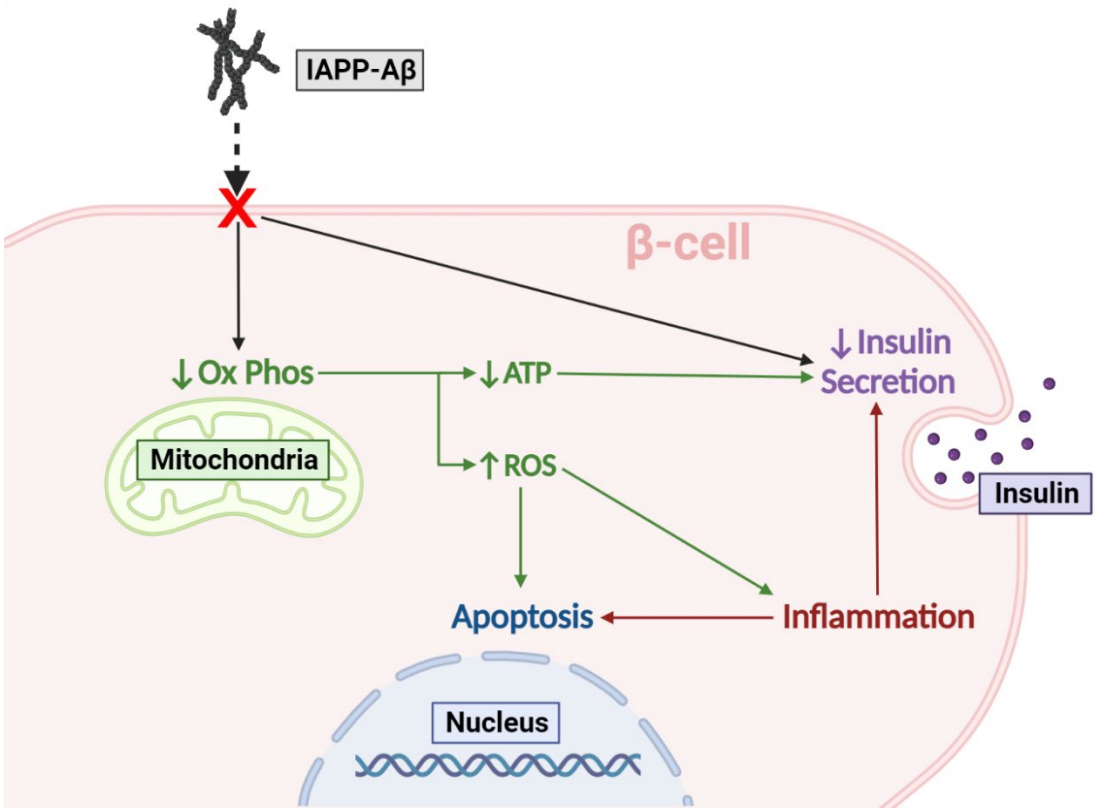

Figure 32. IAPP-Aβ aggregates induce oxidative stress and dysregulation in insulin secretion from BRIN-BD11 pancreatic β-cells. After exposure to IAPP-Aβ co-aggregates, BRIN-BD11 β-cells displayed a reduction in mitochondrial activity associated with oxidative phosphorylation. This resulted in a reduction in ATP production, impaired insulin secretion and an increase in ROS generation. An accumulation of intracellular ROS is correlated with increased expression of inflammatory and apoptotic markers and exacerbation of insulin dysregulation [151]. However, findings from this chapter also indicate that Aβ aggregates, and therefore potentially IAPP-Aβ co-aggregates, are capable of impairing glucose-stimulated insulin secretion directly, regardless of cytotoxicity. Figure created by author with Biorender.com.

Interestingly, Aβ was able to reduce GSIS (Figure 27) without affecting mitochondrial function (Figure 28), indicating it likely did so without ionic dysregulation. The mechanism by which it does this is uncertain, though studies have shown that Aβ can bind to IAPP receptors [410, 526]. As IAPP exerts autocrine functions in β-cells, regulating insulin secretion and β-cell proliferation in response to glucose [527, 528], it is possible that Aβ can regulate insulin secretion via similar mechanisms. Future work could explore receptor-mediated effects of IAPP, Aβ, and IAPP-Aβ on insulin secretion.

Additional future studies could include repeating similar work in other β-cell models. While BRIN-BD11 β-cells have a glucose-responsiveness more similar to isolated primary islets compared to other cell lines [507], disadvantages of their use in this study include that they are rodent cells responding to human peptides, and as such may not be reflective of human β-cell response. With access to isolated human β-cells limited, exploring the response of other cell lines, such as INS-1 and MIN6, or primary islets could be employed to determine if a uniform response to IAPP, Aβ, and IAPP-Aβ is present, and address some limitations of BRIN-BD11 β-cells (including longer treatment times). Future work could also include pre-treatment in diabetic culturing conditions, such as high glucose and high fatty acids [529], to explore if diabetic conditions aggravate amyloidogenic toxicity.

In conclusion, this chapter reports the novel finding that co-oligomerisation of Aβ with IAPP significantly potentiates IAPP toxicity compared to IAPP alone in β-cells and begins to explore underlying mechanisms. IAPP-Aβ hetero-complexes exacerbated apoptosis and dysfunction of BRIN-BD11 β-cells compared to Aβ or IAPP alone. This chapter additionally showed that GSIS was not only reduced by IAPP and IAPP-Aβ aggregates, but also by the non-cytotoxic Aβ aggregates, indicating downregulatory action independent from cytotoxic mechanisms. As T2D is characterised by both insulin secretion dysregulation and insulin resistance in peripheral tissues, the next chapter investigates the role of IAPP and Aβ, individually and in combination, on peripheral insulin resistance in human skeletal muscle cells.

CHAPTER 5 IAPP Cytotoxicity is Potentiated by Co-Aggregation with Aβ in Human Skeletal Myotube Cells

5.1 Abstract

Insulin resistance is an important feature of both Type 2 Diabetes (T2D) and Alzheimer's disease (AD). *In vitro* and *in vivo* evidence indicates that Aβ inhibits insulin signalling, contributing to both CNS and peripheral insulin resistance. However, the role of IAPP (an amyloidogenic peptide associated with T2D) is less clear. Furthermore, very few studies have investigated the effect of co-aggregation of IAPP-Aβ on peripheral insulin resistance. The previous chapters demonstrated that co-aggregation of IAPP and Aβ further augments β-cell stress. This chapter explores the role of these amyloidogenic aggregates in an insulin-sensitive tissue, skeletal muscle. To address this, the effects of Aβ, IAPP, or a co-aggregation of IAPP-Aβ on cell stress and insulin resistance were evaluated in human skeletal muscle cells (HSMM). Treatment of HSMM cells with IAPP-Aβ potentiated cell death compared to IAPP or Aβ alone, while IAPP had a more significant impact on mitochondrial function than Aβ peptides. In addition, treatment with all aggregates reduced glucose uptake in HSMM cells. These findings demonstrate that while Aβ itself is cytotoxic in isolation, it can reduce insulin sensitivity and potentiate IAPP cytotoxicity in HSMM cells.

5.2 Introduction

T2D is defined by pancreatic islet dysfunction and insulin resistance in peripheral tissues, such as the liver, adipose tissue, and skeletal muscle. Peripheral insulin resistance often precedes and promotes islet dysfunction [1]. To overcome the resistance, a higher insulin demand is required, resulting in an increased burden and stress on pancreatic β-cells to secrete increasing amounts of insulin. As it is co-secreted with insulin, IAPP secretion is also

increased [59]. Under healthy conditions, IAPP aids insulin's function of managing postprandial glucose levels [59], however, under pathological conditions, IAPP aggregates and has been shown to contribute to the disease burden in T2D.

As established in previous research (including observations in previous chapters), IAPP promotes cytotoxicity in pancreatic islets where it aggregates, affecting β-cell viability, function, and mitochondrial bioenergetics [133, 134, 247, 473]. However, the impact of abberant IAPP aggregates on peripheral tissues is largely unknown and still debated. Research on monomeric IAPP has elucidated roles in insulin sensitivity, glucose transport, and glycogen metabolism in peripheral tissues of animal models [23, 241, 242], indicating that these same mechanisms may be disrupted by aggregated IAPP. Although recent research in this area has been lacking, earlier research indicated that IAPP may potentially reduce insulin sensitivity in liver and skeletal muscle [242, 530, 531]. Additionally, studies show that IAPP can deposit not only in pancreatic islets, but also in additional organs such as the brain, heart, liver, and skeletal muscle, often co-aggregated with other amyloidogenic peptides [24, 25, 238-240, 247].

Observed to be co-deposited with IAPP in the brain and pancreas, Aβ has also been shown to deposit in peripheral tissues such as the heart, liver, and skeletal muscle [400]. While the effect of IAPP on peripheral insulin resistance is still deliberated, studies have shown Aβ is capable of inhibiting insulin signalling throughout the body, including in the brain, liver, and skeletal muscle [6, 413, 532]. Consistent with these findings, Wijesekara et al. [247] (Appendix B; 8.2, page 235) noted that transgenic human APP mice had reduced peripheral insulin sensitivity compared to transgenic IAPP and nontransgenic mice. In addition to this finding, Wijesekara et al. [247] also noted no significant impairment in insulin sensitivity of liver or skeletal muscle in transgenic human IAPP mice, despite cytotoxicity the IAPP in pancreatic islets. However, mice expressing both IAPP and Aβ (DTG mice) demonstrated peripheral insulin resistance and pancreatic islet dysfunction, indicating a more advanced state of T2D compared to mice expressing human IAPP or APP only.

While the Wijesekara et al. study [247] indicates that Aβ-induced insulin resistance in peripheral tissue was exacerbated by IAPP, underlying mechanisms remain to be determined and studies are lacking in more relevant human cell lines. To address these gaps in the literature, this chapter evaluates the effects of IAPP, Aβ, or an IAPP-Aβ combination on insulin resistance and cell stress in human skeletal muscle cells. Human skeletal muscle myotubes (HSMM) were exposed to oligomeric preparations of IAPP, Aβ, and IAPP-Aβ *in vitro*, then any changes in insulin signalling, cell viability, markers of cell stress, and alterations in bioenergetics were assessed.

5.3 Aim

Assess function, insulin signalling and cellular metabolism of HSMM cells exposed to Aβ, IAPP alone, or the combination of both IAPP and Aβ.

5.4 Materials and Methods

5.4.1 Amyloidogenic Peptide Preparation

The methodology to prepare an 100 μM oligomeric IAPP, Aβ or IAPP-Aβ peptide stocks in phenol red-free Ham's F-12 media (2% v / v of DMSO) is outlined in both Chapter 2 (2.2.1, page 48) and Chapter 4 (4.4.1, page 100) and based upon established protocols [129, 419, 420].

5.4.2 Cell Culture

The primary human skeletal myoblast cell line, HSMM, was cultured in SkBMTM-2 Basal Medium supplemented with 10% v / v FBS, 50 μg / mL of bovine fetuin, 10 ng / mL of human recombinant epidermal growth factor, 1 ng / mL of human recombinant fibroblast growth factor, and 0.4 μg / mL of dexamethasone (2.2.2.2, page 49). Cells were cultured at 37 °C and 5% CO_2 and subcultured at approximately 50-60% confluency to prevent spontaneous differentiation of mononucleated myoblasts into multinucleated myotubes. Supplemented Basal Medium was changed every 2-3 days, and cells were viable up to passage 10 [422]. Differentiation of HSMM cells was induced by culturing in a fusion medium of 1:1 DMEM:F12 supplemented with 2% horse serum and 1% penicillin streptomycin. Briefly, HSMM cells were subcultured,

counted, and then seeded into cell culture plates (6-, 24- or 96-well) with fresh SkBMTM-2 Basal Medium and left to adhere overnight (2.2.2.4, page 49). After overnight incubation, the supernatant was replaced with fusion medium. The HSMM cells were cultured in the fusion medium for 5 days to allow for differentiation prior to treatment, with the supernatant discarded and fresh Fusion Media added every 2-3 days (Figure 33; 2.2.2.3, page 49). All experimentation was conducted on differentiated HSMM cells, unless otherwise stated.

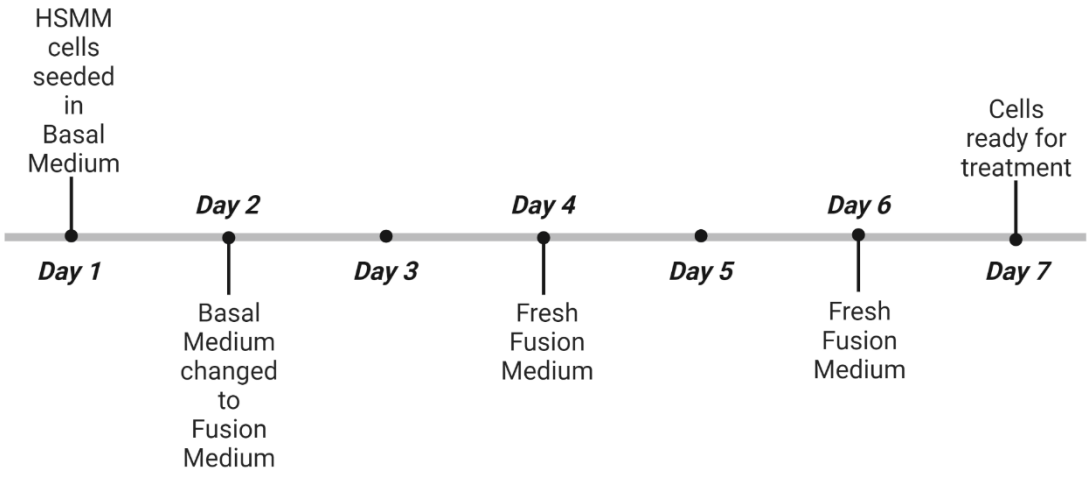

Figure 33. Timeline of HSMM cell differentiation process. Mononucleated human HSMM cells combine and terminally differentiate from myoblasts to multinucleated elongated myotubes in culture via a specialised culturing process over a period of 7 days. Once differentiated, the myotubes were suitable for experimentation.

After differentiation, HSMM cells were treated with SkBMTM-2 Basal Medium supplemented with a concentration of 5-50 µM of oligomeric amyloidogenic peptides for 24-48 h, depending on experimental requirements. All amyloidogenic treatments included appropriate controls, including a media control (Fresh SkBMTM-2 Basal Medium only) and vehicle control (Fresh SkBMTM-2 Basal Medium supplemented with DMSO in Phenol Red-free Ham's F-12 media equivalent to the percentage found in amyloidogenic peptide treatment).

5.4.3 RT-PCR

HSMM cells were seeded into 6-well plates at the manufacturer's recommended density of 1 x 10^5 cells per well, left to adhere overnight before differentiation into myotubes. In addition, densities of 5 x 10^3, 1 x 10^4, 2 x 10^4,

or 4 x 10^4 HSMM cells per well were seeded into 96-well plates, and similarly left to adhere overnight before differentiation. After differentiation, RNA from myotubes, as well as undifferentiated myoblast controls, was extracted and used to synthesise cDNA to perform RT-PCR (2.2.13, page 62) in quadruplicate wells in a 384-well plate. The expression of genetic markers of differentiation Myogenin (MYOG), Myosin Heavy Chain II (MHC2), and Troponin T Type 3 (TNNT3) were analysed via the comparative Ct ($\Delta\Delta$Ct) method. Values were normalised to those achieved with the housekeeping gene β-2 Microglobulin (β2M) and expressed as relative quantification from myoblast controls.

5.4.4 Mitochondrial Stress Test

In initial optimisation experiments, densities of 5 x 10^3, 1 x 10^4, 2 x 10^4, or 4 x 10^4 HSMM cells per well (quadruplicate wells) were seeded into specialised XF^{e}96 cell culture plates and left to adhere overnight before differentiation into myotubes. Once differentiated, densities of 5 x 10^3, 1 x 10^4, 2 x 10^4, or 4 x 10^4 undifferentiated HSMM cells per well were additionally seeded the day prior to the assay and left to adhere overnight before the assay. In later experiments, an optimised density of 1 x 10^4 HSMM cells per well were seeded into specialised XF^{e}96 cell culture plates and left to adhere overnight before differentiation into myotubes. Once differentiation was complete, HSMM cells were treated for 24 h with amyloidogenic peptides in quadruplicate wells.

The Mitochondrial Stress Test (2.2.11, page 56) was performed according to manufacturer's protocol. Briefly, injections of the mitochondrial modulator drugs Oligomycin, FCCP, and an Antimycin A and Rotenone combination were optimised for HSMM cells (Table 6, page 58), and administered at 21min intervals. OCR (pmol / L / min) measurements were recorded before and after the injections by the Agilent Seahorse XFe96 flux analyser, and then used to calculate parameters of mitochondrial function, including basal respiratory rate, maximum respiratory rate, ATP Production, mitochondrial coupling efficiency, proton leak, and spare respiratory capacity (Figure 7, page 59). The BCA Assay (2.2.5, page 51) was used to normalise by protein and results were expressed as the fold change from control measurements.

5.4.5 MTT Assay

A density of 1 x 10^4 HSMM cells per well were seeded into 96-well plates and left to adhere overnight before differentiation into myotubes. Once differentiation was complete, HSMM cells were treated for 24 or 48 h with amyloidogenic peptides in quadruplicate wells. Following treatment, an MTT Assay (2.2.3, page 50) was performed. Results were expressed as relative fold change in cell viability compared to the media control.

5.4.6 PI Staining

A density of 1 x 10^5 HSMM cells per well were seeded into 6-well plates and left to adhere overnight before differentiation into myotubes. Once differentiation was complete, HSMM cells were treated for 24 h with amyloidogenic peptides in duplicate wells. After treatment, HSMM cells were harvested and PI Staining (2.2.9, page 55) was performed, using 40 µg / mL of PI. Using flow cytometry, single cell populations were isolated via gating, and a minimum of 1 x 10^4 events were recorded per sample. The percentage of PI negative (non-apoptotic) cells out of the total cell count were measured. Results were expressed as relative fold change compared to the media control.

5.4.7 Western Blot Analysis

A density of 1 x 10^5 HSMM cells per well were seeded into 6-well plates and left to adhere overnight before differentiation into myotubes. Once differentiation was complete, HSMM cells were treated for 24 h with amyloidogenic peptides. If used for insulin signalling analysis, HSMM cells were cultured in serum-free media for 4 h, before a 20 min incubation with 100 nM insulin. After treatment, HSMM cells were lysed and a BCA Assay (2.2.5, page 51) was conducted for protein quantification to prepare samples for Western Blot Analysis (2.2.8, page 52). Primary antibodies used in this study included anti-Akt, anti-pAkt T308, and anti-pAkt S473 antibodies as markers of insulin signalling [533, 534]. Protein expression of stress markers was also examined using antibodies including anti-Activating Transcription Factor 4 (ATF4), anti-Sirtuin1 (SIRT1), anti-BiP, anti-HSP60, and anti-Active Cas3.

Anti-GAPDH antibodies were used as loading controls. HRP-linked secondary antibodies used in this study include anti-Rabbit IgG and anti-Mouse IgG.

5.4.8 Glucose Uptake Assay

A density of 1 x 10^5 HSMM cells per well were seeded into 6-well plates and left to adhere overnight before differentiation into myotubes. Once differentiation was complete, HSMM cells were treated for 24 h with amyloidogenic peptides in duplicate wells. After treatment, HSMM cells were incubated for 20 min with or without both 100 µM of 2-NDBG and 100 nM of insulin as per Glucose Uptake (2.2.14, page 63) protocol. Using flow cytometry, single cell populations were isolated via gating, and a minimum of 1 x 10^4 events were recorded. Results were expressed as the mean fluorescent intensity.

5.4.9 Intracellular ROS assay

A density of 1 x 10^5 HSMM cells per well were seeded into 6-well plates and left to adhere overnight before differentiation into myotubes. Once differentiation was complete, HSMM cells were treated for 24 h with amyloidogenic peptides in duplicate wells. After treatment, HSMM cells were incubated with the intracellular ROS probe CM-H2DCFDA (2.2.10, page 56) for 30 min at 37 °C, protected from light. Cells were harvested and were incubated with 40 µg / mL of PI as per the PI Staining (2.2.9, page 55) protocol, for simultaneous co-staining of intracellular ROS and to exclude apoptotic cells from measurement. Using flow cytometry, single cell populations were isolated via gating, and a minimum of 1 x 10^4 events were recorded. Each treatment group had additional controls with an absence of any staining to determine blank measurements and assist in optimisation and gating. Results were recorded as the mean fluorescent intensity expressed as the fold change from control, as well as the percentage of total cells positive for intracellular ROS.

5.4.10 Glycolytic Rate Assay

A density of 1 x 10^4 HSMM cells per well were seeded into specialised XFe96 cell culture plates and left to adhere overnight before differentiation into myotubes. Once differentiation was complete, HSMM cells were treated for 24 or 48 h with amyloidogenic peptides in quadruplicate wells. After treatment,

the Glycolytic Rate Assay (2.2.12, page 59) was conducted according to manufacturer's protocol. Briefly, measurements of PER (pmol / L / min) were recorded before and after injection of a combination of the mitochondrial modulators Antimycin A and Rotenone, followed after a 21 min interval by 2-DG (Table 8, page 61). Cell-free control wells were with serial injections of 5 mmol / L HCl to account for buffering capacity of the media. Changes in PER were detected by the Seahorse XFe96 flux analyser through changes in pH (Figure 9, page 62) and used to determine parameters of glycolytic function, including basal and compensatory glycolytic rate. A BCA Assay (2.2.5, page 51) was used to normalise by protein and results were expressed as the fold change from control measurements.

5.4.11 Data Analysis

All experiments were performed a minimum of three times. Statistical analysis was performed by GraphPad Prism Version 8 Software. Normality testing was performed on all data prior to analysis. One-way ANOVA with Tukey multiple comparisons Post-Hoc testing was used to determine statistically significant changes between treatment groups. Two-way ANOVA with Sidak's multiple comparisons Post-Hoc testing was used to determine changes between groups over time. No nonparametric analysis was used in this chapter as normality testing found all data to be normally distributed. All data is expressed as mean ± SEM. The limit of statistical significance was set at 0.05 ($p \leq 0.05$).

5.5 Results

5.5.1 Optimisation of HSMM differentiation in 96-well plates

HSMM cells, as myoblasts, are able to fuse and terminally differentiate into mature myotubes for a more appropriate *in vitro* model of human skeletal muscle [422, 423]. Culturing and differentiation of HSMM in 96-well plates was required for both the MTT assay and mitochondrial stress test, however, previously established laboratory and manufacturer protocols differentiation had been optimised for use in 6-well plates only. As such, optimisation of cell density was needed to confirm differentiation and metabolic activity of HSMM cells in 96-well plates was both appropriate and sufficient.

HSMM cells were seeded at densities of 5 x 10^3, 1 x 10^4, 2 x 10^4, or 4 x 10^4 cells per well in 96-well plates and differentiated. Using RT-PCR, specific markers for differentiated HSMM cells were assessed, including MYOG, MHC2, and TNTT3 (Figure 34). Compared to myoblast controls, both 5 x 10^3 and 1 x 10^4 cells per well of myotubes showed increased expression of MYOG ($p = 0.046$ and 0.047 respectively) and MHC2 (Figure 34A-B; $p = 0.005$ and 0.040 respectively). Only 5 x 10^3 cells per well had significantly increased expression of TNTT3 compared to myoblast controls (Figure 34C; p value= 0.014)

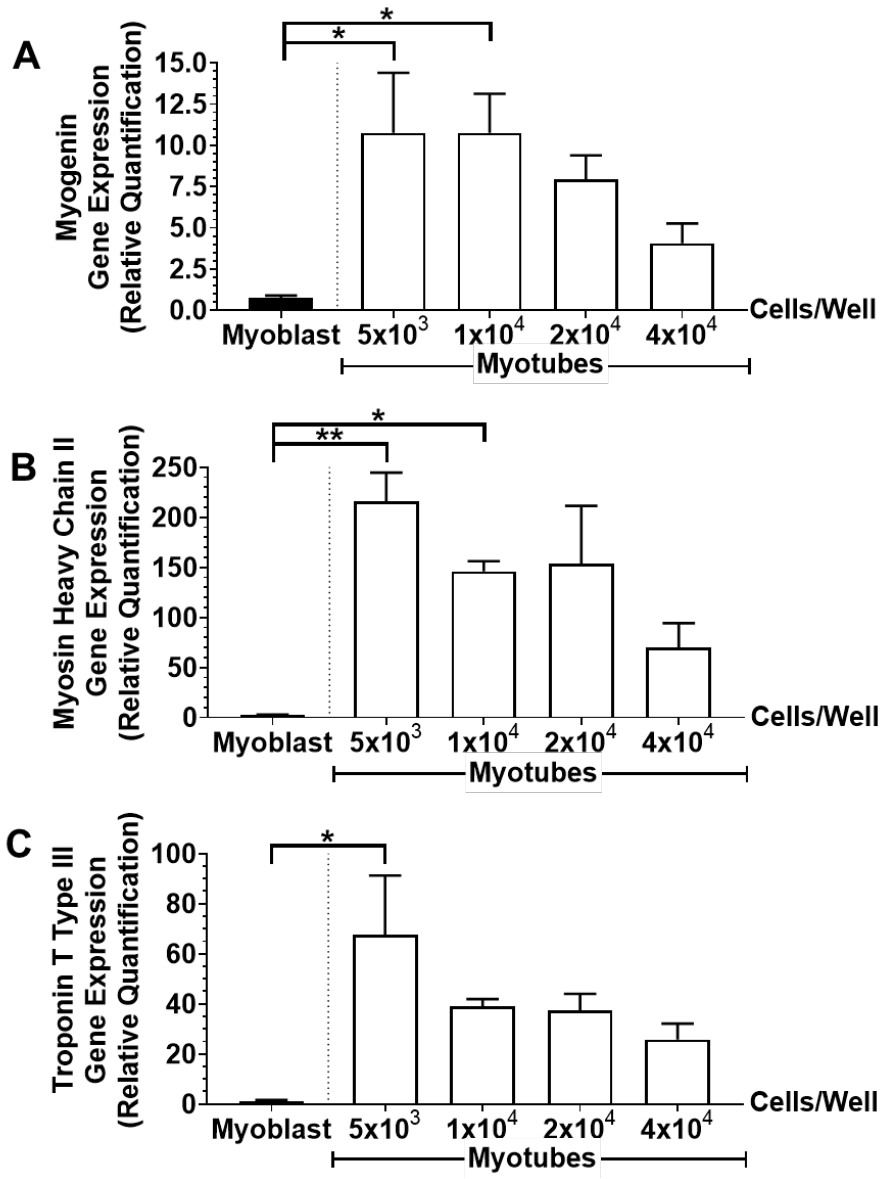

Figure 34. Lower HSMM cell densities showed increased expression of differentiation markers compared to higher cell densities in a specialised 96-well plate. To determine the optimum cell density for human skeletal muscle myoblasts health and differentiation, HSMM cells were subcultured at varying cell densities in 96 well plate and differentiated into myotubes. Expression of markers of differentiation, including (A) Myogenin, (B) Myosin Heavy Chain II, and (C) Troponin T Type III, were analysed via RT-PCR and comparative Ct ($\Delta\Delta$Ct) method, normalised via house-keeping gene β-2 Microglobulin. Results were expressed as the mean relative quantification ± SEM in bar graphs (N=3), with statistical analysis via one-way ANOVA with Tukey's multiple comparisons test to determine variation between experimental groups. * = statistical significance compared to indicated experimental group. *p value=< 0.05, **p value=< 0.01, ***p value=< 0.001, ****p value=< 0.0001.

Despite this result, the OCR of HSMM cells at a density of 5 x 10^3 cells per well (both myotubes and myoblasts) was below the Agilent Seahorse XFe96

flux analyser manufacturer's recommended basal level [535] (Figure 35). While myotubes at densities of 2 x 10^4 and 4 x 10^4 cells per well exhibited OCR measurements above the recommended levels [535]. Compared to equivalent densities of myoblasts, significant reductions in basal OCR, ATP production and maximum OCR of myotubes was noted. These results indicated that at the described densities, myotubes displayed reduced mitochondrial activity (Figure 35A-C; p value=< 0.0001 for all), consistent with metabolic quiescence or potential cellular stress at higher cell densities after differentiation. A density of 1 x 10^4 cells per well showed the appropriate balance between differentiation and sufficient cellular metabolism, as demonstrated by sufficient basal OCR and mitochondrial activity compared to the other cell densities. In addition, the expression of markers of differentiation at this density was similar to that observed for 6-well plates at manufacturer recommended densities (Figure 36). Thus, 1 x 10^4 cells per well was chosen to progress to subsequent experiments in 96-well plates

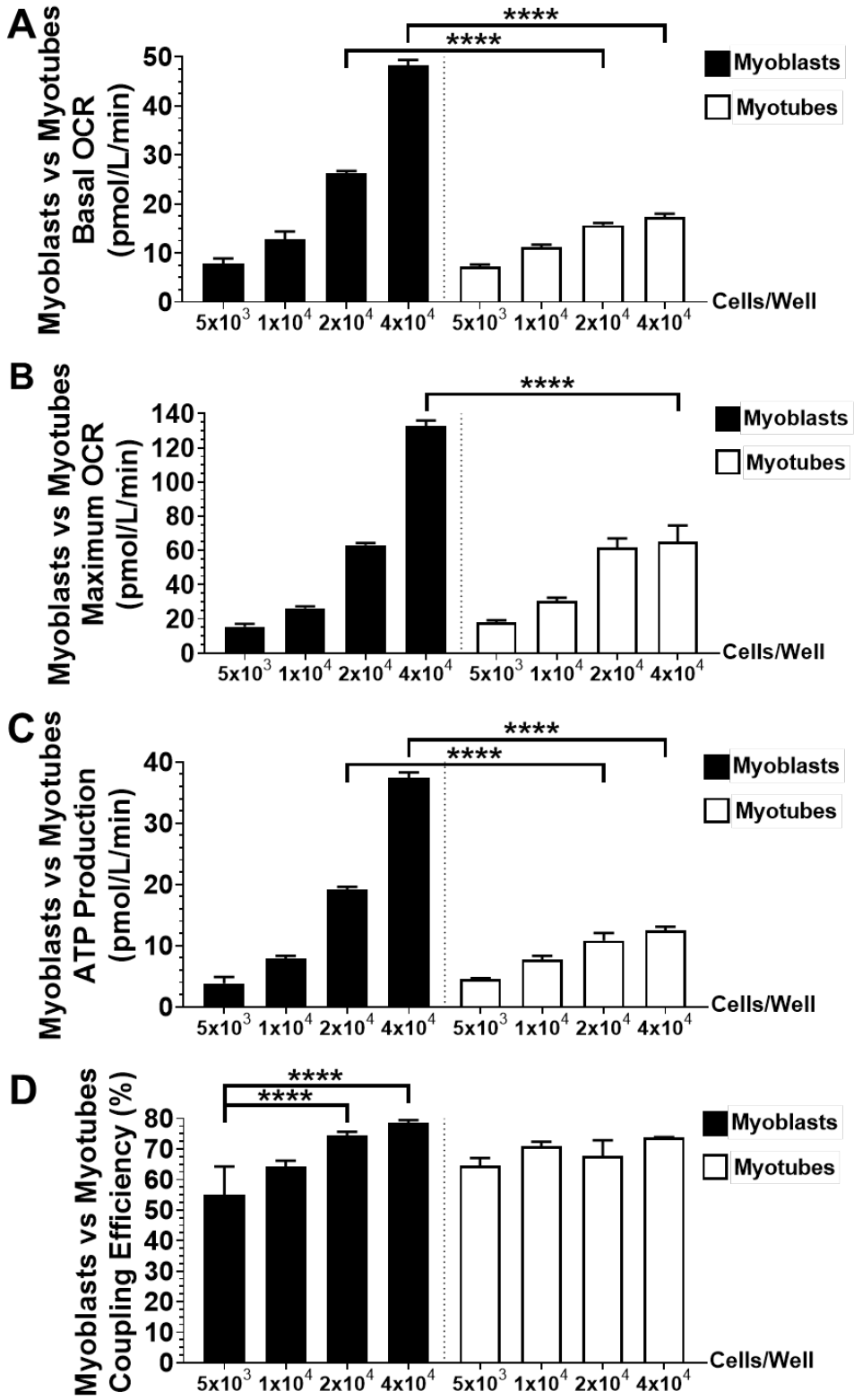

Figure 35. High cell densities of differentiated HSMM cells showed impaired bioenergetics in a specialised 96-well plate. Mitochondrial stress testing was performed on HSMM cells seeded at different cell densities in a specialised 96-well plate. Using a Seahorse XF^{e}96 Flux Analyser, alterations in key parameters of mitochondrial function via changes in the oxygen consumption rate (OCR) upon exposure to mitochondrial modulators were

examined. Results were quantified as mean OCR ± SEM (N=3 in quadruplicate) and expressed as OCR in pmol / L / min in bar graphs, including (A) Basal OCR, (B) Maximum OCR, (C) ATP Production, and (D) % Coupling Efficiency. Statistical analysis via one-way ANOVA with Tukey's multiple comparisons test to determine variation between experimental groups. * = statistical significance compared to indicated experimental group. *p value=< 0.05, **p value=< 0.01, ***p value=< 0.001, ****p value=< 0.0001.

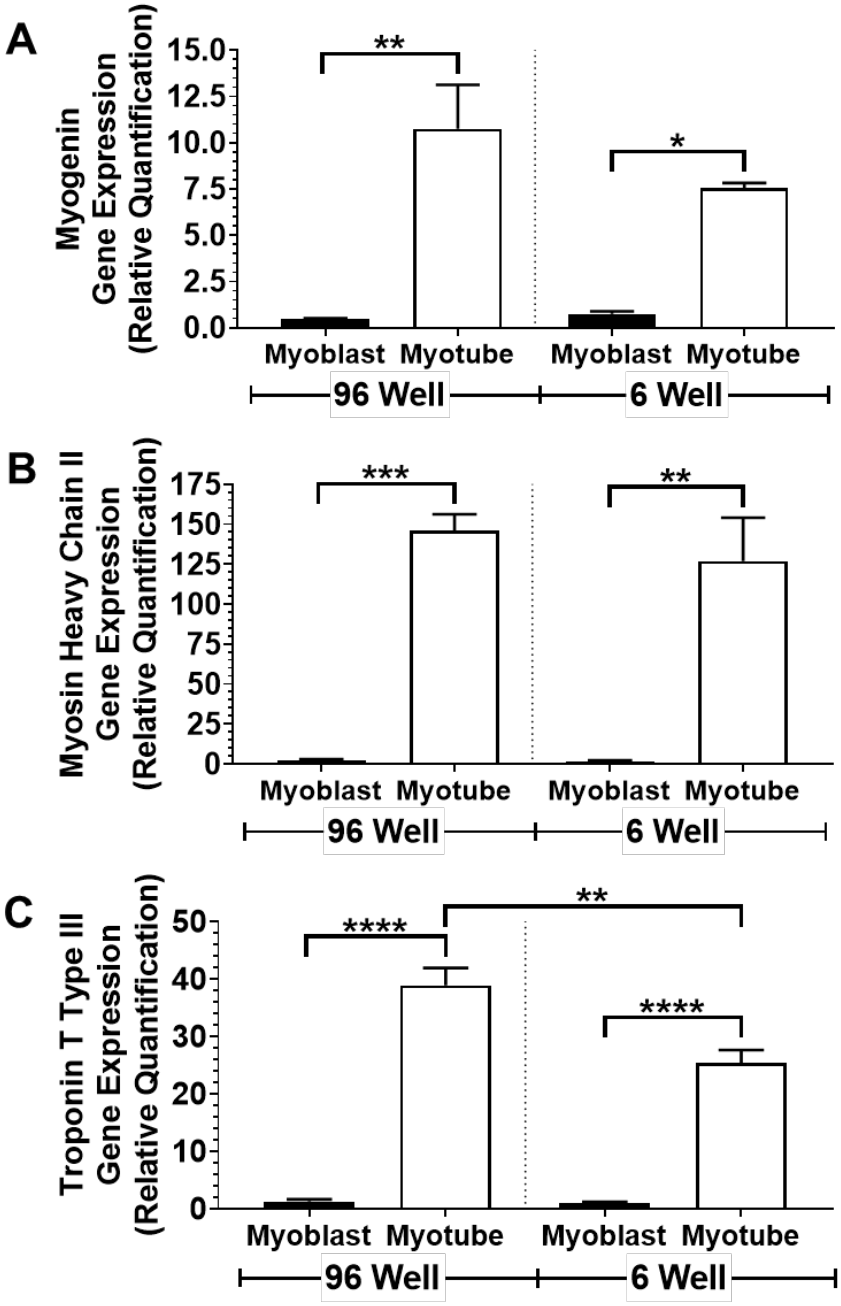

Figure 36. HSMM cells at a density of 1 x 10^4 cells per well in a 96-well plate showed comparable expression of markers of differentiation to the recommended density in a 6-well plate. To determine if the differentiation of HSMM cells at the optimised cell density of 1x10^4 cells per well in a 96-well plate was comparable to the manufacturor's recommended

cell density in a 6-well plate, human skeletal muscle myoblasts were subcultured at a density of $1x10^4$ cells per well in a 96-well plate and $1x10^5$ cells per well in a 6-well plate. Expression of markers of differentiation, including (A) Myogenin, (B) Myosin Heavy Chain II, and (C) Troponin T Type III, were analysed via RT-PCR and comparative Ct ($\Delta\Delta$Ct) method, normalised via house-keeping gene β-2 Microglobulin. Results were expressed as the mean relative quantification ± SEM in bar graphs (N=3), with statistical analysis via one-way ANOVA with Tukey's multiple comparisons test to determine variation between experimental groups. * = statistical significance compared to indicated experimental group. *p value=< 0.05, **p value=< 0.01, ***p value=< 0.001, ****p value=< 0.0001.

5.5.2 The IAPP-Aβ combination reduces viability of differentiated HSMM cells

Having optimised the seeding density, experiments progressed to determining the effect of the amyloidogenic peptides. HSMM cells differentiated into myotubes were exposed to 5-50 μM of IAPP, Aβ or IAPP-Aβ combination for 24 h (Figure 37A) or 48 h (Figure 37B), then assessed for viability using an MTT assay. After 24 h, 25 and 50 μM concentrations of the IAPP-Aβ combination reduced cell viability compared to all controls and amyloidogenic treatments ($p = 0.007$ and < 0.0001 vs vehicle controls, 0.0014 and 0.0235 vs IAPP, and 0.0021 and 0.0007 vs Aβ respectively). Exposure of cells to IAPP-Aβ for 48 h led to further reductions at 25 μM and 50 μM ($p < 0.0001$ vs vehicle controls and Aβ, and 0.0009 and 0.0010 vs IAPP), including a marked reduction in cell viability at a lower concentration (10 μM) compared to controls and other amyloid treatments (p value=< 0.0001 for all).

As there is limited evidence in the literature of peripheral tissue cell loss in T2D, the effective but minimally toxic concentration of 10 μM was selected as preferred concentration of amyloidogenic peptides to proceed. This concentration was further evaluated with PI staining assay (Figure 37C), where the IAPP-Aβ combination concurred with MTT results, demonstrating increased cytotoxicity compared to other treatments at 24 ($p = 0.0312$ vs vehicle control) and 48 h ($p < 0.0001$ vs vehicle control and Aβ, and 0.0101 vs IAPP). PI staining also detected a reduced cell viability in HSMM cells treated with 10 μM of IAPP after 48 h, despite MTT assay only demonstrating a significant reduction in cell viability at higher concentrations (50 μM after 48 h exposure; $p = 0.0051$).

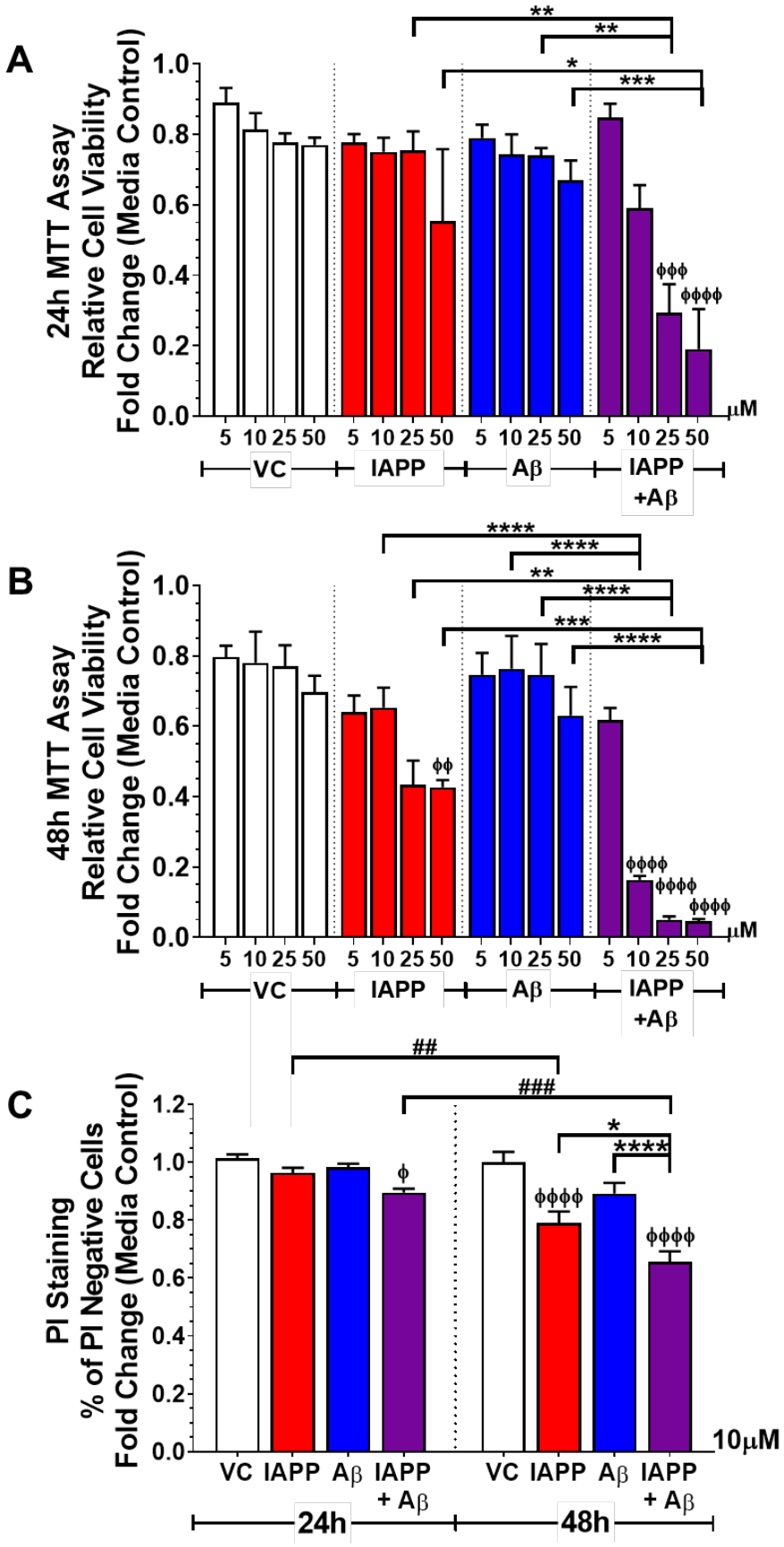

Figure 37. IAPP-Aβ combination exhibits a dose and time-dependent reduction in cell viability of HSMM cells. HSMM cells were treated with 5 μM-50 μM (B) of synthetic human

IAPP, Aβ42, or IAPP-Aβ aggregates for 24 h (A) or 48 h (B) before performing an MTT assay to determine changes in cell viability. Results were quantified as Mean ± SEM and expressed as the fold change from media control in bar graphs (N=3 in quadruplicate), and statistical analysis was performed via one-way ANOVA with Tukey's multiple comparisons test to determine variation between treatment groups. Following this, HSMM cells were treated with 10 μM of synthetic human IAPP, Aβ42 or IAPP-Aβ aggregates for 24 h or 48 h (C) and analysed via PI staining to validate MTT assay and determine changes over time. Results were quantified as mean ± SEM and expressed as the fold change from media control in bar graphs (N=5). Statistical analysis was performed via two-way ANOVA with Sidak's multiple comparisons test to determine variation between treatment groups and between time points. IAPP-Aβ combination = 1 : 1, so 50 μM of IAPP-Aβ = 25 μM IAPP + 25 μM Aβ. Vehicle control = 0.1-1% DMSO (equivalent to 5-50 μM of treatments; A and B) or 0.2% (equivalent to 10 μM of treatments; C). Φ = statistical significance compared to respective vehicle control, # = statistical significance compared to the same treatment over time, * = statistical significance compared to indicated treatment group. ^{Φ} / $^{\#}$ / *p value=< 0.05, ^{ΦΦ} / $^{\#\#}$ / **p value=< 0.01, ^{ΦΦΦ} / $^{\#\#\#}$ / ***p value=< 0.001, ^{ΦΦΦΦ} / $^{\#\#\#\#}$ / ****p value=< 0.0001.

In summary, these findings indicate that of all amyloidogenic peptide treatments assessed, the IAPP-Aβ combination demonstrated the most marked toxicity, with minimal toxicity demonstrated following treatment with IAPP only and no demonstrated cytotoxicity with Aβ only.

5.5.3 Amyloidogenic peptides reduced glucose uptake but did not alter the expression of insulin signalling proteins

To determine if amyloidogenic peptides altered insulin sensitivity of HSMM cells, expression of insulin signalling proteins was assessed. Expression of pAkt T308 and pAkt S473 were assessed as phosphorylation of Akt at these sites is an important step in the insulin signalling cascade activated in human skeletal muscle [533, 534]. Lysates from Chinese hamster ovary (CHO) cells were used as a technical control as they have robust insulin signalling machinery [536] and showed high expression of pAkt (Figure 38A). Compared to CHO cells, expression of pAkt T308 and pAkt S473 were markedly lower in HSMM cells, including controls, despite robust total Akt expression (Figure 31A). The pAkt T308 : Total Akt (Figure 38B) or pAkt S473 : Total Akt (Figure 38C) ratios were not altered following treatment with amyloidogenic peptides. No change in ratio was also observed with the insulin treatment, indicating minimal insulin-induced Akt phosphorylation in HSMM cells.

To investigate if other insulin-dependent mechanisms were altered in the absence of detectable Akt phosphorylation, a functional glucose uptake assay was performed. A trend towards an increase in glucose uptake was observed following exposure to insulin ($p = 0.1065$). Treatment with the amyloidogenic peptides led to a significant decrease in glucose uptake in all amyloidogenic treatments at 10 μM compared to control (Figure 38D; $p = 0.0041$ vs IAPP, 0.0004 vs Aβ, and 0.0011 vs IAPP-Aβ). Together, these data indicate that despite a perceived lack of insulin signalling observed for HSMM cells, all amyloidogenic peptide treatments reduced functional glucose uptake by these cells.

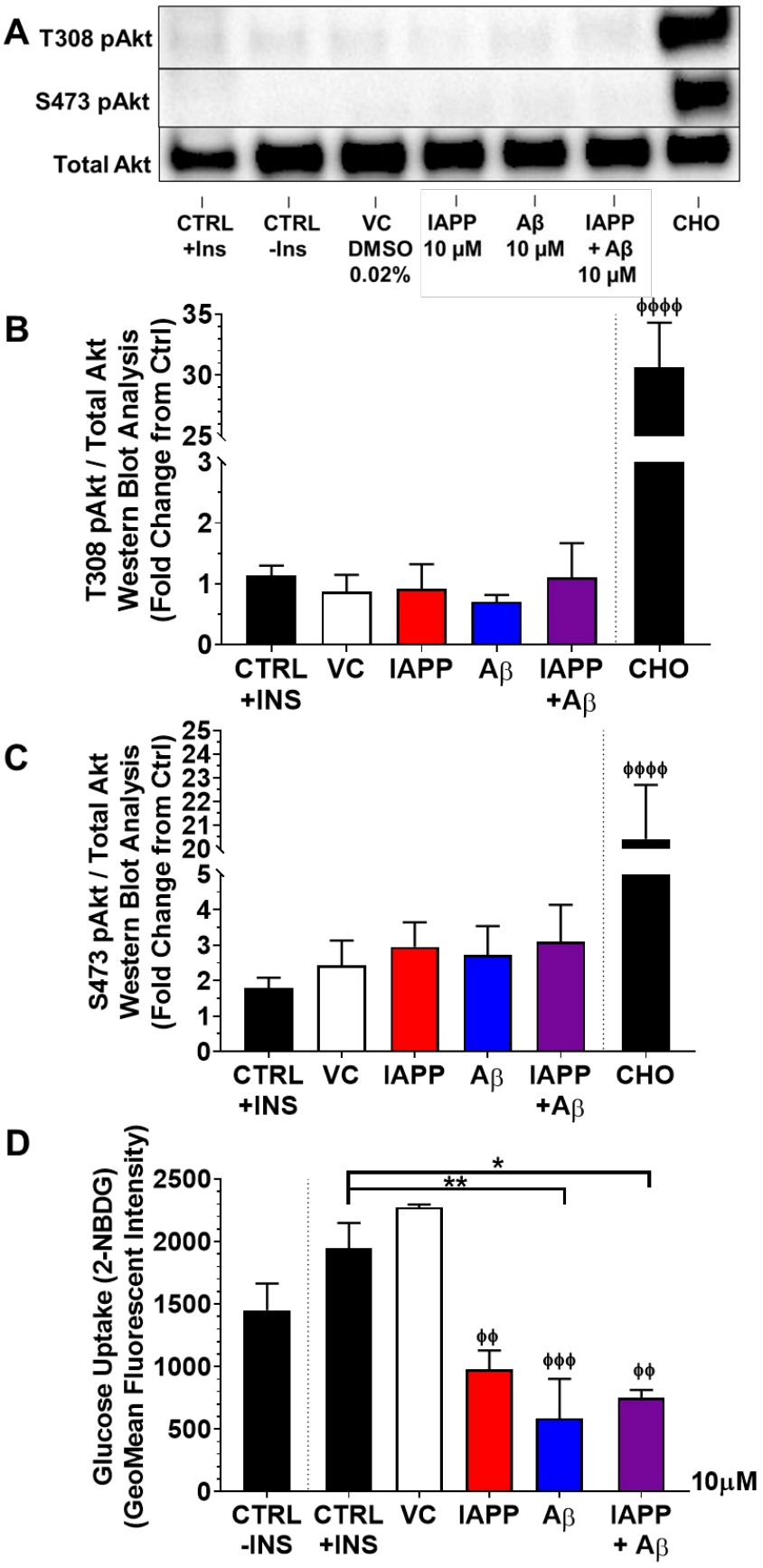

Figure 38. Amyloidogenic peptides did not alter expression of insulin signalling proteins but reduced functional glucose uptake in HSMM cells. HSMM cells were treated

with 10 μM of synthetic human IAPP, Aβ42, or IAPP-Aβ aggregates for 24 h before a 20 min incubation with 100 nM of insulin. Untreated HSMM cells (CTRL -INS), insulin-treated HSMM cells (CTRL +INS) and insulin-treated Chines Hamster Ovary (CHO) cells were used as negative and positive controls respectively. Lysates were then collected for western blot analysis to detect changes in protein expression associated with insulin signalling (A), including Total Akt, P-Akt (Thr308) and P-Akt (Ser473). Results were quantified as the mean ratio of P-Akt (Thr308 / Ser473) to Total Akt ± SEM and expressed as the fold change from media control in bar graphs (B and C, N=3). In addition, a glucose uptake assay was performed to determine functional changes related to insulin signalling. HSMM cells were treated with 10 μM of synthetic human IAPP, Aβ42 or IAPP-Aβ aggregates for 24 h before a 20 min incubation with or without 100 nM of insulin and 100 μM 2-NBDG before cells were harvested and analysed via flow cytometry (D; N=3 in duplicate). Results were expressed as mean fluorescent intensity ± SEM in bar graphs. Statistical analysis via one-way ANOVA with Tukey's multiple comparisons test to determine variation between treatment groups. Ctrl = media only control. Vehicle control = 0.2% DMSO (equivalent to 10 μM of treatments). Φ = statistical significance compared to respective vehicle control, * = statistical significance compared to indicated treatment group. $^{\Phi}$ / *p value=< 0.05, $^{\Phi\Phi}$ / **p value=< 0.01, $^{\Phi\Phi\Phi}$ / ***p value=< 0.001, $^{\Phi\Phi\Phi\Phi}$ / ****p value=< 0.0001.

5.5.4 IAPP, but not Aβ, impaired mitochondrial bioenergetics of HSMM cells

The findings above demonstrated altered glucose uptake and reduced cell viability in differentiated HSMM cells upon exposure to amyloidogenic peptides, particularly following treatment with IAPP-Aβ combination. As impaired mitochondrial function is a common mechanism of amyloidotoxicity, markers of mitochondrial stress were investigated further. Initially, an assay to measure intracellular ROS was performed. Differentiated HSMM cells were treated with 10 μM of amyloidogenic peptides for 24hrs. As a positive control, cells were treated with glucose oxidase (GOx) for 20 min. GOx is an enzyme which catalyses the oxidation of β-D-glucose to gluconic acid resulting in the generation of the intracellular ROS, hydrogen peroxide (H_2O_2) [537]. In response, the cell will increase intracellular glutathione, the target of the ROS probe CM-HF2DCFDA in the assay. Compared to vehicle treatment, the geometric mean fluorescent intensity of the probe did not significantly increase following exposure to the peptides or the positive treatment control, GOx. (Figure 39A). However, GOx treatment resulted in a 5-fold increase in the number of cells with detectable intracellular ROS, as determined by the

increased percentage of total events. No change was observed following amyloidogenic peptide treatment (Figure 39B), where the percentage was similar to that observed for vehicle control.

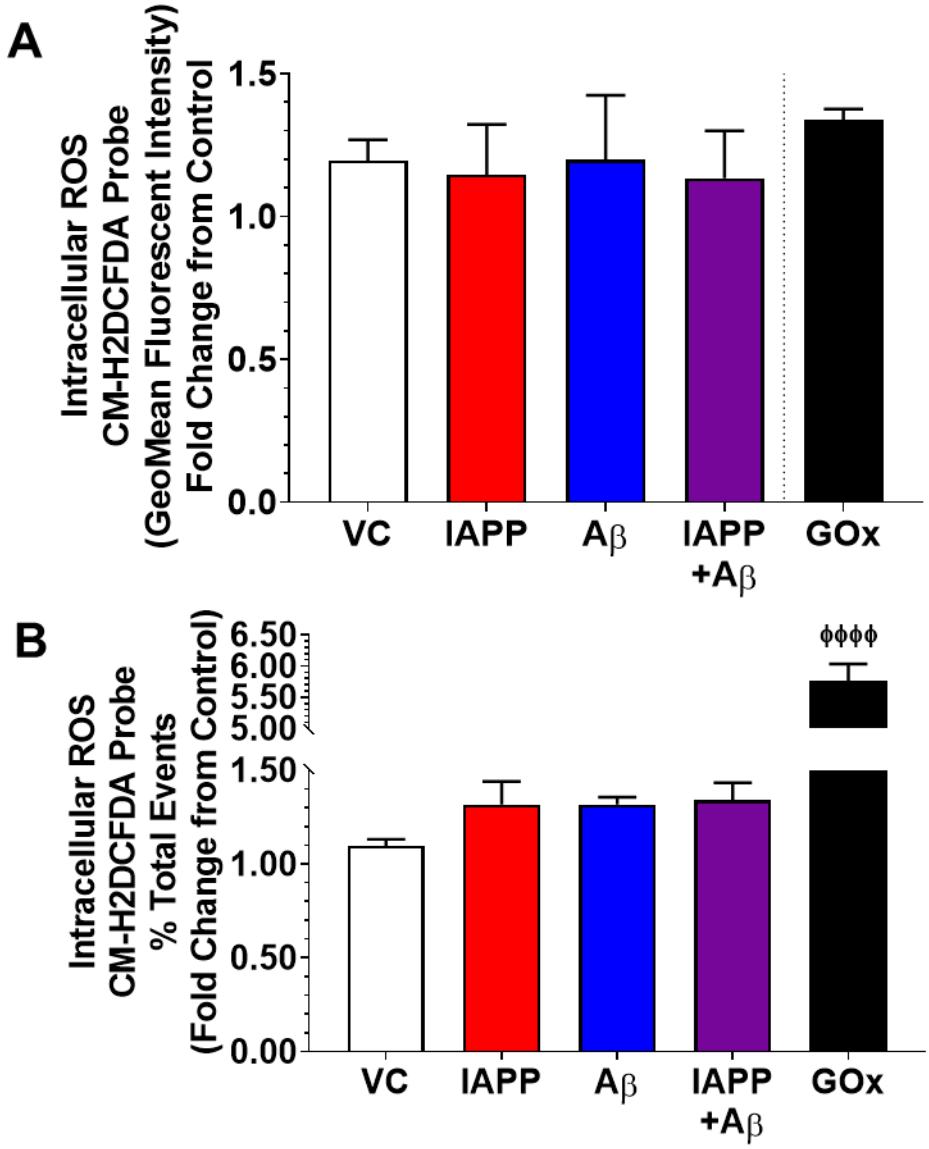

Figure 39. Amyloidogenic peptides did not increase intracellular ROS in HSMM cells. HSMM cells were treated with 10 μM of synthetic human IAPP, Aβ42, or IAPP-Aβ aggregates for 24 h before performing Intracellular CM-H2DCFDA ROS Assay. Intracellular ROS results were quantified as mean fluorescent intensity ± SEM and expressed as fold change from control in a bar graph (A; N=3 in duplicate). Due to minimal change in mean fluorescent intensity of ROS species (including with the positive control glucose oxidase; GOx), the percentage of total events positive for intracellular ROS were also analysed and expressed as fold change from control in a bar graph to confirm experiment validity (B; N=3 in duplicate). Statistical analysis via one-way ANOVA with Tukey's multiple comparisons test to determine variation between treatment groups. Φ = statistical significance compared to respective vehicle

control, * = statistical significance compared to indicated treatment group. $^{\Phi}$ / *p value=< 0.05, $^{\Phi\Phi}$ / **p value=< 0.01, $^{\Phi\Phi\Phi}$ / ***p value=< 0.001, $^{\Phi\Phi\Phi\Phi}$ / ****p value=< 0.0001.

The more sensitive mitochondrial stress test was performed using the Seahorse XF^{e}96 Flux Analyser (Figure 40) to further investigate if amyloidogenic peptides influenced mitochondrial function in HSMM cells. Compared to vehicle control, a reduction in basal OCR was observed following treatment with 10 μM IAPP-Aβ ($p = 0.0249$). Treatment with this peptide combination did not significantly alter any other parameter, while treatment with Aβ did not alter any of the parameters assessed. In contrast, treatment with IAPP resulted in marked reductions in many key parameters at 5 and / or 10 μM. This included basal OCR ($p = 0.004$ and 0.001 respectively), maximum OCR ($p = 0.0174$), ATP production ($p = 0.0013$ and 0.0061 respectively), and spare respiratory capacity ($p = 0.0204$). Compensatory glycolysis in response to reduced oxidative phosphorylation capacity was also investigated via a glycolytic rate test (Figure 41). Compared to the vehicle control, amyloidogenic peptide treatment did not significantly alter basal or compensatory glycolysis.

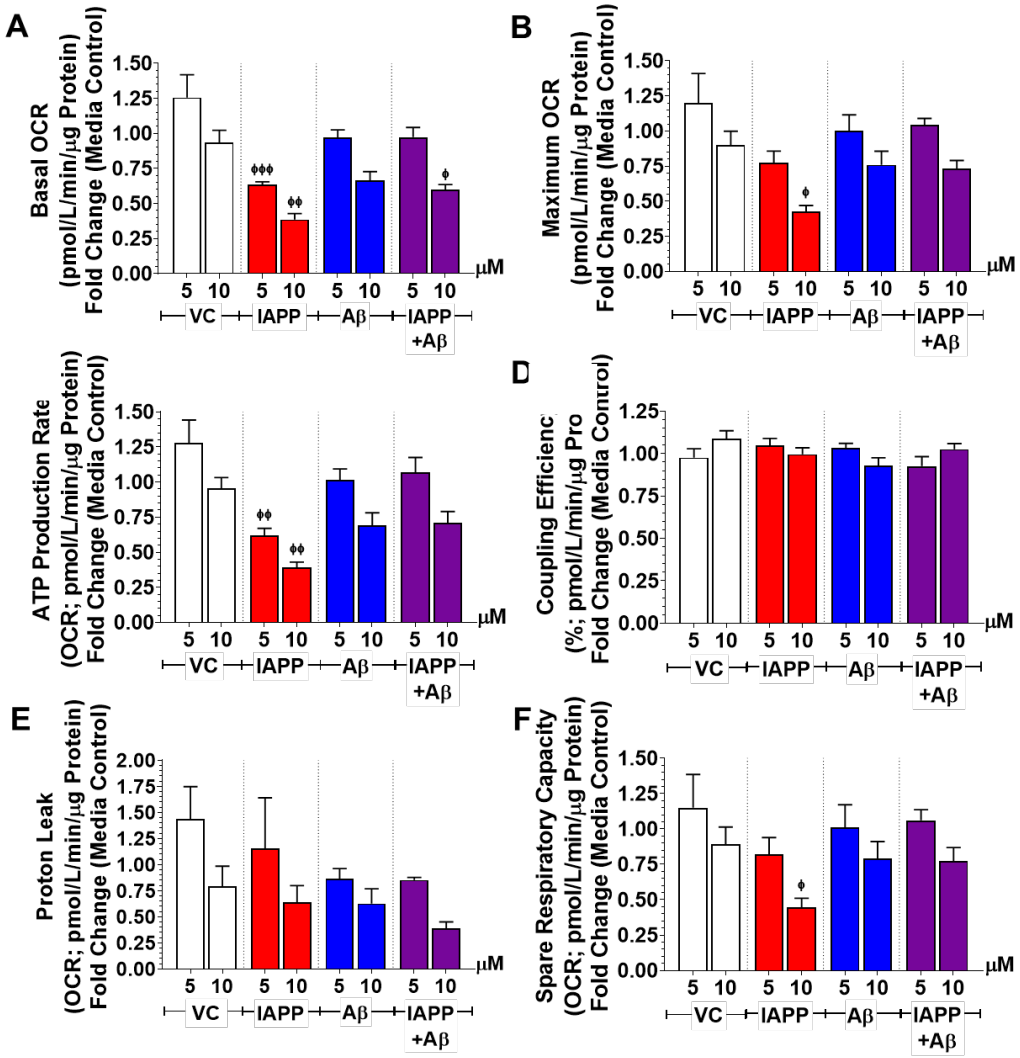

Figure 40. IAPP impacts mitochondrial dysfunction in HSMM cells more significantly than Aβ or IAPP-Aβ combination. HSMM cells were treated with 5 or 10 µM of synthetic human IAPP, Aβ42, or IAPP-Aβ aggregates for 24 h before performing mitochondrial stress testing. Using a Seahorse XF^{e}96 Flux Analyser, key parameters of mitochondrial function were identified via changes in the oxygen consumption rate (OCR) upon exposure to mitochondrial modulators. Results were quantified as mean OCR ± SEM and expressed as the fold change from media control in bar graphs (N=3 in quadruplicate), including (A) Basal OCR, (B) Maximum OCR, (C) ATP Production, (E) Proton Leak, (D) % Coupling Efficiency, and (F) Spare Respiratory Capacity. Statistical analysis via one-way ANOVA with Tukey's multiple comparisons test to determine variation between treatment groups. Φ = statistical significance compared to respective vehicle control, * = statistical significance compared to indicated treatment group. $^{\Phi}$ / *p value=< 0.05, $^{\Phi\Phi}$ / **p value=< 0.01, $^{\Phi\Phi\Phi}$ / ***p value=< 0.001, $^{\Phi\Phi\Phi\Phi}$ / ****p value=< 0.0001.

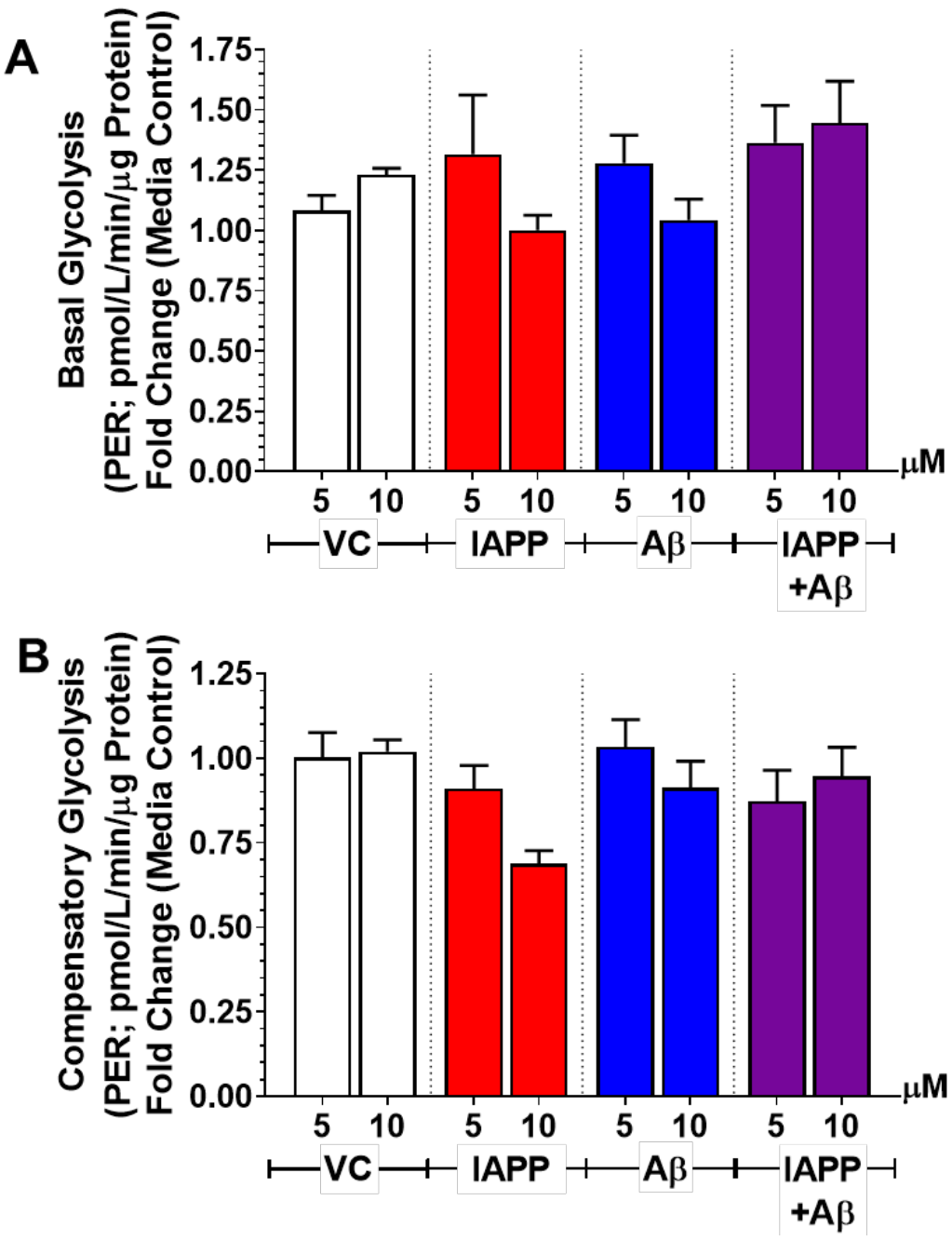

Figure 41. Amyloidogenic peptides do not increase basal or compensatory glycolytic rate in HSMM cells. HSMM cells were treated with 5 or 10 µM of synthetic human IAPP, Aβ42 or IAPP-Aβ aggregates for 24 h before performing glycolytic rate testing. Using a Seahorse XF^{e}96 Flux Analyser, key parameters of glycolysis were identified via changes in the proton efflux rate (PER) upon exposure to mitochondrial and glycolytic modulators. Results were quantified as mean PER ± SEM and expressed as the fold change from media control in bar graphs (N=3 in quadruplicate), including (A) Basal Glycolysis, and (B) Compensatory Glycolysis. Statistical analysis via one-way ANOVA with Tukey's multiple comparisons test to determine variation between treatment groups. Φ = statistical significance compared to respective vehicle control, * = statistical significance compared to indicated treatment group. $^{\Phi}$ / *p value=< 0.05, $^{\Phi\Phi}$ / **p value=< 0.01, $^{\Phi\Phi\Phi}$ / ***p value=< 0.001, $^{\Phi\Phi\Phi\Phi}$ / ****p value=< 0.0001.

Collectively, this data displays that only IAPP appears to alter mitochondrial function in HSMM cells more significantly than other amyloids, particularly impacting the basal metabolic rate and ATP production. However, this change did not result in significant ROS accumulation or compensatory glycolysis.

5.5.5 IAPP and IAPP-Aβ combination altered expression of oxidative stress proteins in HSMM cells

The results above indicated changes in mitochondrial activity following treatment with IAPP in particular. To determine if this was related to mitochondrial stress, levels of the mitochondrial stress proteins, HSP60 and Sirt1 were assessed via western blot analysis. HSP60 is a mitochondria-specific molecular chaperone with functions in clearing unfolded / misfolded proteins [214], while SIRT1 is a mitochondrial modulator with key roles in regulation of insulin resistance and cellular stress response [538]. Differentiated HSMM cells were treated for 24 hrs with 10 μM of the amyloidogenic peptides. As a positive control for mitochondrial stress, cells were also treated with Rotenone. HSP60 and Sirt1 expression was significantly decreased with Rotenone treatment as expected (Figure 42A; Figure 42C; Figure 42D). A trend towards a decrease was observed for HSP60 expression following IAPP-Aβ treatment (Figure 42C) ($p = 0.0920$). Sirt1 expression was significantly reduced following IAPP and IAPP-Aβ treatment (Figure 42D; $p = 0.0375$ and 0.0212 respectively).

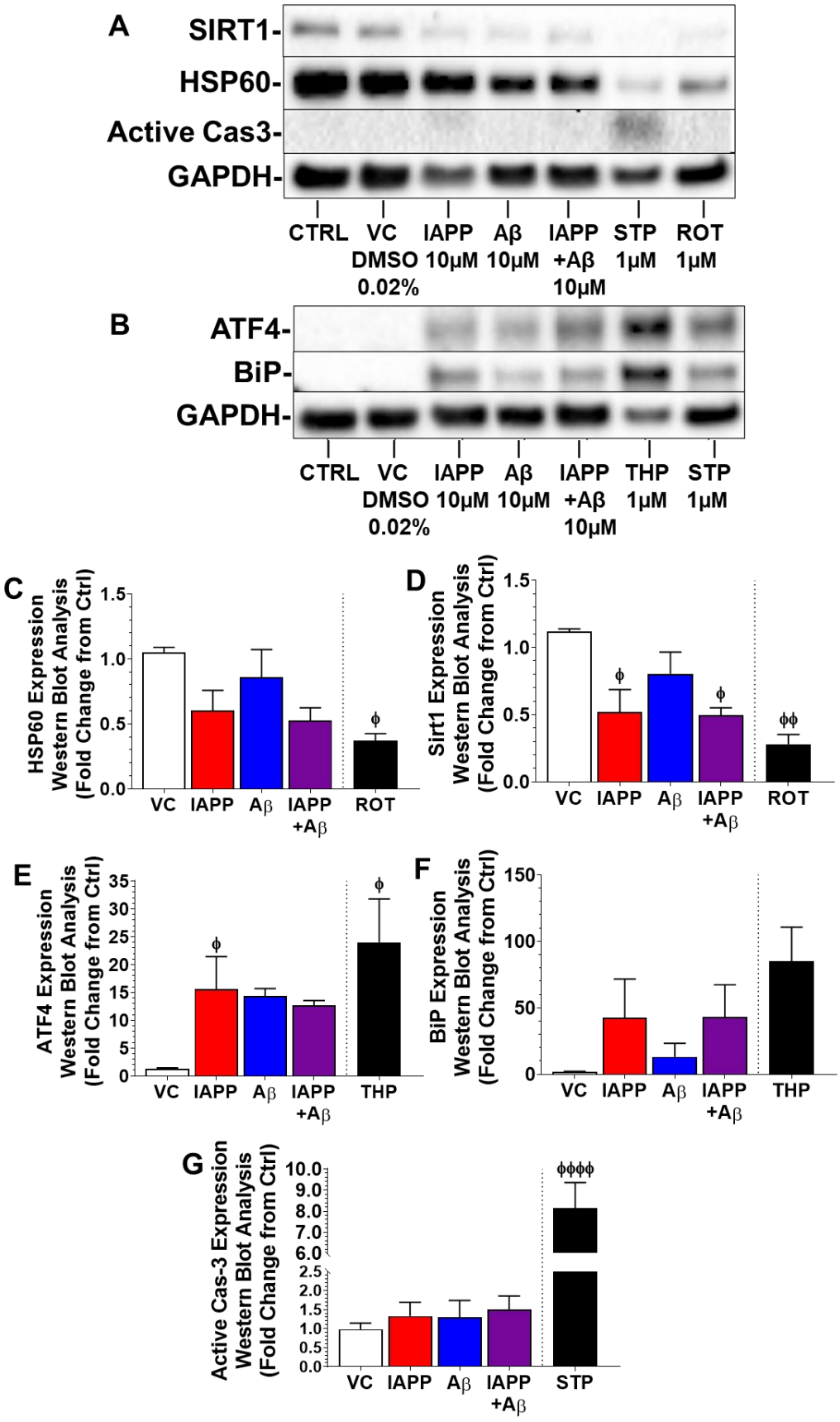

Figure 42. IAPP and IAPP-Aβ combination altered expression of cellular stress markers associated with oxidative stress in HSMM cells. HSMM cells were treated with 10 μM of

synthetic human IAPP, Aβ42, or IAPP-Aβ aggregates for 24 h before performing lysates were collected for western blot analysis to detect changes in protein expression associated with cellular stress and inflammation (A and B). Results were quantified as mean ± SEM and expressed as the fold change from media control in bar graphs (C – G; N=3). 24 h treatment of 1 μM of Rotenone (ROT) used as positive control for mitochondrial stress. 24 h treatment of 1 μM of Staurosporin (STP) used as positive control for apoptosis. 24 h treatment of 1 μM of Thapsigargin (THP) used as positive control for ER stress. Statistical analysis via one-way ANOVA with Tukey's multiple comparisons test to determine variation between treatment groups. Φ = statistical significance compared to respective vehicle control, * = statistical significance compared to indicated treatment group. ^{Φ}/ *p value=< 0.05, ^{ΦΦ}/ **p value=< 0.01, ^{ΦΦΦ} / ***p value=< 0.001, ^{ΦΦΦΦ} / ****p value=< 0.0001.

ATF4 (a pro-apoptotic transcription factor with roles linking oxidative and ER stress [539]), BiP (the HSP and master ER regulator) and Active Cas3 (a marker of apoptosis) were also assessed to determine if any other types of cellular stress were occurring. Cells were also treated with THP or STP as positive controls. Compared to vehicle control, treatment with THP led to a significant increase in ATF4 and a trend toward an increase in BiP expression ($p = 0.0291$ and 0.1021, respectively). Amyloidogenic treatments resulted in a trend towards ($p = 0.0976$ vs Aβ and 0.0621 vs IAPP-Aβ respectively) or a slight significant increase ($p = 0.0449$ vs IAPP) in ATF4 expression (Figure 42E), while no significant changes were observed for BiP expression (Figure 42F). Although, STP significantly increased expression of Active Cas3 (Figure 42G; $p < 0.0001$), no significant activation of active cas-3 expression was noted after treatment with amyloidogenic peptides.

In summation, western blot analysis demonstrated mitochondrial stress in HSMM cells after exposure to IAPP, but not Aβ, with alterations noted in the expression of SIRT1 and a trend toward changes in HSP60. ATF4, a link between oxidative and ER stress, was also significantly increased in the presence of IAPP, indicating potential progression from mitochondrial dysfunction and oxidative stress to ER stress.

5.6 Discussion

T2D and AD share many pathophysiological characteristics, including metabolic disturbances, chronic inflammation, impairment of insulin signalling,

and accumulation of the amyloidogenic peptides Aβ and IAPP in vital organs [4, 10, 24, 25, 214]. Recent evidence implicates IAPP and Aβ in not only the impairment of pancreatic and neuronal cells in T2D and AD, but also suggests these amyloidogenic peptides may have roles in the insulin resistance of peripheral tissues [386, 438]. The previous chapters of this thesis, along with collaborators Wijesekara et al. [247] (Appendix B; 8.2, page 235) and Bharadwaj et al. [129] (Appendix C; 8.3, page 236) demonstrated that IAPP and Aβ in combination potentiates the cytotoxicity of either peptide individually. As such, an investigation into the effect of IAPP and Aβ, individually and in combination on insulin sensitive peripheral tissues was conducted *in vitro* using the HSMM cell line.

Harvested from psoas or quadriceps of healthy donors, HSMM cells are robust primary human skeletal muscle cells [422]. When above 50% confluency in culture or with treatment via fusion medium, HSMM cells will begin to differentiate into mature multinucleated skeletal muscle myotubes [423, 540]. HSMM cells have been shown to physiologically and morphologically respond to environmental stressors, indicating their suitability as tools for studying diseases associated with skeletal muscle [540]. As previously documented work with HSMM cells was predominantly conducted in 6-well plates, initial experiments were aimed at optimising their use in 96-well plates (as required in specific experiments, such as the specialised 96-well culture plates for analysis in the Agilent Seahorse XF^e96 flux analyser). These optimisation experiments confirmed appropriate viability, metabolism, and differentiation of HSMM in specialised 96-well culture plates at a density of $1x10^4$ cells per well, comparable to the manufacturer's recommended density in the standard 6-well culture plate (Figure 34; Figure 35; Figure 36).

As this study represents, to the best of our knowledge, the first investigation of the effects of IAPP and Aβ amyloidogenic peptides on HSMM cells, the next step aimed to determine the cytotoxic potential of IAPP, Aβ, and IAPP-Aβ. HSMM cells were treated with up to 50 μM of amyloidogenic peptides for 24 or 48 h. Treatment with Aβ did not decrease cell viability at any concentration or time point as analysed by MTT assay and confirmed by PI staining (Figure 37). IAPP treatment reduced cell viability only after 48 h, with MTT assay only

showing a significant decrease at the highest concentration of 50 μM, while PI staining revealed a significant decrease at a concentration as low as 10 μM. This discrepancy could result from the higher statistical power in the two-way ANOVA analysis for PI staining data (due to less groups to analyse and less variation within groups), or due to PI staining being a more direct analysis of cellular death, rather than indirectly through mitochondrial function. Regardless, unlike IAPP or Aβ treatments, IAPP-Aβ resulted in significant changes in cell viability beginning at 24 h, with further marked decreases at 48 h. This data is in accordance with the results in previous chapters, as well as studies in neuronal and pancreatic tissues where the co-deposition of IAPP and Aβ promotes cytotoxicity [129, 247].

Despite T2D's correlation with inflammation and cellular stress of peripheral tissues [10, 214, 232, 438], significant muscle atrophy due to apoptosis is rarely a complication of T2D, with only a 3% difference in appendicular skeletal muscle mass between older diabetic and non-diabetic individuals [541]. To best represent this, 5-10 μM concentrations at 24 h exposure to IAPP, Aβ or IAPP-Aβ was selected as the main dosage, as MTT and PI staining data revealed it as an effectual but minimally toxic concentration. Expression of Active Cas3 confirmed 10 μM of any amyloidogenic treatment was not significant at 24 h to cause significant increases in apoptosis (Figure 42) but still may negatively influence cellular function, as amyloidogenic peptides are potentially doing in peripheral tissues of T2D or AD.

In comparison to research on types of cells and cell lines *in vitro*, a concentration of 5-10 μM of Aβ and IAPP (as most commonly used in this chapter) is consistent with concentrations used on neuronal cell [129, 542, 543] and pancreatic β-cell lines [544, 545]. There has been a sparsity of studies investigating Aβ or IAPP oligomers in peripheral tissues *in vitro*. One study treated the rodent skeletal muscle cell line C2C12 with a combination of low levels of Aβ and inflammatory cytokine treatment, rather than separate treatments, significantly increased the levels of nitrite production and iNOS expression (indicating increased inflammation and oxidative stress) [546]. Furthermore, the few *in vivo* murine models exploring Aβ or IAPP perfusions to examine peripheral tissues are inconsistent in their concentrations or units

used, frequency of administration, length of treatment, intervals of measurement, and reported clearance rates [413, 531], making direct comparisons difficult. While the concentration used on HSMM cells in this thesis is supraphysiological (circulatory concentration of IAPP and Aβ are in the pM range in humans [93, 547]), it is comparable to other *in vitro* research on various cell lines from a variety of tissues and to the best of our knowledge represents the first report to investigate the impact of both IAPP and Aβ, separately and in combination, on human skeletal muscle cell viability, bioenergetics and insulin signalling.

The skeletal muscle is a highly insulin-sensitive organ, where insulin has an essential role in promoting glucose uptake by this tissue. Research indicates Aβ can alter insulin signalling and induce an insulin resistance state in both hepatic tissue and skeletal muscle [8, 10, 247, 386, 413]. For IAPP, early research suggested potential roles in glucose sensitivity, transport, and metabolism in peripheral tissues [23, 241, 242], though the ability of IAPP to reduce insulin sensitivity has been widely debated [530, 531]. Of note in this regard is the *in vivo* study by collaborators Wijesekara et al. [247] (Appendix B; 8.2, page 235), where both APP and DTG mice that expressed human Aβ displayed reduced insulin sensitivity in peripheral tissues by 16 weeks and the CNS by 24 weeks, while this effect was absent in IAPP mice.

In this chapter, western blot analysis showed that compared to the technical CHO control, no significant changes in Akt phosphorylation relating to insulin signalling were detected in any of the treatment groups (Figure 38A-C). While the reason for this is unknown, the differentiation process, toxic amyloidogenic treatment, and subsequent serum starvation (as per the protocol to detect changes in insulin signalling through western blot analysis; 5.4.7, page 138) could potentially reduce insulin sensitivity and / or deplete internal HSMM insulin signalling machinery due to excessive stress. This could particularly impact the traditional detection of insulin-induced Akt phosphorylation through activation of phosphatidylinositol 3-kinase (PI3K), as this mechanism also participates in multiple crucial signalling pathways involved in cell stress and survival [548, 549]. Oxidative stress has been shown to directly downregulate the PI3K / Akt signalling pathway [550, 551]. Unfortunately, few papers have

shown direct western blots of pAkt signalling in HSMM cells post-differentiation, with those having done so often having much shorter or less toxic treatments [552-554].

Future experiments could involve in-depth analysis of other markers of insulin signalling in HSMM cells, including GSK3-β expression and GLUT-4 translocation to validate intracellular insulin signalling and sensitivity. Future studies could also re-evaluate this protocol to determine if the levels of cellular stress could be lowered, such as introducing a rest period between differentiation and treatment with toxic peptides (though this would also require reassessment of many other experiments if incorporated). Additionally, alternative cells could be used, such as undifferentiated myoblast cells or murine C2C12 cells (which are more well-established in the field), though this may also decrease the relevance of these models compared to human differentiated myotubes.

Despite the lack of a detectable response in terms of insulin signalling, glucose uptake was reduced in response to 10 μM of all the amyloidogenic treatments compared to controls (Figure 38D). The mechanisms via which amyloidogenic peptides influence insulin sensitivity in peripheral tissues is still largely unknown in the current literature. While GLUT4 is insulin-dependent and insulin signalling via Akt phosphorylation was not confirmed in HSMM cells, theoretically, the glucose uptake could also be occurring via insulin-independent GLUT1 channels. GLUT1 channels are constitutively expressed in a wide variety of organs, including skeletal muscle, as continuous maintenance of blood glucose is critical even at basal (fasting) conditions [555]. Tissue biopsies of T2D patients have demonstrated reduced GLUT1 expression in skeletal muscle compared to controls, despite similar levels of mRNA [556]. Currently, there is very limited information available on the effect of amyloidogenic peptides on GLUT1 expression, though some studies have found Aβ accumulation in the brain is correlated with reduced GLUT1 expression [557, 558]. The order in which it occurs, the decreased GLUT1 expression or Aβ accumulation, is currently being debated. However, the GLUT1 expression in peripheral tissues such as skeletal muscle after

exposure to IAPP, Aβ or IAPP-Aβ aggregates is an avenue for potential future investigation.

If impairments in insulin signalling is occurring but not being detected in HSMM cells, a disruption of the cytoskeletal network could also reduce glucose uptake in myotube cells due to decreased GLUT4 translocation to the cell membrane [51]. While some intracellular GLUT4 is stored in an endosomal pool mediated by the activation of transferrin receptors, approximately 40% of available GLUT4 receptors are stored separately in storage vesicles which rely on an intact microtubule network for translocation to the membrane [559]. In AD, both Aβ and IAPP have been found to interact with, hyperphosphorylate, and co-aggregate with the microtubule-associated protein Tau, causing disruption of the cytoskeletal network and neurofibrillary tangles in neuronal cells [256, 438, 468]. Tau RNA and protein is widely expressed in human and rodent skeletal muscle and other peripheral tissues [560-562], and while pTau has not been identified in the skeletal muscle of AD patients to date, Tau aggregates are present in skeletal muscle in various myopathies [563-565]. IAPP and Aβ could be disrupting the microtubules of the cytoskeletal network in HSMM cells, resulting in decreases in glucose uptake due to reduction in GLUT4 translocation. However, this would likely cause some evidence of cytotoxicity, which is absent upon exposure to the amyloidogenic peptides at the 10 μM concentrations used (and in Aβ entirely).

Alternatively, some evidence suggests that Aβ may induce insulin resistance in murine hepatic tissue via activation of the Janus Kinase 2 (JAK2) signalling pathway *in vivo* and *in vitro* [413, 566]. Research indicates activation of JAK2, a key mediator of cytokine signalling, contributes to Akt downregulation in insulin resistant states in myotubes and hepatocytes, while inhibition of JAK2 improved glucose tolerance and restoration of Akt phosphorylation [567, 568]. Through JAK2 activation and downstream signalling, the amyloidogenic peptides, particularly Aβ, could influence glucose uptake without causing significant changes in cell viability. Though there is currently limited exploration of IAPP activation of JAK2 in myotubes or hepatocytes, IAPP interaction with and activation of JAK2 in human primary adipocytes has been demonstrated [245], creating a potential for future experimentation in this area.

Once glucose has entered skeletal muscle cells via GLUT4 channels, it undergoes glycolysis and enters into the mitochondria for cellular respiration and ATP production. Mitochondrial metabolism is critical for skeletal muscle health and contraction [569]. In fact, mitochondrial dysfunction in skeletal muscle cells has a direct connection with insulin resistance, where oxidative stress and increases in ROS can inhibit insulin action [570]. However, in HSMM cells, flow cytometric analysis was unable to detect significant changes in ROS production across any treatment group when analysing the geometric mean fluorescent intensity. This result essentially indicates that all cells, including the positive control, had a similar 'concentration' of ROS within cells (Figure 39). Interestingly, recent studies have shown that differentiation of HSMM cells into myotubes creates a more than 2-fold upregulation of oxidised glutathione compared to the undifferentiated myoblasts, which could potentially have obscured measurements of oxidative stress and ROS generation [571]. However, when viewing the percentage of cells with detectable intracellular ROS regardless of concentration level (as determined by % of total events rather than fluorescent intensity), cells treated with the positive control were more than five times more likely to contain detectable ROS than control or amyloidogenic treatments.

This discrepancy in data could be also due to the relatively low metabolic activity of HSMM cells post-differentiation, as detected by previous mitochondrial stress testing during optimisation (Figure 35). Compared to undifferentiated myoblasts, HSMM cells had a significantly reduced basal OCR, maximum OCR, and ATP production rate. The maximum cell density of HSMM cells (4×10^4 per well) achieved less than half of the metabolic potential of the undifferentiated myoblasts at a similar density. During differentiation, studies have determined HSMM may undergo significant changes in metabolic profile, with progression towards a pro-oxidative state and reductions in substrate availability for the TCA cycle [571, 572], potentially lowering their metabolic activity. In addition, the differentiated myotubes *in vitro* may have a reduced energetic demand as they are no longer proliferating like myoblasts, but neither are they undergoing the same use (e.g. contraction) as they would be *in vivo*. Essentially, HSMM cells may have both a lower energetic demand

and potential, which could impact their ability to generate substantial enough ROS to influence geometric mean fluorescent intensity, particularly if they already have higher levels of detectable oxidised glutathione.

Despite the low metabolic activity, changes in mitochondrial function were still detected after exposure to amyloidogenic peptides, predominantly IAPP (Figure 40). Basal respiratory rate, maximal respiratory rate, ATP production rate and spare respiratory capacity were all reduced after exposure to IAPP, whilst only the basal metabolic rate was affected by the IAPP-Aβ combination. This is in accordance with the previous Chapter 4, where IAPP also affected the BRIN-BD11 cells more strongly than other treatments. In neuroblastoma cells, Aβ and IAPP downregulate similar mitochondrial genes, but in addition both downregulate complex 4 activity, reducing ATP production and oxygen consumption [155]. However, in addition, IAPP also reduced complex 1 activity, potentially explaining IAPP's greater impact on mitochondrial function on HSMM cells, as well as on the BRIN-BD11 β-cells in Chapter 4 [155].

Another reason for IAPP's greater impact on mitochondria compared to the noticeably more toxic IAPP-Aβ combination could result from the different aggregation states (oligomer, protofibril, fibril, etc) or the morphology of aggregates formed. As shown by collaborators Bharadwaj et al. [129] (Appendix C; 8.3, page 236), IAPP aggregates more rapidly than IAPP-Aβ or Aβ alone, as well as all 3 treatments forming structurally distinct aggregates. These separate morphologies in different states of aggregation may be able to impact the HSMM and / or BRIN-BD11 cells in different ways, where one treatment has a more direct impact on cell viability (e.g., IAPP-Aβ), while another has a greater impact on mitochondrial function directly (e.g. IAPP alone).

While basal respiratory rate, maximal respiratory rate, ATP production rate, and spare respiratory capacity were altered upon exposure to IAPP in HSMM cells, the proton leak and coupling efficiency remained unchanged (Figure 40). Though proton leak can also be up-regulated through increases in uncoupling proteins to assist in management of ROS [426], structural damage to the mitochondria can cause the inner mitochondrial membrane to become more

freely permeable to protons and ions, undermining the electrochemical gradient and reducing the mitochondria's ability to efficiently couple respiration to ATP production (coupling efficiency) [573]. In response to the reduction in mitochondrial respiration, the mitochondria would compensate by increasing the glycolytic rate [433], however the basal glycolytic rate and compensatory glycolytic rate were also unchanged upon exposure to all amyloidogenic treatments in HSMM cells (Figure 41). Together, these findings suggest that, while the function of mitochondria was clearly impacted by IAPP, permanent structural damage to the mitochondria was unlikely.

Despite IAPP's greater disturbance of mitochondrial function than IAPP-Aβ, further analysis via western blot identified reduced expression of other mitochondrial regulatory proteins, such as SIRT1, after exposure to both IAPP and IAPP-Aβ. As a multifunctional protein found in the nucleus and cytoplasm, expression of SIRT1 improves mitochondrial function, reduces oxidative stress, ameliorates insulin resistance, and provides protection from inflammatory cytokines in tissues such as skeletal muscle, adipocytes, hepatic cells, and macrophages / monocytes [538, 574-577]. These actions occur primarily through deacetylation of essential metabolic and other regulatory transcription factors, such as peroxisome proliferator-activated receptor gamma coactivator 1-α (PGC-1α), peroxisome proliferator-activated receptor-α and γ (PPAR-α / -γ), estrogen-related receptor-α (ERR-α), forkhead box O1 and O3 (FOXO1 / 3) and nuclear factor κ-B (NF-κB) [575-582]. SIRT1 is often found to be reduced in the plasma, peripheral blood mononuclear cells (PBMCs), and insulin sensitive tissues (including skeletal muscle) of diabetic patients [538, 583, 584], as well as in the brain of AD patients [585-587], where it typically correlates with insulin resistance, reduced mitochondrial activity, and a decreased ability for the cells to respond to insult [538, 574, 577, 583].

Additionally, a decreased trend in HSP60 expression, particularly for IAPP-Aβ treatment, was identified. HSP60, a stress-responsive mitochondrial chaperone, has similarly previously been found to have decreased expression in the cardiac muscle and adipose tissue of obese diabetic patients [588, 589], though it is currently unknown if it is downregulated in the skeletal muscle tissue. Reduced HSP60 expression is associated with increased oxidative

stress and insulin resistance [590-592]. Importantly, HSP60 is also able to regulate similar master regulators of mitochondrial function and insulin response as SIRT1, such as PGC-1α [593, 594], creating an avenue for further exploration in future experiments. This data together indicates that both IAPP and IAPP-Aβ negatively affects general mitochondrial function and related signalling pathways, though IAPP alone appears to impact oxidative phosphorylation more acutely.

However, contrary to BRIN-BD11 cells, expression of HSP60 in HSMM cells was reduced upon exposure to amyloidogenic peptides and the positive control (rotenone), not increased. This disparate response is not uncommon when examining HSP60, as this mitochondrial chaperone protein is defined by its duality, with both pro-survival or pro-apoptotic functions [595-597]. HSP60 has been found to be both protective and antagonistic in T2D and AD, where it protects against mitochondrial damage from amyloids [362, 363] but also mislocates amyloid precursor proteins to the mitochondria [236] and promotes apoptosis via maturation of pro-caspase-3 [361, 598, 599]. Furthermore, HSP60 can be actively secreted from peripheral tissue cells such as adipocytes and skeletal muscle cells under stress to act as a pro-inflammatory signalling molecule [593, 600-602], with this effect augmented in diabetic patients [589]. While BRIN-BD11 β-cells appear to have accumulated HSP60 after treatment, HSMM cells could have instead secreted HSP60 in response to cell stress. Furthermore, the differences in tissue type, species of origin, concentration of amyloid treatment, level of mitochondrial function, and cell responses to amyloid insult could all lead to differing expression of HSP60 under toxic conditions in the different cell lines

As an oxidative stress-inducible protein with roles in the ER's unfolded protein response, ATF4 was also examined via western blot analysis (Figure 42) [603, 604]. In HSMM cells, ATF4 expression displayed an increasing trend in all amyloidogenic treatment groups, though this was only significantly increased after IAPP treatment. Despite the increase in ATF4, BiP expression was not significantly changed after exposure to amyloidogenic peptides, despite some small increases in expression after IAPP and IAPP-Aβ exposure, suggesting no progression from oxidative to ER stress. This does not rule out the potential

that longer exposure to the amyloidogenic peptides (even at lower concentrations, as present in patients with T2D) could result in eventual ER stress.

In summation, this chapter is in accordance with the previous chapters of this thesis, where co-oligomerisation of IAPP and Aβ potentiated the cytotoxic potential of both peptides. However, despite the higher cytotoxic potential of IAPP-Aβ, IAPP appears to have a more direct effect on mitochondrial function, indicating that IAPP-Aβ may have diverse mechanisms of exerting its toxicity (Figure 43). In addition, all amyloidogenic peptides were able to significantly reduce glucose uptake, including Aβ, even with its apparent lack of effect on HSMM viability. In the next chapter, the findings and implications of the results of this project will be analysed and discussed collectively.

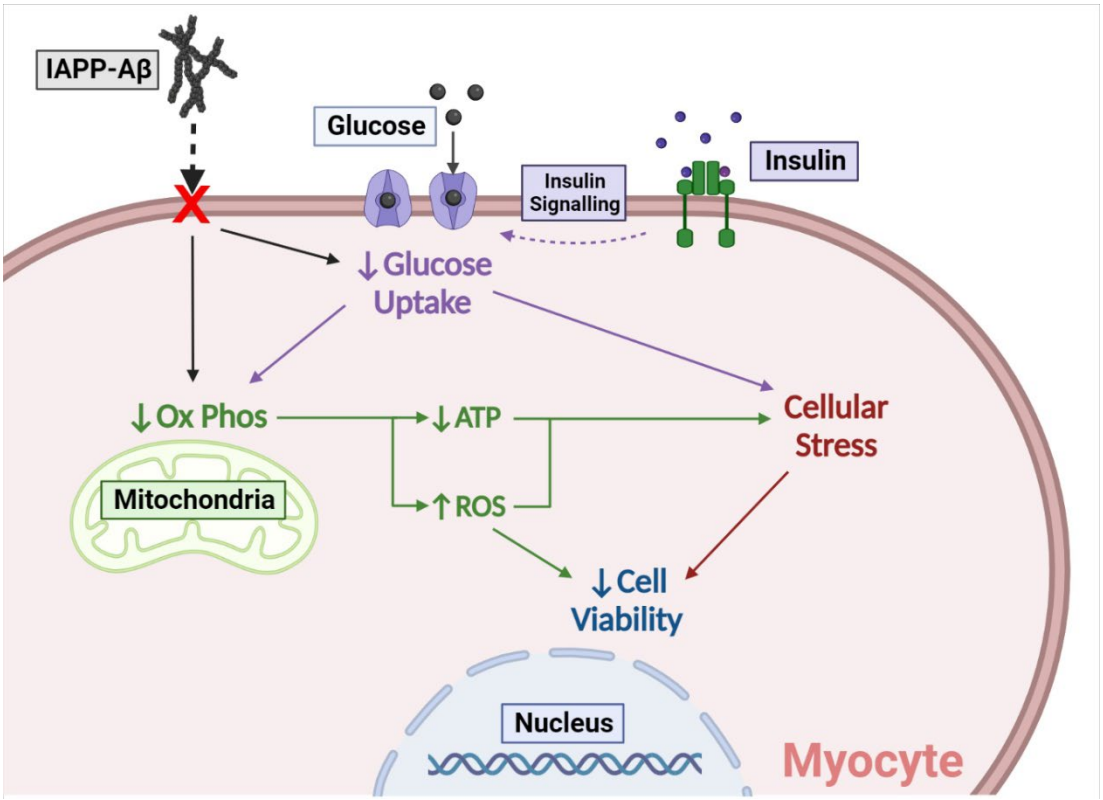

Figure 43. IAPP-Aβ aggregates reduce glucose uptake and cell viability in HSMM cells. After exposure to IAPP-Aβ aggregates, HSMM cells had reduced glucose uptake and a reduction in mitochondrial activity, specifically basal respiration. The reduction in both parameters can result in reduced ATP available for necessary cellular processes, inducing oxidative stress, resulting in cellular stress, and reduced cellular viability. However, as IAPP alone appears to diminish mitochondrial activity more so than IAPP-Aβ, without the same impact on cellular viability, IAPP-Aβ aggregates appear to increase cellular stress and reduce

cellular viability through additional mechanisms as well. Figure created by author with Biorender.com.

CHAPTER 6 Final Discussion

This thesis examined the effects of IAPP, Aβ, and IAPP-Aβ aggregates on tissues related to T2D, including insulin-secreting pancreatic β-cells and insulin-sensitive skeletal muscle cells. The rationale for this investigation is three-fold. 1) The majority of previous studies on IAPP in T2D were conducted many years ago. Without the current knowledge of IAPP binding and aggregation kinetics, these studies often yielded contradictory results [174, 175]. 2) Although previous research has focused mainly on IAPP's role in the β-cell dysfunction and peripheral insulin resistance of T2D, recent evidence also suggests a role for Aβ. The role of Aβ in the brain has been well-studied in context of AD, but its function and indeed its pathogenicity in the periphery is an understudied field. 3) There is accumulating evidence that IAPP and Aβ co-localise and co-aggregate in common tissues, such as the brain, the pancreatic islets, skeletal muscle, and the liver [24, 25, 239, 400]. The cytotoxic profile and underlying mechanisms of this combination remain to be completely determined. This thesis addresses this gap in knowledge by determining and comparing the effects of Aβ, IAPP, or a combination of both on the viability, function, and metabolism of cells from two relevant tissues to T2D, pancreatic islets and skeletal muscle. The primary, novel finding of this work is that IAPP, Aβ, and the IAPP-Aβ combination demonstrated independent effects from one another, providing insight into differential roles of the peptides in inducing dysfunction in these cells. The most notable findings are discussed below

6.1 IAPP induces a more rapid onset of cytotoxicity and has a greater impact on mitochondrial function

IAPP displayed a more rapid cytotoxic effect compared to other amyloidogenic peptide treatments. In Chapter 4 (page 98), IAPP was able to significantly reduce cell viability of BRIN-BD11 β-cells after only 6 h of incubation, the only treatment to do so. Compared to the other amyloid peptides, IAPP was also capable of reducing cell viability at a lower concentration. However, this effect was not dose-dependent and appeared to plateau over time where greater reductions in viability were associated with the IAPP-Aβ combination. The cells

greater sensitivity to IAPP at earlier timepoints maybe explained by different rates of aggregation between amyloidogenic peptides. IAPP has a tendency to aggregate more quickly into relatively inert fibrils, and thus giving only a brief and early window of cytotoxicity [129, 130]. Alternatively, this effect could be due to the different aggregate conformations formed by each individual amyloidogenic treatment, with some perhaps forming more potent conformations than others [129]. Factors such as membrane fluidity, composition, and electrostatic charge can further influence the aggregation and binding of amyloidogenic peptides, with IAPP strongly interacting with β-cell membranes [519-521]. Moreover, different cells may have different vulnerabilities, and since IAPP is natively produced by β-cells, it may have innate autocrine signalling mechanisms that are not induced by other amyloidogenic peptides, allowing for a distinct effect.

These factors may also explain why IAPP had a greater effect on mitochondrial activity of both β-cells and skeletal muscle cells compared to the other amyloidogenic peptides. While not endogenously produced by skeletal muscle cells, these cells are a target tissue for IAPP action [239, 241] and may also have an innate susceptibility to IAPP aggregation. Furthermore, although many studies have confirmed similar tendencies of amyloidogenic peptides to disrupt mitochondrial activity, IAPP may have additional mechanisms to downregulate mitochondrial function compared to other amyloids like Aβ [155]. Future studies could investigate the expression of electron transport chain complexes in detail to determine if IAPP is impairing vital mitochondrial structures to exert the toxic effect. Alternatively, mitochondrial shuttle activity or stress signalling could also be investigated to determine if the effect is more associated with functional rather than structural mitochondrial changes.

6.2 Aβ impaired insulin secretion and glucose uptake despite no cytotoxic effect

In this thesis, it was shown that Aβ did not appear to exert any obvious cytotoxic effects in pancreatic β-cells or human skeletal muscle myotubes. In Chapter 3 (page 65), no amyloid plaque was found in the pancreatic tissue of transgenic mice expressing human APP, despite the fact that the same mice exhibit amyloid plaque deposits in the brain [247]. In Chapter 4 (page 98) and

Chapter 5 (page 133), Aβ displayed no observed cytotoxicity or changes in mitochondrial activity in BRIN-BD11 β-cells or HSMM up to concentrations of 50 μM. This is surprising considering the documented history of cytotoxicity and mitochondrial dysfunction due to Aβ in the CNS. However, there has been limited investigation and evidence of Aβ cytotoxicity in peripheral tissues (outside of specific diseases involving proteostatic dysfunction such as IBM) [605, 606].

The absence of Aβ cytotoxicity in pancreatic β-cells (both primary mouse and BRIN-BD11) could be explained by a potential inherent tissue and / or cell-specific vulnerability of neuronal cells to Aβ, that may be lacking in other tissues [16, 276]. This difference could again be explained by differences in membrane composition and electrostatic mechanisms, where research has shown that unlike IAPP, Aβ does not bind to the β-cell membrane as efficiently [130]. Furthermore, despite both being amyloidogenic peptides with many shared mechanisms, IAPP and Aβ have been shown to react differently to the same stimulus. For example, an agonist for Aβ can be an antagonist of IAPP aggregation under the same conditions [607]. Despite the lack of toxicity in β-cells, Aβ was still able to decrease GSIS in BRIN-BD11 β-cells similar to other amyloidogenic treatments. With a lack of evidence for changes in cell viability or mitochondrial dysfunction after exposure to Aβ, this could potentially mean that Aβ is able to down-regulate insulin secretion via receptor-related mechanisms that are not disruptive to cell viability.

Although there are a number of receptors Aβ is known to interact with, two potential receptors by which Aβ could alter GSIS include the insulin and IAPP receptors, both of which are expressed by β-cells for autocrine regulation of insulin signalling and β-cell proliferation (among other functions) [527, 608]. Aβ is known to be a direct competitive inhibitor of insulin binding and action at insulin receptors [609]. In particular, while monomeric Aβ appears to activate insulin receptors in a similar fashion to insulin itself, toxic aggregations of Aβ can impair insulin receptor function [610]. Research also indicates that the cytotoxic effects of Aβ can be blocked by IAPP receptor antagonists in neurons [611-614]. As both receptors are also expressed in skeletal muscle and other peripheral tissues, disruption of the intracellular signalling mechanisms of

these receptors could also explain the Aβ-induced decrease in glucose uptake despite the lack of cytotoxicity in the HSMM cells of Chapter 5.

With the ability to significantly impact glucose metabolism, both through GSIS and glucose uptake, Aβ-derived pathology could have wide-ranging implications in T2D, even in the absence of peripheral tissue toxicity. Furthermore, while changes in insulin signalling were not able to be detected in HSMM cells via western blot analysis (including controls), Wijesekara et al. [247] provided some support for the notion that Aβ can downregulate insulin signalling and glucose uptake into cells, as the same APP mouse model from Chapter 3 demonstrated both peripheral and central insulin resistance. Future research could investigate specific mechanisms by which Aβ could be reducing insulin secretion and action, including alternate methods of investigating insulin signalling changes in HSMM cells (such as GLUT-4 translocation), and / or through the action of receptors common to both tissues, including insulin and IAPP receptors.

6.3 IAPP-Aβ demonstrated an exacerbated cytotoxic profile in a dose- and time-dependent manner

In all models used in this thesis, IAPP-Aβ in combination was significantly more toxic than Aβ or IAPP alone. In Chapter 3 (page 65), the DTG mice displayed more pancreatic plaque aggregation, insulin dysfunction, islet inflammation, and β-cell apoptosis than other transgenic models and nontransgenic littermates. Similarly, Chapter 4 (page 98) and Chapter 5 (page 133) demonstrated *in vitro* that IAPP-Aβ aggregates exerted significantly more toxicity in both BRIN-BD11 and HSMM cells compared to either Aβ or IAPP treatment alone. This is in agreement with the literature, where Bharadwaj et al [129] and Wijesekara et al [247] both found that IAPP and Aβ in combination was more toxic than IAPP and Aβ alone in neurons and pancreatic islets, respectively.

Bharadwaj et al. [129] previously demonstrated that IAPP-Aβ aggregates are forming distinct, larger oligomers, that are biophysically different from oligomers of either species alone. This may explain the greater cytotoxicity observed by the IAPP-Aβ combination. Alternatively, the binding of Aβ to IAPP

may slow down IAPP's rapid aggregation, stabilising the aggregates in the nucleation and / or elongation phases of aggregation for a longer period of time. This may allow oligomeric complexes more time to exert damage to the cell [615]. The IAPP-Aβ heterocomplexes may also be more difficult for the cells to clear, disrupting proteostasis and inducing cell stress. A study comparing the clearance mechanisms of IAPP and Aβ by BV-2 microglial cells gives insight into potentially independent clearance pathways of each peptide, where IAPP was cleared by IAPP-receptor-mediated endocytosis then targeted to lysosomes, while Aβ appeared to be cleared via a slower non-receptor-mediated mechanism [616]. Although this study also suggested IAPP-Aβ heterocomplex clearance occurs through a similar mechanism to IAPP alone, the study primarily focused on a non-amyloidogenic IAPP mimic and the less-aggregatory Aβ40 species. As such, many questions remain about how more amyloidogenic IAPP, Aβ, and IAPP-Aβ oligomers may be cleared, and how the state of aggregation could affect these mechanisms. Future studies could analyse further any differences in clearance mechanisms between IAPP, Aβ and IAPP-Aβ aggregates, particularly in peripheral tissues, to elucidate if these mechanisms contribute to the exacerbated cytotoxicity of IAPP-Aβ aggregates.

6.4 Differential effects of IAPP, Aβ, and IAPP-Aβ combination on cellular function in the context of T2D and AD

Discussing the results of the thesis in the context of T2D as a whole-body and multifactorial disease is a crucial component of determining the significance of the findings. The symptoms of T2D resulting from the dysfunction of insulin secretion and signalling can include hyperglycaemia, hyperlipidaemia, and chronic inflammation [27, 438]. These factors are all known to contribute to and exacerbate amyloid toxicity. For example, an environment high in glucose and saturated fatty acids simulating diabetic conditions significantly increased the toxicity of both amyloidogenic peptides in INS1 rat pancreatic β-cells [617]. Furthermore, hyperglycaemic and hyperlipidaemic conditions can further potentiate amyloid formation and aggregation, whereby exacerbating the high nutrient environment, and contributing to a vicious cycle of worsening conditions [386, 618-620]. This could be further investigated *in vitro* by

culturing BRIN-BD11 and HSMM cells in hyperglycaemic and hyperlipidaemic conditions, prior to exposure to IAPP, Aβ or the combination, or *in vivo* under similar conditions with mouse models investigated in this thesis [247].

There are a multitude of other factors that could influence the formation and aggregation of amyloidogenic peptides in T2D that were outside the scope of this PhD, which could be examined further in the future. For instance, Aβ is known to interact with Zn^{2+} ions, where Zn^{2+} can increase the rate of Aβ aggregation *in vivo* [621], and pancreatic islets are known to have a high Zn^{2+} content [622]. Currently, there are conflicting reports about whether a high islet Zn^{2+} concentration promotes or protects against IAPP aggregation [260, 623, 624]. Future studies could also examine further the role of Tau protein and Tau pathologies in their contribution to T2D, considering their close relationship to amyloidogenic peptides in AD. Tau appears to play a crucial role in insulin secretion, where Tau ablation in islets results in impaired GSIS, elevated pro-insulin and a diabetic phenotype in mice [383]. Furthermore, Tau is capable of co-aggregating with both IAPP and Aβ. [256, 263, 273, 438]. Wijesekara et al. [263] provided such evidence *in vivo*, suggesting that the co-aggregation of human Tau and IAPP can impair β-cell viability and function. Future studies could analyse the impact of human Tau, and its contribution to the pathology of T2D in the presence of Aβ and IAPP using the models and tools used in this thesis to investigate impact on cellular functioning.

Overall, the findings of this thesis, as well as previous literature on IAPP and / or Aβ aggregates in the periphery and CNS, indicate that these aggregates contribute to both the peripheral metabolic dysfunction in T2D and neurodegeneration in AD to exacerbate the pathologies of both diseases [10, 129, 247, 438]. Furthermore, the peripheral dysfunction induced by and associated with these aggregates in T2D could also influence CNS dysfunction and promote key neurodegenerative processes, and vice versa [625-631]. However, it is still currently unknown at what stage of the development and progression of T2D (and AD) these aggregates are playing a role. Essentially, whether the accumulation of IAPP and / or Aβ aggregates causative of early metabolic dysfunction and inflammation, or a consequence and exacerbator of these factors is yet unknown. To determine this, further investigation involving

the analysis of additional timepoints prior to pre-clinical symptoms would be required. For animal studies, this would rely on the development of a less aggressive mouse model than the DTG mice, as mentioned previously (3.6, page 89), to accurately determine disease progression. In human studies, this would likely require analysis of fluid and / or imaging biomarkers of amyloid accumulation in T2D patients similar to those currently undertaken in AD studies to elucidate at what stage in the development of T2D pathology the aggregates are playing a role.

Taken as a whole, the role of IAPP, Aβ and IAPP-Aβ aggregates in T2D and AD are complex and multifaceted. This thesis shows that they can not only have distinct tissue-dependent effects, but also independent effects from one another under the same conditions in the same tissues. While IAPP has been implicated in T2D for many decades, the role of Aβ both alone and in potentiating the toxicity of IAPP in T2D is an important factor to consider in our understanding of T2D pathology, its relationship with AD, and the use of existing / discovery of new treatments for both diseases.

CHAPTER 7 References

1. WHO. *Diabetes*. 2021; Available from: https://www.who.int/news-room/fact-sheets/detail/diabetes.
2. Arvanitakis, Z., et al., *Diabetes mellitus and risk of Alzheimer disease and decline in cognitive function.* Arch Neurol, 2004. **61**(5): p. 661-6.
3. Leibson, C.L., et al., *Risk of dementia among persons with diabetes mellitus: a population-based cohort study.* Am J Epidemiol, 1997. **145**(4): p. 301-8.
4. Janson, J., et al., *Increased Risk of Type 2 Diabetes in Alzheimer Disease.* Diabetes, 2004. **53**(2): p. 474-481.
5. WHO. *Dementia*. 2020; Available from: https://www.who.int/news-room/fact-sheets/detail/dementia.
6. Jiménez-Palomares, M., et al., *Increased Aβ production prompts the onset of glucose intolerance and insulin resistance.* Am J Physiol Endocrinol Metab, 2012. **302**(11): p. E1373-80.
7. Bergman, R.N., D.T. Finegood, and S.E. Kahn, *The evolution of β-cell dysfunction and insulin resistance in type 2 diabetes.* European Journal of Clinical Investigation, 2002. **32**(s3): p. 35-45.
8. Burillo, J., et al., *Insulin Resistance and Diabetes Mellitus in Alzheimer's Disease.* Cells, 2021. **10**(5): p. 1236.
9. Candeias, E., et al., *The impairment of insulin signaling in Alzheimer's disease.* IUBMB Life, 2012. **64**(12): p. 951-7.
10. Verdile, G., et al., *Inflammation and Oxidative Stress: The Molecular Connectivity between Insulin Resistance, Obesity, and Alzheimer's Disease.* Mediators Inflamm, 2015. **2015**: p. 105828.
11. Esser, N., et al., *Inflammation as a link between obesity, metabolic syndrome and type 2 diabetes.* Diabetes Research and Clinical Practice, 2014. **105**(2): p. 141-150.
12. Milligan Armstrong, A., et al., *Chronic stress and Alzheimer's disease: the interplay between the hypothalamic-pituitary-adrenal axis, genetics and microglia.* Biol Rev Camb Philos Soc, 2021.

13. Zraika, S., et al., *Oxidative stress is induced by islet amyloid formation and time-dependently mediates amyloid-induced beta cell apoptosis.* Diabetologia, 2009. **52**(4): p. 626-35.
14. Alberdi, E., et al., *Amyloid β oligomers induce Ca2+ dysregulation and neuronal death through activation of ionotropic glutamate receptors.* Cell Calcium, 2010. **47**(3): p. 264-272.
15. Cooper, G.J., et al., *Purification and characterization of a peptide from amyloid-rich pancreases of type 2 diabetic patients.* Proceedings of the National Academy of Sciences, 1987. **84**(23): p. 8628-8632.
16. Arai, H., et al., *Expression patterns of β-amyloid precursor protein (β-APP) in neural and nonneural human tissues from alzheimer's disease and control subjects.* Annals of Neurology, 1991. **30**(5): p. 686-693.
17. Sipe, J.D., et al., *Amyloid fibril protein nomenclature: 2012 recommendations from the Nomenclature Committee of the International Society of Amyloidosis.* Amyloid, 2012. **19**(4): p. 167-170.
18. Chiti, F. and C.M. Dobson, *Protein Misfolding, Amyloid Formation, and Human Disease: A Summary of Progress Over the Last Decade.* Annual Review of Biochemistry, 2017. **86**(1): p. 27-68.
19. Cohen, A.S. and E. Calkins, *Electron Microscopic Observations on a Fibrous Component in Amyloid of Diverse Origins.* Nature, 1959. **183**(4669): p. 1202-1203.
20. Meier, J.J., et al., *Inhibition of human IAPP fibril formation does not prevent beta-cell death: evidence for distinct actions of oligomers and fibrils of human IAPP.* Am J Physiol Endocrinol Metab, 2006. **291**(6): p. E1317-24.
21. Epstein, F.H., et al., *Islet Amyloid and Type 2 Diabetes Mellitus.* The New England Journal of Medicine, 2000. **343**(6): p. 411-419.
22. Kadowaki, H., et al., *Amyloid beta induces neuronal cell death through ROS-mediated ASK1 activation.* Cell Death Differ, 2005. **12**(1): p. 19-24.
23. Cooper, G.J., et al., *Amylin found in amyloid deposits in human type 2 diabetes mellitus may be a hormone that regulates glycogen metabolism in skeletal muscle.* Proceedings of the National Academy of Sciences, 1988. **85**(20): p. 7763-7766.

24. Jackson, K., et al., *Amylin deposition in the brain: A second amyloid in Alzheimer disease?* Annals of Neurology, 2013. **74**(4): p. 517-526.
25. Miklossy, J., et al., *Beta amyloid and hyperphosphorylated tau deposits in the pancreas in type 2 diabetes.* Neurobiology of Aging, 2010. **31**(9): p. 1503-1515.
26. Dunstan, D.W., et al., *The rising prevalence of diabetes and impaired glucose tolerance: the Australian Diabetes, Obesity and Lifestyle Study.* Diabetes Care, 2002. **25**(5): p. 829-34.
27. *IDF Diabetes Atlas, 9th edition*. 2019, International Diabetes Federation: Brussels, Belgium.
28. Emma Sainsbury, Y.S., Jeff Flack, Stephen Colagiuri, *Burden of Diabetes in Australia: It's Time for More Action*. 2018, The Boden Institute: Sydney, Australia.
29. *Diabetes*. 2020, Australian Institute of Health and Welfare, Australian Government: Canberra, Australia.
30. Lambert, P. and P.J. Bingley, *What is Type 1 Diabetes?* Medicine, 2002. **30**(1): p. 1-5.
31. Urakami, T., *Maturity-onset diabetes of the young (MODY): current perspectives on diagnosis and treatment.* Diabetes, Metabolic Syndrome and Obesity: Targets and Therapy, 2019. **Volume 12**: p. 1047-1056.
32. Schienkiewitz, A., et al., *Body mass index history and risk of type 2 diabetes: results from the European Prospective Investigation into Cancer and Nutrition (EPIC)–Potsdam Study.* The American Journal of Clinical Nutrition, 2006. **84**(2): p. 427-433.
33. Lindstrom, J. and J. Tuomilehto, *The Diabetes Risk Score: A practical tool to predict type 2 diabetes risk.* Diabetes Care, 2003. **26**(3): p. 725-731.
34. Guo, Z., et al., *The causal association between body mass index and type 2 diabetes mellitus—evidence based on regression discontinuity design.* Diabetes/Metabolism Research and Reviews, 2021. **37**(8).
35. Wilmot, E. and I. Idris, *Early onset type 2 diabetes: risk factors, clinical impact and management.* Therapeutic Advances in Chronic Disease, 2014. **5**(6): p. 234-244.

36. Haffner, S.M., *Epidemiology of type 2 diabetes: risk factors.* Diabetes Care, 1998. **21 Suppl 3**: p. C3-6.
37. Haines, L., et al., *Rising Incidence of Type 2 Diabetes in Children in the U.K.* Diabetes Care, 2007. **30**(5): p. 1097-1101.
38. Hillier, T.A. and K.L. Pedula, *Characteristics of an Adult Population With Newly Diagnosed Type 2 Diabetes.* The relation of obesity and age of onset, 2001. **24**(9): p. 1522-1527.
39. Levelt, E., et al., *Ectopic and Visceral Fat Deposition in Lean and Obese Patients With Type 2 Diabetes.* Journal of the American College of Cardiology, 2016. **68**(1): p. 53-63.
40. Nauli, A.M. and S. Matin, *Why Do Men Accumulate Abdominal Visceral Fat?* Frontiers in Physiology, 2019. **10**.
41. Nelson, M.D., et al., *Transwomen and the Metabolic Syndrome: Is Orchiectomy Protective?* Transgender Health, 2016. **1**(1): p. 165-171.
42. Shai, I., et al., *Ethnicity, Obesity, and Risk of Type 2 Diabetes in Women: A 20-year follow-up study.* Diabetes Care, 2006. **29**(7): p. 1585-1590.
43. Davis, T.M.E., et al., *Continuing Disparities in Cardiovascular Risk Factors and Complications Between Aboriginal and Anglo-Celt Australians With Type 2 Diabetes: The Fremantle Diabetes Study.* Diabetes Care, 2012. **35**(10): p. 2005-2011.
44. Association, A.D., *Type 2 Diabetes in Children and Adolescents.* Pediatrics, 2000. **105**(3): p. 671-680.
45. Talmud, P.J., et al., *Utility of genetic and non-genetic risk factors in prediction of type 2 diabetes: Whitehall II prospective cohort study.* BMJ, 2010. **340**(jan14 1): p. b4838-b4838.
46. Newsholme, P., L. Brennan, and K. Bender, *Amino Acid Metabolism, β-Cell Function, and Diabetes.* Diabetes, 2006. **55**(Supplement 2): p. S39-S47.
47. Newsholme, P., et al., *Diabetes associated cell stress and dysfunction: role of mitochondrial and non-mitochondrial ROS production and activity.* The Journal of Physiology, 2007. **583**(1): p. 9-24.
48. Keane, K. and P. Newsholme, *Metabolic regulation of insulin secretion.* Vitam Horm, 2014. **95**: p. 1-33.

49. Maechler, P., *Mitochondrial function and insulin secretion.* Molecular and Cellular Endocrinology, 2013. **379**(1): p. 12-18.
50. Petersen, M.C. and G.I. Shulman, *Mechanisms of Insulin Action and Insulin Resistance.* Physiological Reviews, 2018. **98**(4): p. 2133-2223.
51. Leto, D. and A.R. Saltiel, *Regulation of glucose transport by insulin: traffic control of GLUT4.* Nature Reviews Molecular Cell Biology, 2012. **13**(6): p. 383-396.
52. Martins, A.R., et al., *Mechanisms underlying skeletal muscle insulin resistance induced by fatty acids: importance of the mitochondrial function.* Lipids in Health and Disease, 2012. **11**(1): p. 30.
53. Abdul-Ghani, M.A. and R.A. Defronzo, *Pathogenesis of Insulin Resistance in Skeletal Muscle.* Journal of Biomedicine and Biotechnology, 2010. **2010**: p. 1-19.
54. Wu, H. and C.M. Ballantyne, *Skeletal muscle inflammation and insulin resistance in obesity.* Journal of Clinical Investigation, 2017. **127**(1): p. 43-54.
55. Isganaitis, E. and R.H. Lustig, *Fast Food, Central Nervous System Insulin Resistance, and Obesity.* Arteriosclerosis, Thrombosis, and Vascular Biology, 2005. **25**(12): p. 2451-2462.
56. Haugaard, S.B., et al., *Dietary intervention increases n-3 long-chain polyunsaturated fatty acids in skeletal muscle membrane phospholipids of obese subjects. Implications for insulin sensitivity.* Clinical Endocrinology, 2006. **64**(2): p. 169-178.
57. Brown, A.E. and M. Walker, *Genetics of Insulin Resistance and the Metabolic Syndrome.* Current Cardiology Reports, 2016. **18**(8).
58. Rachdaoui, N., *Insulin: The Friend and the Foe in the Development of Type 2 Diabetes Mellitus.* International Journal of Molecular Sciences, 2020. **21**(5): p. 1770.
59. Martin, C., *The physiology of amylin and insulin: maintaining the balance between glucose secretion and glucose uptake.* Diabetes Educ, 2006. **32 Suppl 3**: p. 101s-104s.
60. Cerf, M., *Beta Cell Dysfunction and Insulin Resistance.* Frontiers in Endocrinology, 2013. **4**.

61. Gonzalez, A., et al., *Insulin hypersecretion in islets from diet-induced hyperinsulinemic obese female mice is associated with several functional adaptations in individual β-cells.* Endocrinology, 2013. **154**(10): p. 3515-24.
62. Kasuga, M., *Insulin resistance and pancreatic cell failure.* Journal of Clinical Investigation, 2006. **116**(7): p. 1756-1760.
63. Speier, S., et al., *Cx36-Mediated Coupling Reduces β-Cell Heterogeneity, Confines the Stimulating Glucose Concentration Range, and Affects Insulin Release Kinetics.* Diabetes, 2007. **56**(4): p. 1078-1086.
64. Stožer, A., R. Hojs, and J. Dolenšek, *Beta Cell Functional Adaptation and Dysfunction in Insulin Resistance and the Role of Chronic Kidney Disease.* Nephron, 2019. **143**(1): p. 33-37.
65. Westermark, P., et al., *Amyloid fibrils in human insulinoma and islets of Langerhans of the diabetic cat are derived from a neuropeptide-like protein also present in normal islet cells.* Proceedings of the National Academy of Sciences, 1987. **84**(11): p. 3881-3885.
66. Westermark, P., *Quantitative studies on amyloid in the islets of Langerhans.* Ups J Med Sci, 1972. **77**(2): p. 91-4.
67. Clark, A., et al., *Islet amyloid polypeptide in diabetic and non-diabetic Pima Indians.* Diabetologia, 1990. **33**(5): p. 285-9.
68. Clark, A. and M.R. Nilsson, *Islet amyloid: a complication of islet dysfunction or an aetiological factor in Type 2 diabetes?* Diabetologia, 2004. **47**(2): p. 157-69.
69. Röcken, C., R.P. Linke, and W. Saeger, *Immunohistology of islet amyloid polypeptide in diabetes mellitus: Semi-qantitative studies in a post-mortem series.* Virchows Archiv A Pathological Anatomy and Histopathology, 1992. **421**(4): p. 339-344.
70. Kahn, S.E., S. Andrikopoulos, and C.B. Verchere, *Islet amyloid: a long-recognized but underappreciated pathological feature of type 2 diabetes.* Diabetes, 1999. **48**(2): p. 241-253.
71. Wang, F., et al., *Islet Amyloid Develops Diffusely Throughout the Pancreas Before Becoming Severe and Replacing Endocrine Cells.* Diabetes, 2001. **50**(11): p. 2514-2520.

72. Krampert, M., et al., *Amyloidogenicity of recombinant human pro-islet amyloid polypeptide (ProIAPP).* Chem Biol, 2000. **7**(11): p. 855-71.
73. Westermark, P., A. Andersson, and G.T. Westermark, *Islet amyloid polypeptide, islet amyloid, and diabetes mellitus.* Physiol Rev, 2011. **91**(3): p. 795-826.
74. Wagner, U., et al., *Amylin immunoreactivity in the rat trachea and characterization of the interaction of amylin and somatostatin on airway mucus secretion.* Res Exp Med (Berl), 1995. **195**(5): p. 289-96.
75. Skofitsch, G., et al., *Comparative immunohistochemical distribution of amylin-like and calcitonin gene related peptide like immunoreactivity in the rat central nervous system.* Can J Physiol Pharmacol, 1995. **73**(7): p. 945-56.
76. Ferrier, G.J., et al., *Expression of the rat amylin (IAPP/DAP) gene.* J Mol Endocrinol, 1989. **3**(1): p. R1-4.
77. Hayden, M.R., et al., *Type 2 diabetes mellitus as a conformational disease.* Jop, 2005. **6**(4): p. 287-302.
78. Roberts, A.N., et al., *Molecular and functional characterization of amylin, a peptide associated with type 2 diabetes mellitus.* Proceedings of the National Academy of Sciences, 1989. **86**(24): p. 9662-9666.
79. Clark, A., et al., *Localisation of islet amyloid peptide in lipofuscin bodies and secretory granules of human B-cells and in islets of type-2 diabetic subjects.* Cell and Tissue Research, 1989. **257**(1).
80. Larsson, H. and B. Ahrén, *Effects of Arginine on the Secretion of Insulin and Islet Amyloid Polypeptide in Humans.* Pancreas, 1995. **11**(2): p. 201-205.
81. Qi, D., et al., *Fatty acids induce amylin expression and secretion by pancreatic β-cells.* American Journal of Physiology-Endocrinology and Metabolism, 2010. **298**(1): p. E99-E107.
82. Stridsberg, M., S. Sandler, and E. Wilander, *Cosecretion of islet amylid polypeptide (IAPP) and insulin from isolated rat pancreatic islets following stimulation or inhibition of β-cell function.* Regulatory Peptides, 1993. **45**(3): p. 363-370.
83. Serup, P., et al., *Induction of insulin and islet amyloid polypeptide production in pancreatic islet glucagonoma cells by insulin promoter*

factor 1. Proceedings of the National Academy of Sciences, 1996. **93**(17): p. 9015-9020.

84. German, M.S., et al., *The insulin and islet amyloid polypeptide genes contain similar cell-specific promoter elements that bind identical beta-cell nuclear complexes.* Mol Cell Biol, 1992. **12**(4): p. 1777-88.
85. Lukinius, A., et al., *Co-localization of islet amyloid polypeptide and insulin in the B cell secretory granules of the human pancreatic islets.* Diabetologia, 1989. **32**(4): p. 240-244.
86. Kahn, S.E., et al., *Evidence of Cosecretion of Islet Amyloid Polypeptide and Insulin by β-Cells.* Diabetes, 1990. **39**(5): p. 634-638.
87. Cai, K., et al., *TNF-α acutely upregulates amylin expression in murine pancreatic beta cells.* Diabetologia, 2011. **54**(3): p. 617-626.
88. Cai, K., et al., *MCP-1 Upregulates Amylin Expression in Murine Pancreatic beta Cells through ERK/JNK-AP1 and NF-kappa B Related Signaling Pathways Independent of CCR2.* PLoS One, 2011. **6**(5).
89. Gedulin, B., G.J.S. Cooper, and A.A. Young, *Amylin secretion from the perfused pancreas: Dissociation from insulin and abnormal elevation in insulin-resistant diabetic rats.* Biochemical and Biophysical Research Communications, 1991. **180**(2): p. 782-789.
90. O'Brien, T.D., P. Westermark, and K.H. Johnson, *Islet amyloid polypeptide and insulin secretion from isolated perfused pancreas of fed, fasted, glucose-treated, and dexamethasone-treated rats.* Diabetes, 1991. **40**(12): p. 1701-6.
91. Couce, M., et al., *Treatment With Growth Hormone and Dexamethasone in Mice Transgenic for Human Islet Amyloid Polypeptide Causes Islet Amyloidosis and β-Cell Dysfunction.* Diabetes, 1996. **45**(8): p. 1094-1101.
92. Cluck, M.W., C.Y. Chan, and T.E. Adrian, *The regulation of amylin and insulin gene expression and secretion.* Pancreas, 2005. **30**(1): p. 1-14.
93. Enoki, S., et al., *Plasma islet amyloid polypeptide levels in obesity, impaired glucose tolerance and non-insulin-dependent diabetes mellitus.* Diabetes Research and Clinical Practice, 1992. **15**(1): p. 97-102.

94. Kautzky-Willer, A., et al., *Role of islet amyloid polypeptide secretion in insulin-resistant humans.* Diabetologia, 1994. **37**(2): p. 188-194.
95. Zhang, S. and K.H. Kim, *TNF-alpha inhibits glucose-induced insulin secretion in a pancreatic beta-cell line (INS-1).* FEBS Lett, 1995. **377**(2): p. 237-9.
96. Piemonti, L., et al., *Human pancreatic islets produce and secrete MCP-1/CCL2: relevance in human islet transplantation.* Diabetes, 2002. **51**(1): p. 55-65.
97. Gasa, R., et al., *High Glucose Concentration Favors the Selective Secretion of Islet Amyloid Polypeptide Through a Constitutive Secretory Pathway in Human Pancreatic Islets.* Pancreas, 2001. **22**(3): p. 307-310.
98. Tundo, G.R., et al., *Insulin-degrading Enzyme (IDE).* Journal of Biological Chemistry, 2013. **288**(4): p. 2281-2289.
99. Bennett, R.G., W.C. Duckworth, and F.G. Hamel, *Degradation of Amylin by Insulin-degrading Enzyme.* Journal of Biological Chemistry, 2000. **275**(47): p. 36621-36625.
100. Suire, C.N., M.K. Brizuela, and M.A. Leissring, *Quantitative, High-Throughput Assays for Proteolytic Degradation of Amylin.* Methods and Protocols, 2020. **3**(4): p. 81.
101. Rabkin, R., M.P. Ryan, and W.C. Duckworth, *The renal metabolism of insulin.* Diabetologia, 1984. **27**(3): p. 351-357.
102. Bergman, R.N., M. Kabir, and M. Ader, *The Physiology of Insulin Clearance.* International Journal of Molecular Sciences, 2022. **23**(3): p. 1826.
103. Piccinini, F. and R.N. Bergman, *The Measurement of Insulin Clearance.* Diabetes Care, 2020. **43**(9): p. 2296-2302.
104. Pecoits-Filho, R., et al., *Interactions between kidney disease and diabetes: dangerous liaisons.* Diabetology & Metabolic Syndrome, 2016. **8**(1).
105. Stadler, M., et al., *Increased Plasma Amylin in Type 1 Diabetic Patients After Kidney and Pancreas Transplantation: A sign of impaired β-cell function?* Diabetes Care, 2006. **29**(5): p. 1031-1038.

106. Thomaseth, K., et al., *Amylin Release During Oral Glucose Tolerance Test.* Diabetic Medicine, 1997. **14**.
107. Clodi, M., et al., *Distribution and kinetics of amylin in humans.* American Journal of Physiology-Endocrinology and Metabolism, 1998. **274**(5): p. E903-E908.
108. Ludvik, B., et al., *Increased levels of circulating islet amyloid polypeptide in patients with chronic renal failure have no effect on insulin secretion.* Journal of Clinical Investigation, 1994. **94**(5): p. 2045-2050.
109. Bhowmick, D.C., et al., *Molecular Mechanisms of Amylin Turnover, Misfolding and Toxicity in the Pancreas.* Molecules, 2022. **27**(3): p. 1021.
110. Press, M., et al., *Protein aggregates and proteostasis in aging: Amylin and β-cell function.* Mechanisms of Ageing and Development, 2019. **177**: p. 46-54.
111. Nandi, D., et al., *The ubiquitin-proteasome system.* Journal of Biosciences, 2006. **31**(1): p. 137-155.
112. Kim, J., et al., *An autophagy enhancer ameliorates diabetes of human IAPP-transgenic mice through clearance of amyloidogenic oligomer.* Nature Communications, 2021. **12**(1).
113. Mizushima, N., Y. Ohsumi, and T. Yoshimori, *Autophagosome Formation in Mammalian Cells.* Cell Structure and Function, 2002. **27**(6): p. 421-429.
114. Bustamante, H.A., et al., *Interplay Between the Autophagy-Lysosomal Pathway and the Ubiquitin-Proteasome System: A Target for Therapeutic Development in Alzheimer's Disease.* Frontiers in Cellular Neuroscience, 2018. **12**.
115. Banaei-Bouchareb, L., et al., *Insulin cell mass is altered inCsf1^{op}/Csf1^{op}macrophage-deficient mice.* Journal of Leukocyte Biology, 2004. **76**(2): p. 359-367.
116. Kamata, K., et al., *Islet amyloid with macrophage migration correlates with augmented β-cell deficits in type 2 diabetic patients.* Amyloid, 2014. **21**(3): p. 191-201.

117. Makin, O.S., et al., *Molecular basis for amyloid fibril formation and stability.* Proceedings of the National Academy of Sciences, 2005. **102**(2): p. 315-320.
118. Tracz, S.M., et al., *Role of Aromatic Interactions in Amyloid Formation by Peptides Derived from Human Amylin.* Biochemistry, 2004. **43**(50): p. 15901-15908.
119. Lanzarotti, E., et al., *Aromatic–Aromatic Interactions in Proteins: Beyond the Dimer.* Journal of Chemical Information and Modeling, 2011. **51**(7): p. 1623-1633.
120. Doran, T.M., et al., *Role of amino acid hydrophobicity, aromaticity, and molecular volume on IAPP(20-29) amyloid self-assembly.* Proteins: Structure, Function, and Bioinformatics, 2012. **80**(4): p. 1053-1065.
121. Westermark, P., et al., *Islet amyloid polypeptide: pinpointing amino acid residues linked to amyloid fibril formation.* Proceedings of the National Academy of Sciences, 1990. **87**(13): p. 5036-5040.
122. Noh, D., et al., *Analysis of Amylin Consensus Sequences Suggests That Human Amylin Is Not Optimized to Minimize Amyloid Formation and Provides Clues to Factors That Modulate Amyloidogenicity.* ACS Chemical Biology, 2020. **15**(6): p. 1408-1416.
123. Jotha-Mattos, L., et al., *Amyloidogenesis of feline amylin and plasma levels in cats with diabetes mellitus or pancreatitis.* Domestic Animal Endocrinology, 2021. **74**: p. 106532.
124. Wallin, C., et al., *Alzheimer's disease and cigarette smoke components: effects of nicotine, PAHs, and Cd(II), Cr(III), Pb(II), Pb(IV) ions on amyloid-β peptide aggregation.* Scientific Reports, 2017. **7**(1).
125. Abedini, A., et al., *Time-resolved studies define the nature of toxic IAPP intermediates, providing insight for anti-amyloidosis therapeutics.* eLife, 2016. **5**.
126. Kumar, S. and J. Walter, *Phosphorylation of amyloid beta (Aβ) peptides – A trigger for formation of toxic aggregates in Alzheimer's disease.* Aging, 2011. **3**(8): p. 803-812.
127. Kayed, R., et al., *Common structure of soluble amyloid oligomers implies common mechanism of pathogenesis.* Science, 2003. **300**(5618): p. 486-9.

128. Green, J.D., et al., *Human Amylin Oligomer Growth and Fibril Elongation Define Two Distinct Phases in Amyloid Formation.* Journal of Biological Chemistry, 2004. **279**(13): p. 12206-12212.
129. Bharadwaj, P., et al., *Amylin and beta amyloid proteins interact to form amorphous heterocomplexes with enhanced toxicity in neuronal cells.* Scientific Reports, 2020. **10**(1).
130. Seeliger, J., et al., *The Effect of Aβ on IAPP Aggregation in the Presence of an Isolated β-Cell Membrane.* Journal of Molecular Biology, 2012. **421**(2-3): p. 348-363.
131. de Koning, E.J., et al., *Intra- and extracellular amyloid fibrils are formed in cultured pancreatic islets of transgenic mice expressing human islet amyloid polypeptide.* Proc Natl Acad Sci U S A, 1994. **91**(18): p. 8467-71.
132. Mirzabekov, T.A., M.C. Lin, and B.L. Kagan, *Pore formation by the cytotoxic islet amyloid peptide amylin.* J. Biol. Chem., 1996. **271**(4): p. 1988-1992.
133. Zhang, S., et al., *Induction of apoptosis by human amylin in RINm5F islet β-cells is associated with enhanced expression of p53 and p21(WAF1/CIP1).* FEBS Letters, 1999. **455**(3): p. 315-320.
134. Lorenzo, A., et al., *Pancreatic islet cell toxicity of amylin associated with type-2 diabetes mellitus.* Nature, 1994. **368**(6473): p. 756-60.
135. Lue, L.F., et al., *Soluble amyloid beta peptide concentration as a predictor of synaptic change in Alzheimer's disease.* The American journal of pathology, 1999. **155**(3): p. 853-62.
136. McLean, C.A., et al., *Soluble pool of Abeta amyloid as a determinant of severity of neurodegeneration in Alzheimer's disease.* Annals of neurology, 1999. **46**(6): p. 860-6.
137. He, Y., et al., *Soluble oligomers and fibrillar species of amyloid β-peptide differentially affect cognitive functions and hippocampal inflammatory response.* Biochem Biophys Res Commun, 2012. **429**(3-4): p. 125-30.
138. Sepehri, A., B. Nepal, and T. Lazaridis, *Distinct Modes of Action of IAPP Oligomers on Membranes.* J Chem Inf Model, 2021. **61**(9): p. 4645-4655.

139. Liu, N., M. Duan, and M. Yang, *Structural Properties of Human IAPP Dimer in Membrane Environment Studied by All-Atom Molecular Dynamics Simulations.* Sci Rep, 2017. **7**(1): p. 7915.
140. Ramamoorthy, A., et al., *Cholesterol reduces pardaxin's dynamics—a barrel-stave mechanism of membrane disruption investigated by solid-state NMR.* Biochimica et Biophysica Acta (BBA) - Biomembranes, 2010. **1798**(2): p. 223-227.
141. Abedini, A. and D.P. Raleigh, *A role for helical intermediates in amyloid formation by natively unfolded polypeptides?* Phys Biol, 2009. **6**(1): p. 015005.
142. Knight, J.D., J.A. Hebda, and A.D. Miranker, *Conserved and Cooperative Assembly of Membrane-Bound α-Helical States of Islet Amyloid Polypeptide.* Biochemistry, 2006. **45**(31): p. 9496-9508.
143. Sciacca, M.F., et al., *The Role of Cholesterol in Driving IAPP-Membrane Interactions.* Biophys J, 2016. **111**(1): p. 140-51.
144. Engel, M.F.M., et al., *Membrane damage by human islet amyloid polypeptide through fibril growth at the membrane.* Proceedings of the National Academy of Sciences, 2008. **105**(16): p. 6033-6038.
145. Casas, S., et al., *Calcium elevation in mouse pancreatic beta cells evoked by extracellular human islet amyloid polypeptide involves activation of the mechanosensitive ion channel TRPV4.* Diabetologia, 2008. **51**(12): p. 2252-2262.
146. Newsholme, P., et al., *Reactive oxygen and nitrogen species generation, antioxidant defenses, and β-cell function: a critical role for amino acids.* Journal of Endocrinology, 2012. **214**(1): p. 11-20.
147. Zhu, H., et al., *Role of Nrf2 signaling in regulation of antioxidants and phase 2 enzymes in cardiac fibroblasts: Protection against reactive oxygen and nitrogen species-induced cell injury.* FEBS Letters, 2005. **579**(14): p. 3029-3036.
148. Newsholme, P., et al., *Oxidative stress pathways in pancreatic β-cells and insulin-sensitive cells and tissues: importance to cell metabolism, function, and dysfunction.* American Journal of Physiology-Cell Physiology, 2019. **317**(3): p. C420-C433.

149. Wang, J. and H. Wang, *Oxidative Stress in Pancreatic Beta Cell Regeneration.* Oxidative Medicine and Cellular Longevity, 2017. **2017**: p. 1-9.
150. Li, X.L., et al., *Involvement of mitochondrial dysfunction in human islet amyloid polypeptide-induced apoptosis in INS-1E pancreatic beta cells: An effect attenuated by phycocyanin.* Int J Biochem Cell Biol, 2011. **43**(4): p. 525-34.
151. Newsholme, P., et al., *Molecular mechanisms of ROS production and oxidative stress in diabetes.* Biochemical Journal, 2016. **473**(24): p. 4527-4550.
152. He, J., et al., *KEAP1/NRF2 axis regulates H2O2-induced apoptosis of pancreatic β-cells.* Gene, 2019. **691**: p. 8-17.
153. Liu, X., et al., *Oligomannuronate prevents mitochondrial dysfunction induced by IAPP in RINm5F islet cells by inhibition of JNK activation and cell apoptosis.* Chinese Medicine, 2020. **15**(1).
154. Montemurro, C., et al., *IAPP toxicity activates HIF1α/PFKFB3 signaling delaying β-cell loss at the expense of β-cell function.* Nature Communications, 2019. **10**(1).
155. Lim, Y.A., et al., *Aβ and human amylin share a common toxicity pathway via mitochondrial dysfunction.* Proteomics, 2010. **10**(8): p. 1621-1633.
156. Lenzen, S., J. Drinkgern, and M. Tiedge, *Low antioxidant enzyme gene expression in pancreatic islets compared with various other mouse tissues.* Free Radical Biology and Medicine, 1996. **20**(3): p. 463-466.
157. Gurlo, T., et al., *Evidence for proteotoxicity in beta cells in type 2 diabetes: toxic islet amyloid polypeptide oligomers form intracellularly in the secretory pathway.* Am J Pathol, 2010. **176**(2): p. 861-9.
158. Idevall-Hagren, O. and A. Tengholm, *Metabolic regulation of calcium signaling in beta cells.* Semin Cell Dev Biol, 2020. **103**: p. 20-30.
159. Rossi, A., P. Pizzo, and R. Filadi, *Calcium, mitochondria and cell metabolism: A functional triangle in bioenergetics.* Biochim Biophys Acta Mol Cell Res, 2019. **1866**(7): p. 1068-1078.
160. Contreras, L., et al., *Mitochondria: the calcium connection.* Biochim Biophys Acta, 2010. **1797**(6-7): p. 607-18.

161. Sukumaran, P., et al., *Calcium Signaling Regulates Autophagy and Apoptosis.* Cells, 2021. **10**(8): p. 2125.
162. Niki, I. and H. Hidaka, Molecular and Cellular Biochemistry, 1999. **190**(1/2): p. 119-124.
163. Saikia, R. and J. Joseph, *AMPK: a key regulator of energy stress and calcium-induced autophagy.* Journal of Molecular Medicine, 2021. **99**(11): p. 1539-1551.
164. Shigeto, M., et al., *A role of PLC/PKC-dependent pathway in GLP-1-stimulated insulin secretion.* Journal of Molecular Medicine, 2017. **95**(4): p. 361-368.
165. Suefuji, M., et al., *The impact of Ca2+/calmodulin-dependent protein kinase II on insulin gene expression in MIN6 cells.* Biochemical and Biophysical Research Communications, 2012. **421**(4): p. 801-807.
166. Culp, D.J., Z. Zhang, and R.L. Evans, *Role of Calcium and PKC in Salivary Mucous Cell Exocrine Secretion.* Journal of Dental Research, 2011. **90**(12): p. 1469-1476.
167. Means, A.R., *Calmodulin: Properties, Intracellular Localization, and Multiple Roles in Cell Regulation11Supported by NIH Research Grant HD-07503 and the Baylor Center for Reproductive Biology and Population Research*, in *Proceedings of the 1980 Laurentian Hormone Conference*, R.O. Greep, Editor. 1981, Academic Press: Boston. p. 333-367.
168. Xie, Y., et al., *The mTORC2/PKC pathway sustains compensatory insulin secretion of pancreatic β cells in response to metabolic stress.* Biochim Biophys Acta Gen Subj, 2017. **1861**(8): p. 2039-2047.
169. Newsholme, P. and M. Krause, *Nutritional regulation of insulin secretion: implications for diabetes.* Clin Biochem Rev, 2012. **33**(2): p. 35-47.
170. Giorgi, C., et al., *Mitochondrial calcium homeostasis as potential target for mitochondrial medicine.* Mitochondrion, 2012. **12**(1): p. 77-85.
171. Costes, S., G. Bertrand, and M.A. Ravier, *Mechanisms of Beta-Cell Apoptosis in Type 2 Diabetes-Prone Situations and Potential Protection by GLP-1-Based Therapies.* International Journal of Molecular Sciences, 2021. **22**(10): p. 5303.

172. Degano, P., et al., *Amylin inhibits glucose-induced insulin secretion in a dose-dependent manner. Study in the perfused rat pancreas.* Regulatory Peptides, 1993. **43**(1-2): p. 91-96.
173. Zhu, T., et al., *Islet amyloid polypeptide acts on glucose- stimulated beta cells to reduce voltage-gated calcium channel activation, intracellular Ca(2+) concentration, and insulin secretion.* Diabetes Metab Res Rev, 2011. **27**(1): p. 28-34.
174. Silvestre, R.A., et al., *Inhibitory effect of rat amylin on the insulin responses to glucose and arginine in the perfused rat pancreas.* Regul Pept, 1990. **31**(1): p. 23-31.
175. Broderick, C.L., et al., *Human and rat amylin have no effects on insulin secretion in isolated rat pancreatic islets.* Biochemical and Biophysical Research Communications, 1991. **177**(3): p. 932-938.
176. O'Brien, T.D., P. Westermark, and K.H. Johnson, *Islet amyloid polypeptide (IAPP) does not inhibit glucose-stimulated insulin secretion from isolated perfused rat pancreas.* Biochem Biophys Res Commun, 1990. **170**(3): p. 1223-8.
177. Hartter, E., et al., *Basal and stimulated plasma levels of pancreatic amylin indicate its co-secretion with insulin in humans.* Diabetologia, 1991. **34**(1): p. 52-4.
178. Castillo, M.J., A.J. Scheen, and P.J. Lefebvre, *Amylin/islet amyloid polypeptide: biochemistry, physiology, patho-physiology.* Diabete Metabolism, 1995. **21**(1): p. 3-25.
179. Knight, J.D., J.A. Williamson, and A.D. Miranker, *Interaction of membrane-bound islet amyloid polypeptide with soluble and crystalline insulin.* Protein Science, 2008. **17**(10): p. 1850-1856.
180. Bram, Y., et al., *Apoptosis induced by islet amyloid polypeptide soluble oligomers is neutralized by diabetes-associated specific antibodies.* Scientific Reports, 2014. **4**(1).
181. Lontchi-Yimagou, E., et al., *Diabetes Mellitus and Inflammation.* Current Diabetes Reports, 2013. **13**(3): p. 435-444.
182. Yang, C.F. and W.C. Tsai, *Calmodulin: The switch button of calcium signaling.* Tzu Chi Med J, 2022. **34**(1): p. 15-22.

183. Baier, G. and J. Wagner, *PKC inhibitors: potential in T cell-dependent immune diseases.* Curr Opin Cell Biol, 2009. **21**(2): p. 262-7.
184. Eguchi, N., et al., *The Role of Oxidative Stress in Pancreatic β Cell Dysfunction in Diabetes.* International Journal of Molecular Sciences, 2021. **22**(4): p. 1509.
185. Morgan, D., et al., *Glucose, palmitate and pro-inflammatory cytokines modulate production and activity of a phagocyte-like NADPH oxidase in rat pancreatic islets and a clonal beta cell line.* Diabetologia, 2007. **50**(2): p. 359-369.
186. Gurgul-Convey, E., et al., *Sensitivity profile of the human EndoC-βH1 beta cell line to proinflammatory cytokines.* Diabetologia, 2016. **59**(10): p. 2125-2133.
187. Shin, J.J., et al., *Damage-associated molecular patterns and their pathological relevance in diabetes mellitus.* Ageing Research Reviews, 2015. **24**: p. 66-76.
188. Dixit, V.D., *Nlrp3 Inflammasome Activation in Type 2 Diabetes: Is It Clinically Relevant?* Diabetes, 2012. **62**(1): p. 22-24.
189. Roh, J.S. and D.H. Sohn, *Damage-Associated Molecular Patterns in Inflammatory Diseases.* Immune Network, 2018. **18**(4).
190. Budd, R.C., *Activation-induced cell death.* Current Opinion in Immunology, 2001. **13**(3): p. 356-362.
191. Ehses, J.A., et al., *Increased Number of Islet-Associated Macrophages in Type 2 Diabetes.* Diabetes, 2007. **56**(9): p. 2356-2370.
192. Richardson, S.J., et al., *Islet-associated macrophages in type 2 diabetes.* Diabetologia, 2009. **52**(8): p. 1686-1688.
193. Inoue, H., et al., *Signaling between pancreatic β cells and macrophages via S100 calcium-binding protein A8 exacerbates β-cell apoptosis and islet inflammation.* J Biol Chem, 2018. **293**(16): p. 5934-5946.
194. Kinney, J.W., et al., *Inflammation as a central mechanism in Alzheimer's disease.* Alzheimer's & Dementia: Translational Research & Clinical Interventions, 2018. **4**: p. 575-590.
195. Lee, Y.H. and R.E. Pratley, *The evolving role of inflammation in obesity and the metabolic syndrome.* Curr Diab Rep, 2005. **5**(1): p. 70-5.

196. Masters, S.L., et al., *Activation of the NLRP3 inflammasome by islet amyloid polypeptide provides a mechanism for enhanced IL-1β in type 2 diabetes.* Nature Immunology, 2010. **11**(10): p. 897-904.
197. Mandrup-Poulsen, T., *IAPP boosts islet macrophage IL-1 in type 2 diabetes.* Nature Immunology, 2010. **11**(10): p. 881-883.
198. Westwell-Roper, C.Y., J.A. Ehses, and C.B. Verchere, *Resident Macrophages Mediate Islet Amyloid Polypeptide–Induced Islet IL-1β Production and β-Cell Dysfunction.* Diabetes, 2014. **63**(5): p. 1698-1711.
199. Westwell-Roper, C., et al., *Differential Activation of Innate Immune Pathways by Distinct Islet Amyloid Polypeptide (IAPP) Aggregates.* Journal of Biological Chemistry, 2016. **291**(17): p. 8908-8917.
200. Yates, S.L., et al., *Amyloid β and Amylin Fibrils Induce Increases in Proinflammatory Cytokine and Chemokine Production by THP-1 Cells and Murine Microglia.* Journal of Neurochemistry, 2000. **74**(3): p. 1017-1025.
201. Zhang, S., et al., *Fas-Associated Death Receptor Signaling Evoked by Human Amylin in Islet β-Cells.* Diabetes, 2008. **57**(2): p. 348-356.
202. Park, Y.J., et al., *Deletion of Fas protects islet beta cells from cytotoxic effects of human islet amyloid polypeptide.* Diabetologia, 2012. **55**(4): p. 1035-1047.
203. Rivera, J.F., et al., *Human-IAPP disrupts the autophagy/lysosomal pathway in pancreatic β-cells: protective role of p62-positive cytoplasmic inclusions.* Cell Death & Differentiation, 2011. **18**(3): p. 415-426.
204. Costes, S., et al., *UCHL1 deficiency exacerbates human islet amyloid polypeptide toxicity in β-cells.* Autophagy, 2014. **10**(6): p. 1004-1014.
205. Casas, S.L., et al., *Impairment of the Ubiquitin-Proteasome Pathway Is a Downstream Endoplasmic Reticulum Stress Response Induced by Extracellular Human Islet Amyloid Polypeptide and Contributes to Pancreatic β-Cell Apoptosis.* Diabetes, 2007. **56**(9): p. 2284-2294.
206. Raimundo, A.F., et al., *Islet Amyloid Polypeptide: A Partner in Crime With Aβ in the Pathology of Alzheimer's Disease.* Frontiers in molecular neuroscience, 2020. **13**: p. 35-35.

207. Lindquist, S. and E.A. Craig, *The heat-shock proteins.* Annu Rev Genet, 1988. **22**: p. 631-77.
208. Dice, J.F., *Chaperone-Mediated Autophagy.* Autophagy, 2007. **3**(4): p. 295-299.
209. Esser, C., S. Alberti, and J. Höhfeld, *Cooperation of molecular chaperones with the ubiquitin/proteasome system.* Biochim Biophys Acta, 2004. **1695**(1-3): p. 171-88.
210. Welch, W.J., *Mammalian stress response: cell physiology, structure/function of stress proteins, and implications for medicine and disease.* Physiol Rev, 1992. **72**(4): p. 1063-81.
211. Santoro, M.G., *Heat shock factors and the control of the stress response.* Biochemical Pharmacology, 2000. **59**(1): p. 55-63.
212. Belhadj Slimen, I., et al., *Reactive oxygen species, heat stress and oxidative-induced mitochondrial damage. A review.* International Journal of Hyperthermia, 2014. **30**(7): p. 513-523.
213. Hirsch, G.E. and T.G. Heck, *Inflammation, oxidative stress and altered heat shock response in type 2 diabetes: the basis for new pharmacological and non-pharmacological interventions.* Archives of Physiology and Biochemistry, 2022. **128**(2): p. 411-425.
214. Rowles, J.E., et al., *Are Heat Shock Proteins an Important Link between Type 2 Diabetes and Alzheimer Disease?* International Journal of Molecular Sciences, 2020. **21**(21): p. 8204.
215. Krause, M.S., et al., *MRP1/GS-X pump ATPase expression: is this the explanation for the cytoprotection of the heart against oxidative stress-induced redox imbalance in comparison to skeletal muscle cells?* Cell Biochemistry and Function, 2007. **25**(1): p. 23-32.
216. Chung, J., et al., *HSP72 protects against obesity-induced insulin resistance.* Proceedings of the National Academy of Sciences, 2008. **105**(5): p. 1739-1744.
217. Chilukoti, N., et al., *Hsp70 Delays Amyloid Aggregation of Amylin by Inhibiting Primary Nucleation.* Biophysical Journal, 2018. **114**(3): p. 78a-79a.

218. Sabbah, N.A., N.A. Rezk, and M.S.S. Saad, *Relationship Between Heat Shock Protein Expression and Obesity With and Without Metabolic Syndrome.* Genet Test Mol Biomarkers, 2019. **23**(10): p. 737-743.
219. Tower, J., *Hsps and aging.* Trends in Endocrinology & Metabolism, 2009. **20**(5): p. 216-222.
220. Kurucz, I., et al., *Decreased expression of heat shock protein 72 in skeletal muscle of patients with type 2 diabetes correlates with insulin resistance.* Diabetes, 2002. **51**(4): p. 1102-9.
221. Hooper, P.L. and P.L. Hooper, *Inflammation, heat shock proteins, and type 2 diabetes.* Cell Stress and Chaperones, 2009. **14**(2): p. 113-115.
222. Stege, G.J.J., et al., *The Molecular Chaperone αB-crystallin Enhances Amyloid β Neurotoxicity.* Biochemical and Biophysical Research Communications, 1999. **262**(1): p. 152-156.
223. Wang, J., et al., *HSPA5 Gene encoding Hsp70 chaperone BiP in the endoplasmic reticulum.* Gene, 2017. **618**: p. 14-23.
224. Pobre, K.F.R., G.J. Poet, and L.M. Hendershot, *The endoplasmic reticulum (ER) chaperone BiP is a master regulator of ER functions: Getting by with a little help from ERdj friends.* Journal of Biological Chemistry, 2019. **294**(6): p. 2098-2108.
225. Chien, V., et al., *The chaperone proteins HSP70, HSP40/DnaJ and GRP78/BiP suppress misfolding and formation of β-sheet-containing aggregates by human amylin: a potential role for defective chaperone biology in Type 2 diabetes.* Biochem J, 2010. **432**(1): p. 113-21.
226. Huang, C.-j., et al., *Induction of endoplasmic reticulum stress-induced β-cell apoptosis and accumulation of polyubiquitinated proteins by human islet amyloid polypeptide.* American Journal of Physiology-Endocrinology and Metabolism, 2007. **293**(6): p. E1656-E1662.
227. Vig, S., et al., *Cytokine-induced translocation of GRP78 to the plasma membrane triggers a pro-apoptotic feedback loop in pancreatic beta cells.* Cell Death & Disease, 2019. **10**(4).
228. Ibrahim, I.M., D.H. Abdelmalek, and A.A. Elfiky, *GRP78: A cell's response to stress.* Life Sciences, 2019. **226**: p. 156-163.

229. Tsai, Y.L., et al., *Characterization and mechanism of stress-induced translocation of 78-kilodalton glucose-regulated protein (GRP78) to the cell surface.* J Biol Chem, 2015. **290**(13): p. 8049-64.
230. Angelini, G., et al., *Upper gut heat shock proteins HSP70 and GRP78 promote insulin resistance, hyperglycemia, and non-alcoholic steatohepatitis.* Nature Communications, 2022. **13**(1).
231. Franklin, J.L., M.O. Amsler, and J.L. Messina, *Regulation of glucose responsive protein (GRP) gene expression by insulin.* Cell Stress and Chaperones, 2022. **27**(1): p. 27-35.
232. Krause, M., et al., *Elevated levels of extracellular heat-shock protein 72 (eHSP72) are positively correlated with insulin resistance in vivo and cause pancreatic β-cell dysfunction and death in vitro.* Clinical Science, 2014. **126**(10): p. 739-752.
233. Schirmer, C., et al., *Hsp90 directly interacts, in vitro, with amyloid structures and modulates their assembly and disassembly.* Biochim Biophys Acta, 2016. **1860**(11 Pt A): p. 2598-2609.
234. Lee, J.H., et al., *Heat shock protein 90 (HSP90) inhibitors activate the heat shock factor 1 (HSF1) stress response pathway and improve glucose regulation in diabetic mice.* Biochem Biophys Res Commun, 2013. **430**(3): p. 1109-13.
235. Törner, R., et al., *Structural basis for the inhibition of IAPP fibril formation by the co-chaperonin prefoldin.* Nature Communications, 2022. **13**(1).
236. Walls, K.C., et al., *Swedish Alzheimer mutation induces mitochondrial dysfunction mediated by HSP60 mislocalization of amyloid precursor protein (APP) and beta-amyloid.* J Biol Chem, 2012. **287**(36): p. 30317-27.
237. Park, Y.J., et al., *Dual role of interleukin-1β in islet amyloid formation and its β-cell toxicity: Implications for type 2 diabetes and islet transplantation.* Diabetes, Obesity and Metabolism, 2017. **19**(5): p. 682-694.
238. Yu, X.L., et al., *Rutin inhibits amylin-induced neurocytotoxicity and oxidative stress.* Food Funct, 2015. **6**(10): p. 3296-306.

239. Reza, M.I., et al., *Pancreastatin induces islet amyloid peptide aggregation in the pancreas, liver, and skeletal muscle: An implication for type 2 diabetes.* International Journal of Biological Macromolecules, 2021. **182**: p. 760-771.
240. Despa, S., et al., *Hyperamylinemia Contributes to Cardiac Dysfunction in Obesity and Diabetes.* Circulation Research, 2012. **110**(4): p. 598-608.
241. Tabata, H., et al., *Islet amyloid polypeptide (IAPP/amylin) causes insulin resistance in perfused rat hindlimb muscle.* Diabetes Res Clin Pract, 1992. **15**(1): p. 57-61.
242. Dimitriadis, G., et al., *Islet amyloid polypeptide decreases the effects of insulin-like growth factor-I on glucose transport and glycogen synthesis in skeletal muscle.* The International Journal of Biochemistry & Cell Biology, 1998. **30**(9): p. 1039-1046.
243. Pieber, T.R., et al., *Amylin-insulin relationships in insulin resistance with and without diabetic hyperglycemia.* American Journal of Physiology-Endocrinology and Metabolism, 1993. **265**(3): p. E446-E453.
244. Kassir, A.A., et al., *Lack of effect of islet amyloid polypeptide in causing insulin resistance in conscious dogs during euglycemic clamp studies.* Diabetes, 1991. **40**(8): p. 998-1004.
245. Moon, H.-S., et al., *Leptin and Amylin Act in an Additive Manner to Activate Overlapping Signaling Pathways in Peripheral Tissues.* Diabetes Care, 2011. **34**(1): p. 132-138.
246. Roth, J.D., et al., *Leptin responsiveness restored by amylin agonism in diet-induced obesity: Evidence from nonclinical and clinical studies.* Proceedings of the National Academy of Sciences, 2008. **105**(20): p. 7257-7262.
247. Wijesekara, N., et al., *Amyloid-β and islet amyloid pathologies link Alzheimer's disease and type 2 diabetes in a transgenic model.* The FASEB Journal, 2017. **31**(12): p. 5409-5418.
248. Benson, M.D., et al., *Amyloid nomenclature 2018: recommendations by the International Society of Amyloidosis (ISA) nomenclature committee.* Amyloid, 2018. **25**(4): p. 215-219.

249. Subedi, S., et al., *Amyloid Cross-Seeding: Mechanism, Implication, and Inhibition.* Molecules, 2022. **27**(6): p. 1776.
250. Morales, R., I. Moreno-Gonzalez, and C. Soto, *Cross-Seeding of Misfolded Proteins: Implications for Etiology and Pathogenesis of Protein Misfolding Diseases.* PLoS Pathogens, 2013. **9**(9): p. e1003537.
251. Martinez-Valbuena, I., et al., *Mixed pathologies in pancreatic β cells from subjects with neurodegenerative diseases and their interaction with prion protein.* Acta Neuropathologica Communications, 2021. **9**(1).
252. Chua, K.P., L.Y. Chew, and Y. Mu, *Replica exchange molecular dynamics simulation of cross-fibrillation of IAPP and PrP106-126.* Proteins: Structure, Function, and Bioinformatics, 2016. **84**(8): p. 1134-1146.
253. Tang, Y., et al., *A new strategy to reconcile amyloid cross-seeding and amyloid prevention in a binary system of α-synuclein fragmental peptide and <scp>hIAPP</scp>.* Protein Science, 2022. **31**(2): p. 485-497.
254. Mucibabic, M., et al., *α-Synuclein promotes IAPP fibril formation in vitro and β-cell amyloid formation in vivo in mice.* Scientific Reports, 2020. **10**(1).
255. Horvath, I. and P. Wittung-Stafshede, *Cross-talk between amyloidogenic proteins in type-2 diabetes and Parkinson's disease.* Proceedings of the National Academy of Sciences, 2016. **113**(44): p. 12473-12477.
256. Zhang, G., et al., *Islet amyloid polypeptide cross-seeds tau and drives the neurofibrillary pathology in Alzheimer's disease.* Molecular Neurodegeneration, 2022. **17**(1).
257. Zhang, Y., et al., *Amyloid cross-seeding between Aβ and hIAPP in relation to the pathogenesis of Alzheimer and type 2 diabetes.* Chinese Journal of Chemical Engineering, 2021. **30**: p. 225-235.
258. Kapurniotu, A., *Enlightening amyloid fibrils linked to type 2 diabetes and cross-interactions with Aβ.* Nature Structural & Molecular Biology, 2020. **27**(11): p. 1006-1008.

259. Moreno-Gonzalez, I., et al., *Molecular interaction between type 2 diabetes and Alzheimer's disease through cross-seeding of protein misfolding.* Molecular Psychiatry, 2017. **22**(9): p. 1327-1334.
260. Nedumpully-Govindan, P. and F. Ding, *Inhibition of IAPP aggregation by insulin depends on the insulin oligomeric state regulated by zinc ion concentration.* Scientific Reports, 2015. **5**(1): p. 8240.
261. Ilitchev, A.I., et al., *Hetero-oligomeric Amyloid Assembly and Mechanism: Prion Fragment PrP(106-126) Catalyzes the Islet Amyloid Polypeptide β-Hairpin.* J Am Chem Soc, 2018. **140**(30): p. 9685-9695.
262. Hu, R., et al., *Seed-Induced Heterogeneous Cross-Seeding Self-Assembly of Human and Rat Islet Polypeptides.* ACS Omega, 2017. **2**(3): p. 784-792.
263. Wijesekara, N., et al., *Combination of human tau and islet amyloid polypeptide exacerbates metabolic dysfunction in transgenic mice.* The Journal of Pathology, 2021. **254**(3): p. 244-253.
264. Consortium, T.U., *UniProt: the Universal Protein Knowledgebase in 2023.* Nucleic Acids Research, 2022. **51**(D1): p. D523-D531.
265. Volicer, L., *Physiological and pathological functions of beta-amyloid in the brain and alzheimer's disease: A review.* Chinese Journal of Physiology, 2020. **63**(3): p. 95-100.
266. Zou, K., et al., *A Novel Function of Monomeric Amyloid β-Protein Serving as an Antioxidant Molecule against Metal-Induced Oxidative Damage.* The Journal of Neuroscience, 2002. **22**(12): p. 4833-4841.
267. Mattson, M.P., *Cellular actions of beta-amyloid precursor protein and its soluble and fibrillogenic derivatives.* Physiol Rev, 1997. **77**(4): p. 1081-132.
268. Yao, Z.X. and V. Papadopoulos, *Function of β-amyloid in cholesterol transport: a lead to neurotoxicity.* The FASEB Journal, 2002. **16**(12): p. 1677-1679.
269. Bailey, J.A., et al., *Functional activity of the novel Alzheimer's amyloid β-peptide interacting domain (AβID) in the APP and BACE1 promoter sequences and implications in activating apoptotic genes and in amyloidogenesis.* Gene, 2011. **488**(1-2): p. 13-22.

270. Verdile, G., et al., *The role of beta amyloid in Alzheimer's disease: still a cause of everything or the only one who got caught?* Pharmacol Res, 2004. **50**(4): p. 397-409.
271. Glenner, G.G. and C.W. Wong, *Alzheimer's disease: initial report of the purification and characterization of a novel cerebrovascular amyloid protein.* Biochem Biophys Res Commun, 1984. **120**(3): p. 885-90.
272. Scheidt, H.A., et al., *Dynamics of Amyloid β Fibrils Revealed by Solid-state NMR.* Journal of Biological Chemistry, 2012. **287**(3): p. 2017-2021.
273. Guo, T., et al., *Molecular and cellular mechanisms underlying the pathogenesis of Alzheimer's disease.* Molecular Neurodegeneration, 2020. **15**(1).
274. Zhang, Y.-W., et al., *APP processing in Alzheimer's disease.* Molecular Brain, 2011. **4**(1): p. 3.
275. Müller, U.C., T. Deller, and M. Korte, *Not just amyloid: physiological functions of the amyloid precursor protein family.* Nature Reviews Neuroscience, 2017. **18**(5): p. 281-298.
276. Uhlén, M., et al., *Proteomics. Tissue-based map of the human proteome.* Science, 2015. **347**(6220): p. 1260419.
277. Bush, A.I., et al., *The amyloid precursor protein of Alzheimer's disease is released by human platelets.* J Biol Chem, 1990. **265**(26): p. 15977-83.
278. Evin, G. and Q.X. Li, *Platelets and Alzheimer's disease: Potential of APP as a biomarker.* World J Psychiatry, 2012. **2**(6): p. 102-13.
279. Walter, J. and C. Haass, *Posttranslational Modifications of Amyloid Precursor Protein*, in *Alzheimer's Disease: Methods and Protocols*, N.M. Hooper, Editor. 2000, Humana Press: Totowa, NJ. p. 149-168.
280. De Strooper, B., et al., *Deficiency of presenilin-1 inhibits the normal cleavage of amyloid precursor protein.* Nature, 1998. **391**(6665): p. 387-90.
281. Hartmann, T., et al., *Distinct sites of intracellular production for Alzheimer's disease Aβ40/42 amyloid peptides.* Nature Medicine, 1997. **3**(9): p. 1016-1020.

282. Ehehalt, R., et al., *Amyloidogenic processing of the Alzheimer β-amyloid precursor protein depends on lipid rafts.* Journal of Cell Biology, 2003. **160**(1): p. 113-123.
283. Liao, Y.-F., et al., *Tumor Necrosis Factor-α, Interleukin-1β, and Interferon-γ Stimulate γ-Secretase-mediated Cleavage of Amyloid Precursor Protein through a JNK-dependent MAPK Pathway.* Journal of Biological Chemistry, 2004. **279**(47): p. 49523-49532.
284. Dovey, H.F., et al., *Functional gamma-secretase inhibitors reduce beta-amyloid peptide levels in brain.* Journal of Neurochemistry, 2001. **76**(1): p. 173-181.
285. Casadesus, G., et al., *Luteinizing hormone modulates cognition and amyloid-beta deposition in Alzheimer APP transgenic mice.* Biochim Biophys Acta, 2006. **1762**(4): p. 447-52.
286. Bowen, R.L., et al., *Luteinizing Hormone, a Reproductive Regulator That Modulates the Processing of Amyloid-β Precursor Protein and Amyloid-β Deposition *.* Journal of Biological Chemistry, 2004. **279**(19): p. 20539-20545.
287. Verdile, G., et al., *Luteinizing hormone levels are positively correlated with plasma amyloid-beta protein levels in elderly men.* J Alzheimers Dis, 2008. **14**(2): p. 201-8.
288. Schmidt, M., et al., *Comparison of Alzheimer Aβ(1–40) and Aβ(1–42) amyloid fibrils reveals similar protofilament structures.* Proceedings of the National Academy of Sciences, 2009. **106**(47): p. 19813-19818.
289. Qiu, T., et al., *Aβ42 and Aβ40: similarities and differences.* Journal of Peptide Science, 2015. **21**(7): p. 522-529.
290. Hansson, O., et al., *Advantages and disadvantages of the use of the CSF Amyloid β (Aβ) 42/40 ratio in the diagnosis of Alzheimer's Disease.* Alzheimer's Research & Therapy, 2019. **11**(1).
291. Doecke, J.D., et al., *Total Aβ₄₂/Aβ₄₀ratio in plasma predicts amyloid-PET status, independent of clinical AD diagnosis.* Neurology, 2020. **94**(15): p. e1580-e1591.
292. Xin, S.-H., et al., *Clearance of Amyloid Beta and Tau in Alzheimer's Disease: from Mechanisms to Therapy.* Neurotoxicity Research, 2018. **34**(3): p. 733-748.

293. Li, Y., et al., *Microglia in Alzheimer's Disease.* BioMed Research International, 2014. **2014**: p. 1-7.
294. Ding-Yuan, T., et al., *Physiological clearance of amyloid-beta by the kidney and its therapeutic potential for Alzheimer's disease.* Molecular Psychiatry, 2021. **26**(10): p. 6074-6082.
295. Wang, Y.-R., et al., *Associations Between Hepatic Functions and Plasma Amyloid-Beta Levels—Implications for the Capacity of Liver in Peripheral Amyloid-Beta Clearance.* Molecular Neurobiology, 2017. **54**(3): p. 2338-2344.
296. Bates, K.A., et al., *Clearance mechanisms of Alzheimer's amyloid-β peptide: implications for therapeutic design and diagnostic tests.* Molecular psychiatry, 2009. **14**(5): p. 469-486.
297. Tarasoff-Conway, J.M., et al., *Clearance systems in the brain—implications for Alzheimer disease.* Nature Reviews Neurology, 2015. **11**(8): p. 457-470.
298. Verghese, P.B., et al., *ApoE influences amyloid-β (Aβ) clearance despite minimal apoE/Aβ association in physiological conditions.* Proceedings of the National Academy of Sciences, 2013. **110**(19): p. E1807-E1816.
299. Yamazaki, Y., et al., *Apolipoprotein E and Alzheimer disease: pathobiology and targeting strategies.* Nature Reviews Neurology, 2019. **15**(9): p. 501-518.
300. Tachibana, M., et al., *APOE4-mediated amyloid-β pathology depends on its neuronal receptor LRP1.* Journal of Clinical Investigation, 2019. **129**(3): p. 1272-1277.
301. Hone, E., et al., *Apolipoprotein E influences amyloid-beta clearance from the murine periphery.* Journal of Alzheimer's Disease, 2003. **5**: p. 1-8.
302. Harris-White, M.E. and S.A. Frautschy, *Low density lipoprotein receptor-related proteins (LRPs), Alzheimer's and cognition.* Curr Drug Targets CNS Neurol Disord, 2005. **4**(5): p. 469-80.
303. Dermattos, R.B., et al., *ApoE and Clusterin Cooperatively Suppress Aβ Levels and Deposition.* Neuron, 2004. **41**(2): p. 193-202.

304. Pascale, C.L., et al., *Amyloid-beta transporter expression at the blood-CSF barrier is age-dependent.* Fluids and Barriers of the CNS, 2011. **8**(1): p. 21.
305. Lührs, T., et al., *3D structure of Alzheimer's amyloid-beta(1-42) fibrils.* Proc Natl Acad Sci U S A, 2005. **102**(48): p. 17342-7.
306. Huang, Y.-R. and R.-T. Liu, *The Toxicity and Polymorphism of β-Amyloid Oligomers.* International Journal of Molecular Sciences, 2020. **21**(12): p. 4477.
307. Kim, W. and M.H. Hecht, *Generic hydrophobic residues are sufficient to promote aggregation of the Alzheimer's Abeta42 peptide.* Proc Natl Acad Sci U S A, 2006. **103**(43): p. 15824-9.
308. Pawar, A.P., et al., *Prediction of "aggregation-prone" and "aggregation-susceptible" regions in proteins associated with neurodegenerative diseases.* J Mol Biol, 2005. **350**(2): p. 379-92.
309. Ahmed, M., et al., *Structural conversion of neurotoxic amyloid-beta(1-42) oligomers to fibrils.* Nat Struct Mol Biol, 2010. **17**(5): p. 561-7.
310. Liu, R., et al., *Residues 17–20 and 30–35 of beta-amyloid play critical roles in aggregation.* Journal of Neuroscience Research, 2004. **75**(2): p. 162-171.
311. Itoh, S.G., et al., *Key Residue for Aggregation of Amyloid-β Peptides.* ACS Chemical Neuroscience, 2022. **13**(22): p. 3139-3151.
312. Shi, H., B. Kang, and J.Y. Lee, *Tautomeric Effect of Histidine on the Monomeric Structure of Amyloid β-Peptide(1–40).* The Journal of Physical Chemistry B, 2016. **120**(44): p. 11405-11411.
313. Ma, K., et al., *Residue-Specific pKa Measurements of the β-Peptide and Mechanism of pH-Induced Amyloid Formation.* Journal of the American Chemical Society, 1999. **121**(38): p. 8698-8706.
314. Przygońska, K., et al., *His6, His13, and His14 residues in Aβ 1–40 peptide significantly and specifically affect oligomeric equilibria.* Scientific Reports, 2019. **9**(1).
315. Johnstone, E.M., et al., *Conservation of the sequence of the Alzheimer's disease amyloid peptide in dog, polar bear and five other mammals by cross-species polymerase chain reaction analysis.* Molecular Brain Research, 1991. **10**(4): p. 299-305.

316. Knopman, D.S., et al., *Alzheimer disease.* Nature Reviews Disease Primers, 2021. **7**(1).
317. Health, A.I.o. and Welfare, *Dementia in Australia*. 2023, AIHW: Canberra.
318. Wenk, G.L., *Neuropathologic changes in Alzheimer's disease.* J Clin Psychiatry, 2003. **64 Suppl 9**: p. 7-10.
319. Braak, H. and E. Braak, *Neuropathological stageing of Alzheimer-related changes.* Acta Neuropathologica, 1991. **82**(4): p. 239-259.
320. Ryan, N.S., M.N. Rossor, and N.C. Fox, *Alzheimer's disease in the 100 years since Alzheimer's death.* Brain, 2015. **138**(12): p. 3816-3821.
321. Grundke-Iqbal, I., et al., *Abnormal phosphorylation of the microtubule-associated protein tau (tau) in Alzheimer cytoskeletal pathology.* Proceedings of the National Academy of Sciences, 1986. **83**(13): p. 4913-4917.
322. Spies, P.E., *Reviewing reasons for the decreased CSF Abeta42 concentration in Alzheimer.* Frontiers in Bioscience, 2012. **17**(7): p. 2024.
323. Liu, T., et al., *Amyloid-β-induced toxicity of primary neurons is dependent upon differentiation-associated increases in tau and cyclin-dependent kinase 5 expression.* Journal of Neurochemistry, 2003. **88**(3): p. 554-563.
324. Glabe, C.C., *Amyloid accumulation and pathogensis of Alzheimer's disease: significance of monomeric, oligomeric and fibrillar Abeta.* Subcell Biochem, 2005. **38**: p. 167-77.
325. Terry, R.D., *The pathogenesis of Alzheimer disease: an alternative to the amyloid hypothesis.* J Neuropathol Exp Neurol, 1996. **55**(10): p. 1023-5.
326. McDade, E., et al., *Longitudinal cognitive and biomarker changes in dominantly inherited Alzheimer disease.* Neurology, 2018. **91**(14): p. e1295-e1306.
327. Loo, D.T., et al., *Apoptosis is induced by beta-amyloid in cultured central nervous system neurons.* Proceedings of the National Academy of Sciences, 1993. **90**(17): p. 7951-7955.

328. Xu, J., et al., *Amyloid-β Peptides Are Cytotoxic to Oligodendrocytes.* The Journal of Neuroscience, 2001. **21**(1): p. RC118-RC118.
329. Hugon, J., et al., *Markers of apoptosis and models of programmed cell death in Alzheimer's disease.* J Neural Transm Suppl, 2000. **59**: p. 125-31.
330. Xue, L.-L., et al., *The age-specific pathological changes of β-amyloid plaques in the cortex and hippocampus of APP/PS1 transgenic AD mice.* Neurological Research, 2022. **44**(12): p. 1053-1065.
331. Smith, M.A., et al., *Amyloid-β Deposition in Alzheimer Transgenic Mice Is Associated with Oxidative Stress.* Journal of Neurochemistry, 2002. **70**(5): p. 2212-2215.
332. Verdier, Y. and B. Penke, *Binding sites of amyloid beta-peptide in cell plasma membrane and implications for Alzheimer's disease.* Current protein & peptide science, 2004. **5**(1): p. 19-31.
333. Jang, H., et al., *Mechanisms for the Insertion of Toxic, Fibril-like β-Amyloid Oligomers into the Membrane.* Journal of Chemical Theory and Computation, 2013. **9**(1): p. 822-833.
334. Good, T.A. and R.M. Murphy, *Aggregation state-dependent binding of beta-amyloid peptide to protein and lipid components of rat cortical homogenates.* Biochem Biophys Res Commun, 1995. **207**(1): p. 209-15.
335. Hong, S., et al., *Soluble Aβ Oligomers Are Rapidly Sequestered from Brain ISF In Vivo and Bind GM1 Ganglioside on Cellular Membranes.* Neuron, 2014. **82**(2): p. 308-319.
336. Yasumoto, T., et al., *High molecular weight amyloid β1-42 oligomers induce neurotoxicity via plasma membrane damage.* The FASEB Journal, 2019. **33**(8): p. 9220-9234.
337. Tang, Y.P., et al., *Differential effects of enrichment on learning and memory function in NR2B transgenic mice.* Neuropharmacology, 2001. **41**(6): p. 779-90.
338. Yan, S.D., et al., *RAGE and amyloid-β peptide neurotoxicity in Alzheimer's disease.* Nature, 1996. **382**(6593): p. 685-691.

339. Mroczko, B., et al., *Cellular Receptors of Amyloid β Oligomers (AβOs) in Alzheimer's Disease.* International Journal of Molecular Sciences, 2018. **19**(7): p. 1884.
340. Roberts, J.P., et al., *Selective coactivation of α7- and α4β2-nicotinic acetylcholine receptors reverses beta-amyloid–induced synaptic dysfunction.* Journal of Biological Chemistry, 2021. **296**.
341. Demuro, A., et al., *Calcium Dysregulation and Membrane Disruption as a Ubiquitous Neurotoxic Mechanism of Soluble Amyloid Oligomers*♦.* Journal of Biological Chemistry, 2005. **280**(17): p. 17294-17300.
342. Atamna, H. and K. Boyle, *Amyloid-β peptide binds with heme to form a peroxidase: Relationship to the cytopathologies of Alzheimer's disease.* Proceedings of the National Academy of Sciences, 2006. **103**(9): p. 3381-3386.
343. Atamna, H., et al., *Heme deficiency may be a factor in the mitochondrial and neuronal decay of aging.* Proceedings of the National Academy of Sciences, 2002. **99**(23): p. 14807-14812.
344. Liu, J., et al., *Delaying Brain Mitochondrial Decay and Aging with Mitochondrial Antioxidants and Metabolites.* Annals of the New York Academy of Sciences, 2002. **959**(1): p. 133-166.
345. Yang, C.-N., et al., *Mechanism mediating oligomeric Aβ clearance by naïve primary microglia.* Neurobiology of Disease, 2011. **42**(3): p. 221-230.
346. Cai, Z., M.D. Hussain, and L.-J. Yan, *Microglia, neuroinflammation, and beta-amyloid protein in Alzheimer's disease.* International Journal of Neuroscience, 2014. **124**(5): p. 307-321.
347. Rather, M.A., et al., *Inflammation and Alzheimer's Disease: Mechanisms and Therapeutic Implications by Natural Products.* Mediators of Inflammation, 2021. **2021**: p. 1-21.
348. Khemk, V., *Raised Serum Proinflammatory Cytokines in Alzheimer's Disease with Depression.* Aging and Disease, 2014. **5**(3).
349. Clark, I.A. and B. Vissel, *Amyloid β: one of three danger-associated molecules that are secondary inducers of the proinflammatory cytokines*

that mediate<scp>A</scp>lzheimer's disease. British Journal of Pharmacology, 2015. **172**(15): p. 3714-3727.

350. Hickman, S.E., E.K. Allison, and J. El Khoury, *Microglial Dysfunction and Defective -Amyloid Clearance Pathways in Aging Alzheimer's Disease Mice.* Journal of Neuroscience, 2008. **28**(33): p. 8354-8360.
351. Yamamoto, M., et al., *Interferon-γ and Tumor Necrosis Factor-α Regulate Amyloid-β Plaque Deposition and β-Secretase Expression in Swedish Mutant APP Transgenic Mice.* The American Journal of Pathology, 2007. **170**(2): p. 680-692.
352. Paouri, E., et al., *Peripheral Tumor Necrosis Factor-Alpha (TNF-α) Modulates Amyloid Pathology by Regulating Blood-Derived Immune Cells and Glial Response in the Brain of AD/TNF Transgenic Mice.* The Journal of Neuroscience, 2017. **37**(20): p. 5155-5171.
353. Ding, Q., et al., *Characterization of chronic low-level proteasome inhibition on neural homeostasis.* Journal of Neurochemistry, 2004. **86**(2): p. 489-497.
354. Homma, T. and J. Fujii, *Chapter 5 - Oxidative Stress and Dysfunction of the Intracellular Proteolytic Machinery: A Pathological Hallmark of Nonalcoholic Fatty Liver Disease*, in *Dietary Interventions in Liver Disease*, R.R. Watson and V.R. Preedy, Editors. 2019, Academic Press. p. 59-70.
355. Homma, T. and J. Fujii, *Emerging connections between oxidative stress, defective proteolysis, and metabolic diseases.* Free Radical Research, 2020. **54**(11-12): p. 931-946.
356. Duff, K., et al., *Increased amyloid-β42(43) in brains of mice expressing mutant presenilin 1.* Nature, 1996. **383**(6602): p. 710-713.
357. Ohta, K., et al., *Autophagy impairment stimulates PS1 expression and γ-secretase activity.* Autophagy, 2010. **6**(3): p. 345-352.
358. Ding, Q. and J.N. Keller, *Proteasome inhibition in oxidative stress neurotoxicity: implications for heat shock proteins.* Journal of Neurochemistry, 2001. **77**(4): p. 1010-1017.
359. Penke, B., et al., *Heat Shock Proteins and Autophagy Pathways in Neuroprotection: From Molecular Bases to Pharmacological*

Interventions. International Journal of Molecular Sciences, 2018. **19**(1): p. 325.

360. Sahara, N., et al., *In vivoevidence of CHIP up-regulation attenuating tau aggregation.* Journal of Neurochemistry, 2005. **94**(5): p. 1254-1263.
361. Muchowski, P.J. and J.L. Wacker, *Modulation of neurodegeneration by molecular chaperones.* Nature Reviews Neuroscience, 2005. **6**(1): p. 11-22.
362. Cappello, F., et al., *Chaperonotherapy for Alzheimer's Disease: Focusing on HSP60*. 2015, Springer International Publishing. p. 51-76.
363. Veereshwarayya, V., et al., *Differential Effects of Mitochondrial Heat Shock Protein 60 and Related Molecular Chaperones to Prevent Intracellular β-Amyloid-induced Inhibition of Complex IV and Limit Apoptosis.* Journal of Biological Chemistry, 2006. **281**(40): p. 29468-29478.
364. Marcuccilli, C., et al., *Regulatory differences in the stress response of hippocampal neurons and glial cells after heat shock.* The Journal of Neuroscience, 1996. **16**(2): p. 478-485.
365. Morimoto, R.I., *Cell-Nonautonomous Regulation of Proteostasis in Aging and Disease.* Cold Spring Harbor Perspectives in Biology, 2020. **12**(4): p. a034074.
366. Batulan, Z., et al., *High Threshold for Induction of the Stress Response in Motor Neurons Is Associated with Failure to Activate HSF1.* The Journal of Neuroscience, 2003. **23**(13): p. 5789-5798.
367. Kuta, R., et al., *Depending on the stress, histone deacetylase inhibitors act as heat shock protein co-inducers in motor neurons and potentiate arimoclomol, exerting neuroprotection through multiple mechanisms in ALS models.* Cell Stress and Chaperones, 2020. **25**(1): p. 173-191.
368. Alagar Boopathy, L.R., et al., *Mechanisms tailoring the expression of heat shock proteins to proteostasis challenges.* Journal of Biological Chemistry, 2022. **298**(5): p. 101796.
369. Mathur, S.K., et al., *Deficient induction of human hsp70 heat shock gene transcription in Y79 retinoblastoma cells despite activation of heat*

shock factor 1. Proceedings of the National Academy of Sciences, 1994. **91**(18): p. 8695-8699.

370. Najarzadegan, M.R., *Najarzadegan MR, Ataei E, Akbarzadeh F, borhani M, Mokhber N, et al. The Role of Heat Shock Proteins in Alzheimer Disease: A Systematic Review. J Syndromes. 2016;3(1): 6.* 2016.
371. May, L.A., et al., *Inner ear supporting cells protect hair cells by secreting HSP70.* Journal of Clinical Investigation, 2013. **123**(8): p. 3577-3587.
372. Guzhova, I., et al., *In vitro studies show that Hsp70 can be released by glia and that exogenous Hsp70 can enhance neuronal stress tolerance.* Brain Res, 2001. **914**(1-2): p. 66-73.
373. Alonso, A.D.C., et al., *Abnormal phosphorylation of tau and the mechanism of Alzheimer neurofibrillary degeneration: Sequestration of microtubule-associated proteins 1 and 2 and the disassembly of microtubules by the abnormal tau.* Proceedings of the National Academy of Sciences, 1997. **94**(1): p. 298-303.
374. Medeiros, R., D. Baglietto-Vargas, and F.M. Laferla, *The Role of Tau in Alzheimer's Disease and Related Disorders.* CNS Neuroscience & Therapeutics, 2011. **17**(5): p. 514-524.
375. Cleveland, D.W., S.-Y. Hwo, and M.W. Kirschner, *Purification of tau, a microtubule-associated protein that induces assembly of microtubules from purified tubulin.* Journal of Molecular Biology, 1977. **116**(2): p. 207-225.
376. Wang, J.Z. and F. Liu, *Microtubule-associated protein tau in development, degeneration and protection of neurons.* Prog Neurobiol, 2008. **85**(2): p. 148-75.
377. Combs, B., et al., *Tau and Axonal Transport Misregulation in Tauopathies*. 2019, Springer Singapore. p. 81-95.
378. Terwel, D., I. Dewachter, and F. Van Leuven, *Axonal Transport, Tau Protein, and Neurodegeneration in Alzheimer's Disease.* NeuroMolecular Medicine, 2002. **2**(2): p. 151-166.
379. Gulisano, W., et al., *Role of Amyloid-β and Tau Proteins in Alzheimer's Disease: Confuting the Amyloid Cascade.* J Alzheimers Dis, 2018. **64**(s1): p. S611-s631.

380. Iqbal, K., C.X. Gong, and F. Liu, *Hyperphosphorylation-induced tau oligomers.* Front Neurol, 2013. **4**: p. 112.
381. Roda, A.R., et al., *Amyloid-beta peptide and tau protein crosstalk in Alzheimer's disease.* Neural Regeneration Research, 2022. **17**(8): p. 1666-1674.
382. Tripathi, T. and H. Khan, *Direct Interaction between the β-Amyloid Core and Tau Facilitates Cross-Seeding: A Novel Target for Therapeutic Intervention.* Biochemistry, 2020. **59**(4): p. 341-342.
383. Wijesekara, N., et al., *Tau ablation in mice leads to pancreatic β cell dysfunction and glucose intolerance.* The FASEB Journal, 2018. **32**(6): p. 3166-3173.
384. Kawarabayashi, T., et al., *Accumulation of beta-amyloid fibrils in pancreas of transgenic mice.* Neurobiol Aging, 1996. **17**(2): p. 215-22.
385. Kulas, J.A., K.L. Puig, and C.K. Combs, *Amyloid precursor protein in pancreatic islets.* Journal of Endocrinology, 2017. **235**(1): p. 49-67.
386. Wijesekara, N., et al., *Impaired peripheral glucose homeostasis and Alzheimer's disease.* Neuropharmacology, 2018. **136**(Pt B): p. 172-181.
387. Figueroa, D.J., et al., *Abetapp secretases are co-expressed with Abetapp in the pancreatic islets.* J Alzheimers Dis, 2001. **3**(4): p. 393-396.
388. Stützer, I., et al., *Systematic Proteomic Analysis Identifies β-Site Amyloid Precursor Protein Cleaving Enzyme 2 and 1 (BACE2 and BACE1) Substrates in Pancreatic β-Cells*.* Journal of Biological Chemistry, 2013. **288**(15): p. 10536-10547.
389. Shigemori, K., et al., *Peripheral Aβ acts as a negative modulator of insulin secretion.* Proceedings of the National Academy of Sciences, 2022. **119**(12).
390. Tu, Z., et al., *Integrative Analysis of a Cross-Loci Regulation Network Identifies App as a Gene Regulating Insulin Secretion from Pancreatic Islets.* PLoS Genetics, 2012. **8**(12): p. e1003107.
391. Ly, H., et al., *The association of circulating amylin with β-amyloid in familial Alzheimer's disease.* Alzheimer's & Dementia: Translational Research & Clinical Interventions, 2021. **7**(1).

392. Wang, Y. and G.T. Westermark, *The Amyloid Forming Peptides Islet Amyloid Polypeptide and Amyloid β Interact at the Molecular Level.* International Journal of Molecular Sciences, 2021. **22**(20): p. 11153.
393. Nandakumar, A., et al., *Human Plasma Protein Corona of Aβ Amyloid and Its Impact on Islet Amyloid Polypeptide Cross-Seeding.* Biomacromolecules, 2020. **21**(2): p. 988-998.
394. Hamzé, R., et al., *Type 2 Diabetes Mellitus and Alzheimer's Disease: Shared Molecular Mechanisms and Potential Common Therapeutic Targets.* International Journal of Molecular Sciences, 2022. **23**(23): p. 15287.
395. Patel, A.N. and J.H. Jhamandas, *Neuronal receptors as targets for the action of amyloid-beta protein (Aβ) in the brain.* Expert Rev Mol Med, 2012. **14**: p. e2.
396. Kroner, Z., *The relationship between Alzheimer's disease and diabetes: Type 3 diabetes?* Alternative medicine review, 2009. **14**(4): p. 373-379.
397. Marciniak, E., et al., *Tau deletion promotes brain insulin resistance.* J Exp Med, 2017. **214**(8): p. 2257-2269.
398. Planel, E., et al., *Insulin Dysfunction Induces In Vivo Tau Hyperphosphorylation through Distinct Mechanisms.* The Journal of neuroscience : the official journal of the Society for Neuroscience, 2008. **27**: p. 13635-48.
399. Vinuesa, A., et al., *Inflammation and Insulin Resistance as Risk Factors and Potential Therapeutic Targets for Alzheimer's Disease.* Frontiers in Neuroscience, 2021. **15**.
400. Roher, A.E., et al., *Amyloid beta peptides in human plasma and tissues and their significance for Alzheimer's disease.* Alzheimer's & Dementia, 2009. **5**(1): p. 18-29.
401. Dalakas, M.C., *Sporadic inclusion body myositis—diagnosis, pathogenesis and therapeutic strategies.* Nature Clinical Practice Neurology, 2006. **2**(8): p. 437-447.
402. Greenberg, S.A., *Inclusion body myositis: Review of recent literature.* Current Neurology and Neuroscience Reports, 2009. **9**(1): p. 83-89.
403. Kitazawa, M., et al., *Immunization with Amyloid-Beta Attenuates Inclusion Body Myositis-Like Myopathology and Motor Impairment in a*

Transgenic Mouse Model. Journal of Neuroscience, 2009. **29**(19): p. 6132-6141.

404. Murphy, M.P. and T.E. Golde, *Inclusion-body myositis and Alzheimer disease: two sides of the same coin, or different currencies altogether?* Neurology, 2006. **66**(2 Suppl 1): p. S65-8.
405. Ruiz, H.H., et al., *Increased susceptibility to metabolic dysregulation in a mouse model of Alzheimer's disease is associated with impaired hypothalamic insulin signaling and elevated BCAA levels.* Alzheimer's & Dementia, 2016. **12**(8): p. 851-861.
406. Mody, N., et al., *Susceptibility to diet-induced obesity and glucose intolerance in the APP SWE/PSEN1 A246E mouse model of Alzheimer's disease is associated with increased brain levels of protein tyrosine phosphatase 1B (PTP1B) and retinol-binding protein 4 (RBP4), and bas.* Diabetologia, 2011. **54**(8): p. 2143-2151.
407. Kohjima, M., Y. Sun, and L. Chan, *Increased Food Intake Leads to Obesity and Insulin Resistance in the Tg2576 Alzheimer's Disease Mouse Model.* Endocrinology, 2010. **151**(4): p. 1532-1540.
408. Mehla, J., B.C. Chauhan, and N.B. Chauhan, *Experimental Induction of Type 2 Diabetes in Aging-Accelerated Mice Triggered Alzheimer-Like Pathology and Memory Deficits.* Journal of Alzheimer's Disease, 2014. **39**(1): p. 145-162.
409. Maesako, M., et al., *Environmental enrichment ameliorated high-fat diet-induced Aβ deposition and memory deficit in APP transgenic mice.* Neurobiol Aging, 2012. **33**(5): p. 1011.e11-23.
410. Jarosz-Griffiths, H.H., et al., *Amyloid-β Receptors: The Good, the Bad, and the Prion Protein.* Journal of Biological Chemistry, 2016. **291**(7): p. 3174-3183.
411. Xie, L., et al., *Alzheimer's beta-amyloid peptides compete for insulin binding to the insulin receptor.* J Neurosci, 2002. **22**(10): p. Rc221.
412. Zhang, Y., et al., *Amyloid-β induces hepatic insulin resistance by activating JAK2/STAT3/SOCS-1 signaling pathway.* Diabetes, 2012. **61**(6): p. 1434-43.
413. Zhang, Y., et al., *Amyloid-β Induces Hepatic Insulin Resistance In Vivo via JAK2.* Diabetes, 2013. **62**(4): p. 1159-1166.

414. Hiltunen, M., et al., *Contribution of genetic and dietary insulin resistance to Alzheimer phenotype in APP/PS1 transgenic mice.* Journal of Cellular and Molecular Medicine, 2012. **16**(6): p. 1206-1222.
415. Ueda, H., et al., *The NSY mouse: a new animal model of spontaneous NIDDM with moderate obesity.* Diabetologia, 1995. **38**(5): p. 503-508.
416. Takeda, S., et al., *Diabetes-accelerated memory dysfunction via cerebrovascular inflammation and Aβ deposition in an Alzheimer mouse model with diabetes.* Proceedings of the National Academy of Sciences, 2010. **107**(15): p. 7036-7041.
417. Chishti, M.A., et al., *Early-onset Amyloid Deposition and Cognitive Deficits in Transgenic Mice Expressing a Double Mutant Form of Amyloid Precursor Protein 695.* Journal of Biological Chemistry, 2001. **276**(24): p. 21562-21570.
418. Janson, J., et al., *Spontaneous diabetes mellitus in transgenic mice expressing human islet amyloid polypeptide.* Proceedings of the National Academy of Sciences, 1996. **93**(14): p. 7283-7288.
419. Stine, W.B., Jr., et al., *In vitro characterization of conditions for amyloid-beta peptide oligomerization and fibrillogenesis.* J Biol Chem, 2003. **278**(13): p. 11612-22.
420. Barr, R.K., et al., *Validation and Characterization of a Novel Peptide That Binds Monomeric and Aggregated β-Amyloid and Inhibits the Formation of Neurotoxic Oligomers.* J Biol Chem, 2016. **291**(2): p. 547-59.
421. McClenaghan, N.H., et al., *Characterization of a Novel Glucose-Responsive Insulin-Secreting Cell Line, BRIN-BD11, Produced by Electrofusion.* Diabetes, 1996. **45**(8): p. 1132.
422. *Clonetics™ Skeletal Muscle Myoblast Cell Systems (HSMM – Technical Sheet)*, I. Lonza Walersville, Editor. 2012, Lonza Walersville, Inc: US.
423. *Clonetics™ Skeletal Muscle Myoblast Cell Differentiation to Form Myotubes (HSMM Differentiation – Supplemental Instructions for Use)*. 2012, Lonza Walkersville, Inc: US.
424. Tapadia, M., et al., *Lupin seed hydrolysate promotes G-protein-coupled receptor, intracellular Ca2+ and enhanced glycolytic metabolism-*

mediated insulin secretion from BRIN-BD11 pancreatic beta cells. Molecular and Cellular Endocrinology, 2019. **480**: p. 83-96.

425. Rogers, G.W., S.E. Burroughs, and B.P. Dranka, *Direct Measurements of Cellular Metabolism for Identification of Mitochondrial Drug Targets*. 2018, Agilent Technologies: US.
426. Jastroch, M., et al., *Mitochondrial proton and electron leaks.* Essays in Biochemistry, 2010. **47**: p. 53-67.
427. Bertholet, A.M., et al., *Mitochondrial uncouplers induce proton leak by activating AAC and UCP1.* Nature, 2022. **606**(7912): p. 180-187.
428. Kim, H., et al., *Structure of Antimycin A1, a Specific Electron Transfer Inhibitor of Ubiquinol−Cytochrome c Oxidoreductase.* Journal of the American Chemical Society, 1999. **121**(20): p. 4902-4903.
429. Heinz, S., et al., *Mechanistic Investigations of the Mitochondrial Complex I Inhibitor Rotenone in the Context of Pharmacological and Safety Evaluation.* Sci Rep, 2017. **7**: p. 45465.
430. Mookerjee, S.A., et al., *Quantifying intracellular rates of glycolytic and oxidative ATP production and consumption using extracellular flux measurements.* Journal of Biological Chemistry, 2017. **292**(17): p. 7189-7207.
431. Keane, Kevin N., et al., *The impact of cryopreservation on human peripheral blood leucocyte bioenergetics.* Clin Sci (Lond), 2015. **128**(10): p. 723-733.
432. Romero, N., P. Swain, and B. Dranka, *Characterization of Glycolysis with a Panel of Common Cellular Models Using Agilent Seahorse XF Technology*. 2018, Agilent Technologies, Inc: US.
433. *Agilent Seahorse XFp: Glycolytic Rate Assay Kit User Guide*. 2019, Agilent Technologies, Inc: Delaware, US.
434. Wick, A.N., et al., *Localization of the primary metabolic block produced by 2-deoxyglucose.* J Biol Chem, 1957. **224**(2): p. 963-9.
435. Montenegro, K.R., et al., *Mechanisms of vitamin D action in skeletal muscle.* Nutr Res Rev, 2019. **32**(2): p. 192-204.
436. Banks, W.A. and A.J. Kastin, *Differential Permeability of the Blood–Brain Barrier to Two Pancreatic Peptides: Insulin and Amylin.* Peptides, 1998. **19**(5): p. 883-889.

437. Berhanu, W.M. and U.H. Hansmann, *Inter-species cross-seeding: stability and assembly of rat-human amylin aggregates.* PLoS One, 2014. **9**(5): p. e97051.
438. Bharadwaj, P., et al., *The Link between Type 2 Diabetes and Neurodegeneration: Roles for Amyloid-β, Amylin, and Tau Proteins.* J Alzheimers Dis, 2017. **59**(2): p. 421-432.
439. Maj, M., et al., *The Microtubule-Associated Protein Tau and Its Relevance for Pancreatic Beta Cells.* J Diabetes Res, 2016. **2016**: p. 1964634.
440. Herting, C.J., et al., *Tumour-associated macrophage-derived interleukin-1 mediates glioblastoma-associated cerebral oedema.* Brain, 2019. **142**(12): p. 3834-3851.
441. Miura, Y., et al., *Phenotypic differences in tumor-associated macrophages between metastatic and primary sites of clear cell renal cell carcinoma.* Journal of Clinical Oncology, 2018. **36**(5_suppl): p. 105-105.
442. Kobayashi, M., et al., *The ratio of CD163-positive macrophages to Iba1-positive macrophages is low in the intima in the early stage of cutaneous arteritis.* Immunologic Research, 2020. **68**(3): p. 152-160.
443. Mikkelsen, H.B., et al., *Ionized calcium-binding adaptor molecule 1 positive macrophages and HO-1 up-regulation in intestinal muscularis resident macrophages.* The Anatomical Record, 2017. **300**(6): p. 1114-1122.
444. Donovan, K.M., et al., *Allograft Inflammatory Factor 1 as an Immunohistochemical Marker for Macrophages in Multiple Tissues and Laboratory Animal Species.* Comp Med, 2018. **68**(5): p. 341-348.
445. Chen, Z., et al., *Monocyte depletion enhances neutrophil influx and proneural to mesenchymal transition in glioblastoma.* Nature Communications, 2023. **14**(1): p. 1839.
446. Chen, Z.-W., et al., *Identification, isolation, and characterization of daintain (allograft inflammatory factor 1), a macrophage polypeptide with effects on insulin secretion and abundantly present in the pancreas of prediabetic BB rats.* Proceedings of the National Academy of Sciences, 1997. **94**(25): p. 13879-13884.

447. Köhler, C., *Allograft inflammatory factor-1/Ionized calcium-binding adapter molecule 1 is specifically expressed by most subpopulations of macrophages and spermatids in testis.* Cell and Tissue Research, 2007. **330**(2): p. 291-302.
448. Tok, S., et al., *Neurophysiological effects of human-derived pathological tau conformers in the APPKM670/671NL.PS1/L166P amyloid mouse model of Alzheimer's disease.* Scientific Reports, 2022. **12**(1): p. 7784.
449. Goedert, M., R. Jakes, and E. Vanmechelen, *Monoclonal antibody AT8 recognises tau protein phosphorylated at both serine 202 and threonine 205.* Neuroscience Letters, 1995. **189**(3): p. 167-170.
450. Sonn, K. and A. Zharkovsky, *The effects of STZ-induced diabetes on cognition and brain amyloid in 5XFAD mouse model of Alzheimer's disease.* SpringerPlus, 2015. **4**(Suppl 1): p. P44.
451. Burke, S.J., M.D. Karlstad, and J.J. Collier, *Pancreatic Islet Responses to Metabolic Trauma.* Shock, 2016. **46**(3): p. 230-238.
452. Saito, T., et al., *Single App knock-in mouse models of Alzheimer's disease.* Nat Neurosci, 2014. **17**(5): p. 661-3.
453. Ledo, J.H., et al., *Amyloid-β oligomers link depressive-like behavior and cognitive deficits in mice.* Molecular Psychiatry, 2013. **18**(10): p. 1053-1054.
454. Lotz, M., et al., *Amyloid beta peptide 1-40 enhances the action of Toll-like receptor-2 and -4 agonists but antagonizes Toll-like receptor-9-induced inflammation in primary mouse microglial cell cultures.* Journal of Neurochemistry, 2005. **94**(2): p. 289-298.
455. Gitter, B.D., et al., *Human amylin stimulates inflammatory cytokine secretion from human glioma cells.* Neuroimmunomodulation, 2000. **7**(3): p. 147-52.
456. Badman, M.K., et al., *Fibrillar islet amyloid polypeptide (amylin) is internalised by macrophages but resists proteolytic degradation.* Cell and Tissue Research, 1998. **291**(2): p. 285-294.
457. De Koning, E.J.P., et al., *Human Islet Amyloid Polypeptide Accumulates at Similar Sites in Islets of Transgenic Mice and Humans.* Diabetes, 1994. **43**(5): p. 640-644.

458. Eguchi, K. and R. Nagai, *Islet inflammation in type 2 diabetes and physiology.* Journal of Clinical Investigation, 2017. **127**(1): p. 14-23.
459. Ohsawa, K., et al., *Microglia/macrophage-specific protein Iba1 binds to fimbrin and enhances its actin-bundling activity.* Journal of Neurochemistry, 2004. **88**(4): p. 844-856.
460. Moore, S., et al., *APP Metabolism Regulates Tau Proteostasis in Human Cerebral Cortex Neurons.* Cell Reports, 2015. **11**(5): p. 689-696.
461. Di Meco, A. and D. Praticò, *Early-life exposure to high-fat diet influences brain health in aging mice.* Aging Cell, 2019. **18**(6).
462. Kadavath, H., et al., *Tau stabilizes microtubules by binding at the interface between tubulin heterodimers.* Proc Natl Acad Sci U S A, 2015. **112**(24): p. 7501-6.
463. Zhu, X., et al., *Microtubules Negatively Regulate Insulin Secretion in Pancreatic β Cells.* Developmental Cell, 2015. **34**(6): p. 656-668.
464. Boyd, A.E., W.E. Bolton, and B.R. Brinkley, *Microtubules and beta cell function: effect of colchicine on microtubules and insulin secretion in vitro by mouse beta cells.* Journal of Cell Biology, 1982. **92**(2): p. 425-434.
465. Cerf, M.E., *High fat diet modulation of glucose sensing in the beta-cell.* Med Sci Monit, 2007. **13**(1): p. Ra12-7.
466. Devos, S.L., et al., *Tau reduction in the presence of amyloid-β prevents tau pathology and neuronal death in vivo.* Brain, 2018. **141**(7): p. 2194-2212.
467. Dawson, H.N., et al., *Loss of tau elicits axonal degeneration in a mouse model of Alzheimer's disease.* Neuroscience, 2010. **169**(1): p. 516-531.
468. Bloom, G.S., *Amyloid-β and Tau: The Trigger and Bullet in Alzheimer Disease Pathogenesis.* JAMA Neurology, 2014. **71**(4): p. 505-508.
469. Selkoe, D.J. and J. Hardy, *The amyloid hypothesis of Alzheimer's disease at 25 years.* EMBO Molecular Medicine, 2016. **8**(6): p. 595-608.
470. Radde, R., et al., *The value of incomplete mouse models of Alzheimer's disease.* European Journal of Nuclear Medicine and Molecular Imaging, 2008. **35**: p. 70-4.

471. Kurt, M.A., et al., *Hyperphosphorylated tau and paired helical filament-like structures in the brains of mice carrying mutant amyloid precursor protein and mutant presenilin-1 transgenes.* Neurobiol Dis, 2003. **14**(1): p. 89-97.
472. Sipe, J.D., et al., *Amyloid fibril protein nomenclature: 2010 recommendations from the nomenclature committee of the International Society of Amyloidosis.* Amyloid, 2010. **17**(3-4): p. 101-104.
473. Fan, R., et al., *Exendin-4 protects pancreatic beta cells from human islet amyloid polypeptide-induced cell damage: potential involvement of AKT and mitochondria biogenesis.* Diabetes Obes. Metab., 2010. **12**(9): p. 815-824.
474. Costes, S., et al., *β-Cell failure in type 2 diabetes: A case of asking too much of too few?* Diabetes, 2013. **62**(2): p. 327-335.
475. Umeda, T., et al., *Intracellular amyloid β oligomers impair organelle transport and induce dendritic spine loss in primary neurons.* Acta neuropathologica communications, 2015. **3**: p. 51-51.
476. Kandimalla, K.K., et al., *Mechanism of neuronal versus endothelial cell uptake of Alzheimer's disease amyloid beta protein.* PLoS One, 2009. **4**(2): p. e4627.
477. Poirier, Y., et al., *Link between the unfolded protein response and dysregulation of mitochondrial bioenergetics in Alzheimer's disease.* Cellular and Molecular Life Sciences, 2019. **76**(7): p. 1419-1431.
478. Jung, E.S., et al., *Acute ER stress regulates amyloid precursor protein processing through ubiquitin-dependent degradation.* Scientific Reports, 2015. **5**(1): p. 8805.
479. Rogers, T.B., et al., *Use of thapsigargin to study Ca2+ homeostasis in cardiac cells.* Bioscience Reports, 1995. **15**(5): p. 341-349.
480. Chae, H.-J., et al., *Molecular mechanism of staurosporine-induced apoptosis in osteoblasts.* Pharmacological Research, 2000. **42**(4): p. 373-381.
481. Erickson, H.P., *Evolution of the cytoskeleton.* BioEssays, 2007. **29**(7): p. 668-677.

482. Shahnawaz, M., T. Bilkis, and I.-S. Park, *Amyloid β cytotoxicity is enhanced or reduced depending on formation of amyloid β oligomeric forms.* Biotechnology Letters, 2021. **43**(1): p. 165-175.
483. Zhang, Y., et al., *Selective cytotoxicity of intracellular amyloid β peptide1–42 through p53 and Bax in cultured primary human neurons.* Journal of Cell Biology, 2002. **156**(3): p. 519-529.
484. Jin, S., et al., *Amyloid-β(1–42) Aggregation Initiates Its Cellular Uptake and Cytotoxicity.* Journal of Biological Chemistry, 2016. **291**(37): p. 19590-19606.
485. Chen, X., et al., *Interplay of Energetics and ER Stress Exacerbates Alzheimer's Amyloid-β (Aβ) Toxicity in Yeast.* Front Mol Neurosci, 2017. **10**: p. 232.
486. Ivins, K.J., et al., *Neuronal apoptosis induced by beta-amyloid is mediated by caspase-8.* Neurobiol Dis, 1999. **6**(5): p. 440-9.
487. Tucker, H.M., et al., *Human Amylin Induces "Apoptotic" Pattern of Gene Expression Concomitant with Cortical Neuronal Apoptosis.* Journal of Neurochemistry, 2002. **71**(2): p. 506-516.
488. Mazibuko-Mbeje, S.E., et al., *Antimycin A-induced mitochondrial dysfunction is consistent with impaired insulin signaling in cultured skeletal muscle cells.* Toxicology in Vitro, 2021. **76**: p. 105224.
489. Celotto, A.M., et al., *Modes of Metabolic Compensation during Mitochondrial Disease Using the Drosophila Model of ATP6 Dysfunction.* PLoS ONE, 2011. **6**(10): p. e25823.
490. Dania, et al., *Mitoenergetic Dysfunction Triggers a Rapid Compensatory Increase in Steady-State Glucose Flux.* Biophysical Journal, 2015. **109**(7): p. 1372-1386.
491. Nichols, C.G., *KATP channels as molecular sensors of cellular metabolism.* Nature, 2006. **440**(7083): p. 470-476.
492. Loo, L.S.W., et al., *BCL-xL/BCL2L1 is a critical anti-apoptotic protein that promotes the survival of differentiating pancreatic cells from human pluripotent stem cells.* Cell Death Dis, 2020. **11**(5): p. 378.
493. Finucane, D.M., et al., *Bax-induced Caspase Activation and Apoptosis via Cytochromec Release from Mitochondria Is Inhibitable by Bcl-xL.* Journal of Biological Chemistry, 1999. **274**(4): p. 2225-2233.

494. Mohammed, F., et al., *Rotenone-induced reactive oxygen species signal the recruitment of STAT3 to mitochondria.* FEBS Letters, 2020. **594**(9): p. 1403-1412.
495. Eckhardt, W., K. Bellmann, and H. Kolb, *Regulation of inducible nitric oxide synthase expression in beta cells by environmental factors: heavy metals.* The Biochemical journal, 1999. **338 (Pt 3)**(Pt 3): p. 695-700.
496. Li, F. and R.I. Mahato, *iNOS gene silencing prevents inflammatory cytokine-induced beta-cell apoptosis.* Mol Pharm, 2008. **5**(3): p. 407-17.
497. Gething, M.-J., *Role and regulation of the ER chaperone BiP.* Seminars in Cell & Developmental Biology, 1999. **10**(5): p. 465-472.
498. Coppola, T., et al., *Neurotensin protects pancreatic beta cells from apoptosis.* Int J Biochem Cell Biol, 2008. **40**(10): p. 2296-302.
499. Li, J., et al., *Imeglimin Ameliorates β-Cell Apoptosis by Modulating the Endoplasmic Reticulum Homeostasis Pathway.* Diabetes, 2022. **71**(3): p. 424-439.
500. Rowlands, J., et al., *Method Protocols for Metabolic and Functional Analysis of the BRIN-BD11 β-Cell Line: A Preclinical Model for Type 2 Diabetes.* Methods Mol Biol, 2019. **1916**: p. 329-340.
501. Dixon, G., et al., *A comparative study of amino acid consumption by rat islet cells and the clonal beta-cell line BRIN-BD11 - the functional significance of L-alanine.* J Endocrinol, 2003. **179**(3): p. 447-54.
502. Lernmark, A., *The preparation of, and studies on, free cell suspensions from mouse pancreatic islets.* Diabetologia, 1974. **10**(5): p. 431-8.
503. Velasco, M., et al., *Rat Pancreatic Beta-Cell Culture.* Methods Mol Biol, 2018. **1727**: p. 261-273.
504. Halban, P.A. and C.B. Wollheim, *Intracellular degradation of insulin stores by rat pancreatic islets in vitro. An alternative pathway for homeostasis of pancreatic insulin content.* J Biol Chem, 1980. **255**(13): p. 6003-6.
505. Weir, G.C. and S. Bonner-Weir, *Islets of Langerhans: the puzzle of intraislet interactions and their relevance to diabetes.* The Journal of clinical investigation, 1990. **85**(4): p. 983-987.

506. Chaffey, J.R., et al., *Investigation of the utility of the 1.1B4 cell as a model human beta cell line for study of persistent enteroviral infection.* Scientific Reports, 2021. **11**(1): p. 15624.
507. Hamid, M., et al., *COMPARISON OF THE SECRETORY PROPERTIES OF FOUR INSULIN-SECRETING CELL LINES.* Endocrine Research, 2002. **28**(1-2): p. 35-47.
508. McClenaghan, N.H., et al., *Molecular characterization of the glucose-sensing mechanism in the clonal insulin-secreting BRIN-BD11 cell line.* Biochem Biophys Res Commun, 1998. **242**(2): p. 262-6.
509. Keane, D.C., et al., *Arachidonic acid actions on functional integrity and attenuation of the negative effects of palmitic acid in a clonal pancreatic β-cell line.* Clin Sci (Lond), 2011. **120**(5): p. 195-206.
510. Ding, X., et al., *Pancreatic cancer cells selectively stimulate islet beta cells to secrete amylin.* Gastroenterology, 1998. **114**(1): p. 130-8.
511. Potter, K.J., et al., *Islet amyloid deposition limits the viability of human islet grafts but not porcine islet grafts.* Proceedings of the National Academy of Sciences, 2010. **107**(9): p. 4305-4310.
512. Shigihara, N., et al., *Human IAPP–induced pancreatic β cell toxicity and its regulation by autophagy.* Journal of Clinical Investigation, 2014. **124**(8): p. 3634-3644.
513. Meng, F., et al., *The Flavanol (−)-Epigallocatechin 3-Gallate Inhibits Amyloid Formation by Islet Amyloid Polypeptide, Disaggregates Amyloid Fibrils, and Protects Cultured Cells against IAPP-Induced Toxicity.* Biochemistry, 2010. **49**(37): p. 8127-8133.
514. Janson, J., et al., *The mechanism of islet amyloid polypeptide toxicity is membrane disruption by intermediate-sized toxic amyloid particles.* Diabetes, 1999. **48**(3): p. 491-498.
515. Ritzel, R.A., et al., *Human Islet Amyloid Polypeptide Oligomers Disrupt Cell Coupling, Induce Apoptosis, and Impair Insulin Secretion in Isolated Human Islets.* Diabetes, 2007. **56**(1): p. 65-71.
516. Konarkowska, B., et al., *The aggregation potential of human amylin determines its cytotoxicity towards islet β-cells.* FEBS Journal, 2006. **273**(15): p. 3614-3624.

517. Pilkington, E.H., et al., *Pancreatic β-Cell Membrane Fluidity and Toxicity Induced by Human Islet Amyloid Polypeptide Species.* Scientific Reports, 2016. **6**(1): p. 21274.
518. Kalita, S., et al., *Site-specific single point mutation by anthranilic acid in hIAPP_{8–37} enhances anti-amyloidogenic activity.* RSC Chemical Biology, 2021. **2**(1): p. 266-273.
519. Niu, Z., et al., *Interactions between amyloid β peptide and lipid membranes.* Biochimica et Biophysica Acta (BBA) - Biomembranes, 2018. **1860**(9): p. 1663-1669.
520. Wong, P.T., et al., *Amyloid-beta membrane binding and permeabilization are distinct processes influenced separately by membrane charge and fluidity.* J Mol Biol, 2009. **386**(1): p. 81-96.
521. Dzień, E., et al., *Thermodynamic surprises of Cu(II)–amylin analogue complexes in membrane mimicking solutions.* Scientific Reports, 2022. **12**(1).
522. Patil, S.M. and A.T. Alexandrescu, *Charge-Based Inhibitors of Amylin Fibrillization and Toxicity.* Journal of Diabetes Research, 2015. **2015**: p. 1-13.
523. Kanatsuka, A., S. Kou, and H. Makino, *IAPP/amylin and β-cell failure: implication of the risk factors of type 2 diabetes.* Diabetology International, 2018. **9**(3): p. 143-157.
524. Bode, D.C., M.D. Baker, and J.H. Viles, *Ion Channel Formation by Amyloid-β42 Oligomers but Not Amyloid-β40 in Cellular Membranes.* J Biol Chem, 2017. **292**(4): p. 1404-1413.
525. Esteras, N. and A.Y. Abramov, *Mitochondrial Calcium Deregulation in the Mechanism of Beta-Amyloid and Tau Pathology.* Cells, 2020. **9**(9): p. 2135.
526. Fu, W., et al., *Amyloid β (Aβ) Peptide Directly Activates Amylin-3 Receptor Subtype by Triggering Multiple Intracellular Signaling Pathways.* Journal of Biological Chemistry, 2012. **287**(22): p. 18820-18830.
527. Visa, M., et al., *Islet amyloid polypeptide exerts a novel autocrine action in β-cell signaling and proliferation.* The FASEB Journal, 2015. **29**(7): p. 2970-2979.

528. Mather, K.J., et al., *Role of amylin in insulin secretion and action in humans: antagonist studies across the spectrum of insulin sensitivity.* Diabetes/Metabolism Research and Reviews, 2002. **18**(2): p. 118-126.
529. Newsholme, P., et al., *Nutrient regulation of insulin secretion and action.* J Endocrinol, 2014. **221**(3): p. R105-20.
530. Sowa, R., et al., *Islet amyloid polypeptide amide causes peripheral insulin resistance in vivo in dogs.* Diabetologia, 1990. **33**(2): p. 118-120.
531. Koopmans, S.J., et al., *Amylin-induced in vivo insulin resistance in conscious rats: the liver is more sensitive to amylin than peripheral tissues.* Diabetologia, 1991. **34**(4): p. 218-224.
532. De Felice, F.G., M.V. Lourenco, and S.T. Ferreira, *How does brain insulin resistance develop in Alzheimer's disease?* Alzheimer's & Dementia, 2014. **10**(1, Supplement): p. S26-S32.
533. Burgering, B.M. and P.J. Coffer, *Protein kinase B (c-Akt) in phosphatidylinositol-3-OH kinase signal transduction.* Nature, 1995. **376**(6541): p. 599-602.
534. Franke, T.F., et al., *The protein kinase encoded by the Akt proto-oncogene is a target of the PDGF-activated phosphatidylinositol 3-kinase.* Cell, 1995. **81**(5): p. 727-36.
535. Agilent Technologies, I. *Characterizing Your Cells: Using OCR Values to Determine Optimal Seeding Density*. 2017; Available from: https://www.agilent.com/cs/library/technicaloverviews/public/5991-7994EN.pdf.
536. Yamauchi, K. and J.E. Pessin, *Enhancement or inhibition of insulin signaling by insulin receptor substrate 1 is cell context dependent.* Mol Cell Biol, 1994. **14**(7): p. 4427-34.
537. Bankar, S.B., et al., *Glucose oxidase — An overview.* Biotechnology Advances, 2009. **27**(4): p. 489-501.
538. Kitada, M., et al., *Sirtuins and Type 2 Diabetes: Role in Inflammation, Oxidative Stress, and Mitochondrial Function.* Frontiers in Endocrinology, 2019. **10**.
539. Wortel, I.M.N., et al., *Surviving Stress: Modulation of ATF4-Mediated Stress Responses in Normal and Malignant Cells.* Trends in Endocrinology & Metabolism, 2017. **28**(11): p. 794-806.

540. Owens, J., K. Moreira, and G. Bain, *Characterization of primary human skeletal muscle cells from multiple commercial sources.* In Vitro Cell Dev Biol Anim, 2013. **49**(9): p. 695-705.
541. Leenders, M., et al., *Patients with type 2 diabetes show a greater decline in muscle mass, muscle strength, and functional capacity with aging.* J Am Med Dir Assoc, 2013. **14**(8): p. 585-92.
542. Palmer, J.C., et al., *Endothelin-1 is elevated in Alzheimer's disease and upregulated by amyloid-β.* J Alzheimers Dis, 2012. **29**(4): p. 853-61.
543. Deng, Z., et al., *Ultrasound-mediated augmented exosome release from astrocytes alleviates amyloid-β-induced neurotoxicity.* Theranostics, 2021. **11**(9): p. 4351-4362.
544. Yang, J., et al., *Silibinin protects rat pancreatic β-cell through up-regulation of estrogen receptors' signaling against amylin- or Aβ 1–42 -induced reactive oxygen species/reactive nitrogen species generation.* Phytotherapy Research, 2019. **33**(4): p. 998-1009.
545. Zhang, S., et al., *Fibrillogenic Amylin Evokes Islet β-Cell Apoptosis through Linked Activation of a Caspase Cascade and JNK1.* Journal of Biological Chemistry, 2003. **278**(52): p. 52810-52819.
546. Baron, P., et al., *Synergistic effect of -amyloid protein and interferon gamma on nitric oxide production by C2C12 muscle cells.* Brain, 2000. **123**(2): p. 374-379.
547. Iwatsubo, T., *Amyloid β Protein in Plasma as a Diagnostic Marker for Alzheimer's Disease.* Neurobiology of Aging, 1998. **19**(2): p. 161-163.
548. Wu, Q., et al., *MicroRNA-126 enhances the biological function of endothelial progenitor cells under oxidative stress via PI3K/Akt/GSK-3β and ERK1/2 signaling pathways.* Bosnian Journal of Basic Medical Sciences, 2020.
549. Nicholson, K.M. and N.G. Anderson, *The protein kinase B/Akt signalling pathway in human malignancy.* Cellular Signalling, 2002. **14**(5): p. 381-395.
550. Tong, C., et al., *Insulin resistance, autophagy and apoptosis in patients with polycystic ovary syndrome: Association with PI3K signaling pathway.* Frontiers in Endocrinology, 2022. **13**.

551. Gong, Y., et al., *Growth hormone activates PI3K/Akt signaling and inhibits ROS accumulation and apoptosis in granulosa cells of patients with polycystic ovary syndrome.* Reproductive Biology and Endocrinology, 2020. **18**(1).
552. Jeon, J., et al., *GLP-1 improves palmitate-induced insulin resistance in human skeletal muscle via SIRT1 activity.* International Journal of Molecular Medicine, 2019.
553. Romeu Montenegro, K., et al., *Effects of vitamin D on primary human skeletal muscle cell proliferation, differentiation, protein synthesis and bioenergetics.* The Journal of Steroid Biochemistry and Molecular Biology, 2019. **193**: p. 105423.
554. Tapadia, M., et al., *Antidiabetic effects and mechanisms of action of γ-conglutin from lupin seeds.* Journal of Functional Foods, 2021. **87**: p. 104786.
555. Ebeling, P., H.A. Koistinen, and V.A. Koivisto, *Insulin-independent glucose transport regulates insulin sensitivity.* FEBS Letters, 1998. **436**(3): p. 301-303.
556. Ciaraldi, T.P., et al., *Skeletal Muscle GLUT1 Transporter Protein Expression and Basal Leg Glucose Uptake Are Reduced in Type 2 Diabetes.* The Journal of Clinical Endocrinology & Metabolism, 2005. **90**(1): p. 352-358.
557. Winkler, E.A., et al., *GLUT1 reductions exacerbate Alzheimer's disease vasculo-neuronal dysfunction and degeneration.* Nature Neuroscience, 2015. **18**(4): p. 521-530.
558. Hooijmans, C.R., et al., *Amyloid beta deposition is related to decreased glucose transporter-1 levels and hippocampal atrophy in brains of aged APP/PS1 mice.* Brain Research, 2007. **1181**: p. 93-103.
559. Fletcher, L.M., et al., *Role for the microtubule cytoskeleton in GLUT4 vesicle trafficking and in the regulation of insulin-stimulated glucose uptake.* Biochem J, 2000. **352 Pt 2**(Pt 2): p. 267-76.
560. Sjöstedt, E., et al., *An atlas of the protein-coding genes in the human, pig, and mouse brain.* Science, 2020. **367**(6482): p. eaay5947.
561. Gu, Y., F. Oyama, and Y. Ihara, *τ Is Widely Expressed in Rat Tissues.* Journal of Neurochemistry, 2002. **67**(3): p. 1235-1244.

562. Dugger, B.N., et al., *Tau immunoreactivity in peripheral tissues of human aging and select tauopathies.* Neuroscience Letters, 2019. **696**: p. 132-139.
563. Lübke, U., et al., *Microtubule-associated protein tau epitopes are present in fiber lesions in diverse muscle disorders.* Am J Pathol, 1994. **145**(1): p. 175-88.
564. Maurage, C.A., et al., *Tau aggregates are abnormally phosphorylated in inclusion body myositis and have an immunoelectrophoretic profile distinct from other tauopathies.* Neuropathology and Applied Neurobiology, 2004. **30**(6): p. 624-634.
565. Chen, X., et al., *Development of AD-Like Pathology in Skeletal Muscle.* Journal of Parkinson's Disease and Alzheimer's Disease, 2019. **6**(1): p. 1-10.
566. Zhang, Y., et al., *Amyloid-β Induces Hepatic Insulin Resistance by Activating JAK2/STAT3/SOCS-1 Signaling Pathway.* Diabetes, 2012. **61**(6): p. 1434-1443.
567. Shi, S.Y., et al., *Hepatocyte-specific Deletion of Janus Kinase 2 (JAK2) Protects against Diet-induced Steatohepatitis and Glucose Intolerance.* Journal of Biological Chemistry, 2012. **287**(13): p. 10277-10288.
568. Thirone, A.C., et al., *Opposite effect of JAK2 on insulin-dependent activation of mitogen-activated protein kinases and Akt in muscle cells: possible target to ameliorate insulin resistance.* Diabetes, 2006. **55**(4): p. 942-51.
569. Hood, D.A., et al., *Maintenance of Skeletal Muscle Mitochondria in Health, Exercise, and Aging.* Annual Review of Physiology, 2019. **81**(1): p. 19-41.
570. Di Meo, S., S. Iossa, and P. Venditti, *Skeletal muscle insulin resistance: role of mitochondria and other ROS sources.* Journal of Endocrinology, 2017. **233**(1): p. R15-R42.
571. Kumar, A., et al., *Metabolomic analysis of primary human skeletal muscle cells during myogenic progression.* Scientific Reports, 2020. **10**(1).
572. Rajasekaran, N.S., et al., *Reductive stress impairs myogenic differentiation.* Redox Biology, 2020. **34**: p. 101492.

573. Crouser, E.D., et al., *Abnormal permeability of inner and outer mitochondrial membranes contributes independently to mitochondrial dysfunction in the liver during acute endotoxemia*.* Critical Care Medicine, 2004. **32**(2): p. 478-488.
574. Michan, S. and D. Sinclair, *Sirtuins in mammals: insights into their biological function.* Biochemical Journal, 2007. **404**(1): p. 1-13.
575. Zhang, H.-H., et al., *SIRT1 attenuates high glucose-induced insulin resistance via reducing mitochondrial dysfunction in skeletal muscle cells.* Experimental Biology and Medicine, 2015. **240**(5): p. 557-565.
576. Lagouge, M., et al., *Resveratrol Improves Mitochondrial Function and Protects against Metabolic Disease by Activating SIRT1 and PGC-1α.* Cell, 2006. **127**(6): p. 1109-1122.
577. Gerhart-Hines, Z., et al., *Metabolic control of muscle mitochondrial function and fatty acid oxidation through SIRT1/PGC-1α.* The EMBO Journal, 2007. **26**(7): p. 1913-1923.
578. Cantó, C., et al., *AMPK regulates energy expenditure by modulating NAD+ metabolism and SIRT1 activity.* Nature, 2009. **458**(7241): p. 1056-1060.
579. Rodgers, J.T., et al., *Nutrient control of glucose homeostasis through a complex of PGC-1α and SIRT1.* Nature, 2005. **434**(7029): p. 113-118.
580. Sun, C., et al., *SIRT1 Improves Insulin Sensitivity under Insulin-Resistant Conditions by Repressing PTP1B.* Cell Metabolism, 2007. **6**(4): p. 307-319.
581. Iwabu, M., et al., *Adiponectin and AdipoR1 regulate PGC-1α and mitochondria by Ca2+ and AMPK/SIRT1.* Nature, 2010. **464**(7293): p. 1313-1319.
582. Wilson, B.J., et al., *An Acetylation Switch Modulates the Transcriptional Activity of Estrogen-Related Receptor α.* Molecular Endocrinology, 2010. **24**(7): p. 1349-1358.
583. Fröjdö, S., et al., *Phosphoinositide 3-kinase as a novel functional target for the regulation of the insulin signaling pathway by SIRT1.* Molecular and Cellular Endocrinology, 2011. **335**(2): p. 166-176.
584. de Kreutzenberg, S.V., et al., *Downregulation of the longevity-associated protein sirtuin 1 in insulin resistance and metabolic*

syndrome: potential biochemical mechanisms. Diabetes, 2010. **59**(4): p. 1006-15.

585. Cao, K., et al., *Reduced expression of SIRT1 and SOD-1 and the correlation between these levels in various regions of the brains of patients with Alzheimer's disease.* J Clin Pathol, 2018. **71**(12): p. 1090-1099.
586. Wong, S.Y. and B.L. Tang, *SIRT1 as a therapeutic target for Alzheimer's disease.* Reviews in the Neurosciences, 2016. **27**(8): p. 813-825.
587. Ng, F., L. Wijaya, and B.L. Tang, *SIRT1 in the brain—connections with aging-associated disorders and lifespan.* Frontiers in Cellular Neuroscience, 2015. **9**.
588. Zhang, D., et al., *Heat shock protein 60 (HSP60) modulates adiponectin signaling by stabilizing adiponectin receptor.* Cell Communication and Signaling, 2020. **18**(1).
589. Khadir, A., et al., *Physical Exercise Enhanced Heat Shock Protein 60 Expression and Attenuated Inflammation in the Adipose Tissue of Human Diabetic Obese.* Frontiers in Endocrinology, 2018. **9**.
590. Tang, H., et al., *Downregulation of HSP60 disrupts mitochondrial proteostasis to promote tumorigenesis and progression in clear cell renal cell carcinoma.* Oncotarget, 2016. **7**(25): p. 38822-38834.
591. Liyanagamage, D.S.N.K. and R.D. Martinus, *Role of Mitochondrial Stress Protein HSP60 in Diabetes-Induced Neuroinflammation.* Mediators of Inflammation, 2020. **2020**: p. 1-8.
592. Kleinridders, A., et al., *Leptin regulation of Hsp60 impacts hypothalamic insulin signaling.* Journal of Clinical Investigation, 2013. **123**(11): p. 4667-4680.
593. Barone, R., et al., *Skeletal muscle Heat shock protein 60 increases after endurance training and induces peroxisome proliferator-activated receptor gamma coactivator 1 α1 expression.* Scientific Reports, 2016. **6**(1): p. 19781.
594. Marino Gammazza, A., et al., *Hsp60 in Skeletal Muscle Fiber Biogenesis and Homeostasis: From Physical Exercise to Skeletal Muscle Pathology.* Cells, 2018. **7**(12): p. 224.

595. Chun, J.N., et al., *Cytosolic Hsp60 Is Involved in the NF-κB-Dependent Survival of Cancer Cells via IKK Regulation.* PLoS ONE, 2010. **5**(3): p. e9422.
596. Chandra, D., G. Choy, and D.G. Tang, *Cytosolic Accumulation of HSP60 during Apoptosis with or without Apparent Mitochondrial Release.* Journal of Biological Chemistry, 2007. **282**(43): p. 31289-31301.
597. Sarangi, U., et al., *Hsp60 Chaperonin Acts as Barrier to Pharmacologically Induced Oxidative Stress Mediated Apoptosis in Tumor Cells with Differential stress Response.* Drug Target Insights, 2013. **7**: p. DTI.S12513.
598. Xanthoudakis, S., et al., *Hsp60 accelerates the maturation of pro-caspase-3 by upstream activator proteases during apoptosis.* Embo j, 1999. **18**(8): p. 2049-56.
599. Samali, A., et al., *Apoptosis: Cell death defined by caspase activation.* Cell Death & Differentiation, 1999. **6**(6): p. 495-496.
600. Merendino, A.M., et al., *Hsp60 is actively secreted by human tumor cells.* PloS one, 2010. **5**(2): p. e9247-e9247.
601. Nativel, B., et al., *Biology of Extracellular HSP60*. 2019, Springer International Publishing. p. 57-80.
602. Märker, T., et al., *Heat Shock Protein 60 as a Mediator of Adipose Tissue Inflammation and Insulin Resistance.* Diabetes, 2012. **61**(3): p. 615-625.
603. Lange, P.S., et al., *ATF4 is an oxidative stress–inducible, prodeath transcription factor in neurons in vitro and in vivo.* Journal of Experimental Medicine, 2008. **205**(5): p. 1227-1242.
604. Deldicque, L., P. Hespel, and M. Francaux, *Endoplasmic Reticulum Stress in Skeletal Muscle.* Exercise and Sport Sciences Reviews, 2012. **40**(1): p. 43-49.
605. Askanas, V. and W.K. Engel, *Molecular pathology and pathogenesis of inclusion-body myositis.* Microscopy Research and Technique, 2005. **67**(3-4): p. 114-120.
606. Benveniste, O., et al., *Amyloid deposits and inflammatory infiltrates in sporadic inclusion body myositis: the inflammatory egg comes before*

the degenerative chicken. Acta Neuropathologica, 2015. **129**(5): p. 611-624.

607. Sahoo, B.R., et al., *A cationic polymethacrylate-copolymer acts as an agonist for β-amyloid and an antagonist for amylin fibrillation.* Chemical Science, 2019. **10**(14): p. 3976-3986.
608. Braun, M., R. Ramracheya, and P. Rorsman, *Autocrine regulation of insulin secretion.* Diabetes, Obesity and Metabolism, 2012. **14**(s3): p. 143-151.
609. Xie, L., et al., *Alzheimer's β-Amyloid Peptides Compete for Insulin Binding to the Insulin Receptor.* The Journal of Neuroscience, 2002. **22**(10): p. RC221-RC221.
610. Molina-Fernández, R., et al., *Differential regulation of insulin signalling by monomeric and oligomeric amyloid beta-peptide.* Brain Communications, 2022. **4**(5).
611. Jhamandas, J.H. and D. Mactavish, *Antagonist of the Amylin Receptor Blocks β-Amyloid Toxicity in Rat Cholinergic Basal Forebrain Neurons.* The Journal of Neuroscience, 2004. **24**(24): p. 5579-5584.
612. Soudy, R., et al., *Short amylin receptor antagonist peptides improve memory deficits in Alzheimer's disease mouse model.* Scientific Reports, 2019. **9**(1).
613. Jhamandas, J.H., et al., *Actions of β-Amyloid Protein on Human Neurons Are Expressed through the Amylin Receptor.* The American Journal of Pathology, 2011. **178**(1): p. 140-149.
614. Fu, W., A. Patel, and J.H. Jhamandas, *Amylin Receptor: A Common Pathophysiological Target in Alzheimer's Disease and Diabetes Mellitus.* Frontiers in Aging Neuroscience, 2013. **5**.
615. Yan, L.-M., et al., *IAPP Mimic Blocks Aβ Cytotoxic Self-Assembly: Cross-Suppression of Amyloid Toxicity of Aβ and IAPP Suggests a Molecular Link between Alzheimer's Disease and Type II Diabetes.* Angewandte Chemie International Edition, 2007. **46**(8): p. 1246-1252.
616. Aftabizadeh, M., et al., *Blocking Inflammasome Activation Caused by β-Amyloid Peptide (Aβ) and Islet Amyloid Polypeptide (IAPP) through an IAPP Mimic.* ACS Chemical Neuroscience, 2019. **10**(8): p. 3703-3717.

617. Voronova, A., et al., *Anti-aggregation effect of carbon quantum dots on diabetogenic and beta-cell cytotoxic amylin and beta amyloid heterocomplexes.* Nanoscale, 2022. **14**(39): p. 14683-14694.
618. Verchere, C.B., et al., *Islet amyloid formation associated with hyperglycemia in transgenic mice with pancreatic beta cell expression of human islet amyloid polypeptide.* Proceedings of the National Academy of Sciences, 1996. **93**(8): p. 3492-3496.
619. Nopparat, C., et al., *Melatonin Attenuates High Glucose-Induced Changes in Beta Amyloid Precursor Protein Processing in Human Neuroblastoma Cells.* Neurochemical Research, 2022. **47**(9): p. 2568-2579.
620. Xu, Z., et al., *The role of peripheral β-amyloid in insulin resistance, insulin secretion, and prediabetes: in vitro and population-based studies.* Frontiers in Endocrinology, 2023. **14**.
621. Huang, J., et al., *The solution structure of rat Aβ-(1–28) and its interaction with zinc ion: insights into the scarcity of amyloid deposition in aged rat brain.* JBIC Journal of Biological Inorganic Chemistry, 2004. **9**(5): p. 627-635.
622. Bosco, M.D., et al., *Zinc Transporters in the Endocrine Pancreas*. 2015, Springer Netherlands. p. 511-527.
623. Nedumpully-Govindan, P., et al., *Promotion or Inhibition of Islet Amyloid Polypeptide Aggregation by Zinc Coordination Depends on Its Relative Concentration.* Biochemistry, 2015. **54**(50): p. 7335-44.
624. Fukunaka, A., et al., *Zinc and iron dynamics in human islet amyloid polypeptide-induced diabetes mouse model.* Scientific Reports, 2023. **13**(1).
625. Fujikawa, T., *Central regulation of glucose metabolism in an insulin-dependent and -independent manner.* J Neuroendocrinol, 2021. **33**(4): p. e12941.
626. Yoon, N.A. and S. Diano, *Hypothalamic glucose-sensing mechanisms.* Diabetologia, 2021. **64**(5): p. 985-993.
627. Grayson, B.E., R.J. Seeley, and D.A. Sandoval, *Wired on sugar: the role of the CNS in the regulation of glucose homeostasis.* Nature Reviews Neuroscience, 2013. **14**(1): p. 24-37.

628. Jayaraman, A. and C.J. Pike, *Alzheimer's Disease and Type 2 Diabetes: Multiple Mechanisms Contribute to Interactions.* Current Diabetes Reports, 2014. **14**(4).
629. González, A., et al., *Glucose metabolism and AD: evidence for a potential diabetes type 3.* Alzheimer's Research & Therapy, 2022. **14**(1).
630. Luna, R., et al., *A Comprehensive Review of Neuronal Changes in Diabetics.* Cureus, 2021.
631. Kumar, V., S.-H. Kim, and K. Bishayee, *Dysfunctional Glucose Metabolism in Alzheimer's Disease Onset and Potential Pharmacological Interventions.* International Journal of Molecular Sciences, 2022. **23**(17): p. 9540.

CHAPTER 8 Appendices

8.1 Appendix A – Review article on the role of Heat Shock Proteins in T2D and AD with a focus on the management of amyloidogenic peptides as published by thesis author in *International Journal of Molecular Sciences* (2020)

Content removed due to copyright restrictions

Rowles JE, Keane KN, Gomes Heck T, Cruzat V, Verdile G, Newsholme P. Are Heat Shock Proteins an Important Link between Type 2 Diabetes and Alzheimer Disease? Int J Mol Sci. 2020 Nov 2;21(21):8204. doi: 10.3390/ijms21218204. PMID: 33147803; PMCID: PMC7662599.

8.3 Appendix B – Relevant data associated with novel double transgenic mouse model as published by Wijesekara et al. in *the FASEB Journal* (2017)

Content removed due to copyright restrictions

Wijesekara N, Ahrens R, Sabale M, Wu L, Ha K, Verdile G, Fraser PE. Amyloid-β and islet amyloid pathologies link Alzheimer's disease and type 2 diabetes in a transgenic model. FASEB J. 2017 Dec;31(12):5409-5418. doi: 10.1096/fj.201700431R. Epub 2017 Aug 14. PMID: 28808140.

8.4 Appendix C - Relevant data associated with characterisation of IAPP-Aβ heterocomplexes as published by Bharadwaj et al. in *Scientific Reports* (2020) with thesis author as contributor

Content removed due to copyright restrictions

Bharadwaj P, Solomon T, Sahoo BR, Ignasiak K, Gaskin S, Rowles J, Verdile G, Howard MJ, Bond CS, Ramamoorthy A, Martins RN, Newsholme P. Amylin and beta amyloid proteins interact to form amorphous heterocomplexes with enhanced toxicity in neuronal cells. Sci Rep. 2020 Jun 25;10(1):10356. doi: 10.1038/s41598-020-66602-9. PMID: 32587390; PMCID: PMC7316712.

8.5 Appendix D – Tau pathology in pancreatic tissue of a cross-bred AD x T2D double transgenic mouse model

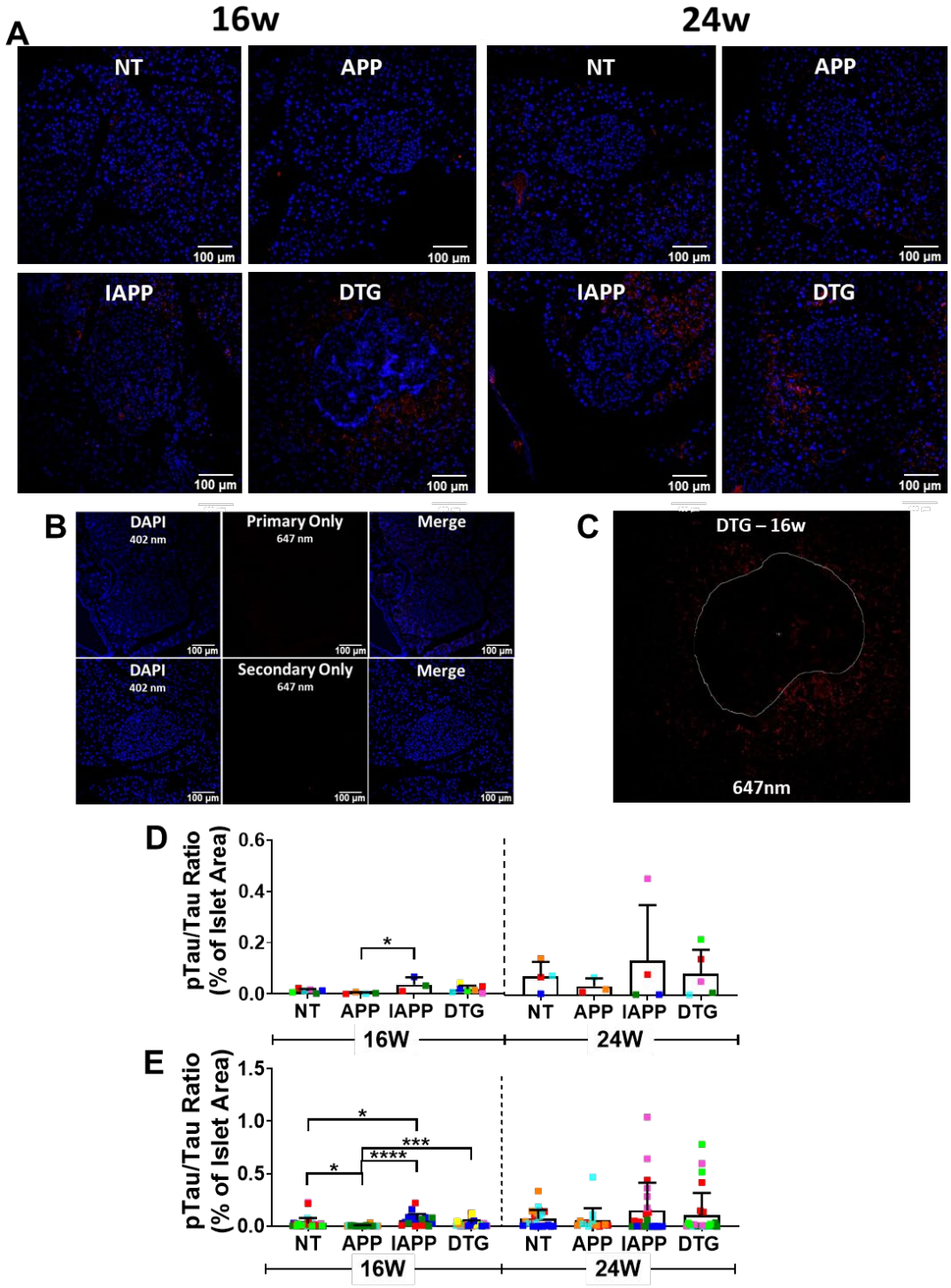

Ratio of phosphorylated Tau to total Tau more variable in islets of nontransgenic, transgenic APP, transgenic IAPP, or crossbred double transgenic APP x IAPP mice at 24 weeks. Paraffin sections were generated from pancreatic tissue of 16- and 24-week-old mice and stained with anti-pTau antibody to detect pTau protein in pancreatic islets. (A)

Representative islet images of pTau staining (anti-pTau antibody; red) and cell nuclei (Hoescht stain; blue) at 20X magnification. During optimisation procedure, primary antibody and isotype controls were conducted with all antibodies a minimum of 3 times. Primary and isotype controls of anti-pTau antibody are included to provide evidence of specific staining due to low expression of pTau staining within islets (B). Very low pTau staining was seen in islets, and extensive staining in the surrounding exocrine portion of the pancreatic tissue (C). The percentage area of islets stained positively with pTau was quantified and expressed as a ratio of pTau to total Tau Coverage (Figure 6) in islets and represented as mixed bar/scattergrams, showing the mean pTau/Tau ratio per animal (D), where each coloured data point represents an individual animal. Data was also plotted as pTau/Tau ratio of total islets per group (E), where each data point represents an individual islet and colour-coded to match individual animals of graph B. All data represented as mean ± SD. Statistical analysis via one-way ANOVA with Tukey multiple comparisons test to determine changes between groups (*), and two-way ANOVA with Sidak's multiple comparisons test was used to determine changes between 16 and 24 weeks(#). # / *p value=< 0.05, ## / **p value=< 0.01, ### / ***p value=< 0.001, #### / ****p value=< 0.0001.

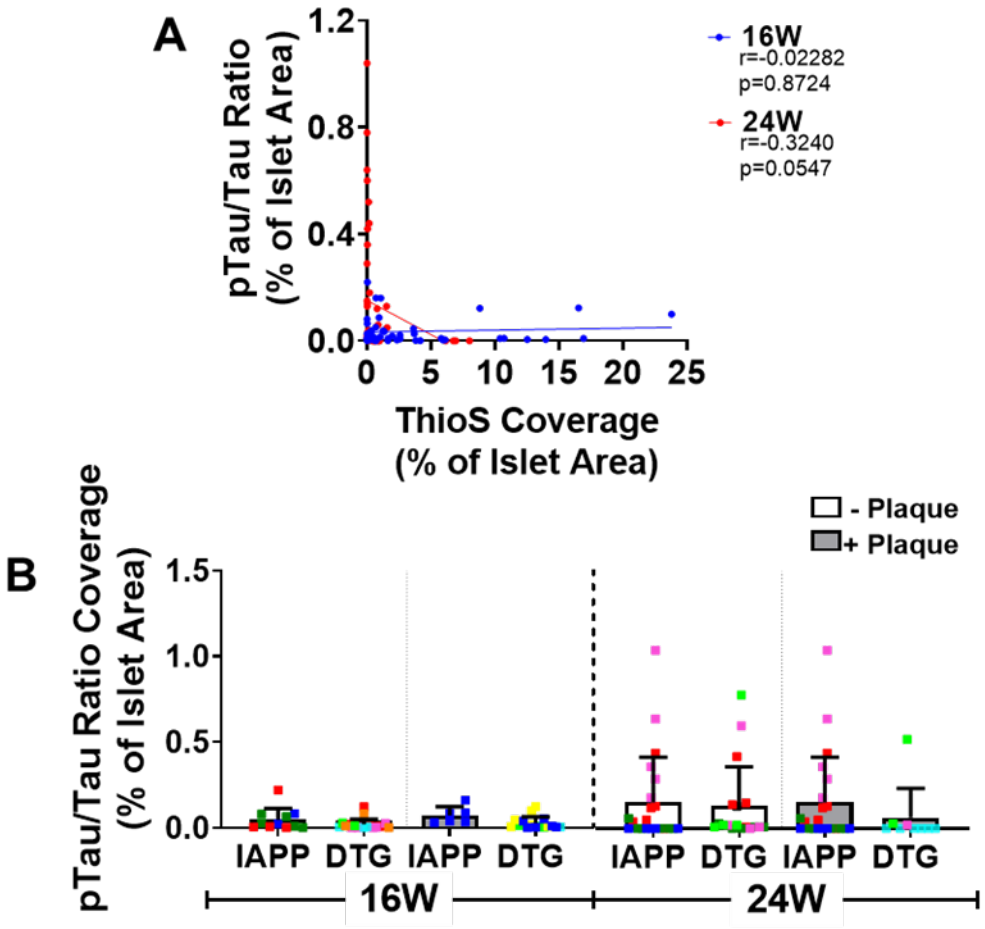

Ratio of phosphorylated Tau to total Tau is not correlated with plaque burden is islets of transgenic IAPP and crossbred double transgenic APP x IAPP mice. Linear regression and

correlation analysis of the relationship between plaque burden and pTau/Tau Ratio (A), where each data point represents an individual islet, showing no significant correlation. Statistical analysis via linear regression and Pearson's correlation test. Correlation explored further via analysis of pTau/Tau Ratio in IAPP and DTG islets with (+) or without (-) plaque accumulation at 16 and 24 weeks (B). All data represented as mean ± SD. Statistical analysis via one-way ANOVA with Tukey multiple comparisons test to determine changes between groups (*), and two-way ANOVA with Sidak's multiple comparisons test was used to determine changes between 16 and 24 weeks(#). **#** / ***p value=< 0.05, **##** / ****p value=< 0.01, **###** / *****p value=< 0.001, **####** / ******p value=< 0.0001